ProQuest LLC.
789 East Eisenhower Parkway
P.O. Box 1346
Ann Arbor, MI 48106 – 1346

Development of a small-scale absorption cooled water chiller

Tan Yuk Wei

A thesis submitted in partial fulfilment of the
requirements of The Nottingham Trent University
for the degree of Doctor of Philosophy

November 2000

ABSTRACT

Legislation to improve environment control has recently led to a number of analytical studies to characterise absorption cooling systems (ACS). ACS play an important role in reducing CFCs and CO_2 since it works on natural fluids and can be driven by waste heat or solar energy. However its current performance is low and the system characteristics are still not well understood. This work aims to provide a better fundamental understanding of existing knowledge on this cooling system technology with the view to improving its performance and establishing the feasibility of developing a small scale unit for the domestic market. The dual pressure water-lithium bromide (H_2O-LiBr) absorption system has been investigated in detail.

The outcome of this work has led to the development of a user friendly software named ABCON, which comprises features of data-logging from a custom built experimental rig, First and Second Laws of Thermodynamic analysis, and components design. The software is a significant improvement over its predecessors especially the monitoring and control of the experimental system integrated with an effective design tool not currently available in the commercial market.

Mathematical models for exergetic analysis based on the Second Law of thermodynamics which have been omitted in most of the published literatures were developed and studied as part of this work. Optimum generator temperatures for establishing maximum exergetic coefficient of performance (ECOP) have been presented in a novel carpet plot form. Two new equations derived for maximum ECOP at optimum generator temperature is conveniently stored in a control system to achieve optimised conditions during operation. For instance, when the condenser and absorber temperatures are equal at 35 °C, and the evaporator temperature is at 8°C, the optimum ECOP will be 0.209 assuming the generator temperature is maintained at 72.5 °C. Analytical and numerical models for different types of absorbers were studied and a coil absorber model has been proposed. The model includes three transport mechanisms namely falling film on the tube, droplets fall and the droplet formation which were not included in previous published literature. The re-circulation spray which can help reduce the absorber load and enhance the absorption rate has been incorporated into the model. The counter-current and parallel absorbers with two coil diameters have been compared with variation of mass concentration, coolant and solution flow rate and number of droplet sites.

An absorption rig was built using borosilicate glass so that the process mechanism can be observed conveniently. It was designed to be flexible and used as a benchmark for comparison in studying and developing new cycles and absorbent/refrigerant combinations in future work. The experimental results show the importance of the effects of the inlet solution conditions on the absorber performance. The changes of heat and mass transfer coefficient, absorber load and mass absorption rate with inlet solution temperatures are reported. The results have been validated against the theoretical model and shown to be in good agreement to the trends predicted for different conditions. Crucial factors for achieving good system performance such as accurate control of the pressure and inlet solution temperature have been identified through experiments. It is recommended that the evaporator and absorber should be combined in future designs. The effects of the non-condensable gas and additives such as 2-ethyl-1-hexanol to the overall performance have been recommended for future work.

The design and development of the rig with viewing and other component interchangebility facilities together with the empirical data generated for a small scale ACS will be an invaluable asset to future development of prototype systems thus making an important contribution to the current debate on environmental control.

ACKNOWLEDGEMENTS

There are many people to whom I am grateful for supporting me during the course of this work. First and foremost, I am very grateful to my director of studies, Professor Nath Jambunathan, for his active support and guidance throughout this work. Without his help in finding the sponsorship and industrial collaboration, this could not have been carried out successfully.

I am indebted to my parents for their encouragement. They instilled in me the desire to complete the work to the best of my abilities. I gratefully acknowledge financial support by the Nottingham Trent University in my studies and Mr. Mark Pontin, the managing director of P.A. Hilton Ltd. for sponsoring the equipment and offering the practical training to build the experimental rig in Winchester. I have to thank Mr. Kim Peeling and Mr. Colin Moss from P.A. Hilton for their precious advice, ideas and tireless efforts to give me a lift during the experimentation periods in Winchester. A special acknowledgement is given to Mr. Colin Moss who always arrived early and leaving late from work, helped me in preparing some of the drawings and labels for the experiment, brazing pipes, solving problems such as crystallisation and leakage. I have greatly benefited from his rich practical experience during my training periods in P.A. Hilton.

I would like to thank Dr. Shenyi Wu and Dr. Ian Eames (University of Nottingham) and Professor R.E. Critoph (Warwick University) for demonstrating their rigs and giving invaluable advice and comments in building my experimental rig. A special thanks to Dr. Jeffrey Seewald (Trane Ltd.) for providing the information to enable me to develop the absorber model for this work.

I would also like to thank the brothers and sisters in the Nottingham Chinese Christian Church who pray constantly for me. I thank God for giving me the intelligence and guiding me throughout this work.

Last but not least, I would like to thank my loving fiancée who is away from her family in Hong Kong. I am greatly indebted to her for the encouragement, support and her patience in the past three years.

LIST OF CONTENTS

CONFERENCES, COURSES AND SEMINAR ATTENDED

Seminar of Low Energy Heat Pump System. Institute of Mechanical Engineering, London. Oct. ,1997

Dr. Y.Yan, MSc course, Lectures on using CFD package (PHOENICS), The Nottingham Trent University. Oct.-Dec., 1998

Refrigeration and Air Conditioning 99' Exhibition. NEC, Birmingham. Mar., 1999.

IMechE Recent Development in Refrigeration and Air Conditioning, 20 Apr., 1999

PUBLICATIONS AND REPORTS

Tan Y.W. and K. Jambunathan, 2000, Development of a small-scale H_20 – LiBr absorption cooling system. *Heat Transfer Science and Technology 2000, Uni. of Tsinghua, Beijing,* 803-808.

Jambunathan, K., Tan, Y.W. and Ashforth-Frost, S., 2000, Optimum design tools for small scale ammonia-water absorption cooling systems. *Int. Conf. & Exhib. On Gearing, Transmissions and Mech. Systems, The Nottingham Trent Uni.,* 791-803.

Tan Y.W. and Jambunathan, K., 2001, A design model for the water-lithium bromide coil absorber. *Applied Thermal Engineering, to be published.*

Tan Y.W. and Jambunathan, K., 2001, Experimental investigations of heat and mass transfer characteristics in a coil absorber. *Int. J. of Refrig., to be published.*

Tan Y.W. and Jambunathan, K., 2001, Development of design tools for absorption systems. *1st Int. Conf. On Experimental & Computational Heat & Mass Transfer, & Fluid Flow, South Africa, to be published.*

Tan Y.W. and Jambunathan, K., 2001, Optimised design tools for small scale water-lithium bromide absorption cooling systems. *1st Int. Conf. On Experimental & Computational Heat & Mass Transfer, & Fluid Flow, South Africa, to be published.*

B.K. Siew, Y.W.Tan and K.Jambunathan, 1999, Feasibility of using different working fluids for absorption cooling system. *B. Eng. (Hons) Mech. Eng. Project report.*

W.Y. Thoo, Y.W. Tan and K. Jambunathan, 1999, Optimisation for 5kW single stage ammonia water system. *B. Eng. (Hons) Mech. Eng. Project report.*

C.K. Tan, Y.W. Tan and K. Jambunathan, 2000, Experimental validation of Second Law analysis using a vapour compression cycle. *B. Eng. (Hons) Mech. Eng. Project report.*

S.M. Ying, Y.W. Tan and K. Jambunathan, 2000, Absorption cooling system using water-lithium bromide. Computer analysis using Second Law. *B. Eng. (Hons) Mech. Eng. Project report.*

NOMENCLATURE

Abbreviations

ACS	absorption cooling system
AACS	ammonia-water absorption cooling system
AG&S HX	generator, absorber and solution heat exchange cycle with precooler
AHE	absorber heat exchanger cycle
AHS	absorber heat recovery cycle
BASIC	basic cycle without Heat Exchanger
BGAX	Branched GAX cycle
BSS	Basic cycle with Heat Exchanger
BWR	Benedict-Webb-Rubin equation
Ca	Carnot
CF	curve fitting
CON	condenser
COP	coefficient of performance
D	mass diffusivity
Do	double stage cycle
E	efficiency
ECOP	exergetic coefficient of performance
EFF	effectiveness method
ES	experimental source
EXPs	expansion/throttling valve at strong solution side
EXPr	expansion/throttling valve at between generator and absorber
G	Gibbs Free Energy
G&S HX	generator and solution heat exchange cycle with pre-cooler
GAX	generator absorber heat recovery cycle
GEN	generator
H	Helmholtz Free Energy
HS	heat source
IS	ideal solution
mol	molecular
MT	modelling type
NOS	number of droplet sites
NTU	number of transfer unit
PAT	process average temperature
PC	basic cycle with precooler
PD	pressure drop
PH	highest pressure
PL	lowest pressure
PR	Peng-Robinson equation
PS	property source
Pv	pressure vapour
RBASIC	basic cycle with rectifier
RHX	basic cycle with rectifier & solution heat exchanger
RK	Redlich Kwong equation
RSHX	Recirculation heat exchanger
SHX	basic cycle with precooler & solution heat exchanger

S-PUMP	solution pump
WF	working fluid

Subscripts

a, abs	absorber
amb	ambient
c	condenser
e	evaporator
ex	excess energy
g	vapour side
ic	inner coil
l	liquid side
ls	lower spray
max	maximum
min	minimum
oc	outer coil
opt	optimum
pc	precooler
r	rectifier
s	saturated
sp	spray
shx	solution heat exchanger
trp, us	upper recirculation spray

List of parameters

a	thermal diffusivity, m/s characteristics dimension associated with time of spreading (t), m (Equation 6.50)
A	area, m^2
C_p	specific heat, kJ/kgK
Cir, f	circulation flow ratio
d	tube diameter, m
D	volumetric diffusivity, sq.cm/sec
$f_{c,t}$	friction factor
g	gravitational acceleration, m^2/s
h	enthalpy , kJ/kg
K_{form}	mass transfer coefficient for droplet formation, m/s
m	mass, kg
M	molecular weight, kg
$\dot{m}$	mass flow rate, kg/s
Nu	Nusselt
P	pressure, bar or kPa as prescribed in equation
Pr	Prandlt number
Q	heat flow (kW)
r	tube radius, m
R	gas constant, 8.314, kJ/kmol K Radius of the absorber coil, m
Re	Reynolds number

s	entropy, kJ/K
Sc	Schmidt number
Sh	Sherwood number
t_{form}	average droplet formation time, seconds
T, t	temperature, K or °C as prescribed in equation
U	overall heat transfer coefficient
v	specific volume, m^3/kg
W	work,kW
X, x,	mass concentration (kg refrigerant/ kg solution)

Greek symbols

η	Efficiency, %
μ	viscosity, m^2/s
λ	thermal conductivity, kW/mK
ρ	density, kg/m^3
δ	film thickness, m
σ	surface tension, N/m
α	nucleate pool boiling coefficient, $W/m^2\,{}^{o}C$ convective heat transfer coefficient, kW/m^2K
Γ	mass flow rate per tube length (kg/ms)
ΔT_{lm}	log mean temperature difference

Chapter 1 Introduction

1.1 Background -Introduction

Although the principle of the Absorption Cooling System (ACS) was invented over a century ago, its exploitation for modern applications has yet to be fully explored. ACS was introduced by Ferdinand Carre (Satha, 1995), who took out a US patent in 1860. It was subsequently replaced by more efficient vapour compression refrigeration systems. However, the absorption cooling process is again becoming increasingly attractive as its advantages in terms of reliability, low noise levels, high effectiveness, reduced impact on global warming and low-level heat energy consumption are being perceived.

Recent implementation of the Montreal Protocol (Davidson, 1999) to phase-out CFC refrigerants has heightened interest in natural fluids for use in refrigeration and air-conditioning applications and has resulted in the resurgence of interest in the development of absorption machines.

Successful introduction of ACS into the domestic market has occurred in Japan and the eastern side of the United States of America. Examination of the climate in these areas shows that there is a need for air-conditioning (refrigeration) in summer and heating in winter. By careful design, it is possible to use the same equipment for both heating and cooling duties. The situation in the UK is different; while heating is generally considered to be an essential requirement, cooling is a luxury. However, cooling by air-conditioning is expected to become popular in the future because the general standard of living improves and as the UK summer temperature continues to increase due to Global Warming. In fact, several European countries have experienced the highest temperature ever recorded.

Examination of the history of the introduction of heat pumps into Europe shows limited success and a number of costly failures (ABO1, 1997). Detailed study of those circumstances, where success for heat pumps had been claimed, shows that the success is dependent upon local energy pricing policies or the use of government subsidies (Ward, 1987). Japan is a good example where the government encourages people to use ACS so that peak electricity demand can be reduced during summer. Details of local climate, housing policy and available energy supplies are also important. It is therefore concluded that the market opportunities and technical requirements for ACS in the United Kingdom can only be established by a detailed study of national conditions and re-education of general perceptions rather than drawing on the experience of other countries.

Chapman (1996) provided an overview of the status and market penetration of gas-fired air conditioning worldwide and identified some of the controlling market forces. The paper stated several barriers to penetrating the market in UK; there is no UK based, and only limited European based, manufacturer of gas cooling equipment. Japanese and USA manufacturers have not generally considered the UK or the European market large enough to develop models tailored to the climate and legislative standards, or to establish distribution and servicing networks for their gas-fired equipment. The other recent useful report (Tozer, 1997) states that the cost of absorption machines is the most important market barrier. Absorption systems tend to be more expensive up to 100% in some instances to install per kW than competing conventional commercial systems.

The few systems currently in operation are mainly in large industrial applications. Tozer (1993) reported that there have been around 2,700 absorption chillers installed in the UK to date and 92% of these chillers are scaled around 18 kW air cooled NH_3/Water, natural gas direct-fired air conditioning units with coefficient of performance (COP) of around 0.5. There are only about ten non-manufacturing suppliers in UK.

The survey found that cooling load below 5 kW would be suitable for a single room or a single-family house. However, most of absorption chillers available in the UK are large in capacity such as the 10 kW Robur unit. Low capacity Japanese chillers have been studied by British Gas and they concluded that the cost was too high. It is therefore timely to investigate ACS technology in the context of domestic applications in the UK. Cost will be the main consideration in this project. As cost is the major criterion of success to penetrate the market of cooling in the UK, research will be aimed to investigate components in the single stage system, which invariably needs fewer components and hence cheaper.

There are many publications on numerical and computer modelling for ACS. However, due to the system's complexity, the predictions are still far from practical. It is hard to determine the effect of size and geometry of the components to the system performance due to the complexity of its structure and transport phenomena. The cost of experimentation will be high as the process consists of complex two-phase flow, which is difficult to determine without proper sensing devices. With the increasing capabilities of computer hardware and software over recent years, it is now possible to simulate the complex two-phase flow, albeit simplistically, using Computational Fluid Dynamics (CFD). Limited validations of the predicted performance of computer models may be achieved by corroboration with experimental results. On this basis, studies can be considerably extended using CFD, reducing time and cost of the design and development process. This project, however, is restricted to fundamental analyses using First and Second Laws of thermodynamics. The study also focused on an analytical model for a coil absorber. The experimental data obtained in this project would be invaluable to provide a strong basis for further CFD model development.

1.2 Project aims and objectives

Aim and Scope

Promising prospects for the application of absorption machines exist due to the increasing ozone depletion and global warming caused by CFC leakage of vapour compression machines into the atmosphere. These prospects include the application of absorption machines for cooling and heating (heat pumps and heat transformers). This study however, is principally restricted to absorption chilling machines for domestic comfort cooling.

Aim

To investigate and optimise single stage absorption cooling systems that use heated water (75^0 C - 95^0 C) supplied from a commercial gas-fired domestic boiler as heat input to the generator. To realise this, it will be necessary to obtain a better fundamental understanding of the factors which determine performance.

Objectives

1. To investigate different options for various absorption systems.
2. To identify relevant properties and recommend optimum parameters for the cooling system.
3. To obtain detailed properties of different working fluids mixtures.
4. To develop simulation software incorporating property data that will facilitate and enhance the future design process of ACS.
5. To develop computer functions for different types of working fluid mixtures for comparison.
6. To investigate the heat transfer and fluid flow characteristics of system components with the view to optimise the overall performance.
7. To select operating conditions which yield the best performance, and assess the limitations of the process. Data for maximising performance will be fitted into equations and design maps to facilitate the selection process.
8. To design and build a glass absorption test rig.
9. To develop data-logging software that is able to control the system parameters.

1.3 Vapour Compression Systems

The Vapour Compression System (VCS) is still one of the most popular systems due to its simplicity and efficiency. **Figure 1.0** illustrates the basic VCS and shows the relative location of the four basic components: compressor, condenser, evaporator and expansion valves. In this system, the main driving force is the compressor, which compresses the refrigerant vapour to a higher pressure so that it can be condensed to liquid refrigerant at the ambient temperature. The pressure difference between the condenser and evaporator is maintained by the expansion valve. The liquid refrigerant then flashes into evaporator to take away heat from the space that requires cooling. The refrigerant evaporates into vapour before entering the compressor in which the cycle is repeated again.

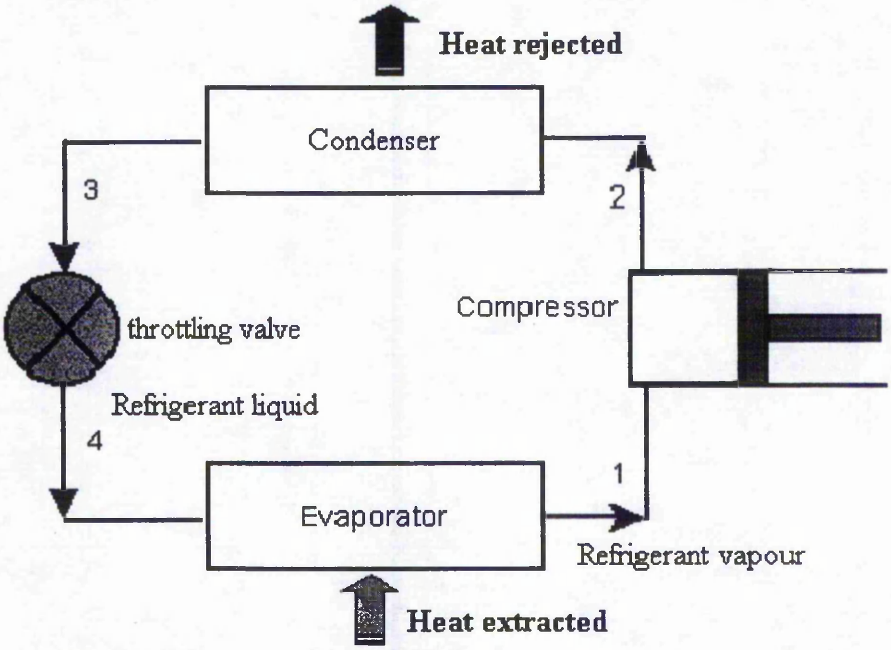

Figure 1.0 Schematic diagram of vapour compression cycle

In vapour compression systems, much work is expended in compressing the vapour from the evaporator pressure to the condenser pressure. This requirement has restricted the usage of the vapour compression system in places that have limited access to electricity supply. Further, the refrigerants used in the vapour compression systems are normally CFCs and HCFCs which are harmful to the earths ozone layer. In recent years, the HFCs such as R134a were introduced to replace these harmful refrigerants but the conversion cost is quite high. Moreover, they were classified as greenhouse gases recently in the Kyoto Protocol. Although the performance of the vapour compression system is good and the cost is low, it is however timely to investigate the alternative absorption systems with a view to reducing the environmental impact in the long run.

1.4 Basic components and principles of ACS

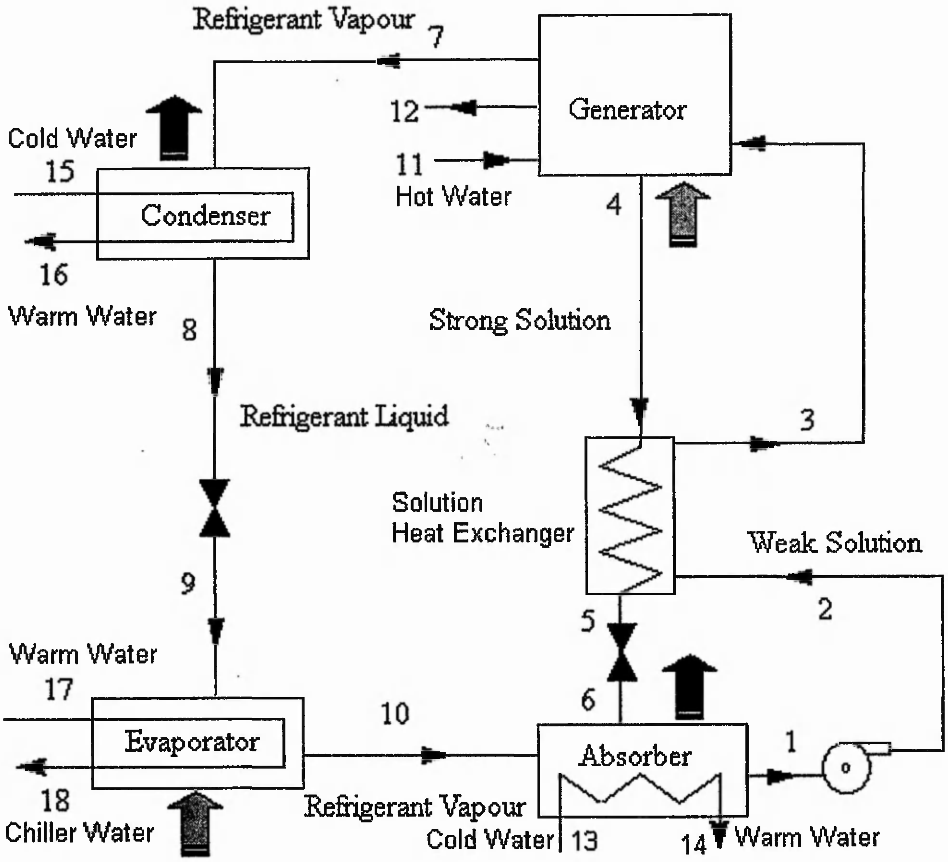

Figure 1.1 Schematic diagram of single effect absorption chiller

ACS works primarily in the same manner as the mechanical vapour compression system with the exception that the compressor is replaced by a solution circuit that absorbs the vapour at low pressure and rejects it at the higher pressure in the generator. Both systems have an evaporator and condenser and expand the refrigerant from high to low pressure through a throttle valve. The heat supplied to the generator is from waste heat from the boiler whilst the evaporator chills the circulating water. ACS operates between two pressures. The high side pressure is normally between 6 to 10 kPa while the low side pressure is between 0.1 to 0.17 kPa. Two needle valves and a solution pump separate both sides (Figure 1.1).

The most common environmentally friendly absorbent-refrigerant combinations in an ACS are ammonia-water (NH_3-H_2O) mixture and water-lithium bromide (H_2O-LiBr) mixture. In this project the ACS uses water as the refrigerant, water and lithium-bromide mixture as the absorbent. The system is mainly divided into four components comprising generator, condenser, evaporator, and absorber. The ACS is driven by any heating that passes through the generator (desorber) from point 11 to point 12. The water is driven out as vapour from the weak (weak refers to low concentration of lithium bromide) water-lithium bromide mixture while the strong solution passes through the throttling valve between point 5 and point 6 and returns to the lower side pressure in the absorber. The water vapour (7) is then condensed by an air-cooled or water-cooled condenser and becomes a saturated or sub-cooled liquid at point 8. In the condenser, heat from the vapour is removed by cooling air or water passing across it from point 15 to point 16. The saturated liquid then passes through the throttling valve from the high pressure side at point 8 to low pressure side at point 9. The liquid water then passes through the evaporator. In the evaporator, the water extracts heat from the cooled area passing through tubes. The heat from water tubes at point 17 is transferred to the liquid refrigerant. The water in the tubes at point 18 returns to the area that needs to be cooled. The heat absorbed by the refrigerant between points 9 and 10 from chilled water circuit causes it to boil and turn into vapour. This vapour is absorbed by the strong water-lithium bromide solution which flows back from the generator to absorber. The weak solution is then pumped to the generator and the process is repeated. This is equivalent to the compression of refrigerant vapour in a vapour compression system but significantly less work is required for the ACS because the specific volume of the liquid solution is much less than that of the refrigerant vapour.

Chapter 2 Literature Review

2.1 A brief historical view of absorption system

Experimental work on absorption systems can be traced back to 1777, which was carried out by Nairne (Cui, 1998). Based on Nairne concept, John Leslie constructed an absorption apparatus in 1810 and used it to produce ice. In 1850, Edmond Carre (Cui, 1998) from France constructed a heat engine using sulphuric acid and water as the working fluids. The first patent of absorption machine that used ammonia and water as the working fluids was registered by Ferdinand Carre (Seewald, 1992), the brother of Edmond. Machines based on this patent were fabricated by manufacturers in European countries for use in various industrial applications such as ice production and food storage. Absorption systems were subsequently replaced by the vapour compression system, which was undergoing active research and development. The principle of these systems is simpler than the absorption system. The absorption system experienced a revival during World War I in 1920 due to awareness of the cost of energy. The absorption technology was improved and the development of absorption theory began. The absorption systems had played a predominant role in air conditioning and refrigeration. In the 1960s, central absorption chiller plants had earned about a 40% share of the domestic market (Katzel, 1992). This market share was maintained for over a decade. The water/lithium bromide absorption system has been widely used since 1950s. The technology was pioneered by several manufacturers.

The energy crisis of the 1970s led the U.S. government to regulate the use of natural gas as a fuel. Electric utility rates were low and the efficiency of electric driven centrifugal chillers was continually improving. Both the government and economic factors drove the U.S. absorption industry to a near halt for roughly 20 years. Meanwhile in Japan, absorption air-conditioning flourished simply because electric power was expensive. Japan encouraged the use of natural gas and fostered an aggressive programme to stimulate absorption research. The absorption system was quickly being appreciated as a quality air-conditioning system. As a result, Japanese manufacturers were the first to introduce direct-fired double-effect chillers, which now account for the majority of absorption chiller sales throughout the world.

As the biggest contributor to pollution and Global Warming, US has greatly contributed in recent years through research on energy efficient systems such as ACS. The development of ACS in the UK is slow compared to US and Japan because of the low market driven force that exist here. Other major reasons include the lack of education on the benefits and unavailability of reliable published data for designers. The perception of lower performance and high initial costs are the prime cause for lack of incentive to progress this technology in Europe.

There is however, increasing research interest in recent years in UK due to the phasing out of CFCs and HCFCs used in conventional vapour compression systems. It is now generally acknowledged by scientists that the world is experiencing extreme weather, such as increasing rainfall, typhoon and tornado due to Global Warming effects. In fact, this year, most of the parts in UK experienced the worst flooding in fifty years. The Global Warming effect is largely caused by the increased Carbon Dioxide (CO_2) and waste heat released to the atmosphere. Absorption cooling system can play an important role in reducing the emission of CO_2 by utilising the waste heat and energy effectively. However, the current ACS technology still has a lot of room for improvement in terms of cost, effectiveness and simplicity compared to conventional cooling systems. Information on ACS is increasing rapidly especially in the past two decades which has created a steep learning curve for designers of ACS. An article aimed at providing a brief guide has been published to address this problem which include references for thermodynamic properties, thermodynamic analysis, software tools and component design. (Tan & Jambunathan, 2000).

Massive research into absorption systems include theoretical modelling of different absorption systems, investigating alternative working fluids and improving system components. In Section 2.2, comprehensive literature reviews on computer/mathematical modelling for different ACS has been compiled into a table (Table 2.1). Most of the literatures reviewed, however, are ammonia based. Part of the reason for this has been the use of ammonia for more than a century for these applications. Despite its flammability, ammonia absorption systems have gained a large market foothold in the commercial sector. Ammonia based absorption systems have enjoyed the benefit of high working pressure which is insensitive to pressure drops compared to water-lithium bromide machines. Hence, the components and pipe connections required are comparatively small. The low freezing point also makes it suitable for ice production and storing food. For air-conditioning, water-lithium bromide is the more suitable candidate. As ammonia is strictly prohibited for domestic applications in some countries such as Japan, water-lithium bromide is used in this project.

Lithium bromide has the benefit of non-flammable, non-toxic and low working pressure which has made it suitable for domestic applications.

In Section 2.3, literature reviews on working mixtures are divided into ammonia (Section 2.3.1) and water based working fluids (Section 2.3.2) respectively. The last section in this chapter provides an overview of the theoretical modelling of an absorber.

2.2 Computer/Mathematical modelling of ACS

The use of computers for thermodynamic analysis has brought a revolutionary change in conventional approaches. Before the 1970's, solving problems using numerical analysis techniques such as Finite Difference, Finite Volume and Finite Elements involves enormous number crunching and hence time consuming. Uses of these techniques have become popular in recent years due to the great improvements in computer power together with significant decrease in their costs.

With the help of a computer, thermodynamic analysis and design can be carried out effectively in a short period. Thus, it is important to capture the benefit of computer modelling and apply it in designing the ACS. It is also important to study various types of ACS models proposed in recent years the necessary enhancements and advantages of each model can be incorporated into a new system. In this section, various types of absorption systems were studied and are reported in brief. These systems are categorized as follows:

System Type

*Type I, **BASIC** cycle without solution heat exchanger (BASIC)*
*Type II, **Basic** cycle with **Solution Heat** e**X**changer(BSHX)*
*Type III, **Basic** cycle with **Precooler** & **Solution Heat** e**X**changer (BPSHX)*
*Type IV, **Basic** cycle with **Rectifier** & **Solution Heat** e**X**changer (BRSHX)*
*Type V, **Basic** cycle with **Rectifier**, **Precooler** & **Solution Heat** e**X**changer (BRPSHX)*
*Type VI, **Basic** cycle with **Rectifier** (BR)*
*Type VII, **Basic** cycle with **Precooler** (BP)*
*Type VIII, **Generator Absorber Heat Recovery** cycle (GAX)*
*Type IX, **Generator** & **Solution Heat** e**X**change cycle with **Precooler** (G&SHXP)*
*Type X, **Absorber**, **Generator** & **Solution Heat** e**X**change cycle with **Precooler** (AG&SHXP)*
*Type XI, **Absorber Heat Exchange** cycle (AHE)*
*Type XII, **Branched GAX** cycle (BGAX)*
*Type Do, **DOUBLE** Stage cycle (Double)*
*Type Ca, **CARNOT** cycle (Carnot)*

The analysis of the absorption cooling system can be traced to as early as 1971, which was carried by Stoecker and Reed (1971). While most of the studies before the 1970's were based on basic single effect cycle with (Figure 2.2) or without (Figure 2.1) a solution heat exchanger, Stoecker & Reed theoretically proved that the performance of refined absorption cycle (Figure 2.3) with inclusion of generator-absorber heat exchanger and rectifier is better. In this cycle, the excess heat in rectifier preheats the solution from the absorber before it enters the solution heat exchanger. Studies on changes of system performance with varying generator temperature (T_g), absorber temperature (T_a), condenser temperature (T_c) and evaporator temperature (T_e) were also performed.

The ideal Carnot cycle is generally used as a benchmark for comparisons. The comparison of refined cycles (Figure 2.4) with *BASIC* (Figure 2.1) and *CARNOT* cycles by Stoecker and Reed (1971) shows that COP of the refined cycle is shifted more toward that of the *CARNOT* cycle, not only in magnitude, but also in the shape of the curve.

Design data for basic system Type I (Figure 2.1) were published by Best et al (1987). However, this system has not attracted much research interest, as the COP is quite low. This is due to the irreversibility of heat transfer between generator and absorber. A system of equations that provide a static simulation of NH_3-H_2O plants (Figure 2.2) had been worked out by Knudsen (1980). The sensitivity analysis has shown that the solution heat exchanger has the largest influence on the COP. As discussed earlier in Chapter 1, the use of a solution heat exchanger can improve the system performance as high as ten percent.

Huang (1978) analysed a similar system as Stocker (1971) with an addition of a precooler between the condenser and evaporator (Type V) (Figure 2.4). The pre-cooler (PRE) use the cold exit refrigerant vapour to cool down the refrigerant leaving the expansion valve from condenser. This will help to increase the evaporator load. Five independent characteristic variables (T_g, T_c, T_e, X_3, r) were used in the rigorous system analyses. In this cycle, the function of the rectifier is to capture the evaporated water vapour from the generator. The rectifier is normally required for ammonia-water systems. There are also two connection pipes between condenser and rectifier. One of the pipes is used to transfer pure refrigerant vapour (ammonia) to the condenser. The other pipe is used to transfer any water trapped in the condenser, which may bypass the rectifier.

A similar approach to Stocker (1971) was carried out by Phillips (1976) and Huang (1978). Phillips studied several advanced systems such as *Generator Absorber Heat eXchange* (***GAX***) cycle (Figure 2.6), Absorber **Heat Exchange** (***AHE***) cycle (Figure 2.9) and double effect cycles. The performance of these cycles is generally better than basic cycles (Type I-II).

GAX is an advanced cycle based on the *AG&SHXP* cycle (Figure 2.8). The *AG&SHXP* is simply a combination of *Generator & Solution Heat eXchange* (***G&SHXP***) cycle (Figure 2.6) and *AHE* cycle (Figure 2.5). Basically, there is an extra internal generator heat exchanger in *G&SHX* cycle compared to *BPSHX* (Figure 2.3). The hot strong solution leaving the generator is passed back through the coolest end of the generator to provide a portion of the heat of generation. This will help to reduce the energy input to the generator.

An extra absorber heat exchanger can be placed either in the absorber or between the solution heat exchanger and absorber. This was named as Absorber Heat exchange (***AHE***) (Figure 2.9) cycle (Kandlikar, 1982). Normally, the strong solution leaving the generator after passing the solution heat exchanger is still hot. By adding an absorber heat exchanger, the hot solution can be cooled by the colder weak solution leaving the absorber. The temperature of the cool weak solution will then increase. This means that the energy input to the generator is reduced, as less energy is necessary to raise the temperature of weak solution to the required level. Detailed methodology for analysing *AHE* cycle were presented by Kandlikar (1982). The results show that improvement of 10% can be obtained as compared to the conventional cycle. A similar cycle was proposed by Kumar and Kaushik (1991). It was found that after adding the second solution heat exchanger between the generator and absorber, 10% improvement in COP can be achieved for an evaporator temperature of 0 °C.

The *AG&SHXP* (Figure 2.8) combines the benefits of both of the *G&SHXP* and *AHE* into one. As the generator exit temperature increases in *AG&SHXP* cycle, the warmest temperature in the absorber will be increased and may eventually exceeds the lowest temperature in the generator. In *GAX* cycle (Figure 2.6), the solution heat exchanger is replaced by a generator-absorber heat exchanger which allows the heat to be exchanged directly between these two components. The compromise of the overlap between the warm end of generator and the cool end of the absorber will help to reduce energy input and increase the absorption rate.

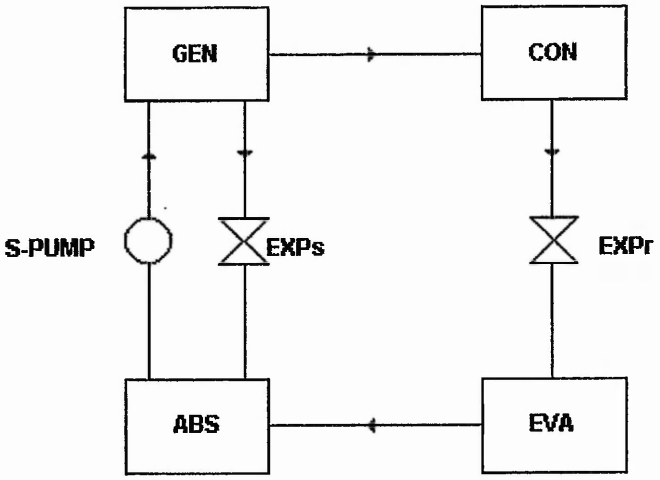

Figure 2.1 Type I – ***(BASIC) Basic*** **single effect cycle without solution heat exchanger**

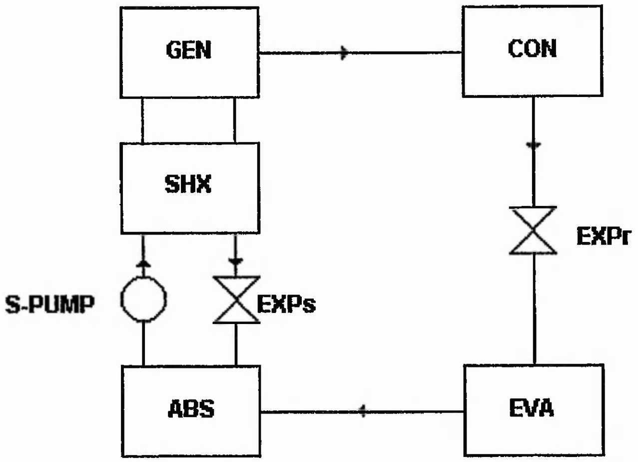

Figure 2.2 Type II – ***(BSS)*** **Basic single effect cycle with solution heat exchanger**

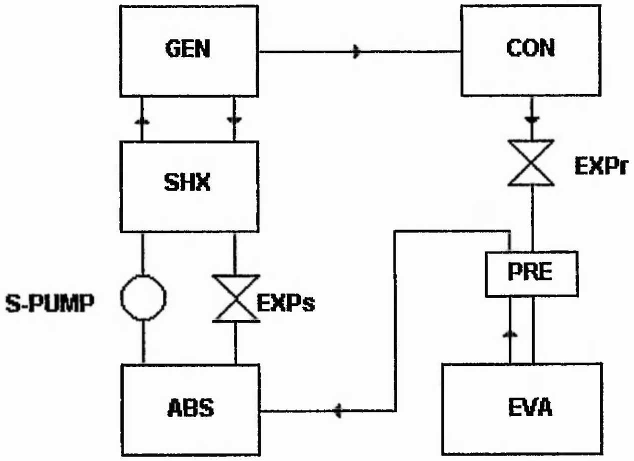

Figure 2.3 Type III – ***(BPSHX)*** **Basic cycle with precooler and solution heat exchanger**

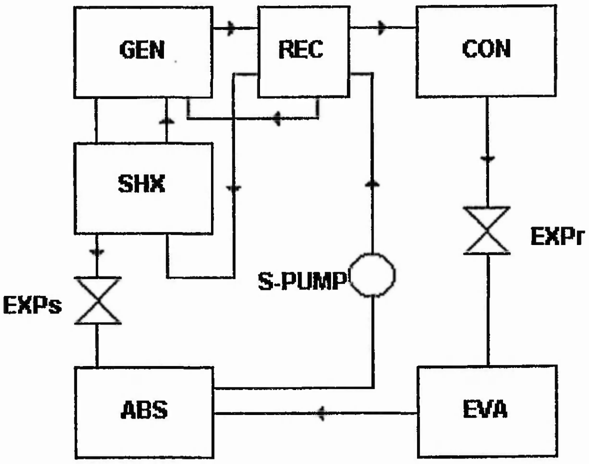

Figure 2.4 Refined cycle with inclusion of generator-absorber heat exchanger & rectifier

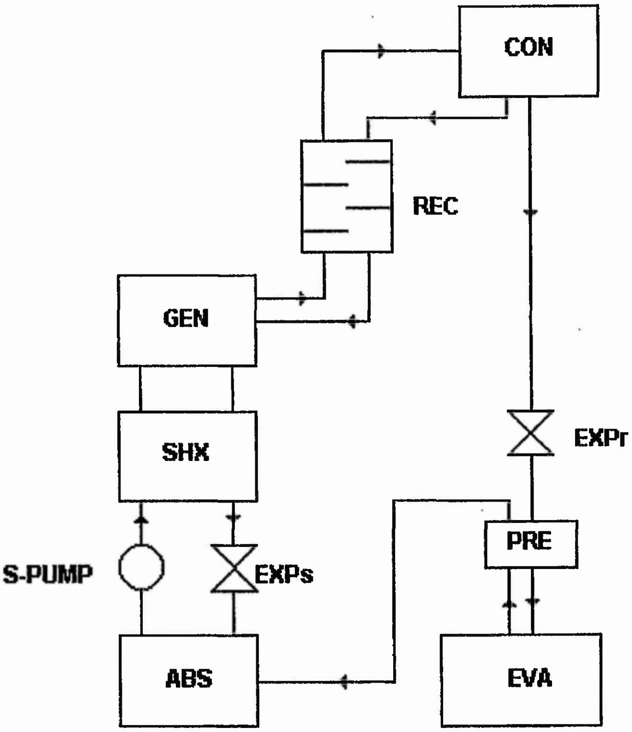

Figure 2.5 Type V-(*BRPSHX*), Basic cycle with rectifier, precooler, and solution heat exchanger

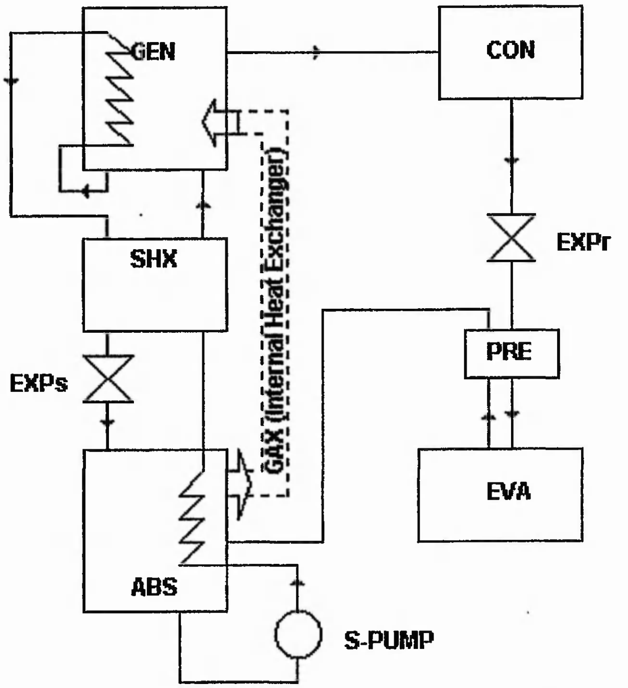

Figure 2.6 Type VIII – (GAX) Generator absorber heat exchanger cycle

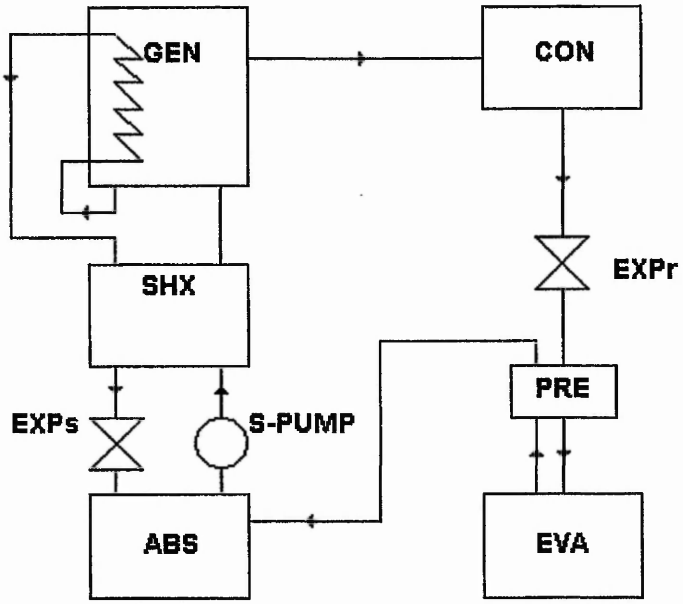

Figure 2.7 Type IX, (G&SHXP) Generator & solution heat exchange cycle with precooler

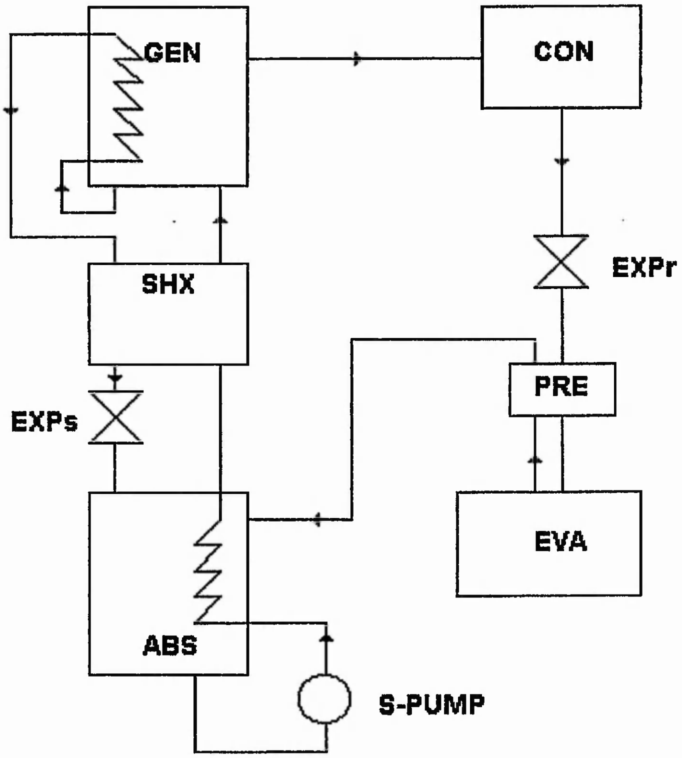

Figure 2.8 Type X, (AG&SHXP) - Absorber, generator & solution heat exchange cycle with precooler

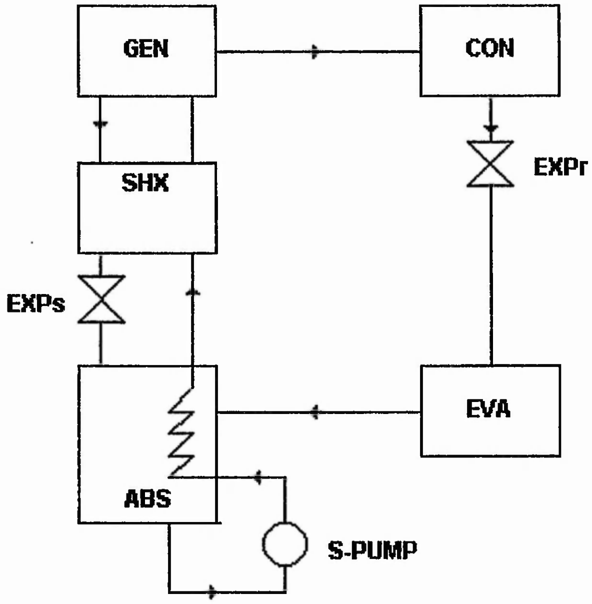

Figure 2.9 Type XI – *(AHE)* Absorber heat exchanger cycle

Other than the temperatures of the four main components Alizadah et al (1979) used the cooling load and heat exchanger as the parameters in their studies. This article performed theoretical studies considering in particular design and optimisation of an absorption refrigeration system operated by solar energy using NH_3-H_2O and LiBr-H_2O as working fluid.

One of the advantages of absorption system is that any kind of energy source as low as 70°C can be used to drive the system. Solar energy is an example. Solar energy is freely available in hot countries where electricity or gas supply are not readily available. The use of solar energy for fridges can also help third world countries keeping their food cold without incurring a high cost. The cost of solar collectors which has generally been high have begun to drop to affordable levels which allow it to be used in ACS. Most of the research are focusing on the storage of energy for usage when solar energy is not available and improvement of the performance of the solar collector. Four systems using solar energy input were analysed by Shiran et al (1982). Type and cost of solar collectors as well as system components were considered in detail.

Tyagi (1988a) published a chart using pressure-temperature-concentration and an empirical equation for finding the cut-off temperatures (the minimum temperature at which the binary solution begins to boil). A chart for finding COP of system Type II (Figure 2.2) was also presented (Tyagi, 1988b).

The optimisation method and theoretical model were developed for system Type V (Figure 2.5) by Bulgan (1995). In this optimisation study, a maximum theoretical value of 0.888 for the COP had been indicated. Sensitivity analyses were reported for the same type of system that has a cooling capacity of 1000 kW and input temperature higher than 120 °C. (Bayramoglu & Builgan, 1995). Later, Bulgan (1997) investigated the use of low temperature source (85-110 °C) in ACS Type V. Optimum design maps for system Type II were also published by others. (Jambunathan et al, 2000; Sun, 1997a; Sun, 1997b).

Apart from using First Law of thermodynamics, exergy analyses were also applied to achieve a better understanding of the irreversible nature of real processes and systems (Karakas et al, 1990; Best et al, 1993). Individual exergy (Second Law) analyses for components were reported by Alvares & Trepp (1987) without studying the effects of other parameters. The gap was then addressed by the studies of Ataer & Gogus (1991). The dimensionless total exergy loss, energy loss of each component, as well as the COP, ECOP and circulation ratio of the system, were calculated. However, the entropy at several points published in this paper as well as the discussion of circulation ratio changes with respect to generator, absorber, condenser and evaporator temperature were misleading. Thus, another article based on this work was recently published (Jambunathan, K., Tan, Y.W and Ashforth-Frost, S., 2000).

Other advanced systems (GAX and AG&S HX) have been analysed using Second Law (Carmody & Shelton, 1993). Apart from steady state simulation, dynamic (Jeong et al, 1993) and transient (Dence et al, 1996) models have been developed for ACS as well. Detailed calculations of ACS are complicated, particularly in a complex cycle such as GAX. Only a few studies have investigated the various advanced cycles, with operating conditions and different design parameters varying over a wide range to compare their performance (Engler et al, 1997; Carmody & Shelton, 1993;). The COP of these cycles are high, however, these cycles require more components and higher energy at temperature above 120 °C. This will obviously increase the capital cost. The required temperature is also well above the normal low temperature heat source such as solar energy, waste heat and domestic boiler.

As a summary (See Table 2.1), the above review has highlighted analyses of the most popular absorption cycles and the improvement achieved through utilisation of heat effectively by adding extra heat exchangers. Ammonia-water is used in most of the advanced cycles. The working pressure of ammonia-water mixture is high (5 – 20 bar) and the pressure drop in pipeline can sometimes be neglected. The problems of excess pressure drop may not occur if additional heat exchangers are placed between the main components. However, this is not true for the case of water-lithium bromide absorption systems. Water-lithium bromide system works at pressures below atmospheric where any small changes in pressure especially in lower side of the system will greatly affect the system performance. Thus, addition of heat exchangers may not always be a sensible way in improving the water-lithium bromide system unless the input temperature is sufficiently high when double effect cycle can be used. In this work, the basic cycle (Type II) was developed as a benchmark for comparison. The cycle was further modified by including a two recirculation spray which pass through a recirculation heat exchanger before entering the absorber.

Other methods of improving the system performance include using alternative working fluids (Section 2.32). There are numerous alternative working fluids being researched. Increase of component efficiency will also improve the overall system performance (See section 2.4). Most of the reviewed modelling and analyses dealt with large scale industrial ACS. Though many cycles were studied and analysed, the design data particularly for the system components are not available. An introductory guide to absorption cooling was published recently by DETR (1999). This guide is intended to help identify the right technology. However, it still lacks any computer analysis and recommended design data for domestic size chiller. There is also insufficient data for designing individual components of the system. This work addresses some of these gaps identified in the literature for future designers of ACS.

Table 2.1 Computer and mathematics modelling reference table

N	Q_E	Name	Year	H.S	P.S	M.T.	S.T	T_G, °C	T_C, °C	T_A, °C	T_E, °C	E_{SHX}	E_{SC}	X_3, %	X_4, %	X_7, %	PH/PL, bar	P.D	COP_{max}
1	n/a	Stoecker	1971	n/a	Ps1	S	I,IV, Ca	93 - 160	27 - 70	10 - 68	-12 – 18	n/a	n/a	n/a	n/a	n/a	n/a	N	0.7
2	n/a	Phillips	1976	So	N/a	S	II, VIII, XII, Do	> 93	43	43	4	n/a	n/a	48	36.5	100	17.94/5.18	N	0.55
3	8.4	Huang	1978	A	N/a	S	V	60 - 100	50	x	-30 – 10	x	x	60 (max)	n/a	99.5	n/a	N	0.6
4	3.52 , 17.6	Alizadeh	1979	So	N/a	S	III	59 - 160	35	21	1.7	n/a	n/a	58	40	n/a	13.3/4.5	N	0.73
5	n/a	Knudsen	1980	W	Ps2	S	II,V	130 - 145	36 - 44	36 - 44	n/a	60-90	60-90	n/a	n/a	n/a	n/a	N	0.52
6	n/a	Kaushik	1982	So	Ps1	S	V	80 - 150	25 - 45	25 - 45	10 - 15	80	70	n/a	n/a	n/a	n/a	N	0.65
7	n/a	Kandlikar	1982	n/a	Ps1	S	I, III, XI	90 - 180	30 - 50	30 - 50	0	80	80	n/a	n/a	n/a	n/a	N	0.67 0.71
8	n/a	Shiran	1982	So	Ps1	S	I,II,IV,VI	55 - 185	38	35	7	50	n/a	49.2	46.5	99.4	14.9/4.14	N	0.65
9	0-2	Keizer	1983	So	Ps2	S	II,III,Do	90 - 130	15 - 45	15 - 45	-20 – 0	90	50	n/a	n/a	99	n/a	Y	0.68
10	n/a	Best	1987	N/a	Es2	S	I	60 - 200	30 - 50	30 - 50	-30 – 10	n/a	n/a	25.58 – 62.13	1.66 – 58.12	100.0	n/a	N	0.58
11	10.51	Clerx	1987	So	Ps1	Ex	III	121.1	37.6	35	-5.61	67.5	63	41.2	28.1	100.0	14.5/2.8	N	0.47
12	n/a	Alvares	1987	So	Ps4	E	I,II,V,VII	85 - 175	Δ9	Δ6	Δ10	n/a	n/a	Kays, 64	Kays, 64	99.9	n/a / 2-2.9	Y	0.6
13	n/a	Tyagi	1988a	N/a	n/a	S	II	60 - 160	20 - 55	20 - 55	-20 – 15	n/a	n/a	20> <100	20> <100	30 – 100	20/0.2	N	No
14	n/a	Tyagi	1988b	N/a	n/a	S	II	55 - 115	25 - 40	25 - 40	-5 – 10	n/a	n/a	n/a	n/a	n/a	n/a	N	0.82
15	4642	Karakas	1990	So	Ps3	E	II	50 - 100	15	15	2 & 10	n/a	n/a	66	25	100	7.29/4.62	N	0.65
16	n/a	Kumar	1991	N/a	n/a	S	XII	90 - 150	30 - 50	30 - 50	0 & -10	n/a	n/a	n/a	n/a	n/a	n/a	N	0.63
17	1	Ataer.	1991	N/a	Ps1	E	III	50 - 130	22 - 28	24 - 30	-20 – 10	80	80	45.9	17	99.9	9.09/2.57	Y	0.82
18	n/a	Carmody	1993	DG	Es3	E	I, III, VII,IX,X	100 - 200	35	n/a	5	n/a	n/a	n/a	n/a	99	n/a	n/a	0.9
19	n/a	Best	1993	So	Es1	E	V	75 – 110	23 - 35	21 - 30	-16 – - 6	0 – 100	n/a	n/a	n/a	99.3	n/a	N	0.7
20	10	Jeong	1993	n/a	n/a	D	III	115.4	42	42	3	90	90	43.5	33.5	98.85	16.28/3.95	Y	0.59
21	12.1	Wu	1993	W	n/a	S	II	97	45.2	45.2	4.9	n/a	n/a	n/a	n/a	n/a	n/a	N	0.66
22	n/a	Mumah	1994	DG	Ps4	S	II	60 - 120	25 - 45	25 - 45	0 – 20	n/a	n/a	34 – 60	n/a	n/a		N	0.63
23	n/a	Bulgan	1995		Ps4, Ps6	S	III	40 - 100	22 - 26	24 - 28	-20 – 0	80	80	30 – 99.9	n/a	99.9	n/a	Y	0.88
24	1000	Bayramoglu	1995	A	Ps4	S	V	110	Δ8,Δ10	Δ6,Δ15	Δ6	n/a	n/a	43.05	n/a	n/a	n/a	Y	0.382
25	10.5 4.74	Dence	1996	n/a	Ps10	S D	III III	148.33 151.66	43.33 43.33	43.33 43.33	7.22 7.22	70 70	50 50	35 35	20 19	99.5 99.5	17.04/5.66 17.80/5.93	Y Y	0.56 0.43
26	1000	Bulgan	1997	A	Ps4	S	V	85 - 110	Δ6,Δ10	Δ6-Δ20	-5	n/a	n/a	30 - 50	n/a	100	n/a	Y	.6

Table 2.1 Computer and mathematics modelling reference table

N	Q_E	Name	Year	H.S	P.S	M.T	S.T	T_G, °C	T_C, °C	T_A, °C	T_E, °C	E_{SHX}	E_{SC}	X_3, %	X_4, %	X_7, %	PH/PL, bar	P.D	COP_{max}
28	18.89 -20.67	Sun	1997a	n/a	Ps10	S	III	43 – 98	20 - 40	20 - 40	2 – 7.5	n/a	n/a	31.4 – 55.8	48.7 – 68.7	100	n/a	N	0.87
29	10.6	Engler	1997	DG	Ps9	S	IV,VIII, XII,XIII	100 - 200	30 - 55	30 - 55	-40 – 20	80	80	n/a	n/a	99.5	n/a	N	1.25
30	n/a	Sun	1997b	n/a	Ps10	S	III	50 - 170	26 - 34	28	-10 – 0	80	80	30 – 99	n/a	99.0	n/a	N	0.95
31	18.6	Sun	1998	n/a	Ps10	S	II	60 - 100	25 - 30	25	-12 – 10	80	n/a	52.24	33.55	100	11.67/3.54	N	0.73
32	6.89	Ng	1998	n/a	Ps4	E, P	VIII	194	44	41	5	n/a	n/a	47.56	4.71	99.9	18.75/4.72	Y	0.87

H.S.- Heat Source
B – Boiler
G – Geothermal
W – Waste heat
DG – Direct gas fired
So - Solar energy
A – All mentioned above

M.T. – Modelling Type
S – Static
D – Dynamic
E – Exergy
P – Process Average Temperature

P.S. – Property source
Ps1- Ps9 – See Table 2.2

S.T. – System Type
*Type I, **BASIC** cycle without solution heat exchanger (BASIC)*
*Type II, Basic cycle with **Solution Heat eXchanger**(BSHX)*
*Type III, Basic cycle with **Precooler & Solution Heat eXchanger** (BPSHX)*
*Type IV, Basic cycle with **Rectifier & Solution Heat eXchanger** (BRSHX)*
*Type V, Basic cycle with **Rectifier**, **Precooler & Solution Heat eXchanger** (BRPSHX)*
*Type VI, Basic cycle with **Rectifier** (BR)*
*Type VII, Basic cycle with **Precooler** (BP)*
*Type VIII, **Generator Absorber Heat Recovery** cycle (GAX)*
*Type IX, **Generator & Solution Heat eXchange** cycle with **Precooler** (G&S HXP)*
*Type X, **Absorber, Generator & Solution Heat eXchange** cycle with **Precooler** (AG&S HXP)*
*Type XI, **Absorber Heat Exchanger** cycle (AHE)*
*Type XII, Branched **GAX** cycle (BGAX)*
*Type Do, **DOUBLE** Stage cycle (Double)*
*Type Ca, **CARNOT** cycle (Carnot)*

Others
PH – Highest pressure, bar
PL – Lowest pressure, bar
PD – Pressure drop, bar
X_3 – mass concentration - Strong solution, %
X_4 – mass concentration - weak solution, %
X_7 – mass concentration – vapour mixture, %
E_{SHX} – Efficiency of solution heat exchange, %r
Esc – Efficiency of precooler (second heat exchanger), %

2.3 Working fluids

2.3.1 Thermodynamic properties of ammonia based mixtures

Ammonia-water

Ammonia-water mixture was selected as a benchmark working fluid for comparison as it has been in use for more than a century. Most of the data before 1970's were raw data from experimental work in tabular or graphical form. Correlations of the available binary ammonia-water thermodynamic data were published in Germany in 1929 by Merkel and Bosnjakovic and Zinner in 1934. More compilations were published in the United States by Jennings and Shannon (1938), Scatchard et al. (1947). One of the most frequently used experimental data was from The Institute of Gas Technology (IGT) (Macrisis et al, 1964).

Isobaric vapour-liquid equilibrium of the mixture NH_3-H_2O was experimentally determined at 14.69 and 65 psia by Polak and Lu (1975). Jennings (1981), published thermodynamic properties of ammonia-water mixtures (P-T-x) in tabular format for pressure range 0.01 to 28 bar. Vapour liquid equilibrium (VLE) data for NH_3-H_2O at three temperatures, 403.1, 453.1 and 503.1 K, and pressures up to 7 MPa were obtained by Guillevic et al (1985). The data were extended to a wider range of temperatures between 306 to 618 K and at pressures up to 22 MPa by Reid and Heidemann (1987). VLE for the mixture NH_3-H_2O up to critical region were measured by Sassen et al (1990). Bubble points, dew points, and critical points were measured in the system for six different mixture ratios varying in composition from 18.9 to 80.0 mol % ammonia over a temperature range of 389.4 – 613.5 K and a pressure range of 1.29 – 21.52 MPa. Dew point were measured for 15 compositions between 19.4 and 90.0 mol % ammonia over a temperature range of 373.2 – 453.2 K and a pressure range of 0.14 – 9.70 MPa.

Thomas et al (1991) converted VLE data for five temperatures between 20 – 140 °C and up to 500 psia into T-P-x data and calculated vapour phase compositions by means of Redlich-Kwong equation of state. There are three comprehensive reviews up to date, which are from Jennings and Shannon (1938), Macriss et al (1964) and Tillner-Roth and Friend (1998).

In the past, thermodynamic cycle calculations for NH_3-H_2O absorption machines were performed manually, using state point property data from a graphical or tabulated source such as the data published by Jennings (1981). A lot of experimental work on NH_3-H_2O has been performed. Until 1971 there had not been a systematic approach, ending up in an analytical correlation for the obtained experimental results.

Researchers in the 1970's started to use equation of state derived from experimental data for thermodynamic properties of NH_3-H_2O to facilitate the calculations in the design process. The use of electronic computer enabled calculations to be performed in a considerably greater quantity, detail and accuracy. Iterative calculations, for instance, for the purpose of optimisation are easily performed. Two of the earliest equations were published by Jain and Gable (1971) and Schulz (1972). Schulz developed equations of state for the range of pressure 0.01 to 25 bar in the form of a virial equation of state for the vapour region and Gibbs free energy for the liquid region. His work is based on the IGT data (Macriss et al, 1964) in the liquid region and assumptions of validity of a virial equation of state for vapour phase of water and ammonia, truncated after the second virial coefficient.

Both Jain & Gable (1971) and Schulz (1972) presented the data in an analytical form. Jain and Gable provided polynomial equations for the equilibrium property data of NH_3-H_2O mixtures. Though equations developed by Jain and Gable are easier to implement, their data are restricted to a limited range. Thus, many computer modelling were based on Schulz's equation until his data were extended to a higher pressure with sufficient accuracy (50 bar) by Ziegler & Trepp (1984). New correlations for equilibrium properties of NH_3-H_2O mixtures were presented in this paper. The equations presented are in principle the same as Schulz. The coefficients in this paper are based on data published by Haar (1978) for ammonia and Keenan (1967) for water respectively. Gomez & Mansoori (1983) developed a methodology using Redlich-Kwong (RK) equation. El-Sayed and Tribus (1986) took the approach of establishing separate equations for different properties which were then incorporated into cycle calculations. Their work covered the pressure and temperature up to 110 bar and 770 K respectively. Bourseau & Bugarel (1986) presented similar type of equations to Schulz and Ziegler & Trepp. The coefficients published in this paper were obtained from their own research (Bourseau, 1983). Ruiter (1990) developed a simplified method for describing ammonia-water mixtures as well as seventeen other working pairs. In his approach, the vapour pressure is assumed negligible compared to the vapour pressure of the refrigerant.

Both Park & Sonntag (1990) and Ibrahim & Klein (1993) noticed that the range of thermodynamic properties of NH_3-H_2O based on IGT data did not cover the operating range of pressure and temperature for future use of power cycles. Park & Sonntag published a set of data based on a generalised equation of state. A Benedict-Webb-Rubin (BWR)-type equation was presented. The pressure and temperature ranges were extended to 200 bar and 650 K respectively. Ibrahim and Klein modified the correlation for the Gibbs excess energy from Ziegler and Trepp to include Wiltec experimental data (Gillespie et al., 1987) at higher temperatures and pressures to 600 K and 110 bar respectively.

The time needed to construct and compute equations using Gibbs free energy as the basis may be large, as iteration process has to be used. Patek & Klomfar (1995) used variable dependence of technical relevance, which make it possible to avoid iteration evaluations. Five equations were constructed by fitting critically assessed experimental data using simple functional forms. Curve fit experimental data from (Reistad,1969), ideal solution model (IS), and the Peng-Robinson equation of state model were discussed in detail by Palmer, 1995. Abovsky (1996) fitted experimental data on phase equilibrium in ammonia-water mixture on the basis of the author's version of thermodynamic perturbation theory in the range of temperature (200-640 K) and pressure (0.02 – 23 MPa).

In the candidate's opinion, the correlation described by Ibrahim and Klein (1993) was the best available correlation for ammonia-water mixtures, until very recently a new correlation has been developed by Tillner-Roth and Friend (1998) at the National Institute of Standards and Technology (NIST). It provides reliable information on the thermodynamic properties of ammonia-water for the entire composition range and in a wide range of temperature and pressure. It provides property data for all compositions from pure water to pure ammonia, VLE-properties between the solid-liquid-vapour boundary (195.5 K to 273.16 K) and the critical locus (405 K to 647 K), properties of liquid and vapour up to 40 MPa and good predictions in the supercritical range.

In this work, the thermodynamic properties model proposed by Ibrahim and Klein was used. The recent correlations developed by Tillner-Roth were not used due to its complexity which may increase the computation time. The extended data range is also beyond the interest of this work Unfortunately, the correlations presented by Ibrahim and Klein were in the form of differential equations and not readily usable for computer modelling. The differential equations were solved in this work (Section 3.1). All the thermodynamic properties relationship such as enthalpy and entropy were presented in a simple form that can then be conveniently programmed into computer functions.

Ammonia-salts

Other ammonia-based working fluids include ammonia/sodium thiocyanate and ammonia/lithium nitrate (Sun, 1998), ternary working fluids such as ammonia-water-salt mixtures (McLinden & Radermacher, 1985; Ibrahim et al, 1997). These mixtures generally provide higher performance than the traditional ammonia-water mixture. Further, NH_3-salt solutions do not require rectification. However, problems of crystallisation, high viscosity and corrosiveness of these solutions need to be considered.

Table 2.2 *Thermodynamic properties of ammonia-water reference table – Analytical*

Ref. No	Investigator	Year	Range T (K)	Range P (bar)	Methods
Ps1	Jain & Gable	1971	267.45 – 280.22 *1 316.3 – 328.56 *2	3.45 - 5.52 17.15 - 24.15	P
Ps2	Schulz	1972	200 – 450	0.01 – 25	G
Ps3	Gomez & Mansoori	1983	-	-	RK
Ps4	Ziegler & Trepp	1984	230 – 500	0.2 – 50	G
Ps5	El-Sayed & Tribus	1985	210.8 - 771.89	0.069 – 110.4	P
Ps6	Bourseau & Bugarel	1986	200 – 450	0.01-25	G
Ps7	Ruiter, J.P.	1990	-	-	BWR
Ps8	Park & Sonntag	1990	650	50-200	H
Ps9	Ibrahim & Klein	1993	230 – 600	0.2 – 110	G
Ps10	Patek & Klomfar	1995	193 – 453	0.02 – 20	P
Ps11	Palmer	1995	-	-	P,PR, IS
Ps12	Abovsky	1996	200 – 700	0.1-300	PT
Ps13	Tillner-Roth	1998	420	400	H

Where G = Gibbs Free Energy, P = Polynomial, RK = Redlich Kwong,

IS = Ideal Solution, BWR = Benedict-Webb-Rubin equation, H = Helmholtz Free Ebergy,

PR = Peng-Robinson equation, PT = Pertubation theory

Table 2.3 *Thermodynamic properties of NH_3-H_2O mixture reference table*

Experimental

Ref No.	Investigator	Year
Es1	Scatchard	1957
Es2	Macriss	1964
Es3	Reistad	1969
Es4	Jennings	1981

ES = Experimental source

2.3.2 Thermodynamic properties of water-based mixtures

Apart from ammonia-based mixtures, numerous other mixtures were investigated (See Section 3.1). Water-based working fluids were studied extensively. Water is non-toxic in its nature and cheap in comparison with ammonia and TFE based refrigerant. Water has the advantage of high latent heat of vaporisation. The working pressure of water is also sufficiently low so that an expensive thick wall can be avoided. However, the freezing point at 0 °C has made water unfavourable in refrigeration systems. This disadvantage has not prevented its wide use in air-conditioning industry which require lowest evaporator temperature at around 7 °C.

This project focussed on water based working fluids. The water-lithium bromide mixture was studied in detail and employed in the experimental work so that the results can be used as a benchmark to compare with other water based working fluids. Numerous investigations were carried out to look for the availability of the thermodynamic and transport properties data. These working fluids include the binary, ternary and tertiary mixtures. The thermodynamic and transport properties of 22 most popular water based mixtures were studied and compiled into three reference tables; Table 2.4 for binary mixtures, Table 2.5 for ternary mixtures and Table 2.6 for tertiary mixtures. The data of water-lithium bromide and water-lithium chloride mixtures were found to be most complete. From the research, it is clear that lithium bromide is still considered to be one of the best absorbent due to its high affinity for water. It releases water vapour at relatively low temperatures because the boiling point of LiBr is relatively high.

The vapour pressure and enthalpy data of water-lithium bromide (H_2O-LiBr) published by McNeely in 1979 is still widely used. Before his work, there was no single standard in studying absorption systems though the thermodynamic properties might be available to industrial manufacturers. Not long after his publication, the correlations were accepted in ASHRAE handbook. The method of correlation suggested has been used for finding thermodynamic properties of other working fluids (See section 3.3). However, the correlation for enthalpy is limited. The range is as follows:

$40\% < x < 70\%$,

$16\ ^{o}C < T < 166\ ^{o}C$

where x = mass concentration, % and T = solution temperature, ^{o}C

For vapour pressure correlation, the limits are

$-20\ ^{o}C < T' < 110\ ^{o}C$

$5 < T < 180\ ^{o}C$

$45\% < x < 70\%$

where T' = refrigerant temperature, ^{o}C

In 1987, Herold & Moran proposed a new method for finding H_2O-LiBr properties using the expressions of Gibbs free energy. The method suggested is similar to the method used for finding ammonia-water properties introduced in this work (Section 3.1). Most of the literature avoids using this method owing to its high complexity in comparison to polynomial correlations developed by McNeely (1979). Nevertheless, the use of expression in terms of Gibbs free energy has the ability to provide further estimation on the specific heat, density and entropy apart from the vapour pressure and enthalpy expressions that is normally available.

Patterson and Perez-Blanco (1988) performed numerical fits of the H_2O-LiBr properties which extended the range of input variables to cover all of the known data for noncrystalline regions. The fittings range covered were wider compared to the past investigators such as McNeely (1979) and Herold and Moran (1987). The fittings were based on McNeely's data. The number of coefficients was varied for each property in order to obtain the best possible fit. The region of temperature-concentration space covered by the fit is as follows:

$0\ ^{o}C < T < 180\ ^{o}C$

$0 < x < 70\%$

The range covered in the fittings is more useful for analysing advanced absorption systems such as GAX, double and triple effect cycles, which generally need a higher input temperature. The use of Patterson's correlation instead of McNeely's equations may not produce any significant difference in this work as only the single effect cycle was studied. The more useful parts of Patterson's article were the numerical fits of transport properties developed by Patterson which include the thermal conductivity, specific heat, viscosity and surface tension. These properties are crucial in modelling and designing the absorber, which is the heart of an absorption system.

The heat capacity data at low temperature were reported by Hasaba et al (1960) and Ogawa (1980). They measured the heat capacity in the temperature ranges 24 °C to 130 °C and 20 °C to 100 °C respectively. Iyoki and Uemura (1989) further extended the temperature range to 40 °C – 160 °C. Lee et al (1990) correlated the density and viscosity data based on the H_2O-LiBr concentrations between 45% and 60% and temperatures ranging from 20 °C to 200 °C. At the same time, DiGuilio et al (1990) also correlated the thermal conductivity data for lithium bromide solutions, which were measured over the ranges of mass concentrations from 30% to 65% and temperatures from 20 °C to 190 °C. Other transport properties such as diffusion and mass transfer coefficient were presented by Miller (1998) and Yih (1982) respectively. The secondary properties of water lithium bromide solutions such as index of refraction, speed of sound, dielectric constant, electricmagnetic radiation absorption and transmission, magnetic properties and electrical conductivity/resistivity were presented by Heinonen and Tapscott (1999). These properties are used to measure the concentration of water-lithium bromide mixtures.

Table 2.4 Reference table for thermodynamic and transport properties of binary mixture

Refrigerant absorbent combinations	Thermodynamic and transport properties										
	p-t-x	t-t-x	h-t-x	C_p (kJ/kgK)	H_m (kJ/kg)	ρ (kg/m^3)	μ (mPas)	σ (mN/m)	λ (wt%)	s (kJ/kgK)	Solubility
(B1) H_2O-LiBr	2 5 9 17 20	1 2 5 9 10 17	2 4 5 9 10 17	2 4 20		2 9 12 18	12 18	21	18 12	2 4 6	13
(B2) H_2O-LiCl	29 30	7	7 29	29 30	29	12 29 30	12 30		29 30	30	
(B3) H_2O-LiI	3 8	3	3 8								
(B4) H_2O-NaOH		25									25
(B5) H_2O-$ZnBr_2$						12	12				
(B6) H_2O-$CaCl_2$						12	12				
(B7) H_2O-$LiNO_3$						12	12				

p-t-x = Pressure-Solution Temperature-Concentration
t-t-x = Solution Temperature-Refrigerant Temperature-Concentration
h-t-x = Enthalpy-Solution Temperature-Concentration
s = Entropy
H_m = Heat of mixtures
Solubility = chart or equation showing crystallisation line

Note: (A look up table (Table 2.7) is provided, for the reference source of the number shown in Table 2.4, Table 2.5 and Table 2.6)

Table 2.5 Reference table for thermodynamic and transport properties of ternary mixture

Refrigerant absorbent combinations	Thermodynamic and transport properties										
	p-t-x	t-t-x	h-t-x	C_p (kJ/kgK)	H_m (kJ/kg)	ρ (kg/m^3)	μ (mPas)	σ (mN/m)	λ (wt%)	s	So
(T1) H_2O-LiBr-LiI (4:1)				11	15			14			16
(T2) H_2O-LiCl-$LiNO_3$ (2.8:1)					15			14			16
(T4) H_2O-LiBr + $ZnBr_2$ (2:1)	23	23	23	23							
(T5) H_2O-KOH+NaOH (1:1)		24	24			24	24				
(T6) H_2O-LiBr+LiCl						27	27				
(T7) H_2O-LiBr+$LiNO_3$						27	27				
(T8) H_2O-LiBr+$CaCl_2$						27	27				
(T9) H_2O-LiBr+$ZnBr_2$						27	27				

Table 2.6 Reference table for thermodynamic and transport properties of tertiary mixture

Refrigerant absorbent combinations	Thermodynamic and transport properties										
	p-t-x	t-t-x	h-t-x	C_p (kJ/kgK)	H_m (kJ/kg)	ρ (kg/m^3)	μ (mPas)	σ (mN/m)	λ (wt%)	s	So
H_2O-LiBr + $ZnCl_2$ +$CaBr_2$ (1:1:0.13)	19			19	19	19	19				19
H_2O-LiBr + $ZnBr_2$ + LiCl (1:1.8:0.26)	26 20	26	26	26 20		26	26	26			26
H_2O-NaOH + KOH + CsOH (4.3:3.6:2.4)	22	22	22								
H_2O-$LiNO_3$ + KNO_3 + $NaNO_3$ (5.3:2.8:1.9)	25	25									
H_2O-LiBr+LiI+LiCl (4.5:1:2)	28					28	28				28

Table 2.7 References source for Table 2.4 to Table 2.6

Ref. No.	Authors' Name	Year
1.	Sabir and Eames	1998
2.	Feuerecker et al	1993
3.	Patil et al	1991b
4.	Herold and Moran	1987
5.	Rogdakis and Antonopoulos	1991
6.	Aphornratana and Eames	1995
7.	Grover et al	1988
8.	Patil et al	1991a
9.	Hellmann and Grossman	1996
10.	Akiyama et al	1996
11.	Iyoki et al	1990
12.	Wimby and Berntsson	1994a
13.	Boryta	1970
14.	Iyoki et al	1993a
15.	Iyoki et al	1993b
16.	Iyoki et al	1990
17.	Rogdakis and Antonopoulos	1992
18.	Lee et al	1990
19.	Iyoki and Uemura	1989a
20.	Iyoki and Uemura	1989b
21.	Patterson and Perez-Blanco	1988
22.	Herold et al	1991
23.	Adegoke and Gosney	1991
24.	Beutler et al	1996
25.	Rane et al	1988
26.	Iyoki and Uemura	1990
27.	Wimby and Berntsson	1994b
28.	Koo et al	1998
29.	Wood et al	1992
30.	Ru	1987

2.4 Absorber Modelling

Enormous research have been carried out on absorber, which is the core component of absorption chillers. While information on evaporator and condenser are readily available due to active developments on conventional chillers and heat pumps in the last few decades, this review focuses on absorber designs.

There are generally four basic types of absorber, which are vertical flat plates, vertical tubes, horizontal tubes and coil tubes. Most of the absorbers are based on these four arrangements, which are considered to be more robust and provide better performance.

Vertical tube and plate absorber

There are various types of fins to improve the heat and mass transfer such as pin fins and fins with fluted, twisted and grooved surfaces. These types of absorbers are too complicated to model because of their complex geometry. Most of the models developed were based on the smooth surface by incorporating experimental data. The semi-empirical method is still widely used. Advanced surfaces for vertical tube absorbers mentioned above were studied experimentally by Miller et al (1992). A number of design charts were presented.

There are three mechanisms to be considered when modelling absorbers. The first is the flow of strong solution from generator to the entrance of absorber heat exchanger, which might be dripping, spraying or jet impinging. The second part is the absorption in falling films which may be laminar or turbulent. The third mechanism is the descending of droplet from one tube to the next and this only occurs in coil and horizontal tubes absorber.

The most comprehensive experimental work to study the first type was carried out by Miller (1995). Full-Jet, Vee-Jet, and Atomising nozzles were used in their experiments.

There are numerous work on modelling absorption in falling films, the second mechanism. The vertical tube and flat plate are normally modelled in a similar way.

One of the most important publication was by Grossman (1983). This article describes a theoretical analysis of the combined heat and mass transfer process taking place in the absorption of a gas or vapour into a laminar liquid film. The energy and diffusion equations were solved simultaneously to give the temperature and concentration variations at the liquid-gas interface and at the wall. Both the analytical and numerical solutions were performed. Absorption in laminar films was also modelled and analysed by Gregor'eva and Nakoryakov (1977), Yih and Seagave (1980). Most of the literatures today are still based on this pioneer work. These models have been extended by including the analyses of the effect of non-condensable gases on the performance of film absorbers (Grossman, 1990; Grossman and Gommed, 1997; Ameel et al, 1997; Sabir and Eames, 1999) and wave motion (Patnaik and Perez-Blanco, 1996; Sabir and Suen, 1996). Yang and Jou (1998) included both effects in their analysis.

Apart from the analytical solution, several numerical studies of heat and mass transfer in falling film (Figure 2.10) were performed by solving simultaneous parabolic second-order partial differential energy (Equation 2.1) and diffusion equations (Equation 2.2) using Finite Difference (Yigit, 1999) and Finite Element (Wekken and Wassenaar, 1988) formulations.

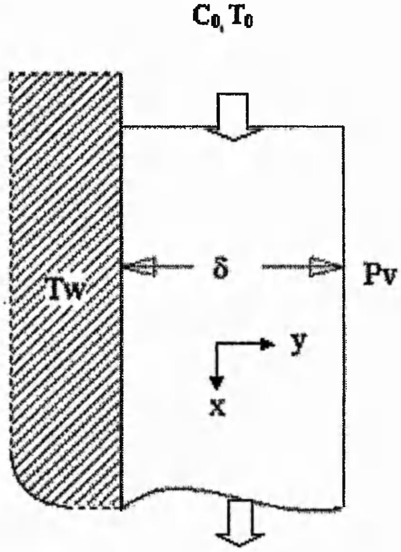

Figure 2.10 Absorption in falling film on a flat plate

$$D\frac{\partial^2 C}{\partial y^2} = u\frac{\partial C}{\partial x} + C\frac{\partial u}{\partial x} \qquad (2.1)$$

$$a\frac{\partial^2 T}{\partial y^2} = u\frac{\partial T}{\partial x} + C\frac{\partial T}{\partial x} \qquad (2.2)$$

where D = mass diffusivity (m^2/s)

a = thermal diffusivity (m^2/s)

Pv = vapour pressure (kPa)

And $u = \frac{3}{2}U_m\left(2\frac{y}{\delta} - \left(\frac{y}{\delta}\right)^2\right)$ (velocity profile) **(2.3)**

where

$$U_m = \frac{\mathrm{Re}\,\mu}{4\pi\delta} \qquad (2.4)$$

δ = film thickness (m)

A problem normally occurs at the point x = 0 and y = δ, where there is a discontinuity in temperature and concentration between the film interface and the entrance plane. This problem has been solved by applying a simplified analytical solution and hybrid method by Patnaik et al (1993) and Ibrahim (1991). Other simple analytical models were proposed for designing the vertical tube and flat plate absorbers (Patnaik, 1994; Sabir, 1993). The theoretical model was construct from two energy balances and a mass balance on an infinitesimally thin slice of the absorber which yields three first-order ordinary differential equations.

Horizontal tube and coil absorber

There has been little work done on the analysis of the absorption process on horizontal tube and coil absorber. The published literature deals extensively with modelling in falling film flowing down a vertical flat plate and tube as discussed earlier. The modelling of horizontal tube and coil absorbers have not attracted much research despite the fact that it is widely used in industrial absorption systems. The mechanisms in horizontal tube and coil absorbers are much more complex due to their circular geometry. It also poses several additional problems. Film thickness changes as it flows down the surface, the angular position determines the thickness and flow field within the film. The droplets effects such as droplet formation and free falling are hard to be modelled accurately.

A physical model was developed by Choudhury et al (1993). In the method of solution presented, governing equations and corresponding boundary equations were transformed in such a way that the variable film thickness has been accommodated in a numerical mesh system. The surface mesh was divided into a finer mesh to achieve better convergence.

Andberg (1986) solved the Navier-Stokes equations, the energy equation, and the diffusion equation for a falling film over a horizontal tube. The solution includes the flow over a top tube and an interior tube in an absorber tube bundle.

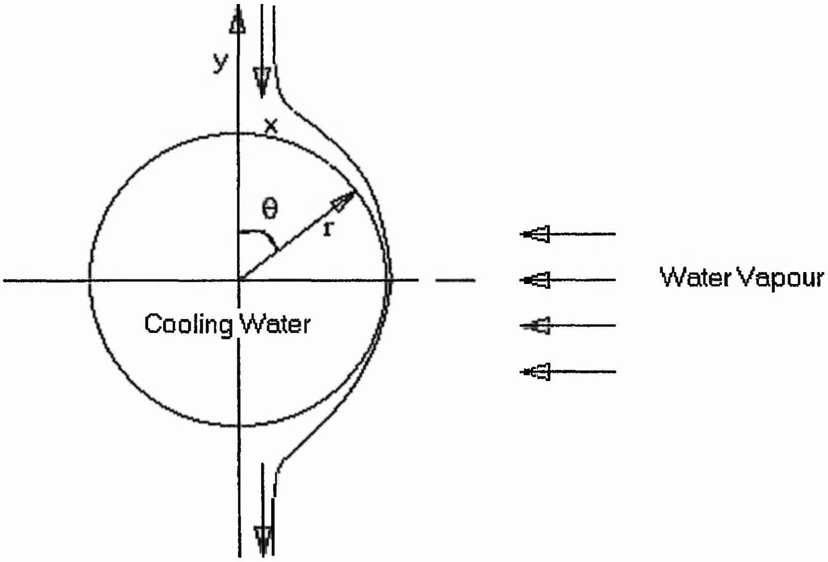

Figure 2.11 Geometrical configuration of the flowing film on horizontal tube

The energy (Equation 2.5) and mass transport (Equation 2.6) equation for a single horizontal tube, assuming constant properties and neglecting pressure gradients, viscous dissipation, transport of energy by mass diffusion, and heat of dilution, are shown as follows:

$$a\frac{\partial^2 T}{\partial y^2} = u\frac{\partial T}{\partial x} + v\frac{\partial T}{\partial y} \qquad (2.5)$$

$$D\frac{\partial^2 C}{\partial y^2} = u\frac{\partial C}{\partial x} + v\frac{\partial C}{\partial y} \qquad (2.6)$$

The velocity profile at a section is determined from the film thickness, viscosity of liquid, and angle of inclination which can be represented as follows :

$$u = \frac{g}{2\nu}\sin\theta(2\delta y - y^2)$$

where

δ = film thickness (m)

ν = kinematic viscosity (m^2/s)

Velocity in the direction of y is as follows:

$$v = -\frac{g}{2\nu}y^2\left[\frac{d\delta}{dx}\sin\theta + \frac{1}{r}\left(\delta - \frac{y}{3}\right)\cos\theta\right]$$

By applying the initial and boundary conditions, the Equations 2.5 and 2.6 were solved using Finite Difference approach (Choudhury et al, 1993). Most of the models presented solve a simplified form of the governing differential equations. A simplified analysis using ordinary first-order differential equation by incorporating experimentally measured heat and mass transfer coefficient were performed by Kirby and Perez-Blanco (1994) and Vliet and Chen (1993).

For the coil absorber, only limited literatures were available (Seewald, 1994; Mao, 1996; Adegoke, 1987). Seewald developed a simple model for calculating the performance of water-lithium bromide coil absorber. The mass transfer was proved to be predominantly caused by droplet falls. Mao solved the Navier-Stokes for coil absorber rigorously. Unfortunately, Mao (1996) only analysed the fluid flow, heat and mass transfer on a coiled tube with zero pitch. This means that the model suggested neglects the droplet falls and considered the film as continuous across the tube coils. Seewald's model on the other hand, did not consider the droplet formation. This project attempts to address these problems by introducing a model for a twin coils absorber with a 10mm pitch by considering the droplet formation. Two re-circulation sprays were also included in the proposed model.

Chapter 3 Thermodynamic and transport properties of working fluid/mixtures

3.1 Introduction

Absorption system needs a refrigerant and solution mixture as absorbent for operation. The most popular refrigerants used are water (H_2O), ammonia (NH_3) and trifluoroethanol (TFE). There are numerous other absorbent mixtures that are being considered. These include ammonia/sodium thiocyanate and ammonia-lithium nitrate (Sun, 1998), ternary working fluids such as ammonia-water salt mixtures (McLinden & Radermacher, 1985; Ibrahim et al, 1997), water-based working fluid combination (Saravan and Maiya, 1998) and various other combinations (See Table 3.1).

Table 3.1 *Reference for research and development on suitable working fluids*

Name	Year	No. of working fluids
Tyagi	1984	26
Smith	1986	16
Harvey et al	1987	500
Manago	1995	190
Macriss et al	1995	500
Saito	1995	264
Saravan and Maiya	1998	16

Some of these mixtures are for specialised applications, such as high temperature, while others are proposed as possessing improved properties over more conventional fluids. Proposed alternatives often address one weakness of the conventional fluids while contributing several additional weaknesses of their own. For instance, the NH_3 –NaSCN mixtures may perform better than NH_3-H_2O and do not need a rectifier to trap the water vapour, but it can cause more problems because of its toxicity and corrosiveness.

Among these working fluids, ammonia/water and TFE/NMP have been recommended for future prototype study of the single effect cycle (Saito, 1995). Water & TFE based working fluids have high values of coefficient of performance (COP) than ammonia based working fluid. However, systems that use these working fluids are larger and involve more design complications than the ammonia-based system because the pressures in such cycles are sub-atmospheric.

Ammonia-water (Tan, 1999) and water-lithium bromide have been chosen in this project because they have commonly been used for several decades and their properties are well established. The excellent thermophysical properties of ammonia and water are reflected by its widespread use for heat transfer applications over many years. NH_3-H_2O solution is however, unpreferred due to its requirement of rectification. Other major drawbacks of ammonia include its flammability at concentrations between 16-20% per volume in air and toxicity. The use of ammonia for domestic air conditioning is often prohibited or at least limited in the amount of usage in countries such as China, Japan and some European countries because of its flammability. The need for stainless steel in NH_3-H_2O systems due to its corrosiveness to copper and its high working pressure has added to the cost of the ACS machine. Thus, water-based mixture is generally preferred and considered in detail here while NH_3-H_2O is used mainly for benchmark comparisons.

The decision in favour of H_2O is further emphasised by the scope, which exists for application of salts e.g. LiI and LiBr. These absorbent-refrigerant combinations theoretically offer higher performance than NH_3-H_2O as shown in the next chapter. However, problems of crystallisation, high viscosity and corrosiveness of these solutions need to be considered. Replacement working mixtures such as TFE-mixtures have also been investigated.

In summary, the selection of working fluid depends largely on the type of application, capacity and cost. While ACSs enjoys the advantages of using ozone friendly working fluid or mixture, more research has to be focussed on the toxicity, flammability and corrosiveness of the fluid mixtures. Pointers of selection criteria are proposed by Eisa and Holland, 1987.

3.2. Thermodynamic and transport properties

3.2.1 Ammonia-Water mixture

3.2.1.1 Equation of State

The equation of a state is the relationship between pressure, volume and temperature of a substance. In the context of a mixture, this concept must be generalised to include composition as a variable. Gibbs free energy is defined as the fundamental function associated with the independent variables temperature and pressure. Should the temperature and volume be chosen as independent variables, the Helmholtz free energy would be the fundamental functions. The distinction has no physical significance. The use of Helmholtz free energy was explained in detail by Tillner-Roth (1998). Once the independent variables are chosen for a given analysis, the remainder of the analysis can frequently be simplified if it is done in terms of the fundamental function. If an equation of state is formed as an expression relating the fundamental function to the so-called natural variables associated with that function (for example, $g = g(T,P)$), then all other thermodynamic properties can be derived from the fundamental function with minimum effort, starting with Equations 3.2 and 3.3.

$$\mathbf{dG = VdP - SdT} \qquad \textbf{(3.1)}$$

At constant P, dP = 0 and from Equation 3.1,

$$\mathbf{(dG/dT)_p = -S} \qquad \textbf{(3.2)}$$

At constant T, dT = 0 and Equation 3.1 gives,

$$\mathbf{(dG/dP)_T = V} \qquad \textbf{(3.3)}$$

This approach has been used for pure fluids (Haar and Gallaghar, 1978) as well as mixtures (Schulz, 1972; Ziegler, 1984; Ibrahim, 1993). However for a mixture an additional independent variable is needed to define the mixture composition.

Once the fundamental function is known as a function of the independent variables, other properties can be computed from it. As a summary, the following relations hold (based on the choice of temperature, pressure and mass fraction as independent variables and Gibbs free energy as the fundamental function):

$$V = \left(\frac{dG}{dP}\right)_{T,x_1} \tag{3.4}$$

$$U = G - T\left(\frac{dG}{dT}\right)_{P,x_1} - P\left(\frac{dG}{dP}\right)_{T,x_1} \tag{3.5}$$

$$H = G - T\left[\frac{dG}{dT}\right]_{P,x_1} \tag{3.6}$$

$$-S = \left(\frac{dG}{dT}\right)_{P,x_1} \tag{3.7}$$

$$C_P = -T\left(\frac{d^2G}{dT^2}\right)_{P,x_1} \tag{3.8}$$

3.2.1.2 The fundamental equations for pure constituents

Substituting Equation 3.7 in 3.6 yields

G = H – TS

At constant temperature

$$\Delta G = \Delta H - T\Delta S$$

$$\Delta G - T\left(\frac{d\Delta G}{dT}\right)_p = \Delta H$$

Dividing both sides by $-T^2$,

$$\frac{-\Delta G + T\left({d\Delta G}/{dT}\right)_p}{T^2} = -\frac{\Delta H}{T^2}$$

L.H.S. is the differential $\frac{d}{dT}\left(\frac{\Delta G}{T}\right)$

$$\frac{d}{dT}\left(\frac{\Delta G}{T}\right) = \frac{d(\Delta G T^{-1})}{dT} = T^{-1}\left(\frac{d\Delta G}{dT}\right) - \Delta G T^{-2}$$

$$= \frac{T(d\Delta G/dT) - \Delta G}{T^2}$$

$$\therefore \qquad \left[\frac{d(\Delta G/T)}{dT}\right]_P = -\frac{\Delta H}{T^2} \tag{3.9}$$

Integration of Equations 3.3 and 3.9 yield the dependence of the molar Gibbs free energy with regard to the pressure and temperature respectively.

$\int(dG)_T = \int VdP$ **(Integrating Equation 3.3)**

$$G(P,T) = G(P_o,T) + \int_{P_o}^{P} V(P,T)dP \tag{3.10}$$

$\int d\left(\frac{\Delta G}{T}\right)_P = \int \left(\frac{\Delta H}{T^2}\right)dT$ **(Integrating Equation 3.9)**

$$\frac{G(P_o,T)}{T} = \frac{G(P_o,T_o)}{T_o} - \int_{T_o}^{T} \frac{H(P_o,T)}{T^2}dT \tag{3.11}$$

Substituting Equation 3.11 into 3.10 yields

$$G(P,T) = \frac{T}{T_o}G(P_o,T_o) - T\int_{T_o}^{T} H(P_o,T)T^{-2}dt + \int_{P_o}^{P} V(P,T)dP$$

or

$$G(P,T) = H(P_o,T_o) - T.S(P_o,T_o) - T\int_{T_o}^{T}[H(P_o,T) - H(P_o,T_o)]T^{-2}dt + \int_{P_o}^{P} V(P,T)dP \tag{3.12}$$

The equation can be translated knowing Cp(P$_o$,T) where

$$H(P_o,T) - H(P_o,T_o) = \int_{T_o}^{T} C_P(P_o,T)dT \tag{3.13}$$

Inserting Equation 3.13 into 3.12 gives

$$G(P,T) = H(P_o,T_o) - T.S(P_o,T_o) + \int_{T_o}^{T} C_p(P_o,T)dT - T\int_{T_o}^{T} C_p(P_o,T)T^{-1}dT + \int_{P_o}^{P} V(P,T)dP$$

(Keizer, 1982) **(3.14)**

This relationship is valid for both the gaseous and the liquid phase. To bring equations into a dimensionless form, reduced thermodynamic properties are defined as follows:

$T_r = T/T_b$
$P_r = P/P_b$
$G_r = G/RT_b$
$H_r = H/RT_b$
$C_{pr} = C_p/R$
$S_r = s/R$
$V_r = vP_b/RT_b$ **(3.15)**

Where $T_b = 100$ K ; $P_b = 10$ bar ; R = 8.3143 kJ/(kmole.K)

3.2.1.3 Liquid Mixture Volume, Entropy and Enthalpy

Mixture volume, entropy and enthalpy can be expressed by formulating the real mixture characteristics as an ideal mixture with a term added to account for the non-ideal behaviour. The non-ideal term is called the excess energy.

The liquid mixture volume, entropy and enthalpy are expressed as

$$V_m^l = xV_a^l + (1-x)V_w^l + V^E \tag{3.16}$$

$$S_m^l = SV_a^l + (1-x)S_w^l + S^E + S^{mix} \tag{3.17}$$

$$S^{mix} = -R\{xLn(x) + (1-x)Ln(1-x)\} \tag{3.18}$$

$$H_m^l = xH_a^l + (1-x)H_w^l + H^E \tag{3.19}$$

Equations 3.20 and 3.21 show the correlation of the specific volume and specific heat of pure liquid respectively

$$\mathrm{V}^l(T,P) = a_1 + a_2P + a_3T + a_4T^2 \tag{3.20}$$

$$C_P^l(T,P_o) = b_1 + b_2T \tag{3.21}$$

Substituting Equations 3.15, 3.20 & 3.21 into Equation 3.14, Gibbs free energy equation of the pure liquid components are derived as shown below:

$$\begin{aligned} G_r^l(P_r, T_r) = {} & H_{or}^l(P_{or}, T_{or}) - T_r . S_{or}^l(P_{or}, T_{or}) + \\ & + b_1(T_r - T_{or}) + \frac{b_2}{2}(T_r^2 - T_{or}^2) + \frac{b_3}{3}(T_r^3 - T_{or}^3) \\ & - b_1 T_r \ln({}^{T_r}\!/_{T_{or}}) - b_2 T_r (T_r - T_{or}) - \frac{b_3}{2} T_r (T_r^2 - T_{or}^2) \\ & + a_1(P_r - P_{or}) + a_2(P_r^2 - P_{or}{}^2)/2 + a_3 T_r (P_r - P_{or}) + a_4 T_r{}^2 (P_r - P_{or}) \end{aligned} \qquad (3.22)$$

The Gibbs excess energy of liquid mixtures is proposed by Ziegler & Trepp(1984) as follows:

$$G^E = \{F_1 + F_2(2x-1) + F_3(2x-1)^2\} \times (1-x) \qquad (3.23)$$

Where

$$F_1 = E_1 + E_2 P_r + (E_3 + E_4 P_r) T_r + E_3 / T_r + E_6 / T_r^2$$

$$F_2 = E_7 + E_8 P_r + (E_9 + E_{10} P_r) T_r + E_{11} / T_r + E_{12} / T_r^2$$

$$F_3 = E_{13} + E_{14} P_r + E_{15} / T_r + E_{16} / T_r^2$$

<u>Molar Specific Enthalpy (liquid)</u>

The molar specific enthalpy of pure liquid and enthalpy of excess energy are derived by combining Equations 3.9 and 3.15 as follows:

$$H^l = -R_i T_b T_r^2 \left[\frac{d(G_r^l / T_r)}{dT_r} \right]_{P_r} \qquad (3.24)$$

$$H^E = -R_m T_b T_r^2 \left[\frac{d(G_r^E / T_r)}{dT_r} \right]_{P_r} \qquad (3.25)$$

Equations 3.24 and 3.25 are further simplified to Equations 3.26 and 3.27 respectively in this work to incorporate them into computer analysis.

$$\begin{aligned} H^{l} &= -RT_bT_r^2\left[\frac{d(G_r^l/T_r)}{dT_r}\right]_{P_r} \\ &= -RT_b[-H_{or}^l + b_1(T_{or}-T_r) + \frac{b_2}{2}(T_{or}^2 - T_r^2) + \frac{b_3}{3}(T_{or}^3 - T_r^3) \\ &\quad + (a_4T_r^2 - a_1)(P_r - P_{or}) - \frac{a_2}{2}(P_r^2 - P_{or}^2)] \end{aligned} \tag{3.26}$$

$$\begin{aligned} H^{E} &= -R_mT_bT_r^2\left[\frac{d(G_r^E/T_r)}{dT_r}\right]_{P_r} \\ &= -R_mT_b\Bigg(x.(1-x).\Big\{-E_1 - E_2P_r - \frac{2}{T_r}E_5 - \frac{3}{T_r^2}E_{6r} + \\ &\quad + (2x-1)[-E_7 - \frac{2}{T_r}E_{11} - \frac{3}{T_r^2}E_{12})] + \\ &\quad + (2x-1)^2[-E_{13} - E_{14}P_r - \frac{2}{T_r}E_{15} - \frac{3}{T_r^2}E_{16})]\Big\}\Bigg) \end{aligned} \tag{3.27}$$

where

$$R_m = \frac{R}{M_ax + (1-x)M_w} \tag{3.28}$$

By substituting Equations 3.26 and 3.27 into Equation 3.19, the molar specific enthalpy of liquid mixture is computed.

Molar Specific Volume (liquid)

From Equation 3.15 and 3.4

$$V = \frac{RT_b}{P_b}\left(\frac{dG_r^i}{dP_r}\right)_{T_r} \tag{3.29}$$

Substituting Equation 3.20 into 3.29, specific volume of the pure component is derived as shown below:

$$V^i = \frac{RT_b}{P_b}(a_1 + a_2P + a_3T + a_4T^2) \tag{3.30}$$

$$V^E = \frac{R_mT_b}{P_b}\left[x.(1-x)\{E_2 + E_4T_r + (2x-1).(E_8 + E_{10}T_r) + (2x-1)^2E_{14}\}\right] \tag{3.31}$$

Equations 3.30 and 3.31 are substituted into Equation 3.16 to find molar specific volume of NH_3-H_2O liquid mixture.

Molar Specific Entropy (liquid)

From Equation 3.7 and 3.15

$$S = -R\left(\frac{dG_r^l}{dT_r}\right)_{P_r} \tag{3.32}$$

The molar entropy for the pure liquid component is given as

$$S^l = -R.\left[-S_{or}^l - b_1 \ln(T_r / T_{or}) - b_2(T_r - T_{or}) - \frac{b_3}{2}(T_r^2 - T_{or}^2) + \right.$$
$$\left. + \{a_3 + 2a_4 T_r\}(P_r - P_{or})\right] \tag{3.33}$$

The excess entropy is given as

$$S^E = -R_m x.(1-x)\left[E_3 + E_4 P_r - \frac{E_5}{T_r^2} - \frac{2E_6}{T_r^3} + (2x-1).\{E_9 + E_{10} P_r - \frac{E_{11}}{T_r^2} - \frac{2E_{12}}{T_r^3}\}\right.$$
$$\left. + (2x-1)^2\{-\frac{E_{15}}{T_r^2} - \frac{2E_{16}}{T_r^3}\}\right] \tag{3.34}$$

Equations 3.33, 3.34 and 3.18 are substituted into Equation 3.17 to find the molar specific entropy for NH_3-H_2O liquid mixture.

3.2.1.4 Vapour Mixture Volume, Entropy and Enthalpy

Ammonia-water vapour mixtures are assumed to be ideal solutions. The volume, entropy and enthalpy of the vapour mixture are computed by Equations 3.35 – 3.37.

$$V_m^g = yV_a^g + (1-y)V_w^g \tag{3.35}$$

$$S_m^g = yS_a^g + (1-y)S_w^g + S^{mix} \tag{3.36}$$

$$H_m^g = yH_a^g + (1-y)H_w^g \tag{3.37}$$

Equations 3.38 and 3.39 show the correlation of the specific volume and specific heat of pure vapour respectively

$$.V^g(T,P) = R.T/P + c_1 + c_2/T^3 + c_3/T^{11} + c_4P^2/T^{11} \tag{3.38}$$

$$C_p^g(P_o,T) = d_1 + d_2T + d_3T^2 \tag{3.39}$$

By inserting Equations 3.15, 3.38 & 3.39 in Equation 3.14, Gibbs free energy equation of the pure vapour components are derived as shown below:

$$\begin{aligned} G_r^g(P_r,T_r) = {} & H_{or}^g(P_{or},T_{or}) - T_r.S_{or}^g(P_{or},T_{or}) + \\ & + d_1(T_r - T_{or}) + \frac{d_2}{2}(T_r^2 - T_{or}^2) + \frac{d_3}{3}(T_r^3 - T_{or}^3) \\ & - d_1T_r \ln({}^{T_r}\!/\!_{T_{or}}) - d_2T_r(T_r - T_{or}) - \frac{d_3}{2}T_r(T_r^2 - T_{or}^2) \\ & + T_r \ln({}^{T_r}\!/\!_{T_{or}}) + c_1(P_r - P_{or}) \\ & + c_2(P_r / T_r^3 - 4P_{or} / T_r^3 + 3P_{or}T_r / T_{or}^4) \\ & + c_3(P_r / T_r^{11} - 12P_{or} / T_{or}^{11} + 11P_{or}T_r / T_{or}^{12}) \\ & + \frac{c_4}{3}(P_r^{\,3} / T_r^{11} - 12P_{or}^3 / T_{or}^{11} + 11P_{or}^3T_r / T_{or}^{12}) \end{aligned} \tag{3.40}$$

Molar Specific Enthalpy (vapour)

The molar specific enthalpy of pure liquid and the enthalpy of excess energy are derived by combining Equations 3.9 and 3.15 as shown in Equation 3.41. This equation has been simplified for inserting into computer functions.

$$\begin{aligned} H^g &= -RT_bT_r^2\left[\frac{d(G_r^g / T_r)}{dT_r}\right]_{P_r} \\ &= -RT_b\Bigg[-H_{or}^g + d_1(T_{or} - T_r) + \frac{d_2}{2}(T_{or}^2 - T_r^2) + \frac{d_3}{3}(T_{or}^3 - T_r^3) + \\ &\quad - c_1(P_r - P_{or}) + 4c_2\left(\frac{P_{or}}{T_{or}^3} - \frac{P_r}{T_r^3}\right) + 12c_3\left(\frac{P_{or}}{T_{or}^{11}} - \frac{P_r}{T_r^{11}}\right) + 4c_4\left(\frac{P_{or}^3}{T_{or}^{11}} - \frac{P_r^3}{T_r^{11}}\right)\Bigg] \end{aligned} \tag{3.41}$$

The enthalpy of mixture in vapour phase can be obtained by inserting Equation 3.41 into 3.37.

Molar Specific Entropy (vapour)

From Equations 3.7 and 3.15

$$S^g = -R\left(\frac{dG_r^g}{dT_r}\right)_{P_r} \qquad (3.42)$$

Molar entropy for the pure vapour component is given as

$$\mathbf{S}^g = -\mathbf{R}_i\left(\frac{\mathbf{dG}_r^g}{\mathbf{dT}_r}\right)_{\mathbf{P}_r}$$

$$= -R_i\left(-S_{or}^g + ln(\frac{P_r}{P_{or}}) + c_2\left(\frac{-3P_r}{T_r^4} + \frac{-3P_{or}}{T_{or}^4}\right) + c_3\left(\frac{-11P_r}{T_r^{12}} + \frac{11P_{or}}{T_{or}^{12}}\right) + \frac{c_4}{3}\left(\frac{-11P_r}{T_r^{12}} + \frac{11P_{or}}{T_{or}^{12}}\right)\right.$$

$$\left. -d_1 ln\left(\frac{T_r}{T_{or}}\right) - d_2(T_r - T_{or}) - \frac{d_3}{2}(T_r^{\,2} - T_{or}^{\,2})\right) \qquad (3.43)$$

Molar specific entropy for NH_3-H_2O vapour mixture can be calculated by substituting Equations 3.43 and 3.18 into 3.36.

Pressure-Temperature-Concentration relationship (Bourseau and Bugarel, 1986)

Log P = A – B/T [Unit of P = Pascal, T = K] (3.44)

Where $\mathbf{A = 10.440 - 1.767.x + 0.9823.x^2 + 0.3267.x^3}$
$\mathbf{B = 2013.8 - 2155.7x + 1540.9x^2 + 194.7.x^3}$

3.2.2 Water-Lithium Bromide (H_2O-LiBr) mixture

3.2.2.1 Thermodynamic and transport properties of the refrigerant - Water

Superheated enthalpy (Equation 3.45) and entropy (Equation 3.46) for liquid refrigerant are obtained from Irvine and Lilly, 1984 as follows

Enthalpy of superheated water vapour

$$h_g^s(T,P) = \sum_{n=0}^{2} A_n T^n - A_3.\exp[(T_s - T)/M] \qquad [\text{kJ/kg}] \qquad (3.45)$$

where,

$\mathbf{A0 = b(1, 1) + b(1, 2).P + b(1, 3).P}$
$\mathbf{A1 = b(2, 1) + b(2, 2).P + b(2, 3).P^2}$
$\mathbf{A2 = b(3, 1) + b(3, 2).P + b(3, 3).P^2}$
$\mathbf{A3 = b(4, 1) + b(4, 2).T_s + b(4, 3).\ T_s^{\,2} + b(4, 4).T_s^{\,3} + b(4, 5).\ T_s^{\,4}}$
b(1, 1) = 2041.21   b(1, 2) = -40.40021   b(1, 3) = -0.48095
b(2, 1) = 1.610693   b(2, 2) = 0.05472051   b(2, 3) = 7.517537E-4
b(3, 1) = 3.383117E-4   b(3, 2) = -1.975736E-5   b(3, 3) = -2.87409E-7
b(4, 1) = 1707.82   b(4, 2) = -16.99419   b(4, 3) = 6.2746295E-2
b(4, 4) = -1.0284259E-4   b(4, 5) = 6.4561298E-8   m = 45
T_s = Saturation temperature, K and P = Pressure, bar

Entropy for superheated water vapour

$$s = e + b(1)\left(\frac{T_s - T}{85}\right) \cdot \mathrm{Log}_{10}\left(10 \cdot \frac{P}{10} + b(2)\right) - f \cdot \mathrm{Exp}\left(\frac{T_s - T}{85}\right) \quad [\mathrm{kJ/kgK}] \quad (3.46)$$

where

$a(0) = 4.6162961$
$a(1) = 0.01039008$
$a(2) = -9.873085E-06$
$a(3) = 5.43411E-09$
$a(4) = -1.170465E-12$

$b(1) = -0.4650306$
$b(2) = 0.001$

$c(0) = 1.777804$
$c(1) = -0.01802468$
$c(2) = 6.854459E-05$
$c(3) = -1.184424E-07$
$c(4) = 8.142201E-11$

$$T_s = 42.6776 + \frac{-3892.7}{\log\left(\frac{P}{10}\right) - 9.48654} - 273.16$$

$$e = \sum_{x=0}^{x=4} a(x) \cdot T^x$$

$$f = \sum_{y=0}^{y=4} c(y) \cdot T^y$$

$T = T_g$, in Kelvin; $P = P_g = P_c$, in bar

Volume of saturated vapour (Kashinath et al, 1991)

$$V' = (-2.6295E\text{-}06 . T'^2 + 8.6144E\text{-}04 . T' - 0.07968) + (4.614E\text{-}03 . T' + 1.260734)/P \quad [m^3/kg] \quad (3.47)$$

where T' = water temperature in °C

Volume of superheated vapour (Kashinath et al, 1991)

$$V' = (-2.6295E\text{-}06 . T^2 + 8.6144E\text{-}04 . T - 0.07968) + (4.614E\text{-}03 . T + 1.260734)/P \quad [m^3/kg] \quad (3.48)$$

where T-T' = degree of superheat

The author has correlated the thermal conductivity of liquid water (Equation 3.49) and vapour (Equation 3.50) using data from the steam tables (Rogers & Mayhew, 1995). The percentage of deviation are shown in Figures 3.1 and 3.2 respectively.

Thermal conductivity of saturated water liquid

$$\lambda_l\,(T\ ^0C) = (a + b.T + c.T^2 + d.T^3 + e.T^4 + f.T^5 + g.T^6).10^{-6}\ [kW/mK] \qquad (3.49)$$

a = 568.91507597
b = 1.874258819
c = -7.888751E-3
d = -6.46045E-7
e = 5.69404E-8
f = -1.98121E-10
g = 2.15875E-13

Thermal conductivity of saturated water vapour

$$\lambda_g\,(T\ ^0C) = (a + b.T + c.T^2 + d.T^3 + e.T^4 + f.T^5 + g.T^6).10^{-6}[kW/mK] \qquad (3.50)$$

a = 16.347623406
b = 7.018478E-2
c = 3.77774E-4
d = -5.21139E-6
e = 3.92543E-8
f = -1.2771E-10
g = 1.8328E-13

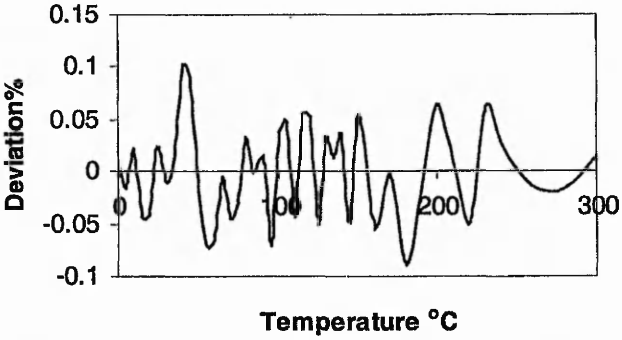

Figure 3.1 Percentage deviation of fitted equations of thermal conductivity of saturated water liquid

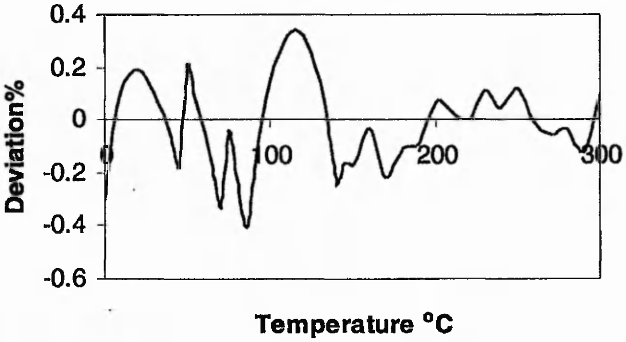

Figure 3.2 Percentage deviation of fitted equations of thermal conductivity of saturated water vapour

The author has correlated the specific heat of liquid water (Equation 3.51) and vapour (Equation 3.52) using data from the steam tables (Rogers & Mayhew, 1995). The percentage of deviation are shown in Figures 3.3 and 3.4 respectively.

Specific heat capacity of saturated liquid water

$$\mathbf{Cp_l\,(T\,^{\circ}C) = a + b.T + c.T^2 + d.T^3 + e.T^4 + f.T^5 + g.T^6 \quad [kJ/kgK] \qquad (3.51)}$$

a = 4.212237644　　b = -2.475189E-3　　c = 6.2983E-5
d = -7.22209E-7　　e = 4.78682E-9　　f = -1.50601E-11
g = 1.8969E-14

Specific heat capacity of saturated water vapour

$$\mathbf{Cp_g\,(T\,^{\circ}C) = a + b.T + c.T^2 + d.T^3 + e.T^4 + f.T^5 + g.T^6 \quad [kJ/kgK] \qquad (3.52)}$$

a = 1.871159484　　b = -2.324751E-3　　c = 1.31937E-4
d = -2.18643E-6　　e = 1.76339E-08　　f = -6.12104E-11
g = 7.96242E-14

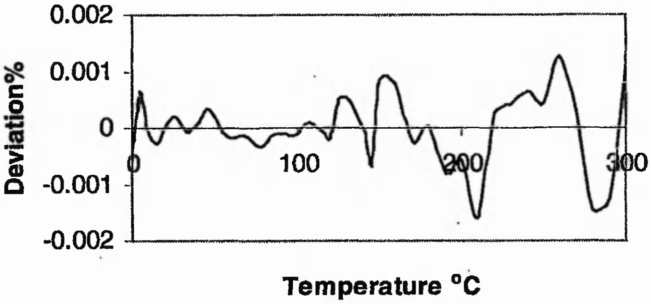

Figure 3.3 Percentage deviation of fitted equations of specific heat capacity of saturated water liquid

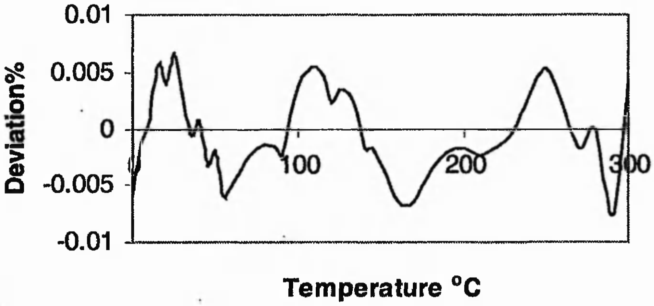

Figure 3.4 Percentage deviation of fitted equations of specific heat capacity of saturated water vapour

Saturated pressure and temperature of liquid water [McNeely, 1979]

$$\mathbf{P_s\ (T,\ ^{o}K) = exp(K_0 + K_1 / T + K_2 / T^2)\ \ [bar]} \tag{3.53}$$

$$\mathbf{T_s\ (P,\ bar) = (-2.K_2 / (K_1 + (K_1^2 - 4.K_2.(K_0 - lnP))^{0.5})) - 273.15\ \ [^{o}C]} \tag{3.54}$$

$K_0 = 11.5923$
$K_1 = -3669.89$
$K_2 = -243093$

Density of saturated liquid water [Wagner, 1993]

$$\mathbf{\rho_l(T,\ ^{o}C) = (1 + b_1.\theta^{1/3} + b_2.\theta^{2/3} + b_3.\theta^{5/3} + b_4.\theta^{16/3} + b_5.\theta^{43/3} + b_6.\theta^{110/3}).\rho_c\ \ [m^3/kg]} \tag{3.55}$$

where,
$b_1 = 1.99274064$ $\quad b_2 = 1.09965342$ $\quad b_3 = -0.510839303$
$b_4 = -1.75493479$ $\quad b_5 = -45.5170352$ $\quad b_6 = -6.7469445 * 10^5$
$\rho_c = 322$ $\quad T_c = 647.096$ $\quad T = T + 273.16$ $\quad K$
$\theta = (1 - T / T_c)$

Density of saturated water vapour [Wagner, 1993]

$$\mathbf{\rho_g(T,\ ^{o}C) = exp(c_1.\theta^{2/6} + c_2.\theta^{4/6} + c_3.\theta^{8/6} + c_4.\theta^{18/6} + c_5.\theta^{37/6} + c_6.\theta^{71/6}).\rho_c\ \ [m^3/kg]} \tag{3.56}$$

where,
$c_1 = -2.0315024$ $\quad c_2 = -2.6830294$ $\quad c_3 = -5.38626492$
$c_4 = -17.2991605$ $\quad c_5 = -44.7586581$ $\quad c_6 = -63.9201063$
$\rho_c = 322$ $\quad T_c = 647.096$ $\quad T = T + 273.16\ K$
$\theta = (1 - T / T_c)$

The viscosity of water liquid (Equation 3.57) and vapour (Equation 3.58) are fitted in this work using data from Rogers and Mayhew, 1995. The percentage deviation of both fitted equations are shown in Fig 3.5 and Fig 3.6 respectively.

Viscosity of saturated water liquid

$$\mathbf{\mu_l(T,\ ^{o}C)\ =\ (1 / (a + b.T + c.T^2 + d.T^3 + e.T^4 + f.T^5 + g.T^6)).10^{-6}\ \ [kg/ms]} \tag{3.57}$$

$a = 5.74248E-4$ $\quad b = 1.7491E-5$ $\quad c = 1.97487E-7$
$d = -9.56102E-10$ $\quad e = 2.9877E-12$ $\quad f = -6.25077E-15$
$g = 5.91498E-18$

Viscosity of saturated water vapour

$$\mu_g(T, {}^\circ C) = (a + b.T + c.T^2 + d.T^3 + e.T^4 + f.T^5 + g.T^6).10^{-6}$$
[kg/ms] **(3.58)**

$a = 8.473425067$ $b = 0.03834896$ $c = -1.90836E-4$
$d = 3.16925E-6$ $e = -2.08229E-8$ $f = 5.9236E-11$
$g = -6.01449E-14$

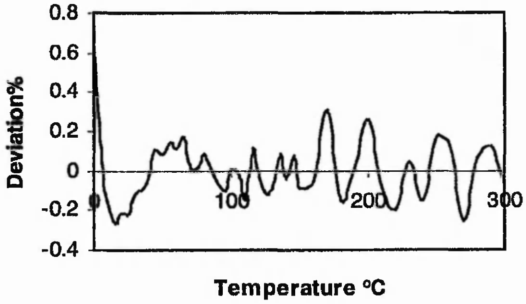

Figure 3.5 Percentage deviation of fitted equations of viscosity of saturated water liquid

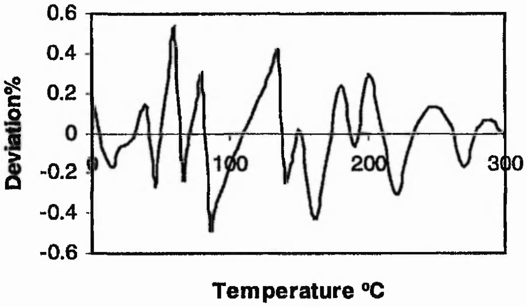

Figure 3.6 Percentage deviation of fitted equations of viscosity of saturated water vapour

3.2.2.2 Thermodynamic and transport properties of mixture – Water-LiBr

Entropy of H_2O-LiBr

$$s(T, x) = \sum_{j=0}^{j=3}\sum_{k=0}^{k=3} a(j,k)\cdot x^j \cdot T^k \qquad [kJ/kg.K] \qquad (3.59)$$

where T = temperature, K.

The entropy of H_2O-LiBr was derived by the author using data from Koehler et al, 1987. (The correlations indexes are shown in Appendix A).

Constants for Equation 3.59.

For 0% $\leq X \leq$ 30%	For 30% $< X <$ 55 %	For 55 $\leq X \leq$ 70 %
a(0, 0) = -7.417100748	a(0, 0) = -9.290712095	a(0, 0) = 19.772820215
a(0, 1) = 0.042904116	a(0, 1) = 0.054835733	a(0, 1) = 0.12433496
a(0, 2) = -7.2384E-05	a(0, 2) = -1.09396E-04	a(0, 2) = -9.3605E-04
a(0, 3) = 5.39369E-08	a(0, 3) = 9.20634E-08	a(0, 3) = 1.44446E-06
a(1, 0) = 0.166314986	a(1, 0) = 0.307819887	a(1, 0) = -1.372844036
a(1, 1) = -1.107228E-03	a(1, 1) = -2.011269E-03	a(1, 1) = -3.914023E-03
a(1, 2) = 2.59684E-06	a(1, 2) = 5.40241E-06	a(1, 2) = 4.2821E-05
a(1, 3) = -2.3296E-09	a(1, 3) = -5.22157E-09	a(1, 3) = -6.96848E-08
a(2, 0) = -1.096469E-03	a(2, 0) = -4.40768E-03	a(2, 0) = 0.030679396
a(2, 1) = 5.57828E-06	a(2, 1) = 2.69E-05	a(2, 1) = 2.91454E-06
a(2, 2) = -1.33234E-08	a(2, 2) = -7.99608E-08	a(2, 2) = -5.48904E-07
a(2, 3) = 1.1879E-11	a(2, 3) = 8.10737E-11	a(2, 3) = 1.01284E-09
a(3, 0) = 9.07416E-06	a(3, 0) = 3.2104E-05	a(3, 0) = -2.25582E-04
a(3, 1) = -4.78769E-08	a(3, 1) = -2.00229E-07	a(3, 1) = 4.52593E-07
a(3, 2) = 1.33503E-10	a(3, 2) = 6.1963E-10	a(3, 2) = 1.72826E-09
a(3, 3) = -1.21532E-13	a(3, 3) = -6.3688E-13	a(3, 3) = -4.37987E-12

Enthalpy of H_2O – LiBr (McNeely, 1979)

$$h_l(T, x) = 2.326 \cdot (a + b \cdot d + c \cdot d^2) \qquad [\mathrm{kJ/kg}] \tag{3.60}$$

where,

$a = -1015.07 + 79.5387.x - 2.358016.x^2 + 0.03031583.x^3 - 1.400261E\text{-}04.x^4$

$b = 4.68108 - 0.3037676.x + 0.00844845.x^2 - 1.047721E\text{-}04.x^3 + 4.80097E\text{-}07.x^4$

$c = -4.9107E\text{-}03 + 3.83184E\text{-}04.x - 1.078963E\text{-}05.x^2 + 1.3152E\text{-}07.x^3 - 5.897E\text{-}10.x^4$

$d = 1.8 * T + 32$

Viscosity of H_2O-LiBr (Lee et al, 1990)

$$\ln \mu[T, x] = A_1 + A_2 / T + A_3 . \ln T \quad [\mathrm{N.s/m^{\wedge}2}] \tag{3.61}$$

$A_1 = -494.122 + 16.3967.x - 0.14511.x^2$
$A_2 = 28606.4 - 934.568.x + 8.52755.x^2$
$A_3 = 70.3848 - 2.35014.x + 0.0207809.x^2$
where t = Temperature, K

Density of H_2O-LiBr (Wimby and Berntsson, 1994)

$$\rho(T\ ^{\circ}C, x) = d_1 + d_2.T + d_3.T^2 + d_4.x + d_5.x^2 + d_6.x.T + d_7.x^2.T + d_8.T^2.x + d_9.x^3 + d_{10}.x^4 \quad [kg/m^3] \qquad (3.62)$$

$d_1 = 1002$ $d_2 = -8.7932\ E\text{-}2$ $d_3 = -3.79848\ E\text{-}3$
$d_4 = 8.5425$ $d_5 = -2.9368\ E\text{-}2$ $d_6 = -5.7606\ E\text{-}3$
$d_7 = -8.2838\ E\text{-}5$ $d_8 = 7.3685\ E\text{-}5$ $d_9 = 1.4834\ E\text{-}3$
$d_{10} = 4.2006\ E\text{-}7$

Specific heat capacity of H_2O-LiBr (Feuerecker, 1993)

$$C_p(T\ ^{\circ}C, x) = \sum_{n=0}^{3} a_n x^n + 2 \cdot T \cdot \sum_{n=0}^{2} b_n x^n + 3 \cdot T^2 \cdot c_0 \quad [kJ/kg] \qquad (3.63)$$

$a_0 = -3.293E\text{-}1$, $a_1 = 4.076E\text{-}2$, $a_2 = -1.36E\text{-}5$, $a_3 = -7.1366E\text{-}6$
$b_0 = 7.4285E\text{-}3$, $b_1 = -1.5144E\text{-}4$, $b_2 = 1.3555E\text{-}6$, $c_0 = -2.269E\text{-}6$

Thermal conductivity of H_2O-LiBr (DeGuilio et al, 1990)

$$\lambda(T, x) = ((-1407.53 + 11.0513 \cdot T - 1.46741E\text{-}2 \cdot T2) + (38.9855 - 0.240475 \cdot T + 3.48073E\text{-}4 \cdot T^2) \cdot x + (-0.265025 + 1.51915E\text{-}3 \cdot T - 2.32262E\text{-}6 \cdot T^2) \cdot x^2) / 1000 \quad [W/mK] \qquad (3.64)$$

where T = Temperature in K

3.3 Derivation of property equations from experimental data

In order to study the absorption cooling system using the First Law of thermodynamic analysis, the three properties needed are the pressure-temperature-concentration relationship, the enthalpy concentration chart and density of the solution mixtures, which are widely available and can be measured easily without using expensive apparatus. The First Law is used not only because of its simplicity, but also because its requirement for only a small number of thermodynamic properties compared to detailed modelling of components is also crucial in the initial stages of selecting working mixtures.

A detailed study of the ACS including the analysis of the various components will need the transport properties such as thermal conductivity, surface tension and viscosity which may not be available from past literature. The time needed and the cost of building experimental rigs to obtain the transport properties will be considerably increased to enable a study of a variety of working fluids. Thus, the First Law is a useful tool at an early stage to filter the potential candidates from the massive database of working fluids.

McNeely (1979) was the first person to publish the correlation method of finding the enthalpy-concentration relationship of water-lithium bromide data obtained from a commercially. This correlation was used in this project for comparisons of alternative working mixtures. It is briefly discussed below:

Once the relations of pressure and temperature at different concentration are measured, the Duhring equation for the mixture can be represented by

$$\mathbf{T = A.T' + B} \tag{3.65}$$

where A and B are constants obtained in terms of solution concentrations using a polynomial fit while t and t' are saturation temperatures of the solution and refrigerant respectively.

The enthalpy-concentration chart can be constructed simply by using vapour pressure values with data for the liquid specific heat capacity and enthalpy of solution at a base concentration over a temperature range of 20 °C to 100 °C. The latent heat of a solution ΔH has to be found using the relationship derived from the Clapeyron equation as follows:

$$\Delta H = \frac{\Delta H'}{AV'}\frac{VT}{T'} \tag{3.66}$$

Where V = specific volume of superheated water vapour

V' = specific volume of saturated water vapour

The latent heat of saturated water is calculated as $\Delta H' = H_g - H_l$ and constant A being the slope of the Duhring line as shown in Equation 3.65.

Using the Haltenberger equation,

$$H_l(T,x) = \frac{H_0 - \int_{x_0}^{x_1} \bar{H} d(1 - x_o / x)}{x_o / x_1} \tag{3.67}$$

where,

$\overline{H} = H_g - \Delta H$ and $1\text{-}x_o/x$ is generally represented by the symbol ω

By setting the reference state of zero enthalpy at 0 °C for water and the solution, at the chosen concentration, the enthalpy of the base concentration is given as:

$$H_o = \int_0^{t_1} C_{P_m} dT \tag{3.68}$$

where Cp_m at the base concentration can be fitted using a polynomial. The integral of Equation 3.66 can be solved either graphically by plotting $\overline{H}$ versus ω and finding the area under the curve, or using a computer program which can deduce the entire isotherm from an input of H_o, x_o, x_n and T by step integration. The corresponding values of H_l were correlated by the following equation:

$$H_l\,(T, x) = A + Bx + Cx^2 \tag{3.69}$$

Where A, B and C are fitted using fourth order polynomial.

3.4 Methods for solving non-linear equations of properties

Non-linear equations such as Equation 3.59 can be solved using interpolations and extrapolations methods. Newton-Raphson, Bisection and False position methods are the most commonly used methods. Some of them need less computing power and few number of calculations whilst others result in better accuracy but take longer. As most of the thermodynamic and transport properties equations are non-linear, it was considered important to choose a suitable method for this work. A brief outline of these methods are as follows:

False position method

Suppose the interpolation guesses are x_n and x_{n+1}. The false position method interpolates linearly between $[x_n, f(x_n)]$ and $[x_{n+1}, f(x_{n+1})]$. The improved guess replaces either the lower or upper bounds of the previous guess. The interpolation can be written as

$$x_{new} = x_n - f(x_n)\left[\frac{x_{n+1} - x_n}{f(x_n + 1) - f(x_n)}\right] \tag{3.70}$$

Newton-Raphson method

The speciality of this method is the need to calculate the derivative of the function, and this may present difficulties when handling with complex equations such as many correlations of transport and thermodynamic properties. The Newton-Raphson formula is shown below:

$$x_{n+1} = x_n - \frac{f(x_n)}{f'(x_n)} \qquad (3.71)$$

where $f'(x_n)$ is the derivative of function $f(x_n)$

Bisection method

In this method, two roots are first estimated by establishing a change of sign of function f(x). The middle value of the function is then found, i.e.,

$$f\left[\frac{(x_{n+1} + x_n)}{2}\right] \text{ or } f(x_{mid})$$

If the sign of the function at this midpoint is the same as that of $f(x_n)$, the root is closer to x_{n+1} and x_{mid} replaces x_n for the next bisection. Alternatively, it replaces x_{n+1}. When successive values of x_{mid} are close enough and within the tolerance required, the iteration is stopped.

Table 3.2 *Comparison of methods for solving PTX equation for H_2O-LiBr*

Method	Iteration	Time (s)	Tolerance	Deviation %
Bisection	114	1.880	1E-4	0.390407
False Position	12	0.144	1E-4	0.391778
Newton Raphson	3	0.020	1E-4	-0.001038
Bisection	121	2.011	1E-6	0.390407
False Position	17	0.219	1E-6	0.390487
Newton Raphson	5	0.053	1E-6	-7.50E-05

It is clear from Table 3.2 that the False position and Newton-Raphson methods are better than Bisection in terms of computing time and number of iterations when solving the pressure-temperature-concentration equation of water-lithium bromide mixtures. The computing time of the False position method is approximately ten times faster than the Bisection method while the deviation percentages only differ slightly. Among these methods, Newton-Raphson is the fastest and most accurate. However, this method needs a proper initial guess and can sometimes be unstable and never converge thus creating overflow problems. Thus the False position method was chosen in the current work.

Chapter 4 Thermodynamic Analysis

4.1 First Law Analysis

Over the past few decades, there has been numerous publications on ACS using First Law analysis. Over 30 of these publications have been scrutinized recently (Tan, 1999). The most common cycle namely the single effect ACS is shown in Figure 4.0. The dual pressure absorption type has been used as a benchmark for comparison in studying and developing new cycles and new working mixture combinations. Generally, when using the First Law of thermodynamics analysis the assumption of endoreversibility is made.

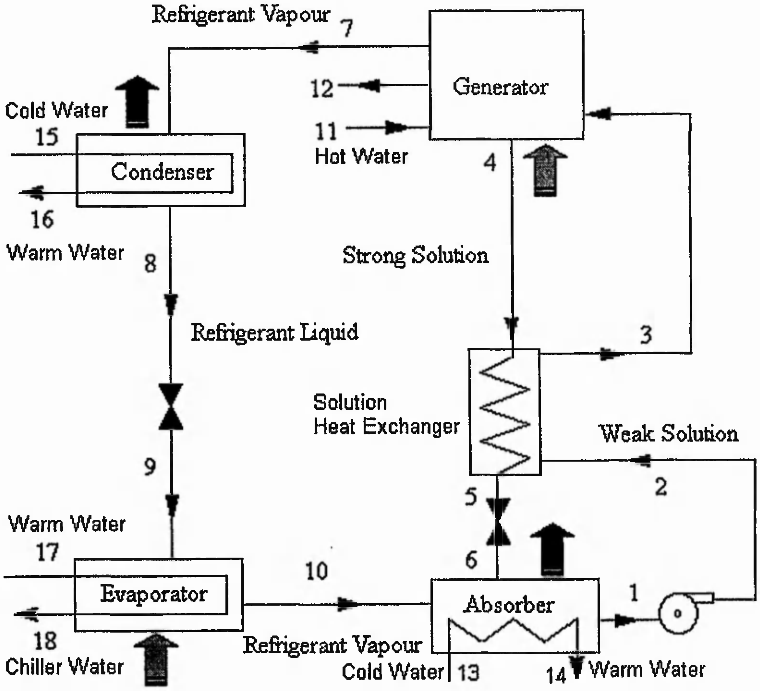

Figure 4.0 Schematic diagram of single effect ACS

The governing equations for mass and species conservation for a steady state and steady-flow system are, respectively,

$$\sum(\dot{m})_{in} - \sum(\dot{m})_{out} = 0 \quad \textbf{(4.0)} \quad \text{and} \quad \sum(\dot{m}x)_{in} - \sum(\dot{m}x)_{out} = 0 \quad \textbf{(4.1)}$$

The First Law of thermodynamics readily yields the energy balance of each component of the absorption chiller.

$$\sum(\dot{m}h)_{in} - \sum(\dot{m}h)_{out} + [\sum\dot{Q}_{in} - \sum\dot{Q}_{out}] + W = 0 \qquad (4.2)$$

where Q's are the heat transfer rates between the control volume and its environment, and W is positive if work is performed on the system. Two important dimensionless variables, namely the coefficient of performance **(COP)** and circulation ratio **(f)**, are defined as follows:

$$COP = \frac{\dot{Q}_{evaporator}}{\dot{Q}_{generator} + W_{pump}} \qquad (4.3) \quad \text{and} \quad circulation\ flow\ ratio(f) = \frac{\dot{m}_3}{\dot{m}_7} \qquad (4.4)$$

4.1.1 The mathematical model

Absorber

$T_a = T_1$ **A0**

$P_a = P_e(T_e)$ (If pressure drop is neglected) **A1a**

$P_a = 0.925\ P_e$ **A1b**

$\dot{m}_{10} + \dot{m}_6 = \dot{m}_1$ (mass balance) **A2**

$\dot{m}_{10}x_{10} + \dot{m}_6x_6 = \dot{m}_1x_1$ (H_2O-LiBr balance) **A3**

$x_3 = x(T_e, T_a)$ (state equation) **A4**

$h_1 = h_l(T_a, x_3)$ (state equation) **A5**

$\dot{Q}_a = \dot{m}_{10}h_{10} + \dot{m}_6h_6 - \dot{m}_1h_1$ (energy balance) **A6a**

or $\dot{Q}_a = \dot{Q}_g + \dot{Q}_e - \dot{Q}_c$ **A6b**

Condenser

$T_c = T_8$ **A7**

$P_c = P(T_c)$ (assumption 1) **A8**

$\dot{m}_7 = \dot{m}_8$ (mass balance) **A9**

$h_8 = h_l(T_c, P_c)$ (assumption 6) **A10**

$\dot{Q}_c = \dot{m}_7h_7 - \dot{m}_8h_8$ (energy balance) **A11**

Evaporator

$T_e = T_{10}$ **A12**

$P_e = P_s(T_e)$ (assumption 2) **A13**

$\dot{m}_9 = \dot{m}_{10}$ (mass balance) **A14**

$h_{10} = hg(T_e, P_e)$ (state equation) **A15**

$\dot{Q}_e = \dot{m}_{10}h_{10} - \dot{m}_9h_9$ (energy balance) **A16**

Solution pump

$$W_p = \frac{(P_2 - P_1)\dot{m}v}{\eta_p} \text{ or } \frac{(P_2 - P_1)}{\eta_p \rho} \tag{A17}$$

$\mathbf{v = vl(T_a, P_a, x_3)}$ (state equation) A18

$\mathbf{h_l = hl(T_a, x_3)}$ (state equation) A19

$\mathbf{T_{1a} = T_1 + T_{pump}}$ (state equation) A20a

$\mathbf{T_{1a} = T_1 = T_a}$ (if pump work is neglected) A20b

$\mathbf{\dot{m}_1 = \dot{m}_{1a}}$ (mass balance) A21

$\mathbf{x_1 = x_{1a}}$ (H_2O-LiBr balance) A22

$\mathbf{h_{1a} = h_1}$ (if pump work is neglected) (enthalpy balance) A23a

$\mathbf{h_{1a} = h_1 + W_p}$ (energy balance) A23b

Solution expansion valve

$\mathbf{T_6 = T_5}$ A24

$\mathbf{\dot{m}_5 = \dot{m}_6}$ (mass balance) A25

$\mathbf{x_5 = x_6}$ (throttling) A26

$\mathbf{h_5 = h_6}$ (enthalpy balance) A27

Refrigerant Expansion Valve

$\mathbf{T_9 = T_c}$ A28

$\mathbf{T_8 = T_9}$ A29

$\mathbf{\dot{m}_8 = \dot{m}_9}$ (mass balance) A30

$\mathbf{h_8 = h_9}$ (assumption 3) A31

Solution heat exchanger SHX

$\mathbf{\dot{m}_{1a} = \dot{m}_3}$ (mass balance) A32

$\mathbf{\dot{m}_4 = \dot{m}_5}$ (mass balance) A33

$\mathbf{x_{1a} = x_3}$ (H_2O-LiBr balance) A34

$\mathbf{x_4 = x_5}$ (H_2O-LiBr balance) A35

(if heat exchanger efficiency, $\eta_{SHX} = 1$)

$\mathbf{\dot{m}_{1a}h_{1a} + \dot{m}_4h_4 = \dot{m}_3h_3 + \dot{m}_5h_5}$ (energy balance) A36

(if heat exchanger efficiency, $\eta_{SHX} < 1$)

$\mathbf{C_{min} = \dot{m}_4 C_{pl}(T_4, x_4)}$ (state equation) A37

$C_{max} = \dot{m}_3 C_{pl}(T_{1a}, x_3)$ (state equation) **A38**

$Z = Cmin/Cmax$ **A39**

$NTU = UA/Cmin$ **A40**

$$\eta_{SHX} = \frac{1-\exp(-NTU(1-Z))}{1-Z.\exp(-NTU(1-Z))}$$ (effectiveness) **A41**

$T_5 = T_g - \eta_{SHX}(T_g - T_{1a})$ **A42**

$T_3 = T_{1a} - Z(T_4 - T_5)$ **A43**

$h_5 = h_l(T_5, P_g, x_4)$ (state equation) **A44**

$h_3 = h_l(T_3, P_g, x_3)$ (state equation) **A45**

Generator for BSS

$T_4 = T_7$ **A46**

$P_g = P_c$ (If pressure drop is neglected) **A47**

$P_g = 1.05\ P_c$ **A47b**

$\dot{m}_4 + \dot{m}_7 = \dot{m}_3$ (mass balance) **A48**

$\dot{m}_4 x_4 = \dot{m}_3 x_3$ (H_2O-LiBr balance) **A49**

$x_4 = x(T_g, T_c)$ (state equation) **A50**

$h_4 = h_l(T_g, x_4)$ (state equation) **A51**

$h_7 = h_g(T_g, P_g)$ (state equation) **A52**

$\dot{Q}_g = \dot{m}_4 h_4 + \dot{m}_7 h_7 - \dot{m}_3 h_3$ (energy balance) **A53**

The above equations were solved simultaneously using Gaussian elimination. A program has been developed using Visual Basic to solve these equations. A commercial Engineering Equation Solver (EES) is also used for comparison and validation. The energy balance equations can be further modified by including the dimensionless number of flow ratio **f** as follows in order to perform a parametric study. By assuming $m_7 = 1$, equation A48 divided by m_7 becomes

$\dot{m}_4\ /\ \dot{m}_7 = f - 1$ **(4.5)**

where $f = m_3/m_7$ is as defined in equation 4.4

Thus equation **A53** becomes

$$\dot{Q}_g = (f-1).h_4 + h_7 - f.h_3$$ **(4.6)**

and
$$COP = \frac{h_{10} - h_9}{f.(h_4 - h_3) + h_7 - h_4 + W_p} \tag{4.7}$$

By dividing **A48** by m_3 and substituting **A49** in the equation the following equations are formed.

$$\mathbf{x_4/x_3 + \dot{m}_7/\dot{m}_3 = 1 \ \text{and} \ \dot{m}_3/\dot{m}_7 = f = 1/(1 - x_4/x_3)}$$

$$f = \frac{x_3}{x_3 - x_4} = \frac{x_3}{\Delta x} \tag{4.8}$$

From Equation 4.7, it can be observed that when circulation flow-ratio, **f,** in the denominator increases, the COP will decrease. Meanwhile, Equation 4.8 shows the increase in the difference between x_3 and x_4 namely **Δx,** will reduce the circulation flow ratio, **f,** and thus improving the COP.

Fig. 4.1 – Fig. 4.4 show the changes of the COP and the flow ratio, **f,** in three types of mixtures with variations in absorber, condenser, generator and evaporator temperatures. NH_3-H_2O and H_2O-LiBr mixtures are widely used in commercial systems, and are thus included in this analysis. H_2O-LiCl, which has been researched extensively due to its advantage of having a low cut-off temperature (intersection point at zero COP) and higher performance, is also included in the analysis. The word 'strong' in this context refers to rich in absorbent while 'weak' means less refrigerant in the mixture.

4.1.2 Effect of changes of condenser temperature

The effect of condenser temperature on the COP value, with operating temperature (T_g, T_a, T_e) parameters being constant, is analogous to the effect due to the variation in absorber temperature. When the condenser temperature is increased, the pressure at the generator and condenser will become higher. When the generator temperature is kept constant, the amount of water refrigerant separated from the weak solution entering from the absorber is reduced and hence a reduction in **Δx.** In order to maintain the same amount of cooling load, the generator load has to be increased and the COP will fall. With the aim of improving performance, a higher efficiency solution heat exchanger has to be employed to increase the inlet temperature to the generator and absorber.

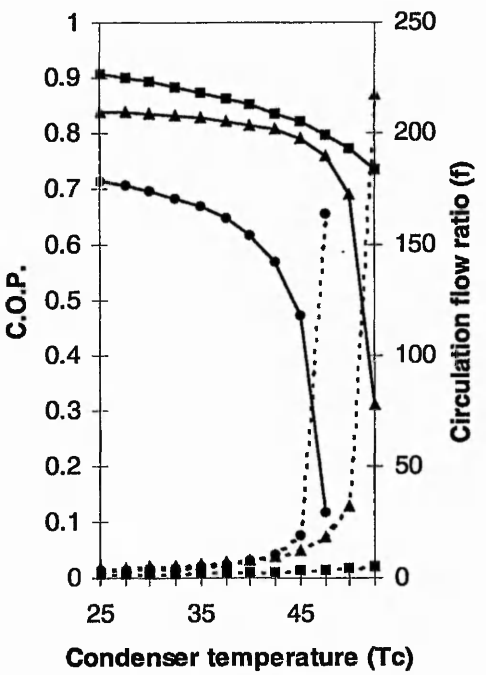

Figure 4.1 Variations in COP with condenser temperatures ($T_e = 8\ ^0C$, $T_a = 30\ ^0C$, $T_g = 80\ ^0C$, $\eta_{SHX} = 0.8$)

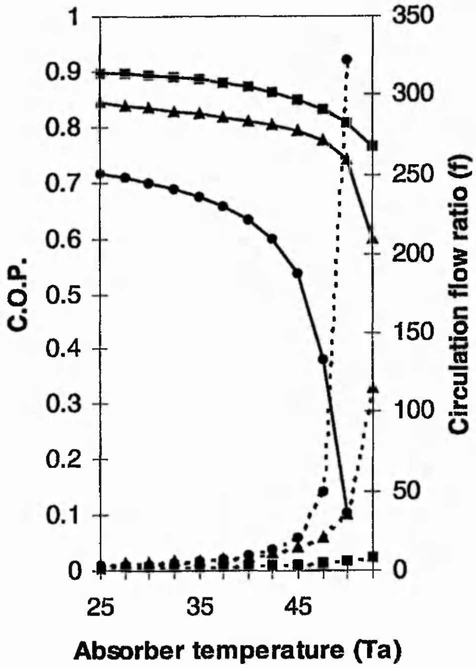

Figure 4.2 Variations in COP with absorber temperatures ($T_e = 8\ ^0C$, $T_c = 30\ ^0C$, $T_g = 80\ ^0C$, $\eta_{SHX} = 0.8$)

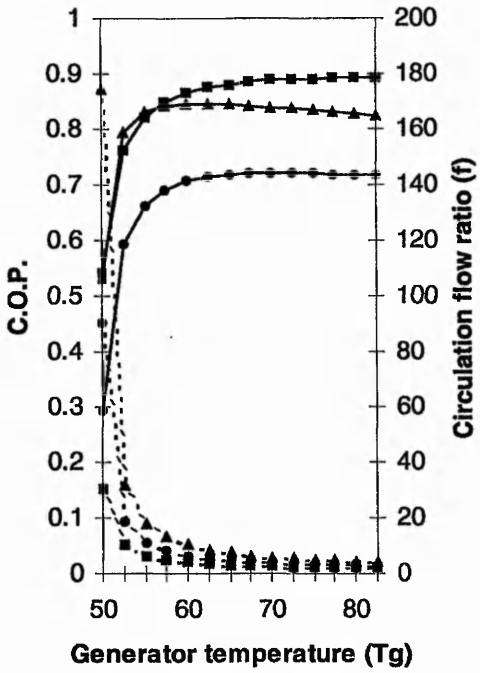

Figure 4.3 Variations in COP with generator temperatures ($T_e = 10\ ^0C$, $T_a = T_c = 30\ ^0C$, $\eta_{SHX} = 0.8$)

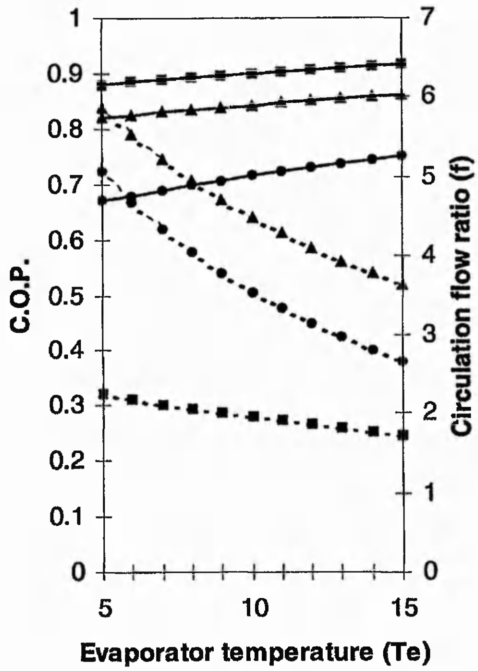

Figure 4.4 Variations in COP with evaporator temperatures ($T_g = 80\ ^0C$,$T_a = T_c\ 30\ ^0C$, $\eta_{SHX} = 0.8$)

┈┈┈ Flow ratio f —— COP ▲ H_2O-LiBr ■ H_2O-LiCl • NH_3-H_2O

Figure 4.1 shows that H_2O-LiBr and H_2O-LiCl are generally performing 15%-20% better than NH_3-H_2O. The analysis also indicates that H_2O-LiCl performs 2% – 7% better than H_2O-LiBr. The cut-off temperature of H_2O-LiBr and H_2O-LiCl is also higher than NH_3-H_2O. The higher the condensing temperature the smaller the size of condenser required. If sufficient difference (10 ^oC) between the condenser and ambient temperature is allowed, air-cooled condenser can be used instead of water-cooled condenser. As the condensing temperature approaches cut-off temperature, circulation flow ratio increases significantly and COP will decrease. A higher power rated pump is therefore required. Therefore, a balance between performance and cost has to be given careful consideration.

4.1.3 Effect of changes in absorber temperature

When the temperature of the evaporator is fixed, elevation in the absorber temperature causes an increase in the concentration of the weak solution x_3. This is because at a constant pressure, the increase in absorber temperature will affect the mass absorption rate. The difference between the strong and weak solution concentration Δx thus decreases, leading to a decrease in the COP value. Increases in absorber temperature might be caused by either inefficiency of the absorber's cooling coil or the solution heat exchanger. A larger and more effective surface area of the absorber coil, A_{eff}, and solution heat exchanger is needed to reduce the temperature at the outlet and inlet of the absorber respectively.

The evaporator load also contributes to increases in absorber temperature if the concentration of the solution mixture is not strong enough for absorption of refrigerant vapour. This is apart from factors caused by the inefficiency of absorber and solution heat exchanger as mentioned earlier.

The effects of increasing absorber temperature and condenser temperature for the three working mixtures have a similar trend. The performance of both water-based mixtures can be 25% - 30% better than NH_3-H_2O. As in the case of condenser temperature changes, a higher absorber temperature is preferable for air-cooling. The temperature is restricted by the performance trend near the cut-off temperature.

From Figure 4.2, it can be seen that with the aim of improving system performance, the absorber temperature has to be kept below 45 °C. The selection of the operating temperature is also limited by the crystallisation temperature (See Appendix E). The analysis in this section does not include consideration to crystallisation. The computer program developed in this work, however, has addressed this problem by providing a function to avoid crystallisation point by setting the minimum difference between the absorber temperature and the crystallisation point.

The dramatic change of circulation flow ratio is also observed in the three working fluids when absorber temperature approaches cut-off temperature. The higher the circulation flow ratio, the more expensive is the start-up and operating costs required for a higher pump power rating. Thus choosing the operating temperature is crucial in the overall design of the ACS.

4.1.4 Effect of changes in evaporator temperature

COP increases with increasing evaporator temperature. This is because when the evaporating pressure becomes higher, the absorber pressure also increases and this will lead to a higher potential for absorption in the absorber. That is to say that the concentration of weak solution decreases whilst Δx increases and thus COP increases. Though the COP increases in this case, the temperature of the evaporator is usually restricted by the cooling requirements.

4.1.5 Effect of changes in generator temperature

Since the evaporator, absorber and condenser temperatures are dependent on ambient conditions, the only two main control parameters are generator temperature and the mass flow rate (m_3) of the weak solution. Controlling the mass flow rate using a variable speed pump is more expensive than controlling the generator temperature, thus the latter is generally adopted and therefore understanding of the effect of generator temperature is vital. Figure 4.4 shows that an incremental change of generator temperature (T_g) initially affects the system performance considerably until a maximum point is reached. After this, any increase in temperature will lead to a gradual decrease of COP. Increasing the generator temperature increases the strong solution concentration, thus decreasing the circulation flow rate and increasing Δx.

The COP of the system therefore increases initially affecting the system performance considerably until a maximum point is reached. After this, any increase of temperature will lead to a gradual decrease of COP. It is often useful to find this optimal point when designing ACS. Equations for finding maximum COP_{max} for a 2kW (specified for a small room or office) ammonia-water ACS at optimal generator temperature $T_{g\ max,\ COP}$ in terms of T_a, T_c, and T_e was developed using non-linear regression analysis. In order to facilitate the design process, an optimal design map has also been devised. This was reported in Tan, 1999.

4.1.6 Summary of results

When kinetic and potential energy are neglected, the conservation of mass and energy equations for steady flow processes are expressed as

$$\sum \dot{m}_i = \sum \dot{m}_e \qquad (4.9)$$

$$\dot{Q} - \dot{W} = \sum \dot{m}_e h_e - \sum \dot{m}_i h_i \qquad (4.10)$$

where subscript ***i*** stands for inlet and ***e*** for exit.

These assumptions have made the analysis of a new system much easier, though, its results as obtained are still far from practical. It is, however, considered a useful tool in the initial stages of any design before further development and a more comprehensive analysis take place. The comparisons of using different working fluids and the effect of COP due to variation in operating parameters have been reported. A further analysis can be made by comparing different designs with the ideal COP as shown in Figure 4.5. The chart shows that utilising a solution heat exchanger can improve the performance between 10 to 20%. The ideal COP is defined by Wang (1992) as

$$C.O.P_{ideal} = \frac{(T_g - T_a).T_e}{(T_c - T_e).T_g} \qquad (4.11)$$

The nearer the actual COP curve to the ideal COP line, the better is the design operating point.

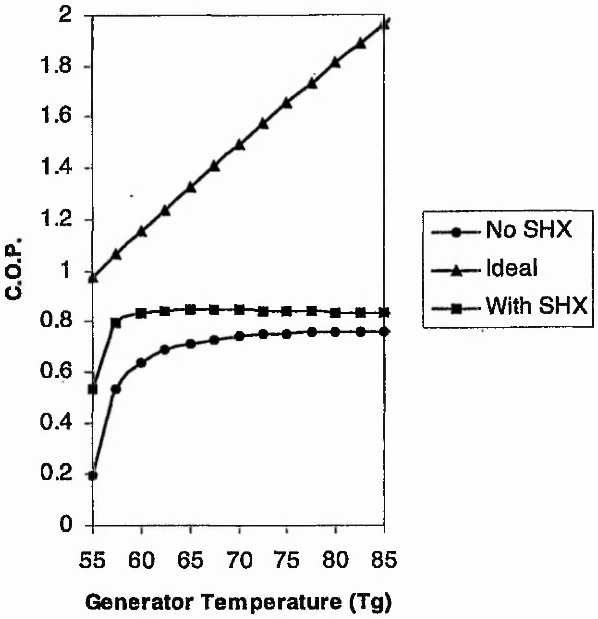

Figure 4.5 Comparison of Ideal COP and COP changes of ACS with and without SHX (Solution heat exchanger) [H_2O-LiBr].

Since no system can violate the First Law of thermodynamics, it is reasonable to conclude that a designed ACS system must at least satisfy the First Law. However, satisfying the First Law alone does not ensure that the process will actually take place. For instance, the First Law can be used to dictate the amount of electrical energy supplied to the resistance wires for heating to be equal to the amount of energy transferred to the room as heat. An attempt to reverse the process by supplying a similar amount of heat to the wire will not cause an equivalent amount of electrical energy to be generated in the wires as before, even though doing so would not violate the First Law.

It is clear that the First Law places no restrictions on the direction of the process. As energy is conserved in the First Law analysis, the effect of irreversible processes, such as chemical changes and pressure drops may be overlooked. The First Law does not distinguish between heat and work, and thus it cannot indicate whether one form of energy can be converted completely to another. These inadequacies of the First Law are overcome by introducing a further analysis namely the Second Law of thermodynamics.

4.2 Second Law of Thermodynamic Analysis

The First Law of thermodynamics only deals with the quantity of energy while the Second Law introduced in this section deals with the quality as well as the quantity of energy. More specifically, it is concerned with the degradation of energy during a process. The Second Law can be used to optimise complex thermodynamic systems by tackling the bottleneck in the system. In this project, exergy ('availability') analysis is used. Exergy always decreases during real irreversible processes and the magnitude is a measure of irreversibility. The irreversibilities include mechanical friction, heat transfer, chemical changes, pressure drop and throttling.

4.2.1 The mathematical model

Exergy is defined as the maximum possible reversible work that can be obtained from a fluid. Exergy of enthalpy is the sum of exergy of internal energy and exergy of flow work.

$$\begin{aligned} E_h &= E_u + E_w \\ &= [(u - u_o) + P_o(\mathrm{v} - \mathrm{v}_o) - T_o(s - s_o)] + (P - P_o)\mathrm{v} \\ &= (u + P\mathrm{v}) - (u_o + P_o v_o) - T_o(s - s_o) \\ &= h - h_o - T_o(s - s_o) \end{aligned} \tag{4.12}$$

If the reference datum state is set at T_o, the exergy of enthalpy is defined as

$$E = h - T_o s - g_o \tag{4.13}$$

Where $g_o = \mu_o = h_o - T_o s_o$

The term h_o and s_o represent the enthalpy and entropy values at reference temperature T_o which is usually taken as ambient temperature. The rate of exergy loss for steady flow can be expressed as

$$\Delta E = \sum \dot{m}_i E_i - \sum \dot{m}_o E_o + \dot{Q}\left(1 - \frac{T_o}{T}\right) + W \tag{4.14}$$

The first two terms on the right hand-side represent the net exergy transfer by mass. The third term is exergy transfer due to heat transferred, $\dot{Q}$ at constant temperature T.

$\dot{Q}$ is positive if heat is added to the system (for eg. $\dot{Q}_{evap}$) The last term is the exergy transfer due to mechanical work, W

For each component, the energy change and exergy production can be calculated as follows:

Energy change

$$\dot{Q}_{evap} = \dot{m}_7(h_{10} - h_9) = \dot{m}_{17}(h_{17} - h_{18}) \tag{4.15}$$

$$\dot{Q}_{con} = \dot{m}_7(h_7 - h_8) = \dot{m}_{15}(h_{16} - h_{15}) \tag{4.16}$$

$$\dot{Q}_{gen} = \dot{m}_7 h_7 + \dot{m}_4 h_4 - \dot{m}_3 h_3 = \dot{m}_{11}(h_{11} - h_{12}) \tag{4.17}$$

$$\dot{Q}_{abs} = \dot{m}_7 h_{10} + \dot{m}_4 h_6 - \dot{m}_3 h_1 = \dot{m}_{13}(h_{14} - h_{13}) \tag{4.18}$$

Exergy production

The exergy changes in water are obtained from

$$\Delta E_{comp,\,water} = \dot{m}_{water,\,i}(E_{hot} - E_{cold}) \tag{4.19}$$

The irreversibility which occurs during the heat transfer process can be measured by the difference between the exergy of the heat flux $\dot{Q}$ and the exergy change in the cooling water or heated water (heat source for generator).

$$\Delta E_{comp,\,ht} = \dot{m}_{water,\,i}(E_i - E_o) + \dot{Q}_{comp}\left(1 - \frac{T_o}{T_{comp}}\right) \tag{4.20}$$

where *comp* in Equations 4.19 and 4.20 represent absorber, generator, condenser and evaporator respectively and $\dot{Q}_{comp}$ is negative for the evaporator and generator and positive for the condenser and absorber. The heat transfer irreversibility of solution heat exchanger is defined as follows:

$$\Delta E_{shx,\,ht} = \dot{m}_4(E_4 - E_5) + \dot{m}_3(E_2 - E_3) \tag{4.21}$$

Internal reversibility is defined as the difference between the exergy change of the working fluid (refrigerant or solution) and the exergy of the heat flux. Internal reversibility for the four reservoirs are obtained as follows:

$$\Delta E_{comp,\,in} = \sum \dot{m}_i E_i - \sum \dot{m}_o E_o + \dot{Q}_{comp}\left(1 - \frac{T_o}{T_{comp}}\right) \tag{4.22}$$

where Q_{comp} is positive for the evaporator and generator and negative for the condenser and absorber. Other irreversibilities for throttling valves and solution pump can be computed as follows:

Solution throttling valve

$$\Delta E_{sol.valve} = \dot{m}_4 v_5 (P_5 - P_6) \qquad (4.23)$$

Refrigerant throttling valve

$$\Delta E_{ref.valve} = \dot{m}_7 (E_8 - E_9) \qquad (4.24)$$

Solution pump

$$\Delta E_{pump} = \frac{\dot{m}_1 (P_1 - P_2) v_1}{\eta_{pump}} \qquad (4.25)$$

Circulation ratio

$$f = \frac{\dot{m}_1}{\dot{m}_7} \qquad (4.26)$$

The coefficient of performance and the exergetic coefficient of performance of the ACS are defined as:

$$COP = \frac{\dot{Q}_{evap}}{W_p + \dot{Q}_{gen}} \qquad (4.27)$$

$$ECOP = \frac{\dot{Q}_{evap}\left(1 - \frac{T_o}{T_e}\right)}{\dot{Q}_{gen}\left(1 - \frac{T_o}{T_g}\right) + W_p} \qquad (4.28)$$

4.2.2 Effect of changes in operating parameters with ECOP

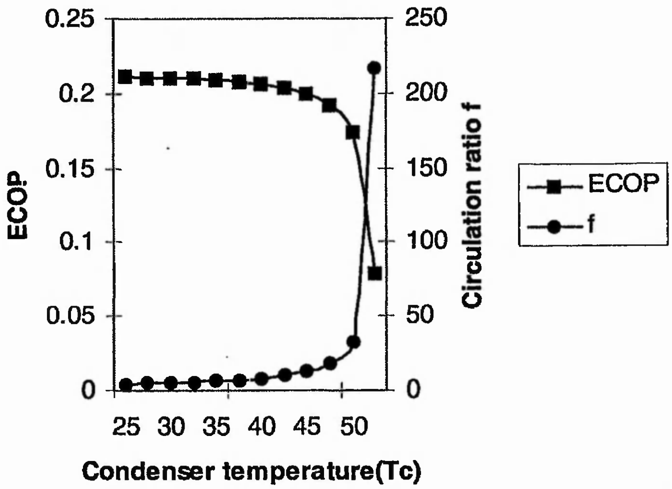

Figure 4.6 Variations in ECOP and circulation ratio with condenser temperature (T_e = 8 °C, T_a = 30 °C, T_g = 80°C, η_{SHX} = 0.8)

The changes of ECOP and circulation flow ratio f with various operating parameters are shown in Figures 4.6 – 4.8. Figure 4.6 and Figure 4.7 show that the ECOP decrease gradually with increasing condenser and absorber temperatures respectively. After the plateau area at around 45 °C, the ECOP decreases rapidly and circulation ratio increase significantly in both cases. Thus the maximum condensing temperature should be maintained to be less than 45°C.

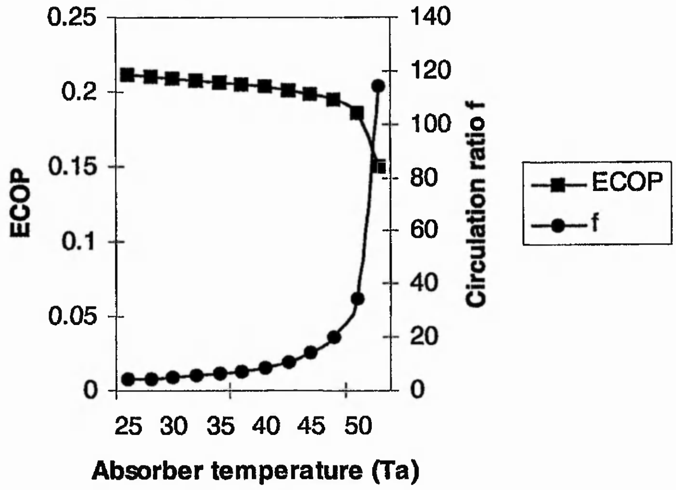

Figure 4.7 Variations in ECOP with absorber temperature (T_e = 8 °C, T_c = 30 °C, T_g = 80°C, η_{SHX} = 0.8)

From Figure 4.7, it is clear that increases in absorber temperature have a similar trend. By selecting a higher absorber temperature, the solution can be easily cooled by air. The size of the absorber can be reduced due to a higher temperature difference between the ambient and the absorber. However, increasing the temperature of the absorber will eventually cause a dramatic drop in ECOP. Although this will have the benefit of using a smaller absorber, without sacrificing much of the performance, the temperature absorber should be kept below 45°C.

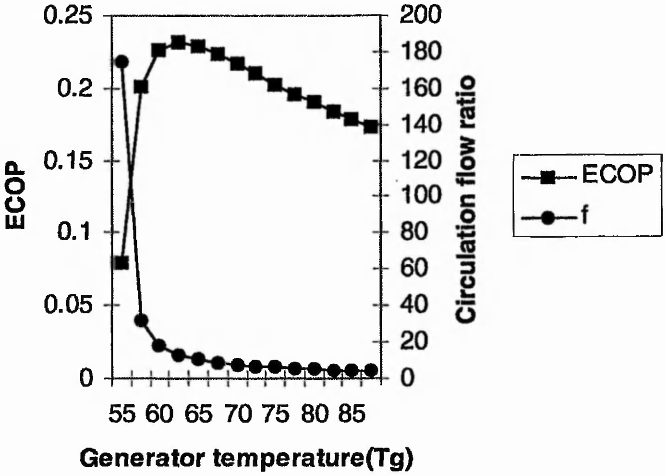

Figure 4.8 Variations in ECOP with generator temperature

($T_e = 8\,^0C$, $T_a = T_c\ 30\,^0C$, $\eta_{SHX} = 0.8$)

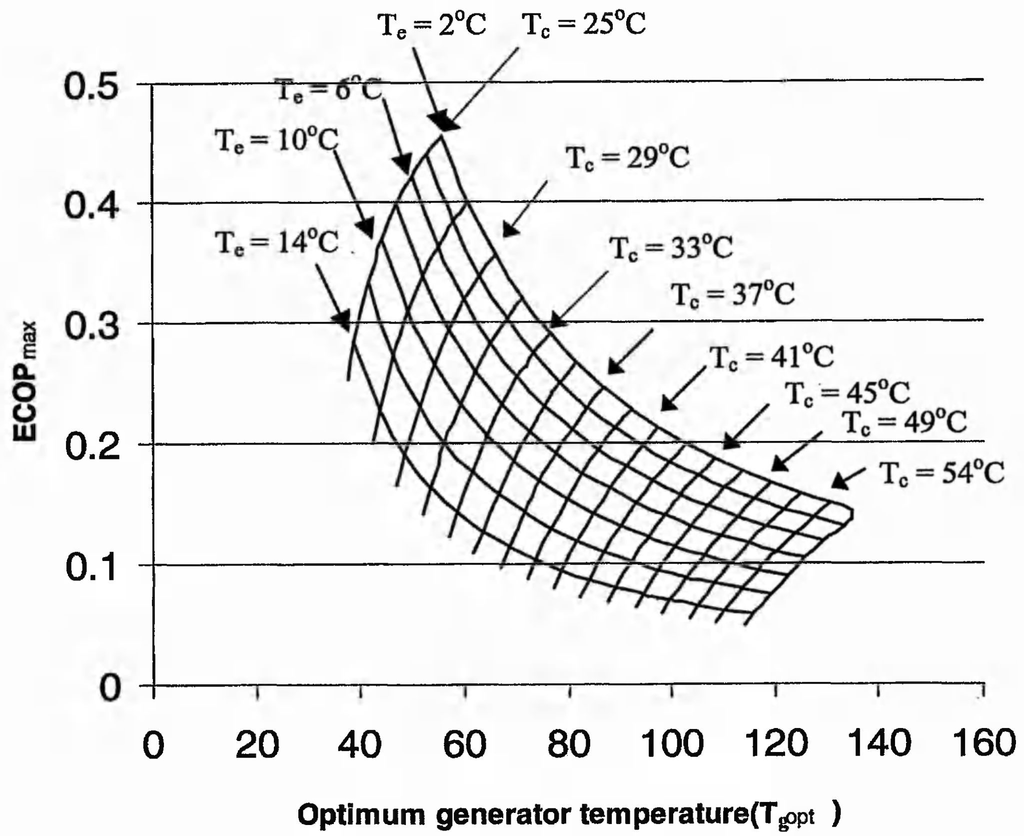

Figure 4.9 Optimum design map giving max. system ECOP for $T_a = T_c$

Note: (The performance is better for $T_a = T_c$ compared to $T_a > T_c$ or $T_c > T_a$)

4.2.3 Optimal design map and equations

Figure 4.8 shows that the incremental change of generator temperature (T_g) initially affects ECOP considerably until a maximum point is reached. After this, any increase of temperature leads to a decrease in ECOP. The maximum point shown is crucial and it is often useful to find this optimal point when designing ACS. Equations for finding maximum COP_{max} for an ACS at optimum generator temperature $T_{g\ opt,\ COP}$ in terms of T_a, T_c, and T_e was developed using non-linear regression analysis (Tan, 1999). The ECOP is defined in Equation 4.28 while the maximum $T_{g\ opt,\ ECOP}$ and $ECOP_{max}$ can be deduced from a numerical fit of the Equations 4.29 and 4.30 respectively for the range of $28 \leq (T_a = T_c) \leq 45$ and $2 \leq T_e \leq 15$.

$$T_{g_{max}} = a + b.T_e + (c + d.T_e).T_a + (e + f.T_e + (g + h).T_a).T_a \tag{4.29}$$

where **a = -2.343219192, b = -1.135652944, c = -4502.586606, d = 26.101749670,**

e = 4504.8869247, f = -26.11224489, g = -15.34085944, h = 15.346014458

$$ECOP_{max} = a + b.T_e + c.T_e^2 + d.T_a + e.T_a.T_e + f.T_a.T_e^2 + g.T_a^2 + h.T_a^2.T_e + i.T_a^3 + j.T_a^4 \tag{4.30}$$

where **a = 3.359594430, b = -.015556309, c = -.001295833, d = -.241988978,**

e = .000584445, f = .000024438, g = .007373192, h = -8.62584E-06,
i = -.000104200, j = 5.63506E-07

The convenient use of the map in Figure 4.9 is described as follows. For given evaporator and absorber temperatures, the two curves intersect at a point. At this point, its coordinates give a value for generator temperature and a value for ECOP. This is the optimum generator temperature and the maximum ECOP the system can achieve. The map enables the deduction of control of parameters to achieve maximum performance for differing requirements.

4.2.4 Effect of changes in evaporator & condenser temperature

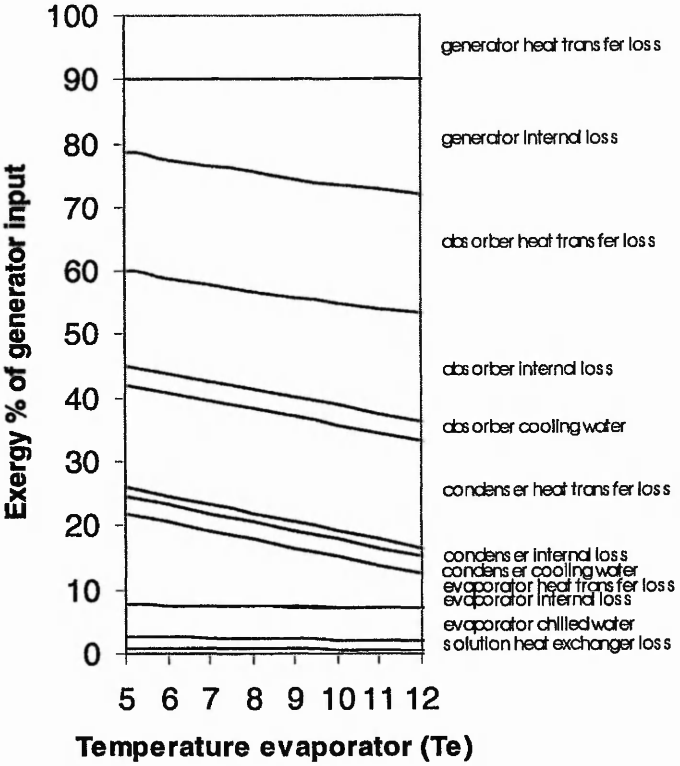

Figure 4.10

In order to understand the overall performance characteristics it is useful to evaluate sensitivity of the effective component using the exergy approach based on the Second Law. Defining the exergy loss for each component as a percentage of the total exergy loss, the variations of these losses due to changes in operating temperatures are plotted in Figure 4.10 to Figure 4.13. From Figure 4.10 and Figure 4.11 a reduction in their heat transfer irreversibility can be achieved if evaporator temperature is increased and condenser temperature is decreased. Although the evaporator heat transfer irreversibility is lower than the exergy loss in the generator and absorber, it has a high impact on the system performance. The height of the band between any two lines is the value of exergy change in each component obtained from Equations 4.15 to 4.28. It can be seen from Figure 4.10 to Figure 4.13 that the generator irreversibility makes up 22% to 33% of the total exergy loss.

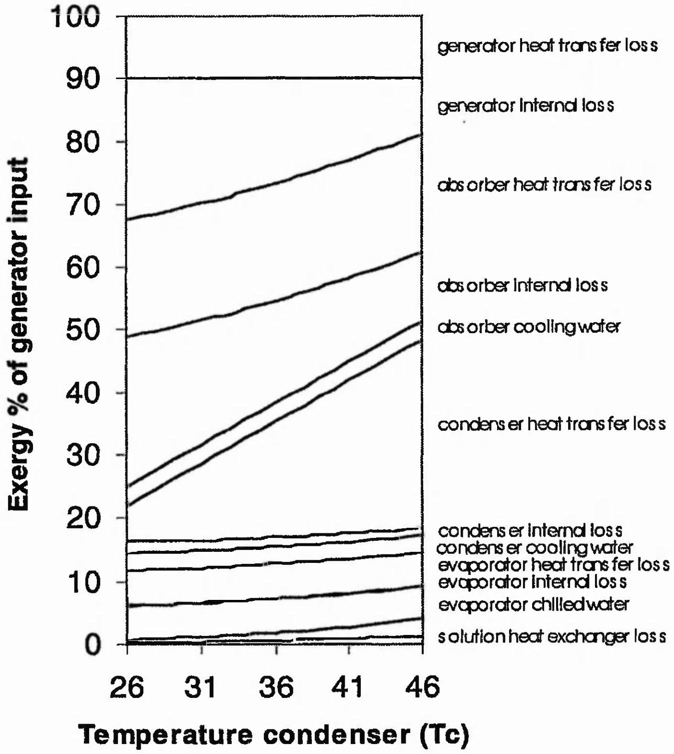

Figure 4.11

It is also seen from the four figures that the irreversibility due to heat transfer is significant compared to the internal loss. The absorber also contributes a large percentage of losses from 15% to 40% of the total exergy change. More than half of the absorber irreversibility is apparently due to internal loss. The internal irreversibility results from the high temperature solution entering from the solution heat exchanger and rejecting heat to low-temperature cooling water. Also, during the absorption process, the chemical potential of the vapour is greater than that of the water component of the solution. These important factors, however, were omitted in most of the past literature. Using a more effective solution heat exchanger can decrease both the generator and absorber irreversibilities. This will also reduce the circulation flow ratio. The use of a solution heat exchanger represents 5% and 3%

improvements in the generator and absorber respectively resulting in nearly 20% reduction of the total irreversibility.

4.2.5 Effect of changes in absorber & generator temperature

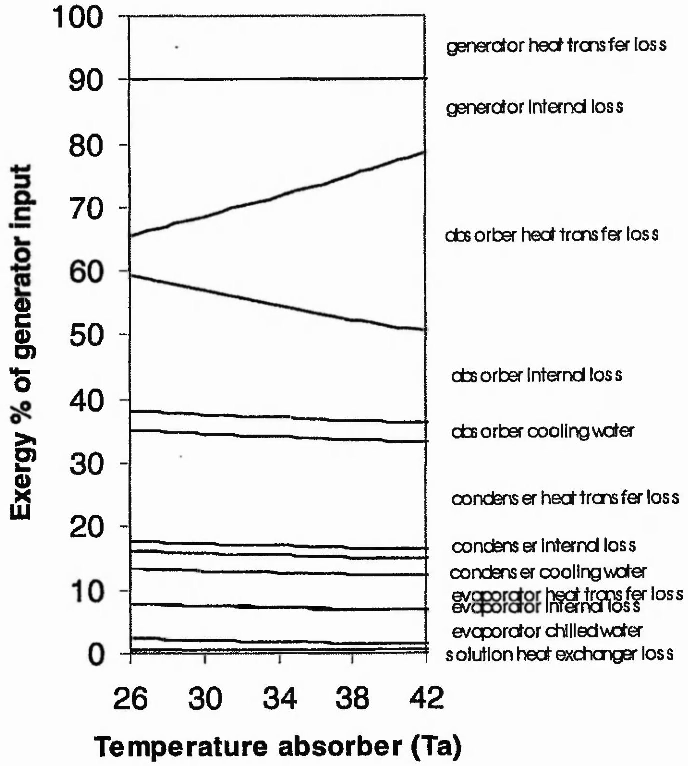

Figure 4.12

It is observed that the total irreversibilities of the absorber are more than the total irreversibilities of the generator as the absorber temperature increases. The decrease of irreversibilities at the generator are due to increase of heat transfer in the solution heat exchanger since the temperature leaving the absorber and entering the solution heat exchanger is increased. The heat transfer loss in the absorber makes the largest contribution of total loss, thus, it is important to pay careful attention when designing the absorber. The heat transfer loss may be decreased if a recirculation circuit is added. In this circuit, part of the weak solution can be diverted back to the absorber so that more absorption can take place, while the returning solution also functions as pre-cooling of strong solution from the generator. The remaining weak solution is pumped to the generator for desorption. This design was used in this project. The details are shown in Chapter 7.

The temperature drop during heat transfer can be reduced by using an effective generator. Figure 4.12 shows that the increase of the temperature generator using an effective generator will reduce the irreversibility of heat transfer. It is seen that the increase of the generator temperature without increasing the effectiveness of the solution heat exchanger and absorber will result in an increase of the total irreversibility in absorber will increase.

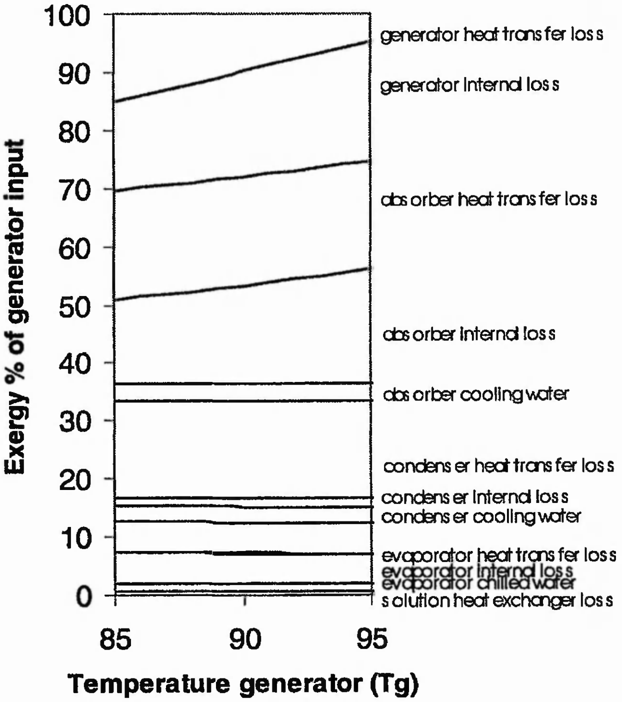

Figure 4.13

The increase in effectiveness of the solution heat exchanger, however, is limited by the crystallisation (See Appendix E) characteristics of salt-mixtures. In order to prevent crystallisation, it is essential to control the lowest temperature to be 5 °C above the crystallisation point at any point on the solution mixtures path. This can be achieved by controlling the solution flow rate or reducing the solution heat exchanger effectiveness. From this analysis, it is possible to establish an optimum point for the pgenerator temperature. A further increase in the temperature generator will only be beneficial if extra components such as a second stage system is employed. Adding components will increase the cost, which is the main barrier of ACS being introduced to the market. Thus, this study is principally aimed at improvements using alternative working fluids and a more effective absorber.

4.3 Critical appraisal of approaches

This chapter has demonstrated the simplicity of using the First Law as a basic tool for analysing an ACS. The assumptions of the ACS being an endoreversible machine has simplified the solutions. The results, however, will not reflect the real situation which is far more complex. The use of First Law has thus far provided a rapid view of system characteristics due to variation in operating parameters. The First Law is also a useful tool for comparing alternative working fluids. The approach only needs basic thermodynamic properties such as enthalpy [h(T,x)], pressure- temperature-concentration [p(T,x)] relationship and the density [ρ(T,x)] of the solution mixture. Further detailed investigation need other properties such as entropy, thermal conductivity, viscosity, diffusion and mass transfer coefficient.

Mathematical models for exergetic analysis based on the Second Law of thermodynamics have also been developed. More effective tools incorporating the Second Law analysis provides a better understanding of cycle performance and an insight which the First Law does not. By evaluating the irreversibility of individual components, improvements can be justified and modified to achieve the best performance. This approach only needs an extra property namely entropy.

The internal irreversibilities, which contribute to nearly half of the total irreversibility, were omitted in most of the past literature. This work has addressed this problem by including the internal irreversibility to achieve a more accurate overall insight into the system characteristics.

In order to simplify the analysis, a computer program has been developed for First and Second Laws analyses. This will be discussed further in the next chapter.

Chapter 5 Computer Simulation of System

5.1 Introduction

Computer modelling is becoming increasingly popular in recent years as microprocessor speed is increasing exponentially while the price of computers is decreasing to an affordable level. This trend has enabled the design and analysis of complex system more effective. Expensive experimental work can be kept to a minimum through practical predictions using semi-empirical and numerical modelling. Analysis of characteristics due to the changes in variation of operating parameters and the development of an optimum design map as discussed in Chapter 4 would have needed more than seven thousand computing cycles and taken months or even years if carried out manually. With the help of Pentium 166 MHz machines, the results were obtained in less than three days. The results were plotted into graphs in seconds. The graphs had provided a better means of understanding the system characteristics. The data-logging software, which will be discussed in Chapter 8, is a good example of the computer power utilisation. The software can capture signals from 70 channels of transducers at intervals of less than 20 seconds, which is impractical if recorded manually, and the possibilities of human error would be very high.

5.2 Computer program

In the development of an absorption cooling system, a number of computer tools were developed and combined into a user-friendly software package named ABCON. The overall developments can be represented by the flow chart as in Figure 5.1 and the main interface as shown in Figure 5.2.

5.2.1 Carpet plot of working fluids

The first step was to construct functions of thermodynamic and transport properties of working fluid/mixtures. The properties of eight working mixtures have been programmed into the software (Figure 5.3). These properties can be plotted using the carpet plot functions for varying parameters. Print preview, paper size and printer selection functions have been included. The x and y axes can be swapped and adjusted to the plot range of interest. These properties are then used in the analysis program using the First and Second Laws of thermodynamics.

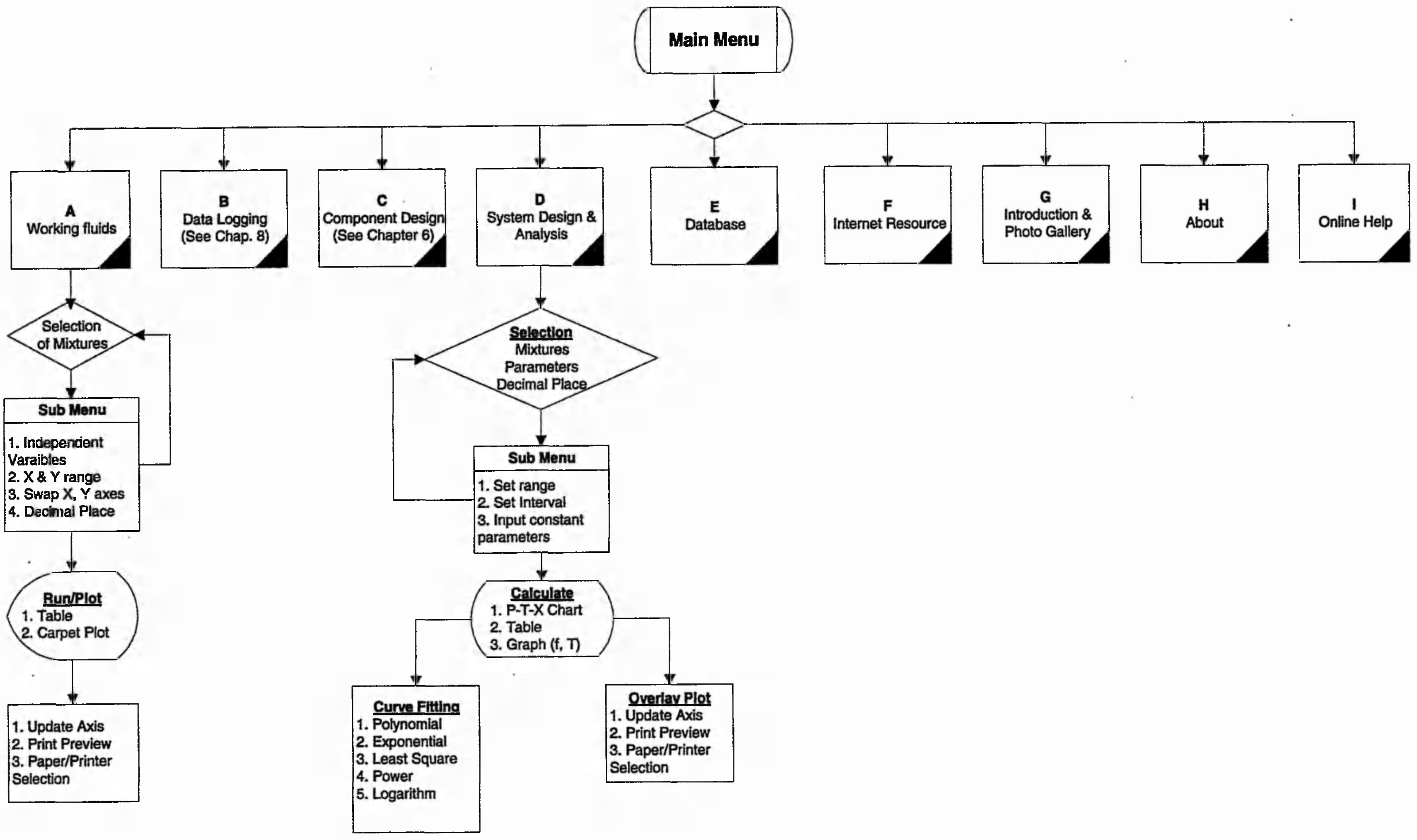

Figure 5.1 Flow Chart of ABCON

Figure 5.2 Main Interface of ABCON

A. Working Fluids - Thermodynamics properties for 8 mixtures.
- Carpet Plot of properties

B. Data Logging - Calibration
- Analogue Computer Gauges
- Library of Sensors
- Online Chart
- Full display of I/O control with LED and Message LED.
- Safety Control
- Print Preview of Table and Chart
- Save Chart to JPEG, Export to Clipboard.

(For details, see chapter 8)

C. Component Design - Model Calculation
- Absorber, Generator, Condenser and Evaporator Design

(For details, see chapter 6)

D. System Analysis & Calculations
- 3 main working mixtures
- 6 parametric studies
- Overlay plot of results
- 6 types of curve fitting
- Detailed results in table

E. Database – Over 400 journals and articles, 100 book references

F. Internet Resources – Internet homepage for absorption chiller.

G. Introduction and Photo Gallery

H. About

I. Online Help

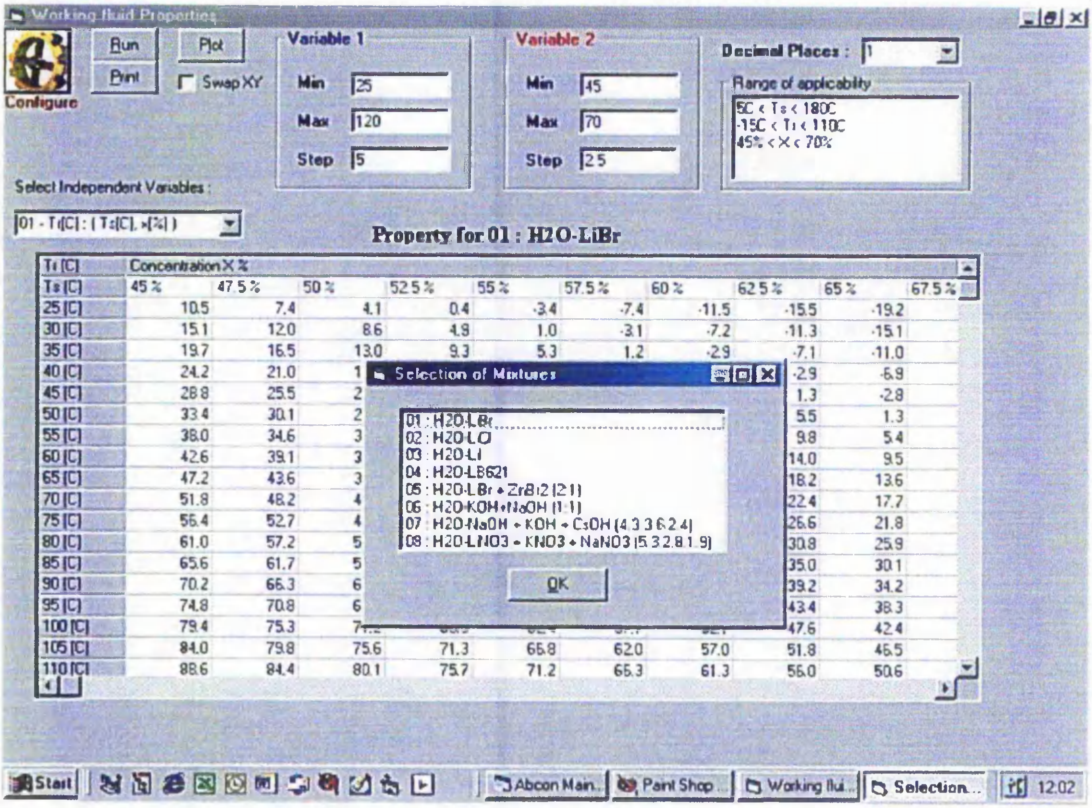

☐ Swap XY

Variable 1
Min 25
Max 120
Step 5

Variable 2
Min 45
Max 70
Step 2.5

Decimal Places : 1

Range of applicabilty
5C < Ts < 180C
-15C < Ti < 110C
45% < X < 70%

Select Independent Variables : 01 - Ti[C] : (Ts[C], x[%])

Property for 01 : H2O-LiBr

Ti [C]	Concentration X %									
Ts [C]	45 %	47.5 %	50 %	52.5 %	55 %	57.5 %	60 %	62.5 %	65 %	67.5 %
25 [C]	10.5	7.4	4.1	0.4	-3.4	-7.4	-11.5	-15.5	-19.2	
30 [C]	15.1	12.0	8.6	4.9	1.0	-3.1	-7.2	-11.3	-15.1	
35 [C]	19.7	16.5	13.0	9.3	5.3	1.2	-2.9	-7.1	-11.0	
40 [C]	24.2	21.0	[illegible]	[illegible]	[illegible]	[illegible]	[illegible]	-2.9	-6.9	
45 [C]	28.8	25.5	[illegible]	[illegible]	[illegible]	[illegible]	[illegible]	1.3	-2.8	
50 [C]	33.4	30.1	[illegible]	[illegible]	[illegible]	[illegible]	[illegible]	5.5	1.3	
55 [C]	38.0	34.6	[illegible]	[illegible]	[illegible]	[illegible]	[illegible]	9.8	5.4	
60 [C]	42.6	39.1	[illegible]	[illegible]	[illegible]	[illegible]	[illegible]	14.0	9.5	
65 [C]	47.2	43.6	[illegible]	[illegible]	[illegible]	[illegible]	[illegible]	18.2	13.6	
70 [C]	51.8	48.2	[illegible]	[illegible]	[illegible]	[illegible]	[illegible]	22.4	17.7	
75 [C]	56.4	52.7	[illegible]	[illegible]	[illegible]	[illegible]	[illegible]	26.6	21.8	
80 [C]	61.0	57.2	[illegible]	[illegible]	[illegible]	[illegible]	[illegible]	30.8	25.9	
85 [C]	65.6	61.7	[illegible]	[illegible]	[illegible]	[illegible]	[illegible]	35.0	30.1	
90 [C]	70.2	66.3	[illegible]	[illegible]	[illegible]	[illegible]	[illegible]	39.2	34.2	
95 [C]	74.8	70.8	[illegible]	[illegible]	[illegible]	[illegible]	[illegible]	43.4	38.3	
100 [C]	79.4	75.3	[illegible]	[illegible]	[illegible]	[illegible]	[illegible]	47.6	42.4	
105 [C]	84.0	79.8	75.6	71.3	66.8	62.0	57.0	51.8	46.5	
110 [C]	88.6	84.4	80.1	75.7	71.2	66.3	61.3	56.0	50.6	

Selection of Mixtures

01 : H2O-LiBr
02 : H2O-LiCl
03 : H2O-LiI
04 : H2O-LB621
05 : H2O-LiBr + ZnBr2 (2:1)
06 : H2O-KOH+NaOH (1:1)
07 : H2O-NaOH + KOH + CsOH (4.3:3.6:2.4)
08 : H2O-LiNO3 + KNO3 + NaNO3 (5.3:2.8:1.9)

OK

Figure 5.3 Computerised table of thermodynamic properties of 8 different mixtures

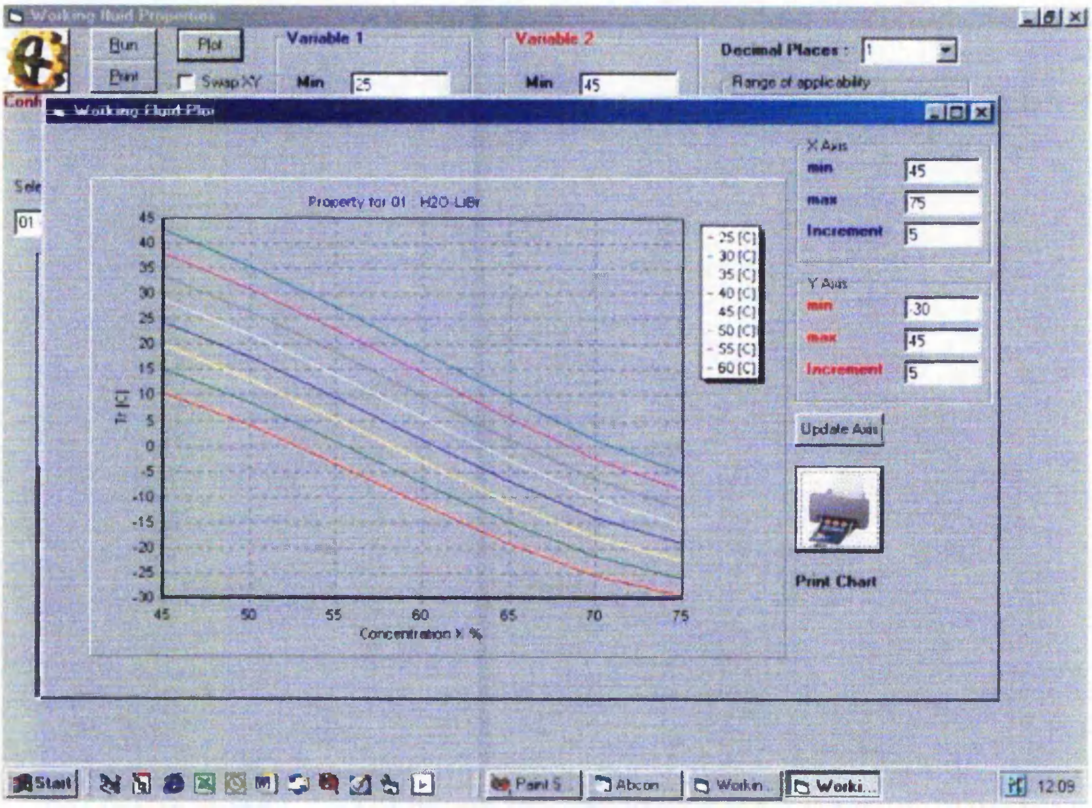

Variable 1 Min: 25

Variable 2 Min: 45

Decimal Places : 1

X Axis
min: 45
max: 75
Increment: 5

Y Axis
min: -30
max: 45
Increment: 5

Figure 5.4 Carpet plot of thermodynamic properties

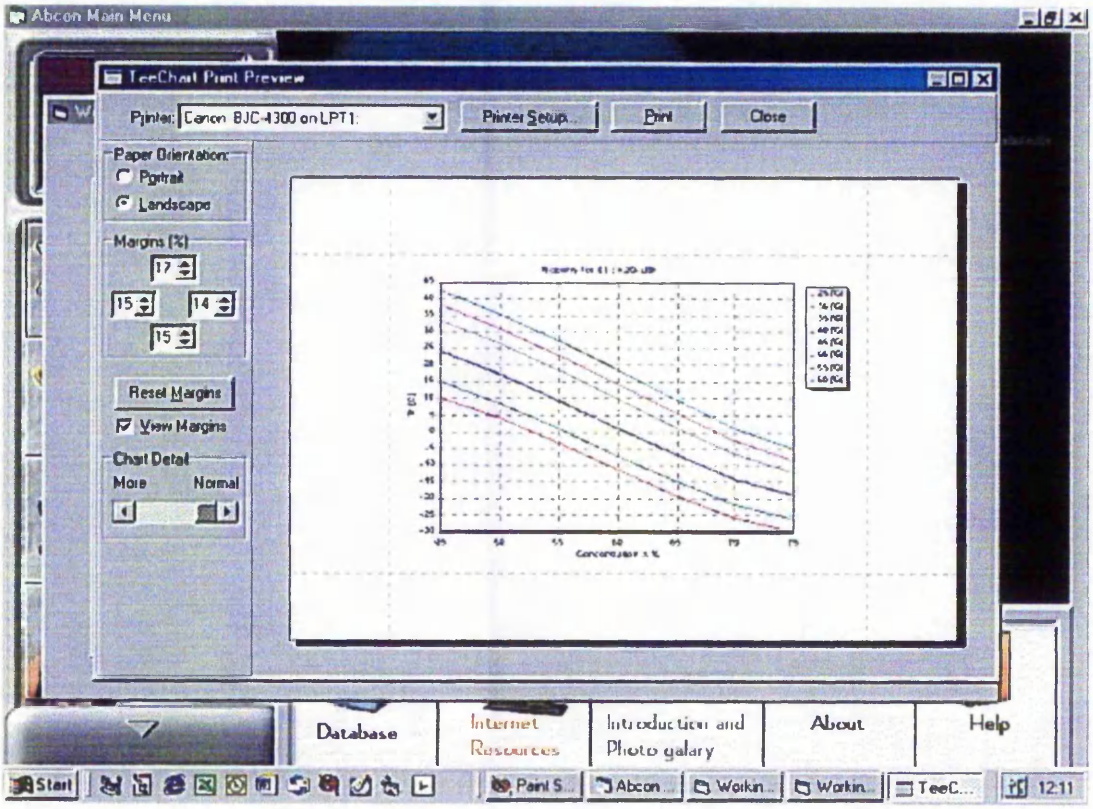

Printer: Canon BJC-4300 on LPT1:

Paper Orientation:
○ Portrait
● Landscape

Margins (%)
17
15
14
15

☑ View Margins

Figure 5.5 Print preview for Carpet plot.

5.2.2 System analysis and calculations

This part of the program is mainly based on the mathematical model discussed in Chapter 4. After clicking the button D as shown in Fig. 5.2, a dialogue box appears. It allows the user to choose the working mixtures, operating parameters and the number of decimal place for analyses. After initial configuration, a sub-menu (Fig.5.6) will appear.

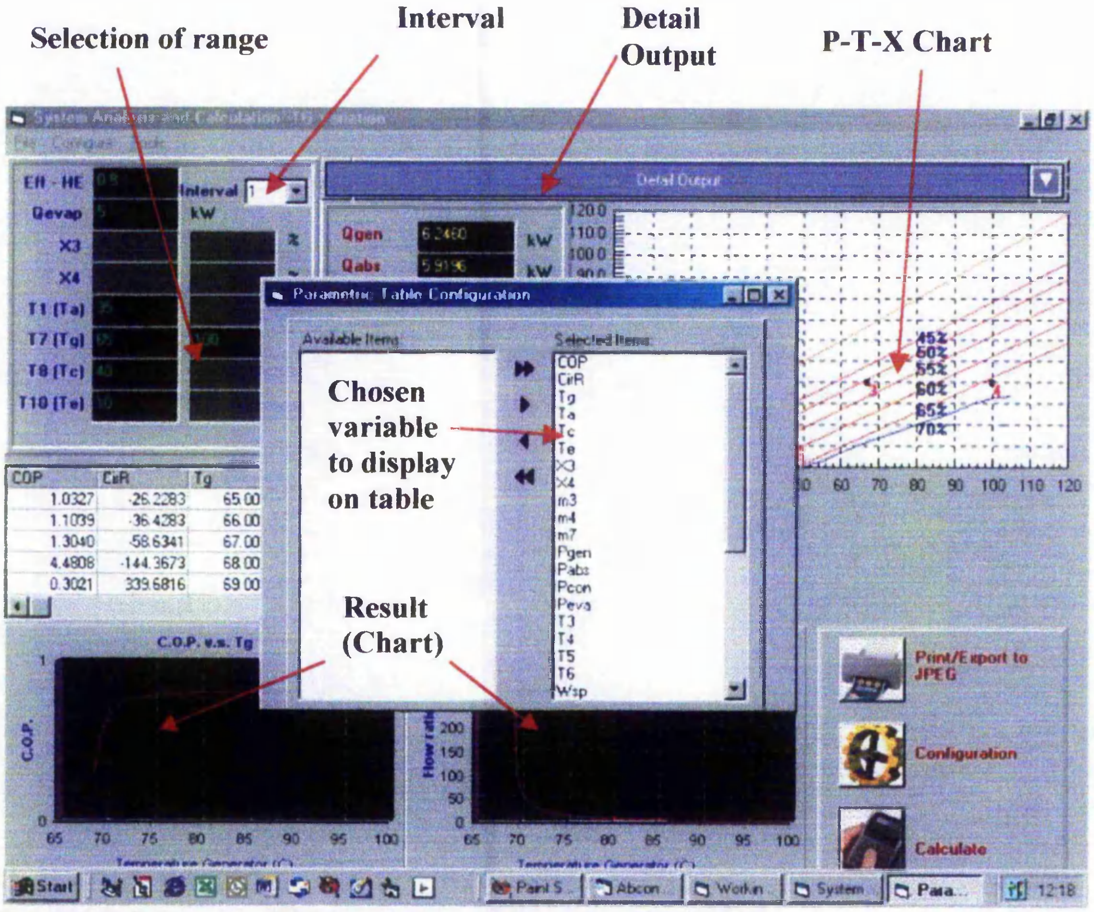

Eff - HE 0.9
Qevap 5
Interval 1
T1 (Ta) 35
T7 (Tg) 65 100
T8 (Tc) 40
T10 (Te) 10
Qgen 6.2460 kW
Qabs 5.9196 kW

COP	CiR	Tg
1.0327	-26.2283	65.00
1.1039	-36.4283	66.00
1.3040	-58.6341	67.00
4.4808	-144.3673	68.00
0.3021	339.6816	69.00

Fig. 5.6 Sub Menu - Selection of variables to be displayed.

A range of operating parameters and intervals/steps can be set for analysis. Upon clicking on the configuration menu and selecting the parametric table, a box with two boxes will emerge as shown in Fig. 5.6. This feature allows the user to choose the parameters, so that it will be shown in the table as well as used for the subsequent overlay plot. In Fig. 5.6, all items are selected. By clicking the 'Calculate' button on the lower right corner, the results will show on the line charts, table and P-T-X chart. These charts can be exported to JPEG file, printed or copied to the clipboard and pasted to other applications such as Microsoft Word. The detailed results are hidden in a drop down box due to the limitation of screen space.

The overlay plot function can be accessed through the Tools menu. Selecting a single operating parameter on the *x*-axis and unlimited number of parameters on *y*-axis an overlay plot graph can be created (See Fig. 5.7). Both axes can be adjusted for the range of interest and set to the required interval. Again this chart can be previewed before printing. Titles of the chart and axes can also be edited.

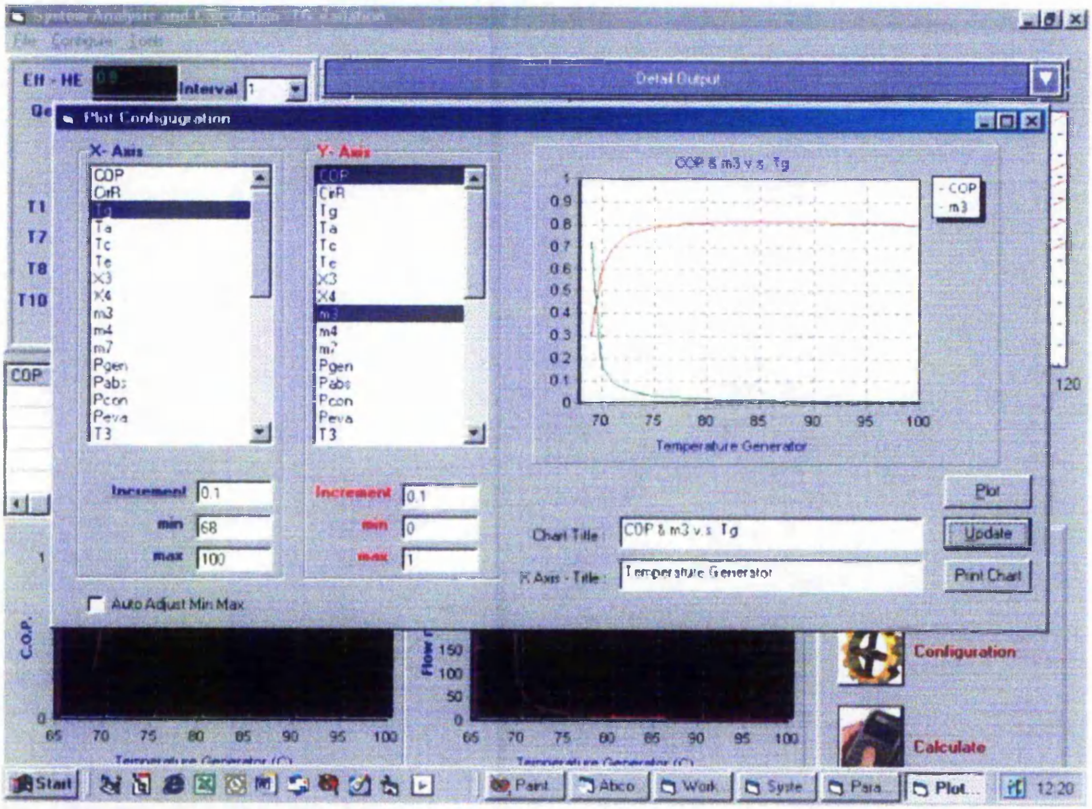

X- Axis: Increment 0.1, min 68, max 100

Y- Axis: Increment 0.1, min 0, max 1

Chart Title: COP & m3 v.s Tg

X Axis - Title: Temperature Generator

☐ Auto Adjust Min Max

Fig. 5.7 Overlay plot of result

5.2.3 Curve fitting

One of the main features in this program is curve fitting. This feature is accessible from the 'Tools' menu only after the first calculation has taken place. A minimum of two other variables have to be chosen. There are, in total, six types of curve fitting routines available in the program (see Fig 5.8). The program can be used to fit any calculated values selected previously as shown in the table.

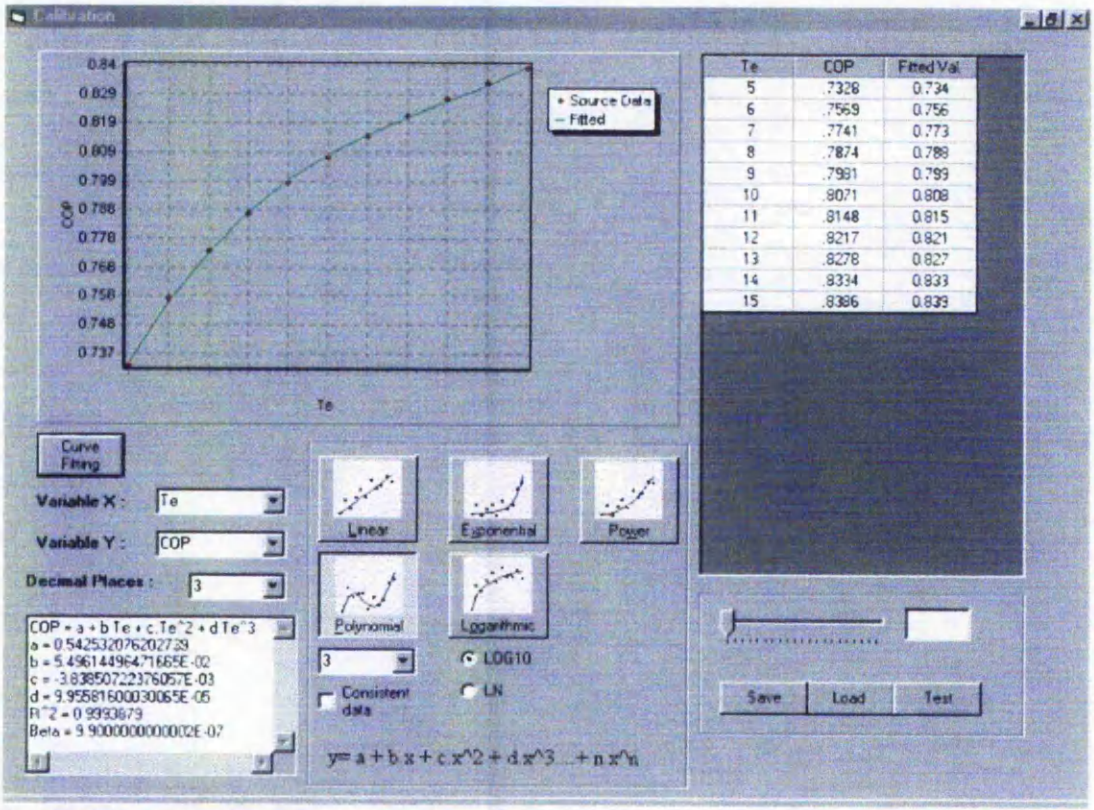

Te	COP	Fitted Val
5	.7328	0.734
6	.7569	0.756
7	.7741	0.773
8	.7874	0.788
9	.7981	0.799
10	.8071	0.808
11	.8148	0.815
12	.8217	0.821
13	.8278	0.827
14	.8334	0.833
15	.8386	0.839

Variable X : Te
Variable Y : COP
Decimal Places : 3

```
COP = a + b.Te + c.Te^2 + d.Te^3
a = 0.542532076202739
b = 5.49614496471665E-02
c = -3.83850722376057E-03
d = 9.95581600030065E-05
R^2 = 0.9993679
Beta = 9.90000000000002E-07
```

3
☐ Consistent data
● LOG10
○ LN

y= a + b.x + c.x^2 + d.x^3 ...+ n.x^n

Fig 5.8 Six options of Curve Fitting

Curve fitting for linear equations (Griffiths and Smith, 1991)

Least square fit is normally used to fit data for linear equations. The following function involving two unknown constants can be used:

$$f(x) = C_1 + C_2 . x \tag{5.1}$$

Following the general form of equation B_A1 in Appendix B, $f_1(x) = 1$ and $f_2(x) = x$. From equation B_A4 (Appendix B), the following system of two equations is to be solved:

$$C_1 = \frac{\sum_{i=1}^{n} y_i - C_2 \sum_{i=1}^{n} x_i}{n} \tag{5.2}$$

After substitution of C_1 and C_2 into the function f(x), the classical linear regression formula is obtained.

$$C_2 = \frac{n\sum_{i=1}^{n} x_i y_i - \sum_{i=1}^{n} x_i \sum_{i=1}^{n} y_i}{n\sum_{i=1}^{n} x_i^2 - \left(\sum_{i=1}^{n} x_i\right)^2} \tag{5.3}$$

Curve fitting for natural and base-10 logarithmic equations

The natural logarithm (base *e*) and base-*n* logarithms are fitted using a similar approach as the least square fit for linear equations. Both equations (Eqn. 5.4 & Eqn. 5.5) have two unknown constants as follows:

$$f(x) = C_1 + C_2.\log_e(x) \qquad (5.4)$$

$$f(x) = C_1 + C_2.\log_{10}(x) \qquad (5.5)$$

The n data points (x_1, y_1), (x_2, y_2).... (x_n, y_n) in linear curve fitting are now changed to $(\log_e(x_1), y_1)$, $(\log_e(x_2), y_2)$.... $(\log_e(x_2), y_n)$ and $(\log_{10}(x_1), y_1)$, $(\log_{10}(x_2), y_2)$.... $(\log_{10}(x_2), y_n)$ for natural and base-10 logarithm least square fit respectively.

Curve fitting for exponential equations

The exponential equation with two unknown constants is shown below

$$y = C_1.\exp(C_2.x) \qquad (5.6)$$

In order to fit the equation, it is linearised by converting the equation to

$$\mathrm{Ln}(y) = \mathrm{Ln}(C_1) + C_2.x \qquad (5.7)$$

The above equation is similar to the following equation

$$f(x) = A + B.x \qquad (5.8)$$

where $A = \mathrm{Ln}(C_1)$ and $B = C_2$

This equation is then solved to find the constants A and B by using least square fit. The equation is then reformed back to Equation 5.6 as follows:

$$\mathrm{Exp}[\ln(y)] = \exp[\ln(C_1)].\exp(C_2.x) \qquad (5.9)$$

Curve fitting for power equations

The power equation with two unknown constants is shown below

$$y = C_1 x^{C_2} \qquad (5.10)$$

To solve this equation, it is linearised into the following form:

$$\log_{10}(y) = \log_{10}(C_1) + C_2.\log_{10}(x) \qquad (5.11)$$

Equation 5.11 has a similar form to Equation 5.8 where $A = \log_{10}(C_1)$ and $B = C_2$. This equation is solved to find the constants A and B by using least square fit. The equation is reformed back to Equation 5.10 as follows:

$$10\text{^}[\log_{10}(y)] = 10\text{^}[\log_{10}(C_1)].x^{C_2} \tag{5.9}$$

Polynomial curve fitting

There are two types of polynomial curve fitting. If the data used is consistent, the exact equation can be fitted using the ***POLCOF*** function. In practice, however, most data obtained is scattered. Thus another method using least square fit (Gerald and Wheatley, 1994) written in Fortran code was converted into Visual Basic function.

The correlation index of the curve fitted is defined as follows:

$$r^2 = 1 - \frac{\sum_{i=1}^{n}\left(y_i - y(x_i)_{fitted}\right)^2}{\sum_{i=1}^{n}\left(y_i - \langle y_i \rangle\right)^2} \tag{5.10}$$

where $$\langle y_i \rangle = \frac{\sum_{i=1}^{n} y_i}{n} \tag{5.11}$$

r^2 = coefficient of determination. For a perfect fit, $r^2 = 1$.

5.2.4 Other features

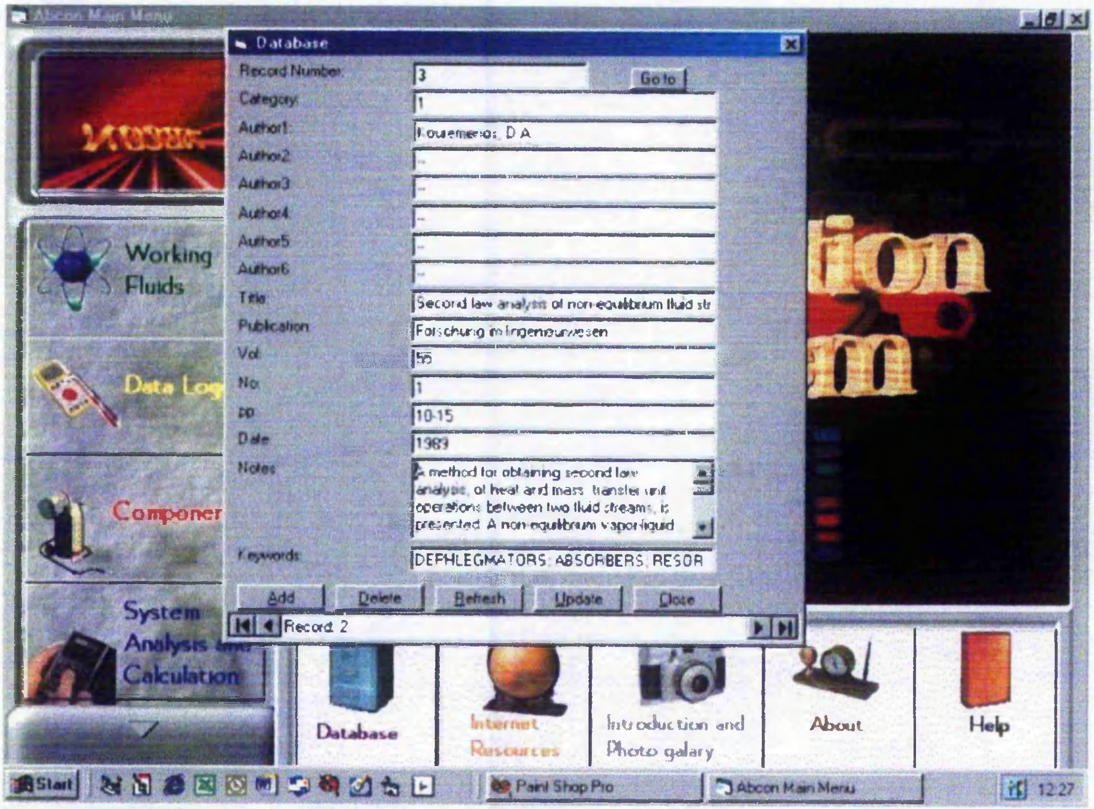

Record Number: 3
Category: 1
Author1: Kouremenos, D A
Author2: --
Author3: --
Author4: --
Author5: --
Author6: --
Title: Second law analysis of non-equilibrium fluid str
Publication: Forschung im Ingenieurwesen
Vol: 55
No: 1
pp: 10-15
Date: 1989
Notes: A method for obtaining second law analysis of heat and mass transfer unit operations between two fluid streams, is presented. A non-equilibrium vapor-liquid
Keywords: DEPHLEGMATORS; ABSORBERS; RESOR
Record: 2

Fig. 5.9 **Database – (~400 article, ~100 books and thesis)**

Other features include a database, which stores references of 400 articles and 100 books/thesis (See Fig. 5.9). The articles are further separated into 8 groups. An internet web page with useful links has also been published. Apart from these, a photo gallery of experimental work and a 'Help' facility is also available.

Chapter 6 Component Design

The Department of Energy, Transport and the Regions (DETR, 1999) recently published a practice guide intended to help identify the right technology for cooling using the absorption principle. This guide however only provides information at an introductory level for ACS users. Neither the DETR guide nor any published literature has provided enough information for the overall design for system components. In this chapter, design details of main components such as generator, evaporator, absorber and condenser are discussed. An estimation of pressure drop in pipelines and the amount of H_2O-LiBr mixture are also considered. Before designing any component for the ACS, identification of the availability of energy source, cooling load requirements and other operating parameters such as cooling water temperature needs to be established.

6.1 Design parameters

Input parameters

The following are the input data required to estimate the performance characteristics of the system and the capacity of components needed.

i) Refrigeration effect Q_e in kW – Cooling load of evaporator.
ii) Condensing temperature in °C (T_8)
iii) Absorber temperature in °C (T_1)
iv) Generator temperature in °C (T_4, T_7)
v) Evaporator temperature in °C (T_{10})
vi) Solution heat exchanger efficiency % (η_{shx})

A maximum evaporator load of 2kW was chosen, which is suitable for a small room. The temperature of absorber (T_a) and condenser (T_c) were chosen as 30 °C based on the assumption that the cooling water with temperature between 20°C to 25 °C is available. If the condenser is air cooled, normal practice, the temperature of absorber and condenser will need to be set at a minimum of 10°C above the ambient temperature, since the specific heat of air is lower than water. The generator temperature was selected based on the water temperature which is available from the domestic boiler. About 5 °C to 10 °C temperature drop is allowed during heat transfer from domestic boiler to the generator. The conditions for designing the experimental ACS are summarised as follows:

Refrigerating effect $\dot{Q}_{e,\max}$ = 2 kW
Temperature of condenser T_c (T_8) = 30 °C
Temperature of absorber T_a (T_1) = 30 °C
Temperature of generator T_g (T_4, T_7) = 80 °C
Temperature of evaporator T_e (T_{10}) = 8 °C
Heat exchanger efficiency = 80%

Pressure of condenser (P_c) and evaporator (P_e) are calculated by assuming saturated temperatures in both components: [Irvine and Lilly, 1984]

Pressure in condenser at 30 °C = 4.25 kPa
Pressure in evaporator at 8 °C = 1.07 kPa

Pressure drop between generator and condenser is only 3.40 Pa/m (Table 6.1). Pressure drop between evaporator and absorber is 8.83 Pa/m (Table 6.1). The pressure drops of two pipes are small enough to be neglected. Thus, pressure in generator $P_g \approx P_c$ and pressure in absorber $P_a \approx P_e$ in the following calculations.

x_3 = weak solution concentration at T_a and T_e = 0.502 wt/wt (50.2%)
x_4 = strong solution concentration at T_g and T_c = 0.629 wt/wt (62.9%)

From (Perez Blanco and Patterson, 1988)
h_1 = enthalpy at 30°C and 50.19% = 62.813 kJ/kg
$h_2 \approx h_1$ = 62.813 kJ/kg
$h_3 = h_1 + m_4/m_3\,(h_4 - h_5)$ = 120.998 kJ/kg
h_4 = enthalpy at 80°C and 62.9 % = 205.339 kJ/kg
h_5 = enthalpy at 40°C and 62.9% = 132.415 kJ/kg
$h_6 \approx h_5$ = 132.415 kJ/kg
From (Patil, K.R., 1991)
h_7 = enthalpy at 80°C (saturated vapour) = 2643.197 kJ/kg

h_8 = enthalpy at 30°C (saturated liquid) = 125.658 kJ/kg

$h_9 \approx h_8$ = 125.658 kJ/kg

h_{10} = enthalpy at 8°C (saturated vapour) = 2515.612 kJ/kg

Mass flow rate m_7 can be found by using the cooling load since h_9 and h_{10} are known.

Evaporator (Cooling) load

$$\dot{Q}_e = \dot{m}_7\,(h_{10} - h_9)$$

$$2\ \text{kW} = \dot{m}_7\,(2515.61 - 125.66)$$

$$\dot{m}_7 = 2 / (2515.61 - 125.66)$$

$$= 0.000837\ \text{kg/s}$$

Mass balance

$$\dot{m}_4 = \dot{m}_3 - \dot{m}_7 \qquad \textbf{(6.2)}$$

LiBr balance

$$\dot{\mathbf{m}}_3\mathbf{x}_3 = \dot{\mathbf{m}}_4\mathbf{x}_4 \qquad \textbf{(6.3)}$$

Therefore

$$\dot{m}_3 x_3 = (\dot{m}_3 - \dot{m}_7)x_4$$

$$m_3 = m_7 / (1 - x_3/x_4)$$

$$\dot{m}_3 = 0.000837 / (1 - 0.502/0.629)$$

$$= 0.00414\ \text{kg/s}$$

and

$$\dot{m}_4 = \dot{m}_3 - \dot{m}_7$$

$$= 0.00414 - 0.000837$$

$$= 0.00330\ \text{kg/s}$$

Condenser load

$$\dot{Q}_c = \dot{m}_7\,(h_7 - h_8) \qquad \textbf{(6.4)}$$

$$= 0.000837\,(2643.20 - 125.66)$$

$$= 2.1068\ \text{kW}$$

Generator load

$$\dot{Q}_g = \dot{m}_7 h_7 + \dot{m}_4 h_4 - \dot{m}_3 h_3 \qquad \textbf{(6.5)}$$

$$= 0.000837 \text{ x } 2643.20 + 0.00330 \text{ x } 205.38 - 0.00414 \text{ x } 121.00$$

$$= 2.3893 \text{ kW}$$

where

$\dot{m}_{10} = \dot{m}_7,\ \dot{m}_6 = \dot{m}_4, \dot{m}_1 = \dot{m}_3$

Absorber load

$$\dot{Q}_a = \dot{m}_{10} h_{10} + \dot{m}_6 h_6 - \dot{m}_1 h_1 \qquad \textbf{(6.6)}$$

$$= 0.000837 \text{ x } 2515.61 + 0.00330 \text{ x } 132.41 - 0.00414 \text{ x } 62.81$$

$$= 2.2826 \text{ kW}$$

6.2 Pipe work

Pressure loss consideration is crucial in systems using water-lithium bromide mixtures compared to ammonia-water mixtures because the sensitivity of performance changes with pressure loss is high. Ideally, there should be no pressure loss in the pipe work connecting the components namely generator, condenser, evaporator and absorber. Thus the selection of pipe was computed iteratively by increasing the pipe size until the pressure drop was acceptable. British Standard (BS EN 1057, 1996) was used as a guideline in designing the pipe work.

The maximum pressure drop is that between the high and low pressure side of the system which is controlled by three needle valves. Two needle valves were placed between the generator and absorber at the strong and weak solution side respectively. Another needle valve was placed in-between the condenser and evaporator to control the refrigerant flow rate and maintaining the pressure drop. Reducing the pressure drop between these pipes will enable a better control of the mass flow rate and pressure difference of the system using these valves.

Darcy-Weisbach equation is used to compute the pressure drop of fluid flowing through straight pipes as follows:

$$\frac{\Delta p}{\rho} = \frac{2fLV^2}{D} \qquad \textbf{(6.7)}$$

Where Δp = pressure drop, N/m^2

ρ = density kg/m^3

f = friction factor (dimensionless)

L = length, m

D = inside diameter of the pipe, m

V = mean velocity, m/s

$$f = \frac{\Delta p D}{2L\rho V^2} \qquad \textbf{(6.8)}$$

This can be further simplified into

$$f = \frac{16}{\mathrm{Re}} \text{ for laminar flow } (\mathrm{Re} < 2000) \qquad \textbf{(6.9)}$$

$$f = \frac{0.08}{\mathrm{Re}^{0.25}} \text{ for turbulent flow } (\mathrm{Re} > 4000) \qquad \textbf{(6.10)}$$

If the Reynolds number of the flow is between 2000 and 4000, the flow is considered to be in transition and the higher friction factor will apply.

The following conditions were used to calculate the pressure drop.

(i) Strong solution line:

Generator temperature, T_g = 80 °C

Strong solution concentration, x_s = 62.9 %

Solution density, ρ_s = 1741.9 kg/m^3

Solution viscosity, μ_s = 0.00344 N.s/m^2

Mass flow rate, $\dot{m}_s$ = 0.00330 kg/s

(ii) Weak solution line:

Temperature absorber, T_a = 30 °C

Weak solution concentration, x_w = 50.2 %

Solution density, ρ_w = 1529.3 kg/m^3

Solution viscosity, μ_w = 0.00299 N.s/m^2

Mass flow rate, $\dot{m}_w$ = 0.00414 kg/s

(iii) Generator-Condenser refrigerant vapour line

Temperature of vapour, T_g = 80 °C

Vapour density = 0.294 kg/m^3

Vapour viscosity, μ_s = 1.127 x10^{-5} kg/m.s

Mass flow rate, $\dot{m}_v$ = 0.00084 kg/s

(iv) Condenser-evaporator refrigerant liquid line

Condensing temperature, T_c = 30 °C

Solution density, ρ_w = 1529.3 kg/m^3

Solution viscosity, μ_w = 0.00299 N.s/m^2

Mass flow rate, $\dot{m}_w$ = 0.00414 kg/s

(v) Evaporator-absorber refrigerant vapour line

Evaporating temperature, T_e = 8 °C

Evaporator pressure, P_e = 1.07 kPa

Vapour density = 0.00828 kg/m^3

Vapour viscosity, μ_s = 8.77 x10^{-6} kg/m.s

Mass flow rate, $\dot{m}_v$ = 0.00084 kg/s

The velocity of flow is calculated as $\mathrm{v} = \frac{\dot{m}}{A\rho}$ **(6.11)**

Where $\dot{m}$ = mass flow rate [kg/s]

ρ = density [kg/m^3]

A = cross section area of pipe = $\frac{\pi d^2}{4}$ **(6.12)**

The Reynolds number is defined as follows:

$$\mathrm{Re} = \frac{\rho v d}{\mu} \quad \textbf{(6.13)}$$

The pressure drop is computed using Equation 6.7 as follows

$$\Delta P = \frac{2 f L V^2 \rho}{d} \quad \textbf{(6.14)}$$

The Table 6.1 shows the selection of tube diameters based on acceptable pressure drops.

Table 6.1 Parameters of pipe flow and pressure drop in tube

Pipe line	Diameter OD(mm)	Cross section A (m^2)	Reynolds Re	Velocity V (m/s)	Pressure Drop ΔP (Pa/m)
1. Strong Solution Line	12.7	9.37E-5	112.11	0.02	16.05
2. Weak Solution Line	12.7	9.37E-5	161.50	0.03	4.52
3. Gen-Con Vapour Line	30	7.1E-4	3151.95	4.03	3.40
4. Con-Eva Liquid Line	12.7	8.27E-5	1707.63	0.13	33.10
5. Eva-Abs Vapour Line	50	1.96E-3	2429.99	51.47	8.83

All the above calculations were done by using Visual Basic Application (VBA) functions in Excel. The VBA share the same thermodynamic and transport properties that are available in ABCON.

6.3 Evaporator

The evaporator is used to boil off the distilled water from condenser under reduced pressure by an immersion heater. The evaporator was designed to contain a 2 kW heater. The position of the evaporator chamber was designed to be horizontal. This was intended to prevent violent boiling, since the height of the water column will cause an increase of pressure at the evaporator. This pressure can affect the smoothness of the boiling. The violent boiling may also form large bubbles which act as an insulation cushion and prevent heat transfer between the heater and the refrigerant. This will cause the temperature to exceed the melting point of the heater wire, resulting in burnout. Thus, during the design of evaporator, correlations to avoid the spheroidal bubble state were used. Rohsenow (1955) correlated experimental data for nucleate pool boiling with the following relationship:

$$\frac{C_l \Delta T_x}{h_{fg}\,\mathrm{Pr}_l^s} = C_{sf}\left[\frac{q/A}{\mu_l h_{fg}}\sqrt{\frac{g_c \sigma}{g(\rho_l - \rho_v)}}\right]^{0.33} \tag{6.15}$$

Where C_l = specific heat of saturated liquid, J/kg. °C

ΔT_x = temperature excess = $T_w - T_{sat}$, °C

h_{fg} = enthalpy of vaporisation, J/kg

Pr_l = Prandtl number of saturated liquid

$\dot{Q}/A$ = heat flux per unit area, W/m^2. °C

μ_l = liquid viscosity, kg/m.s

σ = surface tension of liquid-vapour interface, N/m

g = gravitational acceleration, m/s^2

ρ_l = density of saturated liquid, kg/m^3

ρ_v = density of saturated vapour, kg/m^3

C_{sf} = constant, determined from experimental data

= 0.006 for water with nickel or brass

= 0.013 for water with platigum, copper or stainless steel

s = constant, 1.0 for water and 1.7 for other liquids.

Heat flux can be obtained from Equation 6.16 as follows:

$$q_{flux} = \frac{\dot{Q}}{A} = \mu_f h_{fg} \left[\frac{g(\rho_f - \rho_g)}{\sigma} \right]^{1/2} \left(\frac{C_l \Delta T_x}{C_{sf} h_{fg} \mathrm{Pr}_f^{1.0}} \right)^{1/0.33} \qquad \mathbf{(6.16)}$$

Assuming an evaporator temperature range of 7°C to12°C and for an evaporating temperature of 8°C, the evaporating pressure (saturation) is 0.01 bar or 1kPa. The capacity of the evaporator is 2kW.

$\mu_f = 1376.77 \times 10^{-6}$ kg/m.s
$h_{fg} = 2482.1328 \times 10^{3}$ J/kg
$g = 9.81$ m/s^2
$\rho_f = 999.7990$ kg/m^3
$\rho_g = 8.2830 \times 10^{-3}$ kg/m^3
$\sigma = 74.513011 \times 10^{-3}$ N/m
$C_l = 4.1961 \times 10^{3}$ J/kg.°C
$\mathrm{Pr}_f = 9.9024$
$C_{sf} = 0.006$
$T_w = 22$
Assuming $\Delta T_x = 14$°C,

$$q_{flux} = 1376.77 \times 2482.1328 \times 10^{3} \times \left[\frac{9.81 \times (999.799 - 8.2830 \times 10^{-3})}{74.513011 \times 10^{-3}} \right]^{1/2} \times \left(\frac{4.1961 \times 10^{3} \times 14}{0.006 \times 2482.1328 \times 10^{3} \times 9.9024} \right)^{1/0.33}$$

(6.17)

q_{flux} =Q/A= 7.6212 W/cm^2 = 76.212kW/m^2

This value is checked against the critical heat flux which can be computed using Equation 6.17 (Butterworth, 1977) as follows:

$$q_{crit} = 0.131 \cdot h_{fg} \left[\sigma g (\rho_l - \rho_g) \rho_G^2 \right]^{0.25} \qquad \mathbf{(6.18)}$$

q_{crit} is calculated to be 153.84 kW/m^2. The q_{flux} is about 50% below the q_{crit} thus ensuring dangerous burn out to be avoided.

Figure 6.1 shows the changes of heat flux due to varying design wall temperature. This chart was imported from the component design program in ABCON (Figure 6.2). The design parameters were first chosen from the thermodynamic analysis program (Section 5.2.2). These parameters were then used as the inputs for evaporator design. The program will automate the calculation process and display the results on a chart (Figure 6.1). The figure shows that the heat flux approaches critical value at a wall temperature of 26°C. If the selected wall temperature is above this preset limit then a warning message and suggestion will appear, to ensure avoiding the critical flux value.

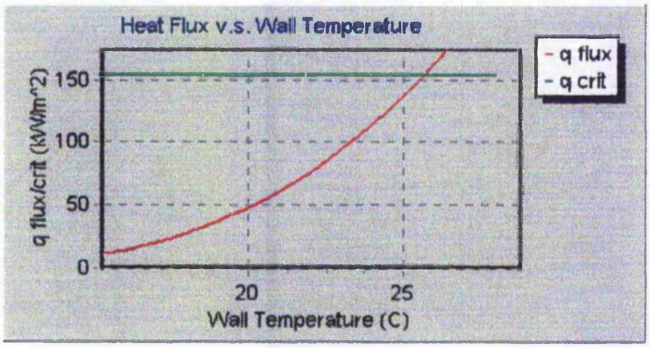

Figure 6.1 The changes of heat flux for varying heater wall temperature

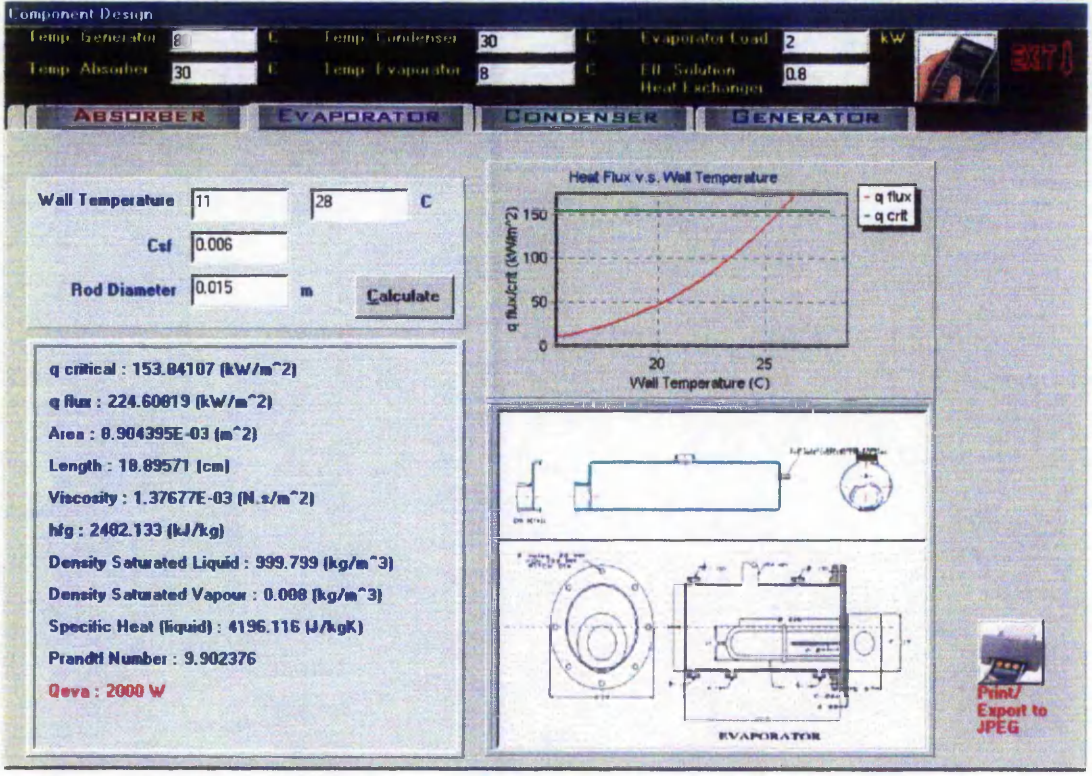

Temp. Generator 80 C
Temp. Absorber 30 C
Temp. Condenser 30 C
Temp. Evaporator 8 C
Evaporator Load 2 kW
Eff. Solution Heat Exchanger 0.8

Wall Temperature 11 28 C
Csf 0.006
Rod Diameter 0.015 m

```
q critical : 153.84107 (kW/m^2)
q flux : 224.60819 (kW/m^2)
Area : 8.904395E-03 (m^2)
Length : 18.89571 (cm)
Viscosity : 1.37677E-03 (N.s/m^2)
hfg : 2482.133 (kJ/kg)
Density Saturated Liquid : 999.799 (kg/m^3)
Density Saturated Vapour : 0.008 (kg/m^3)
Specific Heat (liquid) : 4196.116 (J/kgK)
Prandtl Number : 9.902376
Qeva : 2000 W
```

Figure 6.2 Interface of the program for designing the evaporator

6.4 Generator

Generator is the component used to separate the water content from the water-lithium bromide solution. Falling film on vertical plates and tubes generator have been studied and applied recently in ACS. Horizontal tube generators normally used for transferring heat from supplied hot water or steam to the thin film of solution mixtures that is sprayed on the tube surface. Wang (1996) has studied extensively the heat and mass transfer of lithium-bromide falling film on horizontal tube generator. About eight hundred sets of data were correlated into the Nusselt (Nu) and Sherwood number (Sh) as follows:

$$\boldsymbol{Nu} = \mathbf{0.7084 \cdot Re^{0.4213} \cdot Re_{\mathit{D}}^{0.3872} \cdot Pr^{0.3092}} \qquad \mathbf{(6.19)}$$

$$\boldsymbol{Sh} = \mathbf{0.6232 \cdot Re^{0.2143} \cdot Re_{\mathit{D}}^{0.2301} \cdot Pr^{-0.1743} \cdot} \boldsymbol{Sc}^{\mathbf{0.1027}} \qquad \mathbf{(6.20)}$$

where

$$\boldsymbol{Sc} = \frac{\boldsymbol{v}}{\boldsymbol{D}} \text{ (Schmidt number)}$$

v = viscosity, D = diffusion coefficient

A detailed study of the generator (Falling film or Horizontal tube) was considered to be beyond the scope of this work. For the experimental work, electric heaters were considered to be more proper in terms of ease of control and a more accurate measurement of the overall ACS performance. The above correlations, however, are considered to be a useful tool for verification or development of a prototype of absorption cooling system in the future. The heaters were designed from the following relationship (Butterworth, 1977):

$$\alpha = \mathbf{0.00122} \frac{\mathbf{k_L^{0.79} C_L^{0.45} \rho_L^{0.49}}}{\mathbf{\sigma^{0.5} \mu_L^{0.29} (h_{fg} \rho_G)^{0.24}}} \mathbf{(T_w - T_s)^{0.24} (P_w - P_s)^{0.75}} \qquad \mathbf{(6.21)}$$

$$\mathbf{\dot{Q}} = \alpha \mathbf{\, A \, (T_w - T_l)} \qquad \mathbf{(6.22)}$$

Where

$\dot{Q}$ = 4000 kW (Generator Maximum Load)

α = nucleate, pool coefficient, W/m^2 °C

k_L = liquid thermal conductivity, W/m °C

C_L = liquid heat capacity, J/kg °C

ρ_L = liquid density, kg/m^3

ρ_G = vapour density, kg/m^3

μ_L = liquid viscosity, Ns/m^2

h_{fg} = latent heat, J/kg

T_w = wall, surface temperature, °C

T_S = saturation temperature of boiling liquid °C

P_w = saturation pressure corresponding to the wall temperature, T_w, N/m^2

P_S = saturation pressure corresponding to the wall T_S, Pa

σ = surface tension, N/m

q = heat flux W/cm^2

$T_w = 105$ °C

$T_s = T_g = 80$ °C

$k_L = 0.43412295$ W/m °C

$\alpha = 1013.097094$ N/m

$C_L = 1862.525702$ J/kg °C

$\rho_L = 1741.903076$ kg/m^3

$\rho_G = 0.293767452$ kg/m^3

$\mu_L = 0.003435731$ Ns/m^2

$h_{fg} = 2437.859299 \times 10^3$ J/kg

$P_w = 12885.68262$ N/m^2

$P_s = 4228.162598$ N/m^2

$\sigma = 0.080157779$, N/m

$q = 2.5327427$ W/cm^2

$A = 0.157931556$ m^2

$$\alpha = 0.00122 \frac{0.4341^{0.79} 1862.53^{0.45} 1741.90^{0.49}}{0.0802^{0.5} 0.0034^{0.29} (2437.86 \times 10^3 \times 0.2938)^{0.24}} (25)^{0.24} (8657.52)^{0.75}$$

$$= \mathbf{1013.10\ W/m^{2\circ}C}$$

The heat flux generator heater was calculated as follows:

$$q = \dot{Q} / (A \times \alpha) = 2.5327 \text{ W/cm}^2$$

The value was checked against the critical heat flux equation (Eqn. 6.18) as follows:

$$q_{crit} = 0.131 \cdot h_{fg}\left[\sigma g(\rho_l - \rho_g)\rho_G^2\right]^{0.25}$$

$$= 105.30 \text{ W/cm}^2$$

The program for designing the generator and the comparison of designed heat flux with the critical heat flux are shown in Figure 6.3 and Figure 6.4 respectively.

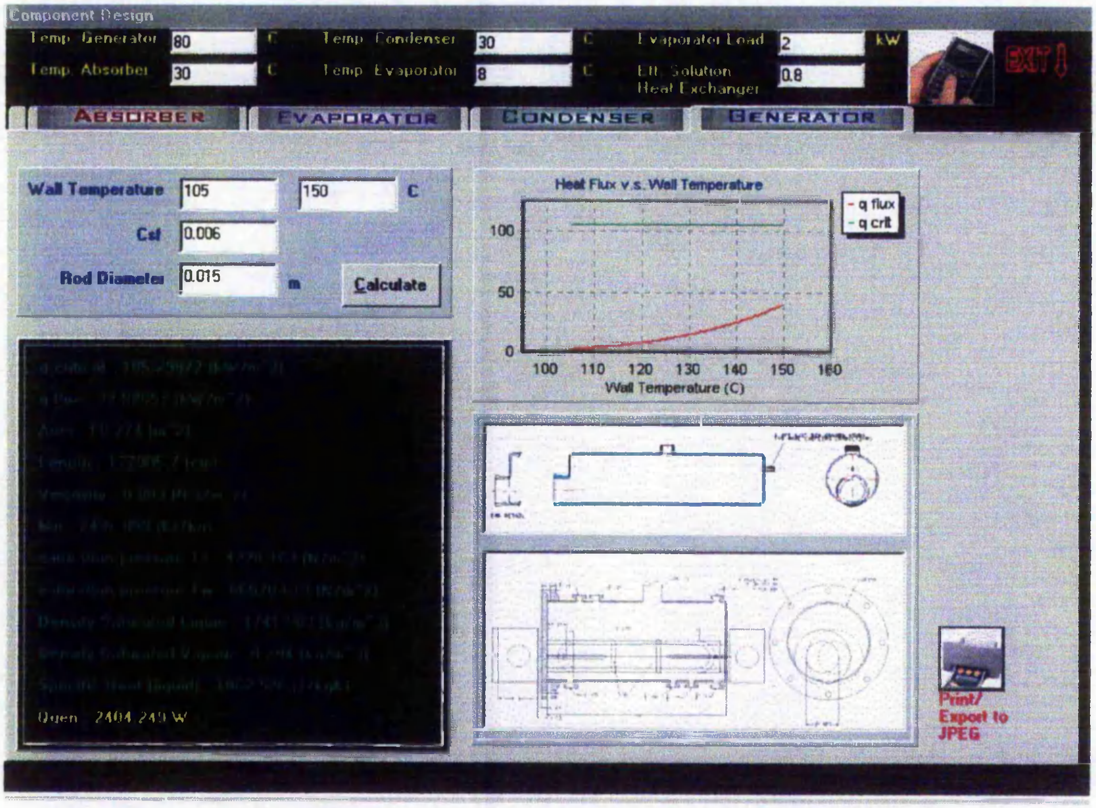
Temp. Generator 80 C
Temp. Absorber 30 C
Temp. Condenser 30 C
Temp. Evaporator 8 C
Evaporator Load 2 kW
Eff. Solution Heat Exchanger 0.8
Wall Temperature 105 150 C
Csf 0.006
Rod Diameter 0.015 m

Qgen 2404.249 W

Figure 6.3 Interface of the program for designing the generator

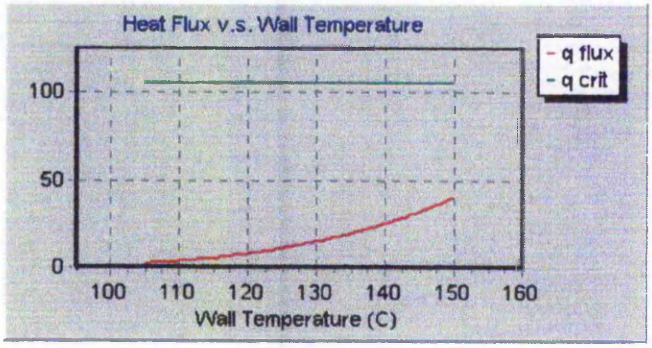

Figure 6.4 The changes of q flux by varying wall temperature of generator heater

6.5 Condenser

The condenser used in this work comprise of a coil tube. The outside of the tube is in touch with water vapour from the generator while cooling water is circulating inside the tube. The condenser load is generally defined as

$$\dot{Q}_c = UA_o\Delta t \tag{6.23}$$

Where $\dot{Q}_c$ = condenser heat load

Δt = the overall temperature difference, K

U is overall heat transfer coefficient for outside surface area $A_{o.}$

$$U = \frac{1}{\frac{1}{h_o} + R_o + \frac{r_o}{k}\ln\left(\frac{A_o}{A_i}\right) + R_i\frac{A_o}{A_i} + \frac{1}{h_i}\frac{A_o}{A_i}} \tag{6.24}$$

Where :

h_o = average unit surface conductance of the fluid on the outside of tubing, W/m^{2}K

h_i = average unit surface conductance of the fluid on the inside of tubing, W/m^{2}K

R_o = Unit fouling resistance on outside of tubing, m^{2}K/W

R_i = Unit fouling resistance on inside of tubing, m^{2}K/W

A_o/A_i = ratio of outside tube surface to inside tube surface

Convection heat transfer coefficient inside a coil tube

Inner tube – Laminar

$$Nu = \left(3.65 + 0.08\left\{1 + 0.8\left(\frac{d}{D}\right)^{0.9}\right\}Re^m Pr^{1/3}\right)\left(\frac{Pr}{Pr_w}\right)^{0.14} \quad \text{(Schmidt, 1966)} \tag{6.25}$$

$100 < Pr < 200$

where $Nu = \frac{h_i d_i}{k}$ **(6.27)**

$$m = 0.5 + 0.2903(d/D_s)^{0.194} \tag{6.28}$$

d = inner diameter of tube

$$Re_{crit} = 2300\left(1 + 8.6\left(\frac{d_o}{D_s}\right)^{0.45}\right) \tag{6.29}$$

$$D_s = \frac{L}{n\pi} \tag{6.30}$$

$$D_w = \sqrt{D_s^2 - \left(\frac{b}{\pi}\right)^2} \tag{6.31}$$

$$D_c = D_w \left[1 + \left(\frac{b}{\pi D_w} \right)^2 \right] \tag{6.32}$$

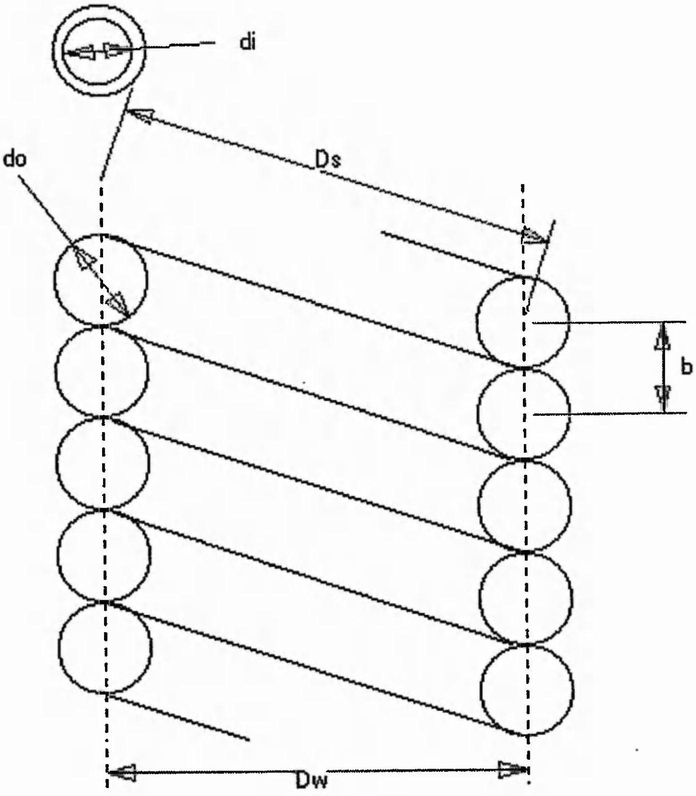

Figure 6.5 Dimensions of a coil tube

Inner Tube - Turbulent

The coolant side heat transfer coefficient can be obtained from Gnielinski (1976) correlation as follows:

$$Nu = \frac{(\mathrm{Re} - 1000) \times \left(\frac{f_{c,t}}{8} \right) \mathrm{Pr}_c}{1 + 1.27 \sqrt{\frac{f_{c,t}}{8}} (\mathrm{Pr}_c^{2/3} - 1)} \tag{6.33}$$

where

$$f_{c,t} = [1.58\ln(\mathrm{Re}_c) - 3.28]^{-2} \tag{6.34}$$

The h_i can be determined by modified Dittus-Boelter equation as follows:

$$\frac{h_i d_{ci}}{\lambda_i} = 0.0225 F_c \left(\frac{4Q_i \rho_i}{\pi \mu_i d_{ci}}\right)^{0.8} \left(\frac{\mu_i c_{pi}}{k_i}\right)^{0.4} \tag{6.35}$$

Where

$$F_c = 1 + 3.4d/D_c \tag{6.36}$$

The critical Reynolds number is calculated as follows:

$$Rcrit = 2x10^4 \left(\frac{d_o}{D_c}\right)^{0.32} \tag{6.37}$$

Outer tube

For outer tube, the flow rate of water vapour is very small and generally considered to be laminar.

$$h_o = 0.725 \left[\frac{k_f^3 \rho_f^2 g h_{fg}}{N D \mu_f \Delta t}\right]^{1/4} \tag{6.38}$$

Where:

N = number of tubes in a vertical row

T_f = mean condensate film temperature

k_f = thermal conductivity of the condensate film evaluated at $t_f = ½(t_c - t_w)$, W/mK

ρ_f = density of the condensate film evaluated at t_f, kg/m^3

μ_f = viscosity of the condensate film evaluated at t_f, Ns/m^2

Δt = temperature differential, °C = $(t_c - t_w)$

t_w = tube wall temperature, °C

t_c = condensation temperature, °C

D = diameter of tube, m

$$Nu = \frac{h_o \delta}{k} \tag{6.39}$$

Where

$$\delta = \left(\frac{\upsilon^2}{g} \right)^{1/3} \quad \text{, (falling film thickness)} \qquad \textbf{(6.40)}$$

Input parameters

Condensing load	Q_c	≈ 2110 W
Condensing temperature	T_c	= 30°C
Cooling water inlet temperature	T_{wi}	= 20°C
Cooling water outlet temperature	T_{wo}	= 26°C
Temperature drop	$T_{w\,Drop}$	= 6°C
Condensing pressure	P_c	= 4.25 kPa
Tubing inner diameter	I.D.	= 10.92 mm
Tubing outer diameter	O.D.	= ½" (12.7 mm)

The following calculations of heat transfer are based on assumption stated above.

Temperature drop through the condensing film,

T_f = 0.5 (30+29) = 29.5

At which the properties of saturated water are:

C_{pi} = 4.179 kJ/kgK

μ_f = 806.66 x 10^{-6} kg/m.s

ρ_f = 995.75 kg/m^3

h_{fg} = 2431.76 kJ/kg

k_f = 617.36 x 10^{-6} kW/mK

$$h_o = 0.725 \left[\frac{k_f^3 \rho_f^2 g h_{fg}}{N D \mu_f \Delta t} \right]^{1/4}$$

$$= 0.725 \left[\frac{617.36 \times 10^3 \times 995.75^2 \times 9.81 \times 2431.76}{39.16 \times 0.0127 \times 806.66 \times 10^{-6} \times 1} \right]^{0.25}$$

$$= 7.869 \text{ kW/m}^2 K$$

μ_i, ρ_w, C_{pi}, λ_i, are estimated at water bulk temperature 23 °C.

$$Volume\ flow\ rate = \frac{\dot{Q}_c}{\rho_w C_{pi} \times 1000 \times T_{wDrop}} \tag{6.41}$$

$$= \frac{2110}{997.50 \times 4.19 \times 1000 \times 6}$$

$$= 8.41 \times 10^{-5} \mathrm{m}^3 / s$$

$$Area_{pipe} = \frac{\pi \times ID / 1000^2}{4} \tag{6.42}$$

$$= 9.36811 \times 10^{-5}\ \mathrm{m}^2$$

V_w = *Volume flow rate / Area*$_{pipe}$ = 0.8982 m/s

$$\mathrm{Re} = \frac{\rho_w v d}{\mu}$$

$$= \frac{997.50 \times 0.8982 \times 10.92 \times 10^{-3}}{9.344 \times 10^{-4}} = 10471.42$$

Pr = 6.43

d_o/D_c = 0.09100

h_i = 5.6754 kW/m^{2}K

R_i = 0.0002

R_o = 0.00005

$$\frac{1}{U} = \frac{1}{\frac{1}{7868.61} + 0.00005 + 0.005621 \times \ln(1.1628) + 0.0002 \times 1.1628 + \frac{1}{5675.41 \times 1.1628}}$$

Thus,

U = 683.87 W/m^{2}K

$$Ao = \frac{\dot{Q}_c}{U \Delta t_m}$$

Δt_m= 6.55

A_o = 0.4712

L = $A_o/\pi d_o$ = 11.81

D_w=120 mm

D_c =120.01 mm

Turn = 39.16

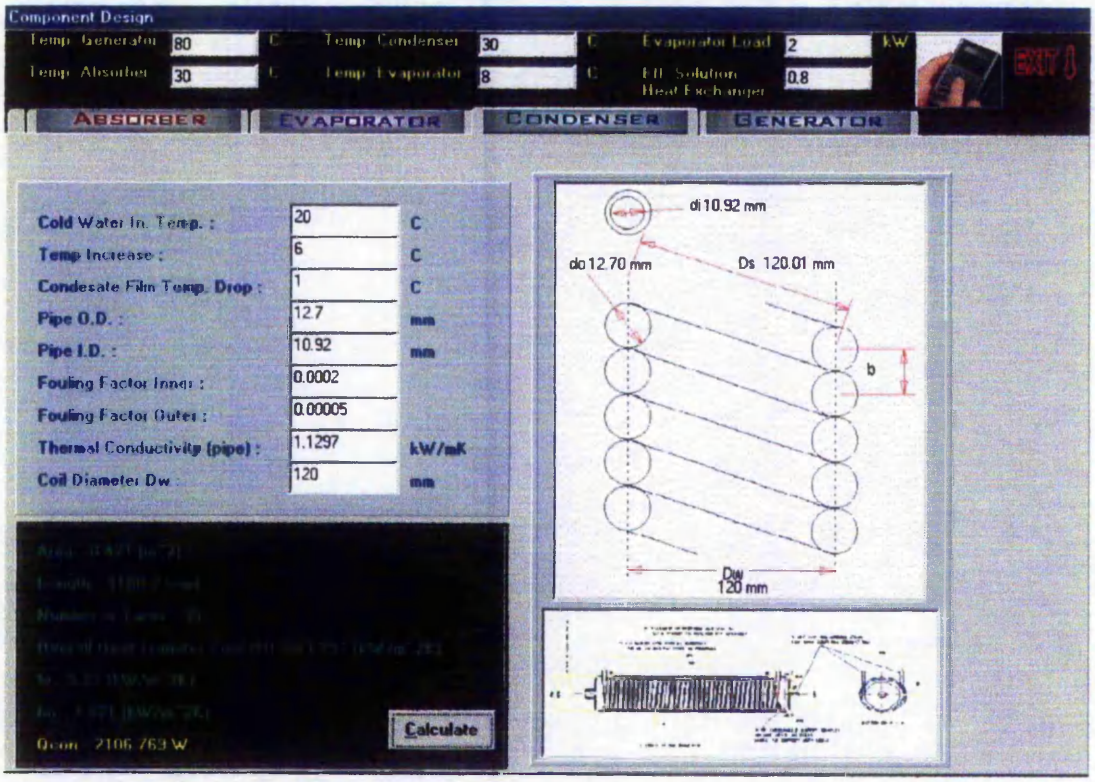

Component Design

Temp. Generator 80 C
Temp. Absorber 30 C
Temp. Condenser 30 C
Temp. Evaporator 8 C
Evaporator Load 2 kW
Eff. Solution Heat Exchanger 0.8

Cold Water In. Temp. : 20 C
Temp Increase : 6 C
Condensate Film Temp. Drop : 1 C
Pipe O.D. : 12.7 mm
Pipe I.D. : 10.92 mm
Fouling Factor Inner : 0.0002
Fouling Factor Outer : 0.00005
Thermal Conductivity (pipe) : 1.1297 kW/mK
Coil Diameter Dw : 120 mm

Qcon : 2106.763 W

Figure 6.6 Program for designing the condenser

Figure 6.6 shows the program developed for facilitating the design of the condenser. By specifying the inputs discussed earlier, the program will automate the computation in seconds. The number of turns, area and length of the tube will be calculated. Other information such as the convection heat transfer coefficient inside (h_i) and outside the (ho) coil tube and the overall heat transfer coefficient (U) are also displayed.

6.6 Absorber

The design of the absorber is more complex than that of condenser or evaporator. This is mainly due to the flow characteristics in absorber, which comprise of weak solution and strong solution mixtures, and water vapour. A Nusselt correlation (Equation 6.43) was used by Adegoke (1987) in his design. The method used, however, omitted the mass transfer, which was later found to be equally important as heat transfer by Seewald (1992). Moreover, the mass transfer takes place primarily during the formation of droplets as shown in Section 6.6.2, was also not considered by Adegoke (1987). Thus, the design of the absorber in this work was largely based on the model proposed by Seewald (1992). In this work, an enhanced model is suggested. In this new model, the formation of droplet neglected in previous literature was included. This consideration has led to a more realistic prediction that could be adapted in practice. Calculations used for the coil sizing and convective heat transfer coefficient for inside of the coil tube are similar to that used previously for the condenser.

$$Nu = 0.67\frac{k}{\sigma}(\mathrm{Re})^{0.11}(\mathrm{Pr}\frac{\sigma}{z})^{0.33} \tag{6.43}$$

6.6.1 Solution side heat transfer

The heat transfer on the solution side of the coil was calculated by assuming that the coil is not completely wet. This assumption is based on the practical observation of the behaviour of droplets and falling film on the coil. A method was devised to estimate the effective wetted area (Seewald, 1992). As a drop of solution descends onto a turn of the coil, a falling film is formed that spreads out as it traverses the circumference of the tube. The shape of this film is assumed to the triangular and the area of half of this triangular shape forms a right triangle (Figure 6.7) and can be estimated as

$$A_{est} = \frac{1}{2}\pi r_o l \tag{6.44}$$

where

r_o = outer radius of the tube

l = the base of triangle

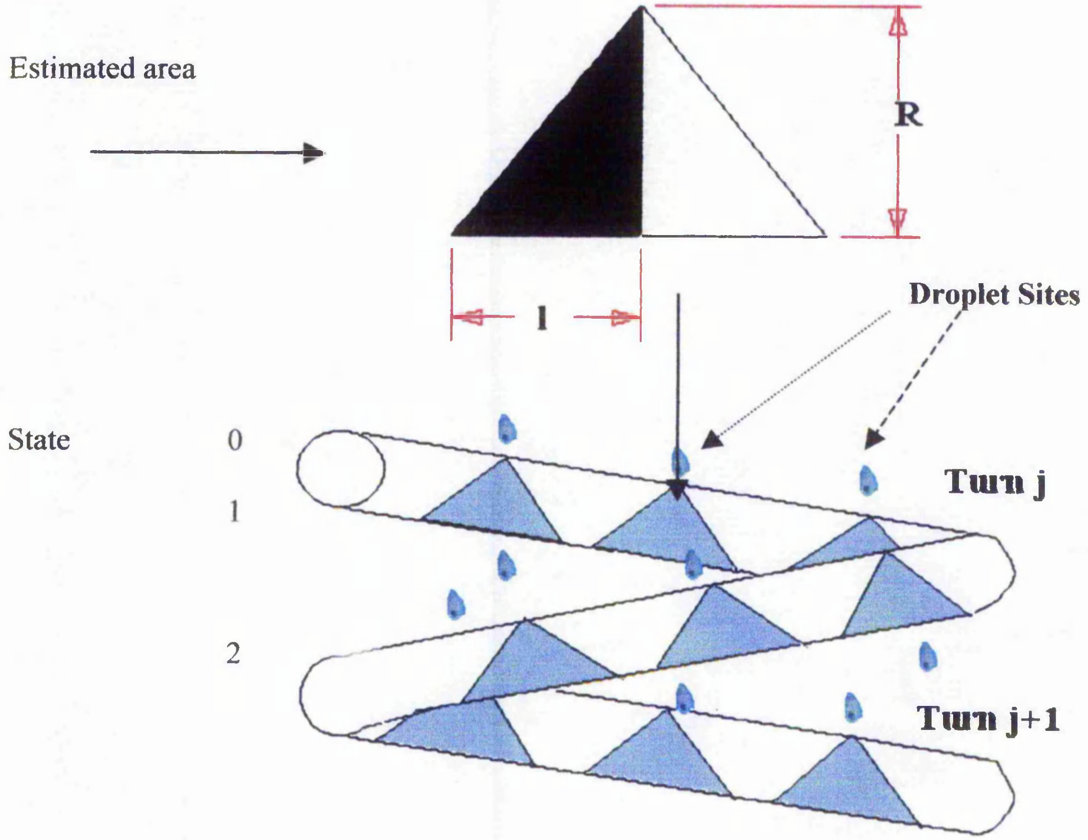

Figure 6.7 Schematic of model solution scheme

Expression in Equation 6.44 yields the area of film due to one droplet. The total wetted area can be estimated by knowing the number of droplet sites (Figure 6.7), n. The solution flow rate for one side can be defined in terms of l as follows:

$$\frac{\dot{m}_s}{n}=\frac{1}{2}\delta l v \rho_s \qquad (6.45)$$

where

$$\mathrm{v}=\frac{\pi r_o}{t} \quad \text{(average velocity)} \qquad (6.46)$$

$$\delta=\left(\frac{6\dot{m}_s\mu_s}{g\,l\,\rho_s^2 n}\right)^{\frac{1}{3}} \quad \text{(falling film thickness)} \qquad (6.47)$$

The average velocity can also be expressed in terms of δ as follows:

$$\mathrm{v} = \delta^2 \left(\frac{g\rho_s}{3\mu_s} \right) \tag{6.48}$$

By substituting Equation 6.47 in Equation 6.45 yields another expression of v as follows:

$$\mathrm{v} = \frac{1}{3} \left(\frac{6\dot{m}_s}{ln} \right)^{\frac{2}{3}} \left(\frac{g}{\mu_s \rho_s} \right)^{\frac{1}{3}} \tag{6.49}$$

The time taken for the solution to fall along the tube is estimated by a correlation for the spreading of liquids on solids (Seewald, 1992). The correlations (Equation 6.50) is defined in terms of viscosity (μ_s), the triangle base (**l**) (Figure 6.7), surface tension (σ), characteristic dimension (**a**) and contact angle (ϕ) which varies from 0° to 20° for copper tube (Adam, 1996).

$$t = \frac{2\mu_s \mathrm{l}^2}{\mathrm{a}\sigma\cos\phi} \tag{6.50}$$

By substituting Equation 6.49 in Equation 6.46 to solve for t and setting the result equal to t in Equation 6.50, the equation can be solved for l as follows:

$$\mathrm{l} = \left(\frac{3\rho_s}{32g} \right)^{\frac{1}{4}} \left(\frac{n}{\dot{m}_s \mu_s} \right)^{\frac{1}{2}} (\pi r_o a \sigma \cos\phi)^{\frac{3}{4}} \tag{6.51}$$

The value of **cos** ϕ is approximated to 1 since it varies only marginally from 0.94 to 1. Thus the Equation 6.51 becomes

$$\mathrm{l} = \left(\frac{3\rho_s}{32g} \right)^{\frac{1}{4}} \left(\frac{n}{\dot{m}_s \mu_s} \right)^{\frac{1}{2}} (\pi r_o a \sigma)^{\frac{3}{4}} \tag{6.52}$$

The Nusselt number is obtained as follows (Blass, 1977),

$$Nu_s = 0.0614\,\mathrm{Re}_s^{0.533}\,\mathrm{Pr}_s^{0.344} \tag{6.53}$$

The $\mathrm{Pr_s}$ and $\mathrm{Re_s}$ are defined as follows

$$\mathrm{Pr}_s = \frac{c_{ps}\mu_s}{k_s} \text{ (Prandtl number)} \tag{6.54}$$

$$\mathbf{Re}_s = \mathbf{v}^{1.5}\left(\frac{3}{gv_s}\right)^{\frac{1}{2}} = \delta^3\left(\frac{g}{3v_s^2}\right) \text{ (Reynolds number)} \qquad \textbf{(6.55)}$$

where

$$v_s = \mu_s/\rho_s \text{ (kinematic viscosity)} \qquad \textbf{(6.56)}$$

The heat transfer coefficient of the solution side can be calculated as follows:

$$h_s = \frac{Nu_s k_s}{\delta} \qquad \textbf{(6.57)}$$

The absorber $\dot{Q}_a$, can be expressed as

$$\dot{Q}_a = UA_a\Delta t_m$$

Where

U = the overall heat transfer coefficient, W/m^{2}K

A_a = absorber cooling coil external surface area, m^2

Δt_m = the logarithmic mean temperature difference

The U- value can thus be obtained from the equation:

$$\frac{1}{U} = \frac{1}{h_c} + \frac{r_i \ln(r_o/r_i)}{k_{pyrex}} + \frac{A_i}{h_s A_{eff}} \qquad \textbf{(6.58)}$$

Where

A_i = inside surface area of one turn of the coil = $4\pi^2 r_i R$

h_e = outside film heat transfer coefficient, W/m^{2}K

h_i = inside film heat transfer coefficient, W/m^{2}K

r_o, r_i = outer and inner radius of tube, m

k_{pyrex} = thermal conductivity of Pyrex tube wall, W/mK

R = radius of the absorber coil, m

6.6.2 Mass transfer

As the falling film of lithium bromide flows to the bottom of a turn of the coil, it collects at the bottom of the turn and forms a drop. At this point, the heat transfer process for that turn is considered complete and the mass transfer begins. The mass transfer process is governed by four equations (Equation 6.59-6.62) by assuming that a mass of solution descending from one turn to the next comes to equilibrium according to its state and its surroundings (Seewald, 1992).

$$\dot{m}_{s1}c_{ps}T_1 - \dot{m}_{s2}c_{ps}T_2 + \dot{m}_a H_v = 0 \tag{6.59}$$
$$\dot{m}_{s1} + \dot{m}_a = \dot{m}_{s2} \tag{6.60}$$
$$\dot{m}_{s1}x_1 = \dot{m}_{s2}x_2 \tag{6.61}$$
$$T_2 = AT_{sat,vapour} + B \tag{6.62}$$

where

m_{s1} and m_{s2} refer to the mass of solutions at state 1 and 2 in Figure 6.7

m_a = mass absorbed per turn of a coil

Equation 6.62 is used to compute the solution temperature, T_2, at the saturation temperature of refrigerant vapour and concentration at state 2. The constants A and B are expressed in the following way (McNeely, 1979):

$$A = -2.00755 + 0.16976x_2 - (3.133362\times10^{-3})x_2^2 + (1.97668\times10^{-5})x_2^3 \tag{6.63}$$
$$B = 321.128 - 19.322x_2 + 0.374382x_2^2 - (2.0637\times10^{-3})x_2^3 \tag{6.64}$$

6.6.3 Absorber performance simulation

The strong solution from the generator that is falling upon the first coil is referred as state 0. The overall heat transfer coefficient is used to compute the amount of heat transferred to the cooling water in the coil through the falling film. The formulation is given by

$$q_j = UA_l(T_{sj} - T_{cj}) \tag{6.65}$$

where

T_{sj} is the average temperature for the turn $= \dfrac{T_{0j} + T_{1j}}{2}$ (6.66)

$$A_l = 2 \times \pi \times r_o \times l \times NOS$$

where

NOS = number of droplet sites (Figure 6.7)

The heat transfer can also be expressed as follows:

$$q_j = \dot{m}_{sj} c_{ps} (T_{0j} - T_{1j}) \qquad (6.67)$$

By combining Equation 6.65 and Equation 6.67, T_{1j} can be expressed in the following way:

$$T_{1j} = \frac{UA_i(-T_{0j} + 2T_{cj}) + 2\dot{m}_{sj} c_{ps} T_{0j}}{(UA_i + 2\dot{m}_{sj} c_{ps})} \qquad (6.68)$$

Once T_{1j} is computed, average temperature T_{sj} can be determined. The amount of heat transferred can then be calculated by using Equation 6.65. By equating the heat transfer rate q in both Equations 6.65 and 6.67, the cooling water temperature of next turn can be determined as follows:

For counter flow flow absorber

$$T_{c(j+1)} = \frac{-q_j}{\dot{m}_{cj} c_{pc}} + T_{cj} \qquad (6.69a)$$

For parallel flow absorber

$$T_{c(j+1)} = T_{cj} + \frac{q_j}{\dot{m}_{cj} c_{pc}} \qquad (6.69b)$$

If conditions at state 1 are known, the Equation 6.59-6.62 can be solved simultaneously. The solved temperature, T_2, is then used as the initial temperature of the next turn, T_{1j}. This temperature is then used to compute the temperature at the bottom of the coil, $T_{0(j+1)}$, by solving the Equation 6.70-6.73 simultaneously and hence the mass transfer can also be computed. The variable x_2 in constants A and B of Equation 6.63 and 6.64 becomes $x_{(j+1)}$ in constants A and B of Equation 6.73.

$$\dot{m}_{si} c_{ps} T_{1i} - \dot{m}_{s(i+1)} c_{ps} T_{0(i+1)} + \dot{m}_{ai} H_v = 0 \qquad (6.70)$$

$$\dot{m}_{si} + \dot{m}_{ai} = \dot{m}_{s(i+1)} \qquad (6.71)$$

$$\dot{m}_{si} x_i = \dot{m}_{s(i+1)} x_{(i+1)} \qquad (6.72)$$

$$T_{0(i+1)} = AT_{sat,vapour} + B \qquad (6.73)$$

After solving the above equations simultaneously, the necessary information for calculating the heat and mass transfer is known at the exit temperature. This process is performed N times for a coil of N turns. If the top re-circulation spray is turned on, the mass flow rate for initial condition is as follows:

$$\dot{m}_{s0} = \dot{m}_{trp} + \dot{m}_w \qquad (6.74)$$

The expression on the left hand side of Equation 6.61 becomes

$$\dot{m}_{s0}x_0 = \dot{m}_{trp}x_w + \dot{m}_w x_s \tag{6.75}$$

where

x_w = concentration of weak solution from generator

x_s = concentration of strong solution from absorber

$\dot{m}_w$ = mass flow rate of weak solution from generator

$\dot{m}_{trp}$ = mass flow rate of top re-circulation spray

If the middle spray is also turned on, the mass transfer equations on the 11th turn are as follows:

$$\dot{m}_{s11} = \dot{m}_{s10} + \dot{m}_{mrp} \tag{6.76}$$

$$\dot{m}_{s11}x_{11} = \dot{m}_{s10}x_{10} + \dot{m}_{mrp}x_w \tag{6.77}$$

For the twin coil absorber, the inlet mass flow rate is divided by two. If only the top re-circulation spray is turned on, the mass flow rate for each coil at the initial condition is as follows:

$$\dot{m}_{s0} = \dot{m}_{trp} + \frac{\dot{m}_w}{2} \tag{6.78}$$

For the solution species mass balance is:

$$m_{s0}x_0 = \dot{m}_{trp}x_s + \frac{\dot{m}_w x_w}{2}$$

The total mass absorbed (Equation 6.79) and heat transfer (Equation 6.80) for the absorber were calculated in the following manner:

$$\dot{m}_{a,total} = \sum_0^N \dot{m}_{j,ic} + \sum_0^N \dot{m}_{j,oc} \tag{6.79}$$

$$q_{total} = \sum_0^N q_{j,ic} + \sum_0^N q_{j,oc} \tag{6.80}$$

where ic and oc represent the inner and outer coil respectively.

6.6.4 A model for droplet formation

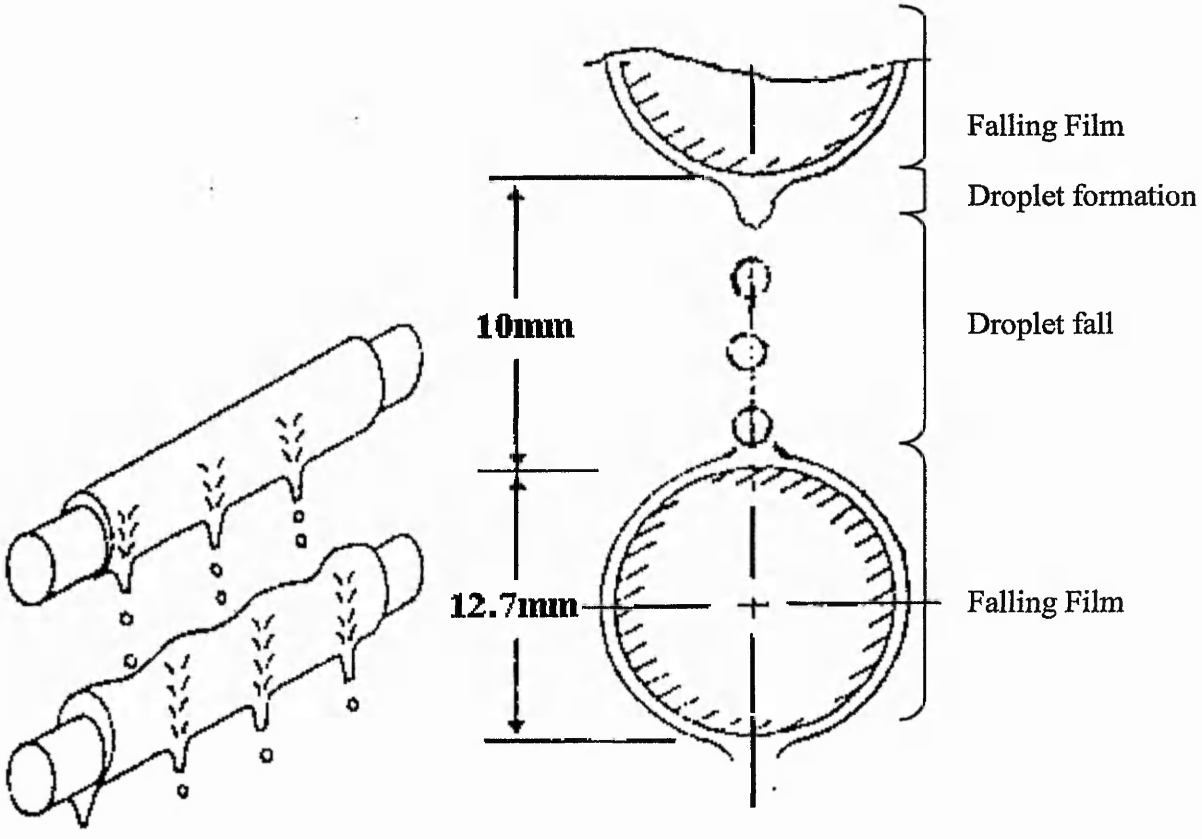

(a) (b)

Figure 6.8 a) Section view of absorber coil b) Side view of absorber flow regimes

For coil absorbers or horizontal tube absorbers, droplets can be observed if the gap of each turn is sufficiently large (Figure 6.8). It can be observed that droplet formation takes place beneath the pipe within a residence time. This behaviour was generally omitted in past literature (Anberg and Vliet, 1987). Most of the previous works focused on modelling of the falling film regime. The importance of droplet formation and droplet flow were raised by Kirby and Perez-Blanco (1994) and Seewald (1992) respectively.

There are generally two types of model for droplet formation (Clift, 1978): 1. Surface Stretch 2. Fresh Surface. The Surface model, which is commonly used for liquid-liquid systems assumes the fluid at the interface to remain throughout the droplet formation. The 'Fresh Surface' model on the other hand, assumes fresh fluid continually substitute the interface during the formation. This model was chosen for modelling droplet formation in this work as the formation is much faster and involves large amount of internal circulation. The Fresh Surface model has also shown to be a better assumption for liquid-vapour systems (Kirby and Perez-Blanco, 1994). The heat and mass transport of the droplet formation that is formed by successive series of thin spherical shells or layers can be defined as follows:

For each layer,

Energy balance,

$$\frac{dT_s}{dt} = \frac{H_v}{m_d C_{ps}} \frac{d\dot{m}_d}{dt} + \frac{\dot{Q}}{m_d C_{ps}} \tag{6.81}$$

Mass transfer,

$$\frac{d\dot{m}_d}{dt} = K_{form} \rho 4\pi R^2 (x_i - x_s) \tag{6.82}$$

where

$$K_{form} = \frac{0.0432d}{t_{form}} \left(\frac{\mathrm{v}_\mathrm{n}^2}{\mathrm{dg}} \right)^{0.089} \left(\frac{d^2}{t_{form} D_d} \right)^{-0.334} \left(\frac{\mu_d}{\sqrt{\rho_d d \sigma}} \right)^{-0.601} \tag{6.83}$$

K_{form} = mass transfer coefficient (Skelland & Minhas, 1971)

D = volumetric diffusivity, sq.cm/sec

d = equivalent drop diameter, cm.

v = velocity of liquid, cm/sec

ρ = density, g/cc

μ = viscosity, poises

σ = interfacial tension, dynes/cm

t_{form} = $\frac{\dot{m}_d N}{\Gamma_s}$, average droplet formation time, s

N = number of dripping sites per tube

Γ_s = solution mass flow rate per tube length (kg/ms)

The ordinary differential equations (Equations 6.81 and 6.82) can be solved using fourth order Runge-Kutta technique to step forward in time. The initial temperature of the droplet is essentially the exit temperature of falling film at the bottom of each turn which is computed analytically. The droplet temperature is solved using the energy balance. This temperature is then used as the initial temperature of the next coil. The mass transport is solved in a similar manner. All the conditions at the inlet and outlet of each turn are stored in the memory temporarily. For the counter current flow absorber, the inlet cooling temperature has to be assumed. This temperature is compared with the computed cooling temperature of the last turn (State 1 of N turn, T_{1N}). The equations are solved iteratively until the desired inlet cooling water temperature is achieved and the results are within the preset tolerance.

6.6.5 Results

The following are the default conditions for the absorber modelling:

1. Tube inner and outer diameters = 9.52 mm and 12.7 mm
2. Tube thermal conductivity = 1.129 kW/mK
3. Inner and outer coil diameters = 90 mm and 128 mm
4. Generator temperature = 80 °C
5. Condenser temperature = 30 °C
6. Absorber temperature = 30 °C
7. Evaporator temperature = 9 °C
8. Number of sites = 6
9. Coolant flow rate = 0.06 kg/s
10. Inlet coolant water temperature = 20 °C
11. Mixture flow rate = 0.0031 kg/s
12. Inlet concentration = 62.8 %

The inlet solution temperature is taken as the saturation temperature at absorber pressure and strong mass concentration. Figures 6.9a and 6.9b shows the total mass absorbed and heat transfer in counter and parallel flow absorbers at different variation of turns. Generally the heat transfer of the counter-flow heat exchanger performs better than parallel flow heat exchanger. In the absorption process, this might be partly true. As shown in Figures 6.9a and 6.9b, the total mass absorbed and heat transfer of parallel flow absorber at coil turns below 30 perform slightly better than the counter-flow absorber. The absorption rate is larger in the early stages when the solution first encounter with vapour from evaporator. This is also helped by the large heat transfer in parallel flow at the first few turns due to the large temperature difference. This can be further explained by theoretical modelling results shown in Figure 6.13 and further experimental results obtained from this work (Figure 9.6).

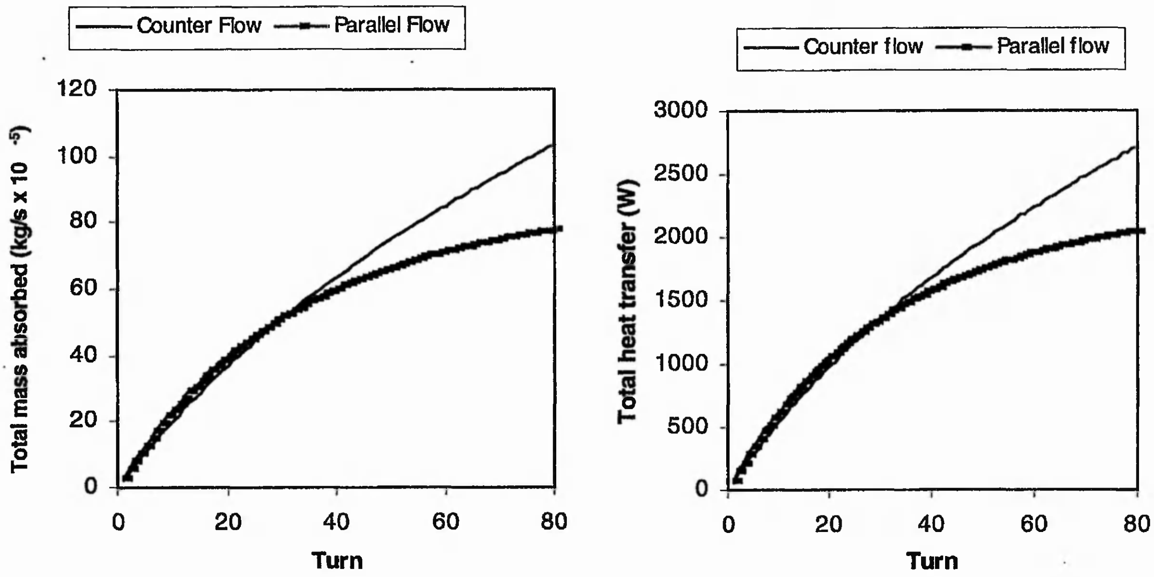

(a) (b)

Figure 6.9 Total mass absorbed (a) and heat transferred (b) by counter and parallel flow absorbers at various turns

Figures 6.10a and 6.10b show the total mass absorbed and heat transferred on the inner and outer coils respectively. The outer coil only performs slightly better than the inner coil due to the assumption of six droplet sites (Figure 6.7) on both coils. That means the wetted surface area of both coils are same. Figures 6.11a and 6.11b compare the changes of total mass absorbed and heat transferred for various number of droplet sites. It can be seen that when the number of droplet sites on the absorber coil is increased, the heat transferred and mass absorbed also increase. This is because increased droplet sites on the absorber coil will creates a larger wetted surface area.

Figure 6.12, compares the effects of flow of two different mass concentrations (58.1% and 62.8%) showing that the heat load and mass absorbed for the higher inlet mass concentration is better. The Figure 6.12 also shows that the heat load and mass absorbed increased sharply for an increase in coolant flow rates of 0.02 kg/s to 0.08 kg/s. The increasing rate gradually decreases until the point where further increase of coolant flow rate provides no significant improvements.

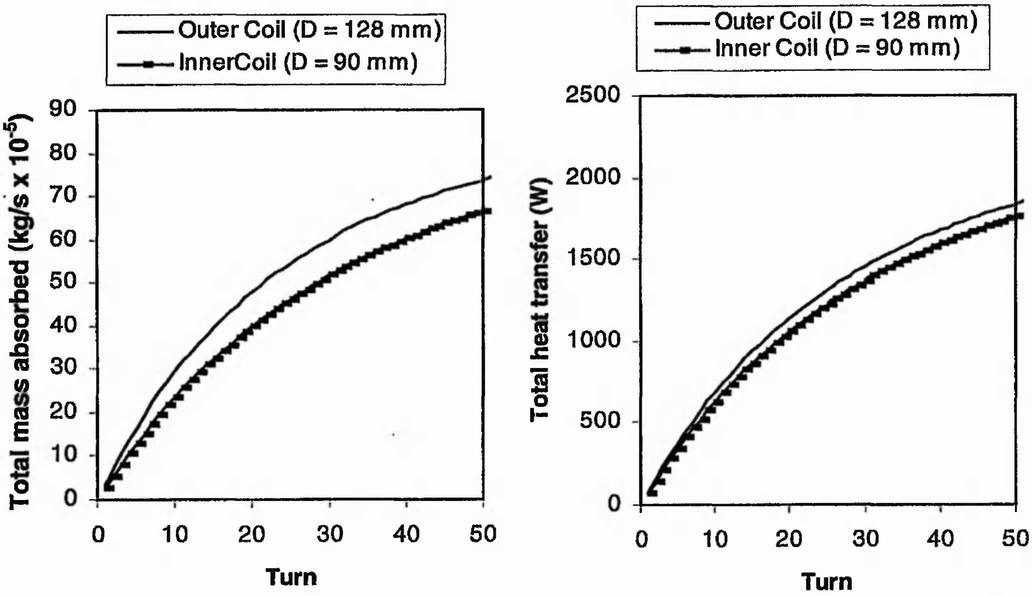

(a) (b)

Figure 6.10 Total mass absorbed (a) and heat transferred (b) for inner and outer coils in the absorber at various of turns. (Droplet sites – Inner = 6, Outer = 6)

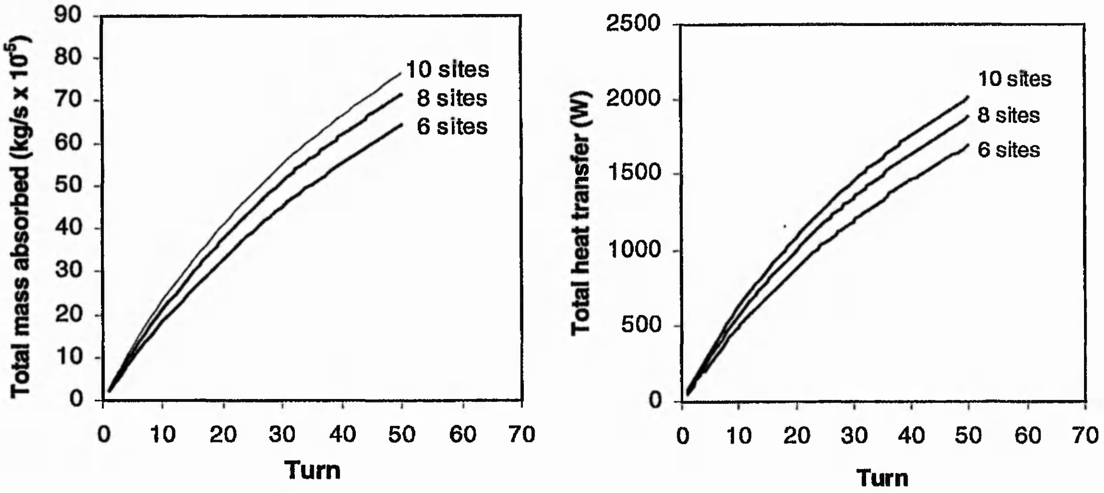

(a) (b)

Figure 6.11 Total mass absorbed (a) and heat transferred (b) on outer coils in the absorber at various of droplet sites (Droplet sites = 6, 8 and 10)

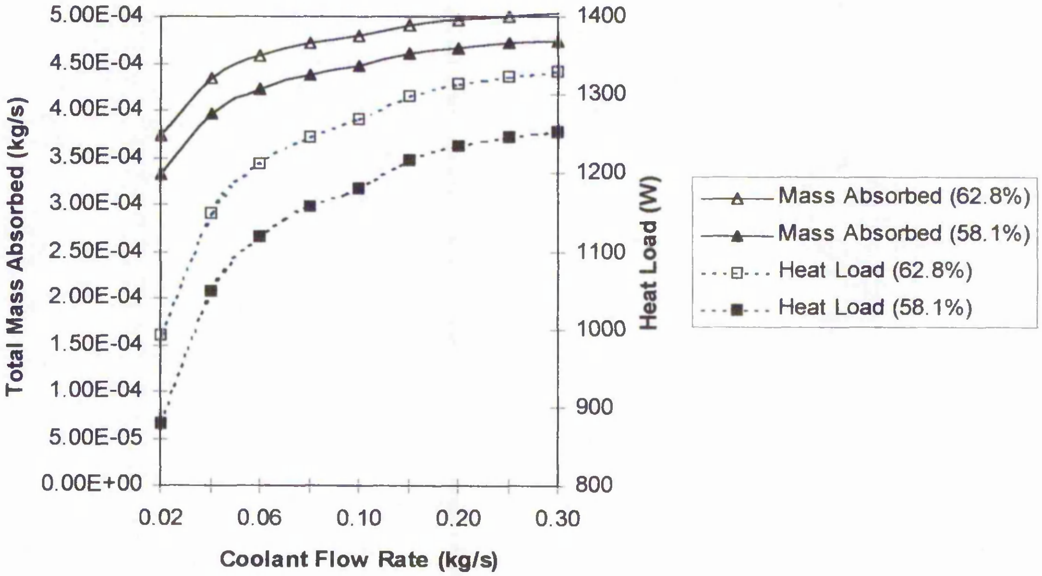

Figure 6.12 Effects of mass concentration and coolant flow rate on the heat load and mass absorbed

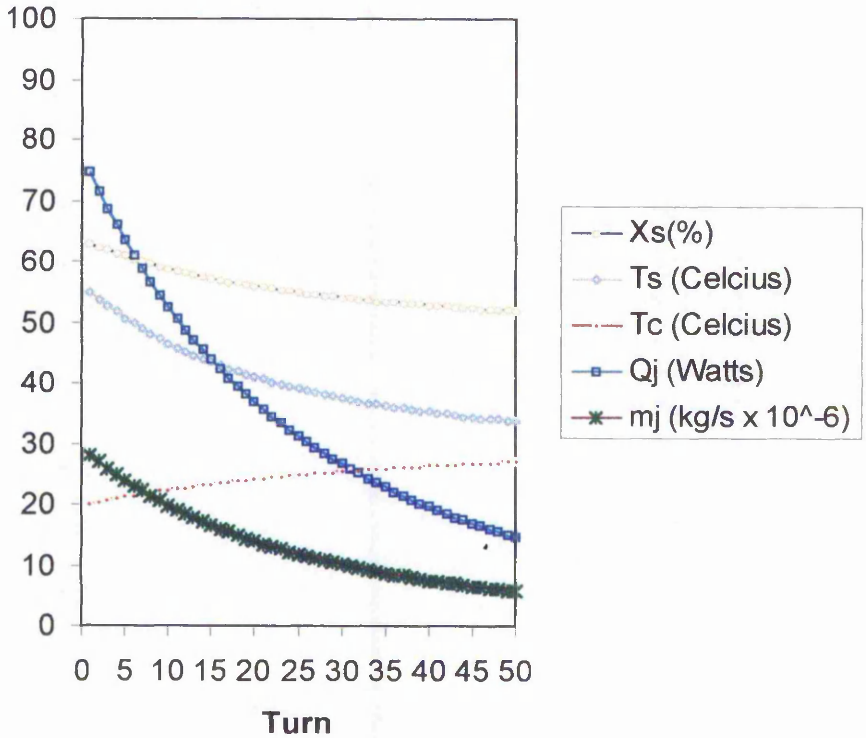

Figure 6.13 Changes of inlet solution concentration, inlet solution temperature, cooling water temperature, heat transferred and mass absorbed at various points

(Note: The unit on Y axis refers to unit in the bracket of the legends)

This feature of designing an absorber for different conditions was incorporated into the computer program ABCON. Figure 6.14 shows the interface of the program developed in this work. The program only requires five initial conditions, which are the efficiency of solution heat exchanger and the temperatures of four components (Absorber, Condenser, Evaporator and Generator). The complexity of computation is hidden from the user, while the more important inputs such as mass flow rates of solution and cooling water, number of drop sites, coil diameter and other inlet conditions remain available for detailed modelling.

In summary, the programs developed for designing these components have shown to be a large improvement over its predecessors, which needs considerable amount of work and assumes a thorough understanding in almost every aspect of the principles of ACS by the user. These programs can be used not only to study the component behaviour numerically such as the conditions of every turn of an absorber coil, it also provides a graphical view of the results which will help towards comparison of results for different set of parameters easily and effectively, features that are invaluable for designers in the industry.

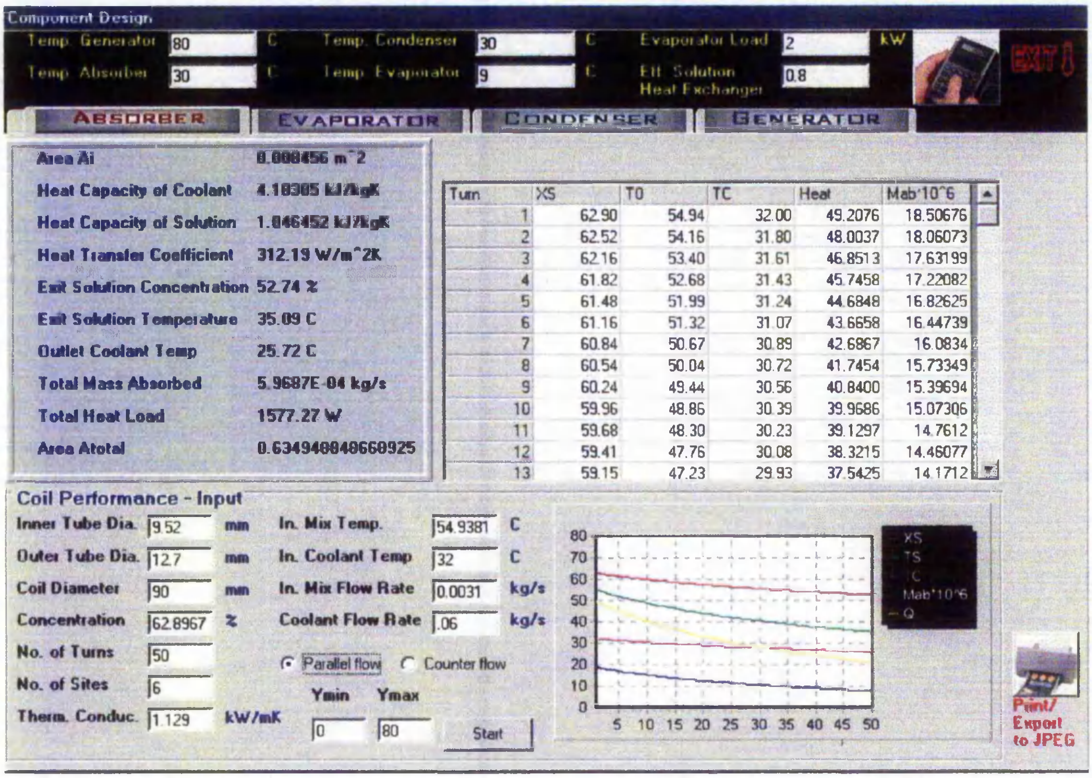

Temp. Generator 80 C
Temp. Absorber 30 C
Temp. Condenser 30 C
Temp. Evaporator 9 C
Evaporator Load 2 kW
Eff. Solution Heat Exchanger 0.8

Area Ai 0.008456 m^2
Heat Capacity of Coolant 4.18305 kJ/kgK
Heat Capacity of Solution 1.846452 kJ/kgK
Heat Transfer Coefficient 312.19 W/m^2K
Exit Solution Concentration 52.74 %
Exit Solution Temperature 35.09 C
Outlet Coolant Temp 25.72 C
Total Mass Absorbed 5.9687E-04 kg/s
Total Heat Load 1577.27 W
Area Atotal 0.634948848668925

Turn	XS	TO	TC	Heat	Mab*10^6
1	62.90	54.94	32.00	49.2076	18.50676
2	62.52	54.16	31.80	48.0037	18.06073
3	62.16	53.40	31.61	46.8513	17.63199
4	61.82	52.68	31.43	45.7458	17.22082
5	61.48	51.99	31.24	44.6848	16.82625
6	61.16	51.32	31.07	43.6658	16.44739
7	60.84	50.67	30.89	42.6867	16.0834
8	60.54	50.04	30.72	41.7454	15.73349
9	60.24	49.44	30.56	40.8400	15.39694
10	59.96	48.86	30.39	39.9686	15.07306
11	59.68	48.30	30.23	39.1297	14.7612
12	59.41	47.76	30.08	38.3215	14.46077
13	59.15	47.23	29.93	37.5425	14.1712

Coil Performance - Input
Inner Tube Dia. 9.52 mm
Outer Tube Dia. 12.7 mm
Coil Diameter 90 mm
Concentration 62.8967 %
No. of Turns 50
No. of Sites 6
Therm. Conduc. 1.129 kW/mK
In. Mix Temp. 54.9381 C
In. Coolant Temp 32 C
In. Mix Flow Rate 0.0031 kg/s
Coolant Flow Rate .06 kg/s
● Parallel flow ○ Counter flow
Ymin 0
Ymax 80
Start

Figure 6.14 Interface of the program for designing the absorber

Chapter 7 Experimental Rig Design

7.1 Main Components

Figure 7.1 and Figure 7.2 show the front view of the experimental rig and solution flow schematic diagram respectively. The system was driven by a gear solution pump with two heaters in the generator simulating the heated water load.

Figure 7.1 Front view of the ACS experimental rig

FIGURE 7.2 - SOLUTION FLOW SCHEMATIC DIAGRAM

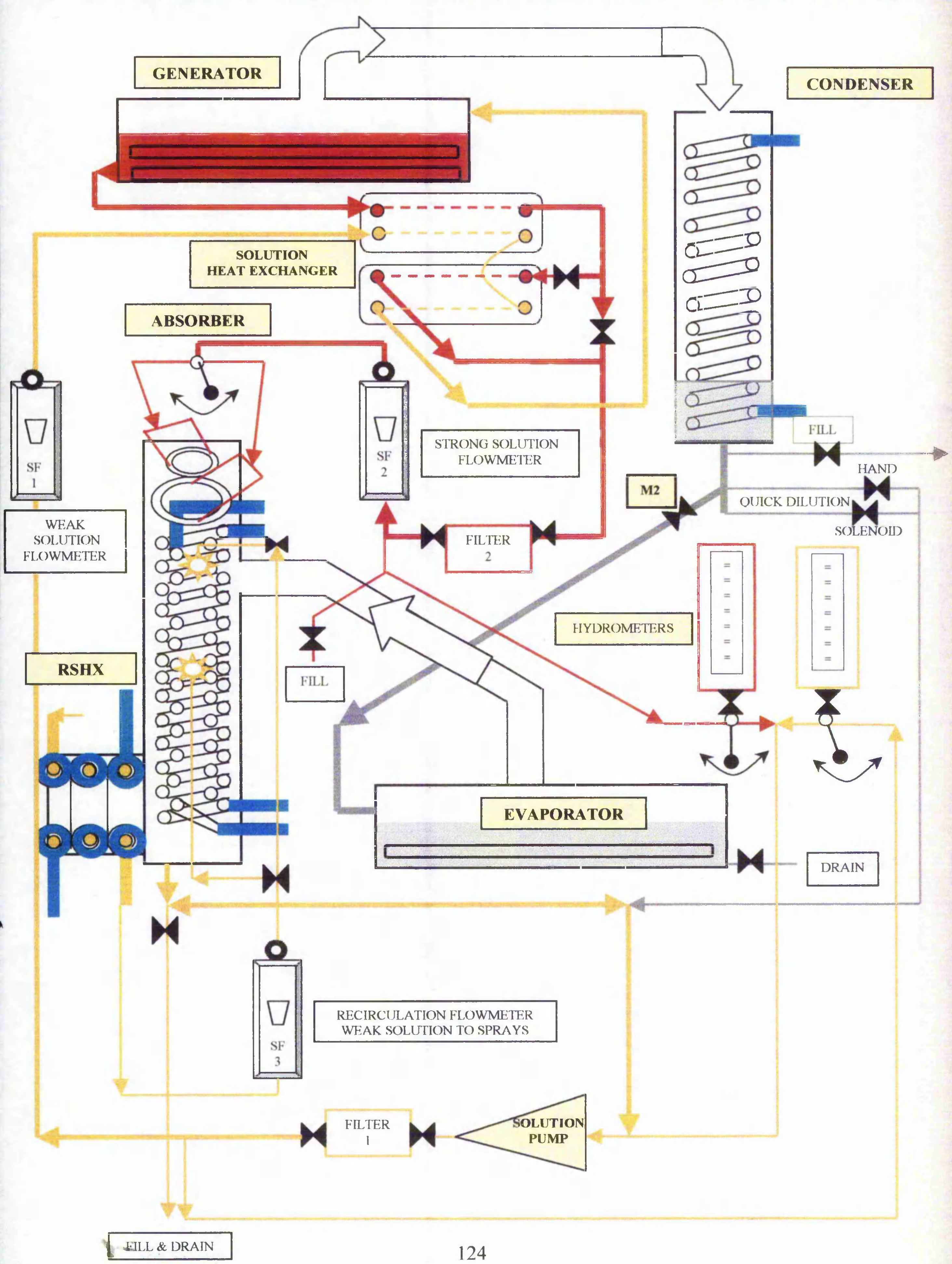

7.1.1 Absorber

The absorber is generally the most expensive component in absorption refrigeration machines. The absorber employed in the current work consisted of two sandblasted borosilicate glass coils which was mounted vertically. Seven type K thermocouples were inserted at every three turns of the inner coil. Two sprays were placed at the top and bottom of the absorber. The top spray was positioned at nearly the same level as the drip coils, while the bottom spray was located in the middle of the absorber. The spray density was controlled using regulator valves to wet the surface as much as possible. A 3-port valve was used to control the solution flow to the inner and outer drip coils. There are two paths from the 3-port valve to each drip coil to achieve even distribution of strong solution from generator. The solution can be directed to flow entirely on the outer or inner coils by switching the valve to the left or right respectively.

The length of the absorber body is 718mm and the diameter 160mm. The space between each turn of the coils is 10mm. A 150mm space at the bottom is designed to hold the excess solution. The tube diameters of both inner and outer coil are each 12.7mm. The inner and outer coil diameters are 90mm and 128mm respectively and each have 22 turns. Diameters of both ends of the absorber (QVF cylinder) are 3". Each end is fitted with a TFE O-ring that is pressed against a brass disc by means of bolts and nuts that join the disc to flange, which encircles the tapered end of the glass tube. This method has been proved to seal off the glass absorber vessel and hold the operational pressure at sub-atmospheric pressure to a positive pressure of up to 1.5 bar gauge without any leakage. A detailed CAD drawing of absorber is shown in Figure 7.3.

7.1.2 Condenser

A borosilicate glass coil condenser was selected and designed to use in the current work. This type of condenser is normally used in small chemical plants or other experimental work and can be found in some small heat pumps that use copper. It was chosen to allow maximum exposure of surface to the water vapour from the generator without sacrificing too much drop in pressure. The coil has 35 turns and made from ½" diameter glass with smooth outer surface. The gaps between the coil turns were designed at 3mm, which allowed exposure of the entire surface without sacrificing too much space. The thread size was designed to fit the 32mm tube link to the condenser inlet while the outlet tube diameter size at the bottom was kept at ½". The details are shown in Figure 7.4.

7.1.3 Generator

The borosilicate glass generator was mounted horizontally to minimise violent boiling. The surface for evaporation in this position is also increased compared to a vertically mounted vessel. Two 2 kW heaters were fitted in the generator with one at the top and the other at the bottom. Each heater is about two meters long. They were wound and bound together with copper wire to fit in the generator. The diameter and length of the generator are 150mm and 600mm respectively. The inlet for weak solution is a ½" diameter ground stubs which was designed at 113mm height and made for wade coupling connections. The outlet of the strong solution was placed at a ½" hole at the bottom of the end plate. The end plate has four ¼" hole for heaters and three 1/8" hole for thermocouples. Another 3/8" BSP hole is used for float switch. An outlet with thread size to suit 32mm tube link was placed at the top for conveying water vapour to condenser. The detailed dimensions are shown in Figure 7.5

7.1.4 Evaporator

The evaporator diameter and length are the same as the generator. The end plate is similar to the one used for generator. There are, however, three holes less than the end plate of generator with 2 holes excluded for a heater and one for the thermocouple measuring the heater surface temperature. The inlet for refrigerant liquid is a ½" diameter ground stubs for wade couplings connection. There is also a charging and discharging hole at the end plate. The outlet hole for the evaporated vapour to the absorber is slightly larger than the generator vapour outlet. The thread size of the outlet was designed to suite 44mm tube link. The evaporator was also filled with matting and sponge (used in gardening) to increase the surface of evaporation. The CAD drawing is shown in Figure 7.6.

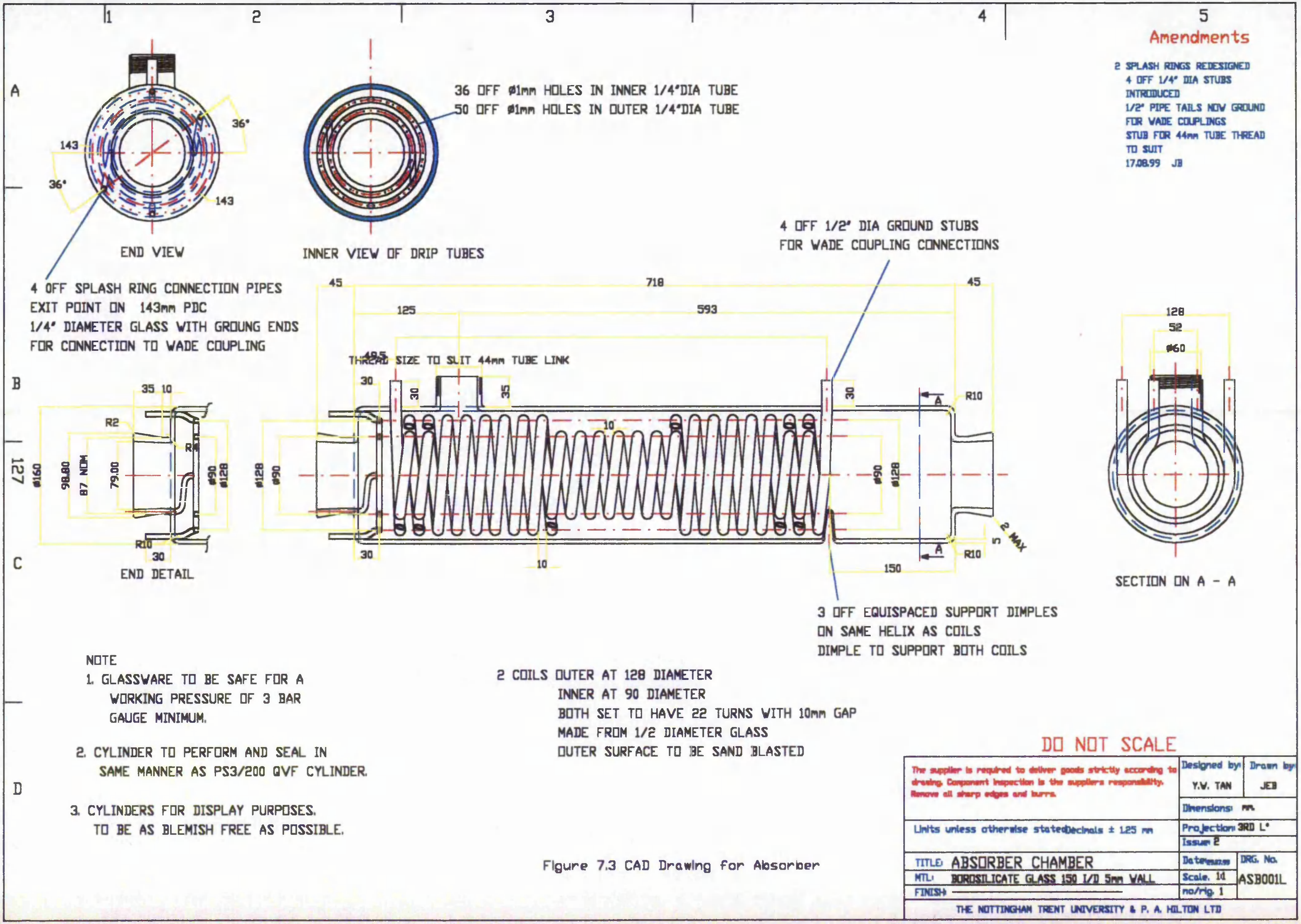

Figure 7.3 CAD Drawing for Absorber

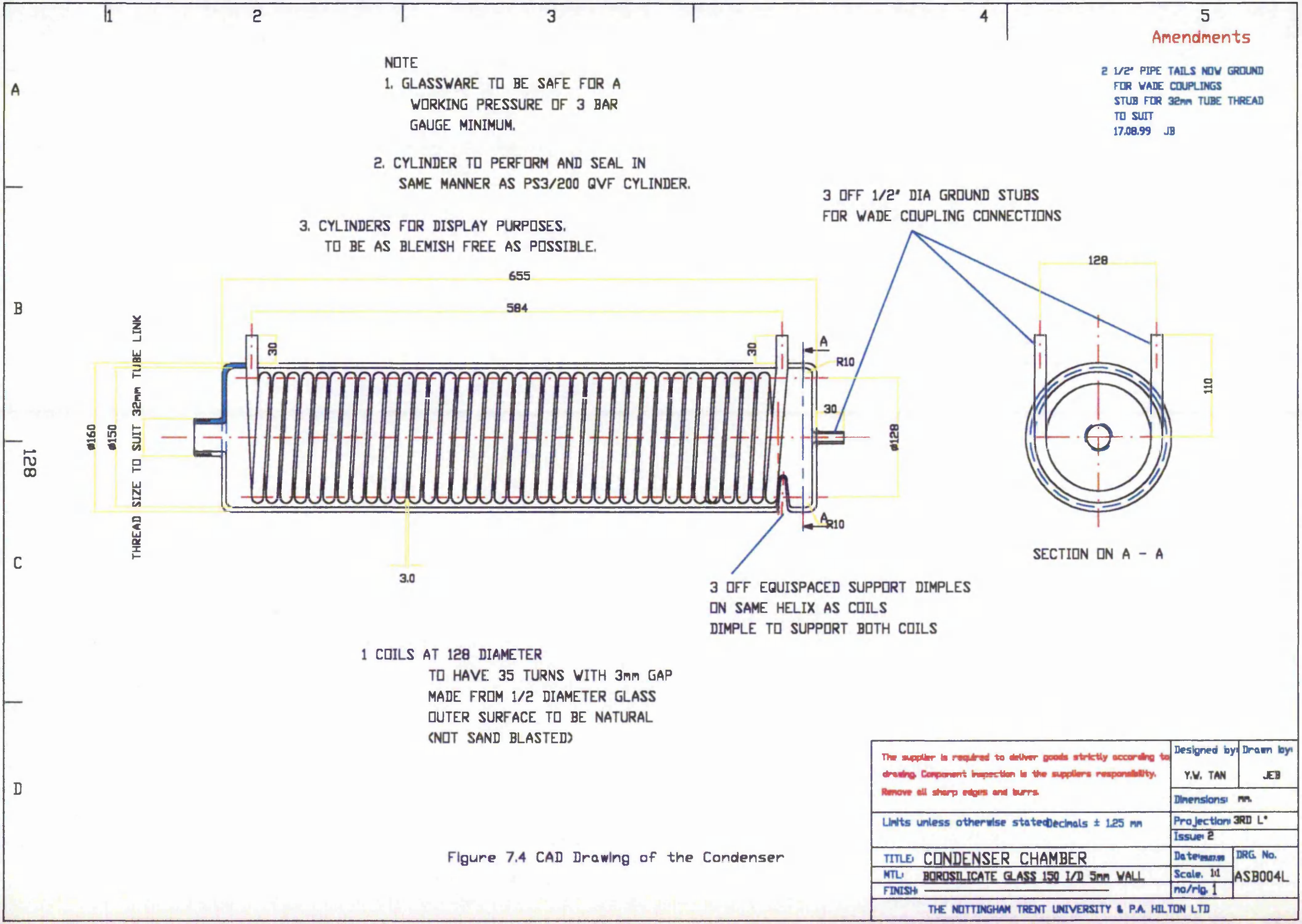

Figure 7.4 CAD Drawing of the Condenser

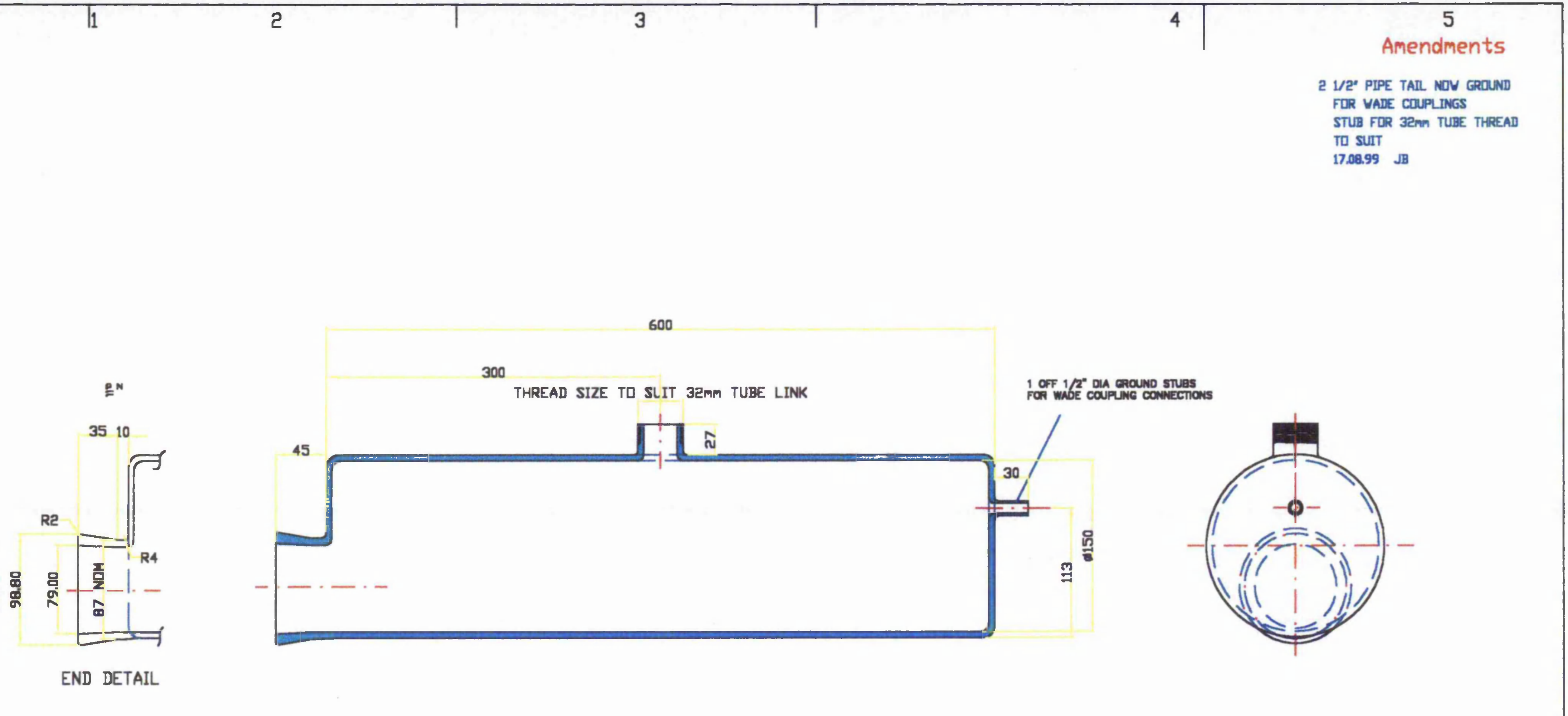

NOTE
1. GLASSWARE TO BE SAFE FOR A WORKING PRESSURE OF 3 BAR GAUGE MINIMUM.

2. CYLINDER TO PERFORM AND SEAL IN SAME MANNER AS PS3/200 QVF CYLINDER.

3. CYLINDERS FOR DISPLAY PURPOSES. TO BE AS BLEMISH FREE AS POSSIBLE.

Figure 7.5 CAD Drawing of the Generator

The supplier is required to deliver goods strictly according to drawing. Component inspection is the suppliers responsibility. Remove all sharp edges and burrs.

Designed by: Y.W. TAN
Drawn by: JEB
Dimensions: mm.
Limits unless otherwise stated Decimals ± 1.25 mm
Projection: 3RD L°
Issue: 2
TITLE: GENERATOR CHAMBER
MTL: BOROSILICATE GLASS 150 I/D 5mm WALL
FINISH: ——
Date:
Scale. 1:1
no/rig. 1
DRG. No. ASB002L
THE NOTTINGHAM TRENT UNIVERSITY & P. A. HILTON LTD

Amendments

2 1/2" PIPE TAIL NOW GROUND
FOR WADE COUPLINGS
STUB FOR 44mm TUBE THREAD
TO SUIT
17.08.99 JB

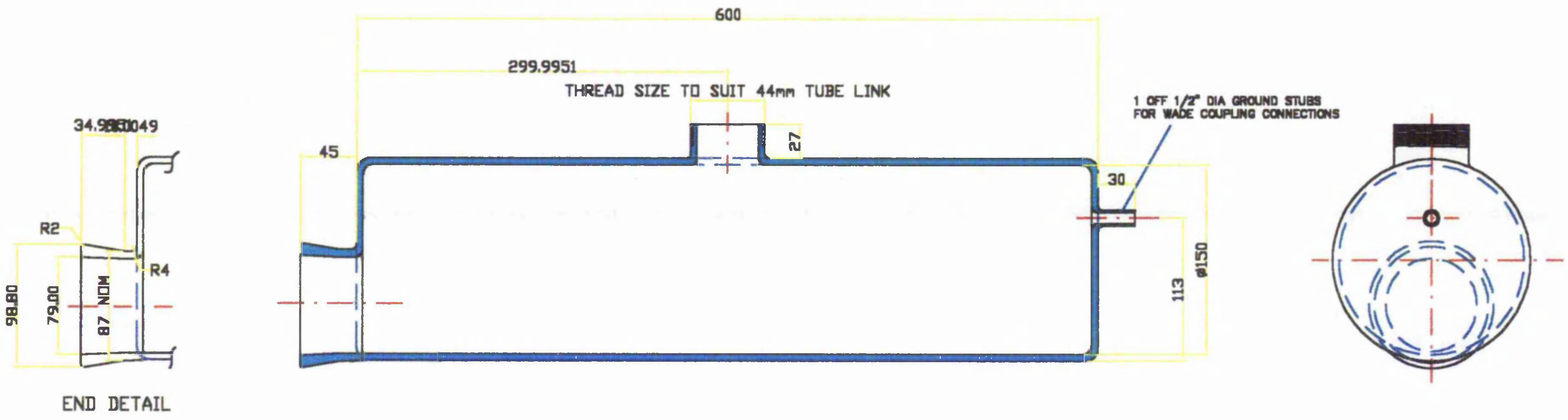

NOTE
1. GLASSWARE TO BE SAFE FOR A
WORKING PRESSURE OF 3 BAR
GAUGE MINIMUM.

2. CYLINDER TO PERFORM AND SEAL IN
SAME MANNER AS PS3/200 QVF CYLINDER.

3. CYLINDERS FOR DISPLAY PURPOSES.
TO BE AS BLEMISH FREE AS POSSIBLE.

DO NOT SCALE

Figure 7.6 CAD Drawing of the Evaporator

The supplier is required to deliver goods strictly according to drawing. Component inspection is the suppliers responsibility. Remove all sharp edges and burrs.

Limits unless otherwise stated :
Decimals ± 1.25 mm

Designed by: Y.W. TAN
Drawn by: JEB
Dimensions: mm.
Projection: 3RD L°
Issue: 2

TITLE: EVAPORATOR CHAMBER
MTL: BOROSILICATE GLASS 150 I/D 5mm WALL
FINISH:

Date:
Scale. 1:1
no/rig. 1
DRG. No. ASB003L

THE NOTTINGHAM TRENT UNIVERSITY & P. A. HILTON LTD

7.1.5 Solution heat exchanger and filter

Two SWEP compact solution heat exchangers were used in this work. Both of them can operate together when connected in series. If only one heat exchanger is needed, the other heat exchanger can be bypassed by turning the isolate valves $\mathbf{i_1}$ and $\mathbf{i_2}$ (Figure 7.7) into a vertical position.

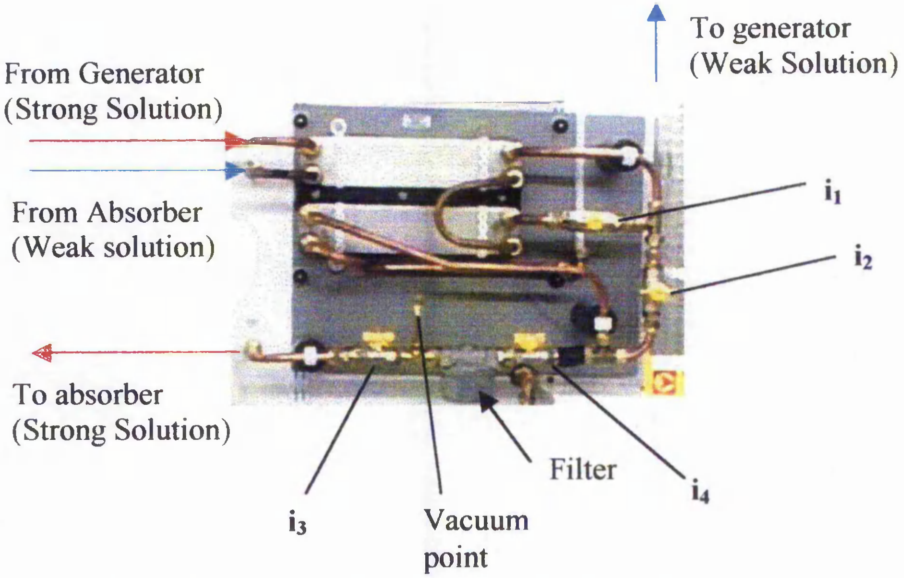

Figure 7.7 Solution heat exchanger and filter

A filter was fitted after the solution heat exchanger. The filter can be removed for cleaning by closing the $\mathbf{i_3}$ and $\mathbf{i_4}$ isolate valves. After the cleaning, the filter can be evacuated through the vacuum point before the isolate valves are switched on again.

7.1.6 Valves

Table 7.1 shows the list of valves used and their functions. The three important valves are metering valves used to control weak and strong solution flow rate and the refrigerant flow rate. Metering valves allow a very fine control over the low flow rate and also used for maintaining the pressure difference between generator and absorber. Most of the valves in Table 7.1 were used for cooling water circuit (See section 7.2). Schraeder valves were used for charging, discharging refrigerant and solution and for evacuating the system without introducing much atmospheric air into the system.

Table 7.1 Valve identification list – Absorption Chiller

VALVE No.	VALVE FUNCTION
1.	Stopcock. Mains water supply to water manifold
2.	Stopcock. Cooling water pump outlet
3.	Stopcock. Cooling water return to tank
4.	Stopcock. Mains water supply from manifold to cold blend flowmeter
5.	Stopcock. Supply from manifold (pumped or mains) to WF1 abs inner cooling coil
6.	Stopcock. Supply from manifold (pumped or mains) to WF2 abs outer cooling coil
7.	Stopcock. Supply from manifold (pumped or mains) to WF3 condenser cooling coil
8.	Stopcock. Supply from manifold (pumped or mains) to WF4 RSHX cooling coil
9.	Stopcock. Abs inner coil cooling water exit. Return to manifold (for re-use or drain)
10.	Stopcock. Abs outer coil cooling water exit. Return to manifold (for re-use or drain)
11.	Stopcock. Condenser cooling water exit. Return to manifold (for re-use or drain)
12.	Stopcock. RSHX cooling water exit. Return to manifold (for re-use or drain)
13.	Drain-down to basin cock. Manifold return line
14.	Drain-down to basin cock. Manifold pumped water line
15.	Drain-down to basin cock. Manifold forced drain line
16.	Drain-down to basin cock. Manifold mains water supply line
17.	Air vent cap. Manifold return line
18.	Air vent cap. Manifold pumped water line
19.	Air vent cap. Manifold mains water supply line
20.	Air vent cap. RSHX cooling water supply line
21.	Air vent cap. Condenser cooling water supply line
22.	Air vent cap. Condenser cooling water return line
23.	Air vent cap. Abs inner coil supply line
24.	Air vent cap. Abs outer coil supply line
25.	Air vent cap. Abs inner coil return line

26.	Air vent cap. Abs outer coil return line
27.	Drain-down to overflow tank. Abs inner coil
28.	Drain-down to overflow tank. Abs outer coil
29.	Drain-down to overflow tank. Condenser coil
30.	Solution system low-point/ solution pump outlet.
31.	Hand operated vent valve for solution system
32.	Schraeder valves. At each solution filter for vac attachment after cleaning
33.	Isolating valves. Each side of both solution filters to facilitate cleaning
34.	M1 Metering valve. At SF2. Strong solution from Gen, via SHX to Abs drip coils
35.	M1a 3-port valve. Strong solution divider between inner and outer drip coils
36.	M2 Metering valve. Liquid refrigerant from Condenser to Evaporator
37.	B1 Metering valve. At SF1. Weak solution from pump to Gen, via SHX
38.	B2 Metering valve. At SF3/Ch29. Weak recirculation from pump to sprays
39.	B2a Needle valve controlling weak solution to upper spray
40.	B2b Needle valve controlling weak solution to lower spray
41.	B3a Cooling water flow control. At WF1/Ch25. Absorber inner coil supply
42.	B3b Cooling water flow control. At WF2/Ch26. Absorber outer coil supply
43.	B4 Cooling water flow control. At WF4/Ch28. RSHX coil supply
44.	B5 Cooling water flow control. At WF3/Ch27. Condenser coil supply
45.	Metering valve. Quick dilution hand valve. Liquid refrigerant direct to Absorber.
46.	Solenoid valve. Automatic Quick dilution controlled by logger Output 1/4
47.	Solenoid valve. Automatic Cold blend controlled by logger Output 2/4
48.	Metering valve. At Cold blend flowmeter Ch30. Hand controlled cold blend.
49.	Schraeder valves. At each solution filter for vacuum attachment after cleaning
50.	Schraeder valve. Air ejector vacuum-access point.
51.	Schraeder valve. Evaporator drain or charge point.
52.	Schraeder valve. Weak solution hydrometer, Vent, bleed or vac point.
53.	Schraeder valve. Strong solution hydrometer, Vent, bleed or vac point.
54.	Absorber low-point. Weak solution - charge & drain (extended tube).
55.	Condenser low-point. Refrigerant - charge & drain (extended tube).
56.	Generator and SHX. Strong solution - charge & drain (extended tube).
57.	Water pump casing drain (extended tube).

7.1.7 Solution pump and vacuum pump

Due to the low pressure of ACS which is normally less than 1kPa during operation, a hermetic pump is essential. Eames and Wu (1999) have tested several types of pumps including vane, gear, solenoid piston, diaphragm and magnetic pumps. Vane and gear pumps were proven to be the most reliable. Magnetic-drive pump has been used in some of the ACS but is not suitable for a small scale ACS development due to its high cost.

Gear pump was selected in this project. Its advantages include the ease of controlling the pump-speed by adjusting a screw. A special water ejector vacuum pump was also used in this work. It functions like a Venturi tube. A conventional pump could be used, however, a cold trap must be added before the entrance to avoid contamination of water. Figure 7.8 shows the solution pump that was connected to a filter at the inlet to capture any small particles or crystals from absorber.

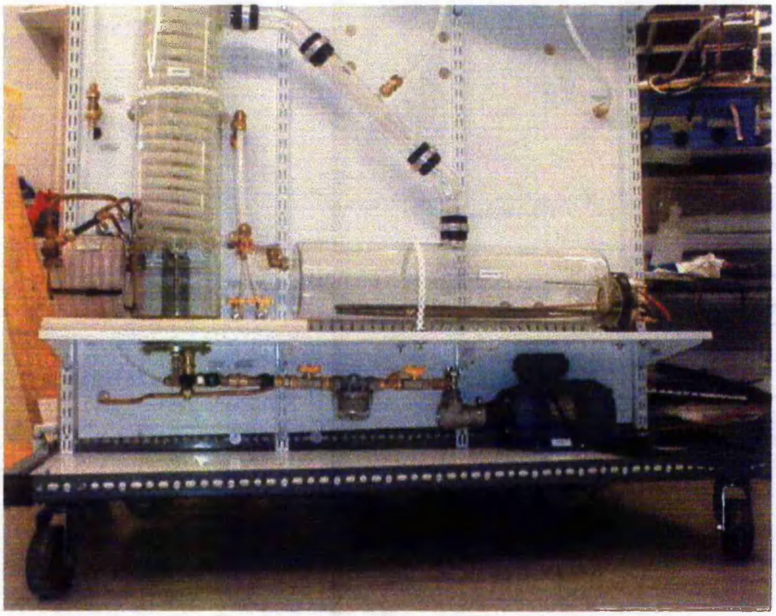

Figure 7.8 Solution pump

7.2 Cooling water circuit

The cooling water was used to remove heat from recirculation heat exchanger, condenser and inner and outer coils of absorber. The heating and cooling water circuit diagram is shown at Figure 7.9. Figure 7.10 shows the system that was fixed under the control panel at the rear side of the experimental rig. The cooling water can be swapped quickly by using mains supply water or a recirculation water circuit driven by a centrifugal pump.

A water tank was fixed for storage and to preheat the water to the required temperature by three heaters (Two 0.5kW heaters and one 2kW heaters). When the water pump is used for recirculation, the water will return to the water tank. When the tank is nearly full the excess water will pass to another tank which is employed for overflow so that the excess water can be drained effectively when flow rate of cold blend is increased.

The cold blend system can be controlled manually or automatically. A float switch was sited near the top of the water tank to stop the cold blend when the level rises to the preset level. Setting a high limit of temperature in the data logging software can also activate the cold blend. The cold blend is activated through a solenoid valve when in automatic mode. The water basin is used for collecting the remaining water in the pipeline when the configuration has to be changed (For example, changing supply of cooling water from using mains water pressure to pump for recirculation). A regulator was fitted to control the mains pressure and a strainer was placed next to it.

FIGURE 7.9 ABSORPTION WATER SYSTEM SCHEMATIC

(MANIFOLD CONFIGURED FOR PUMPED/RECIRCULATED COOLING SYSTEM)

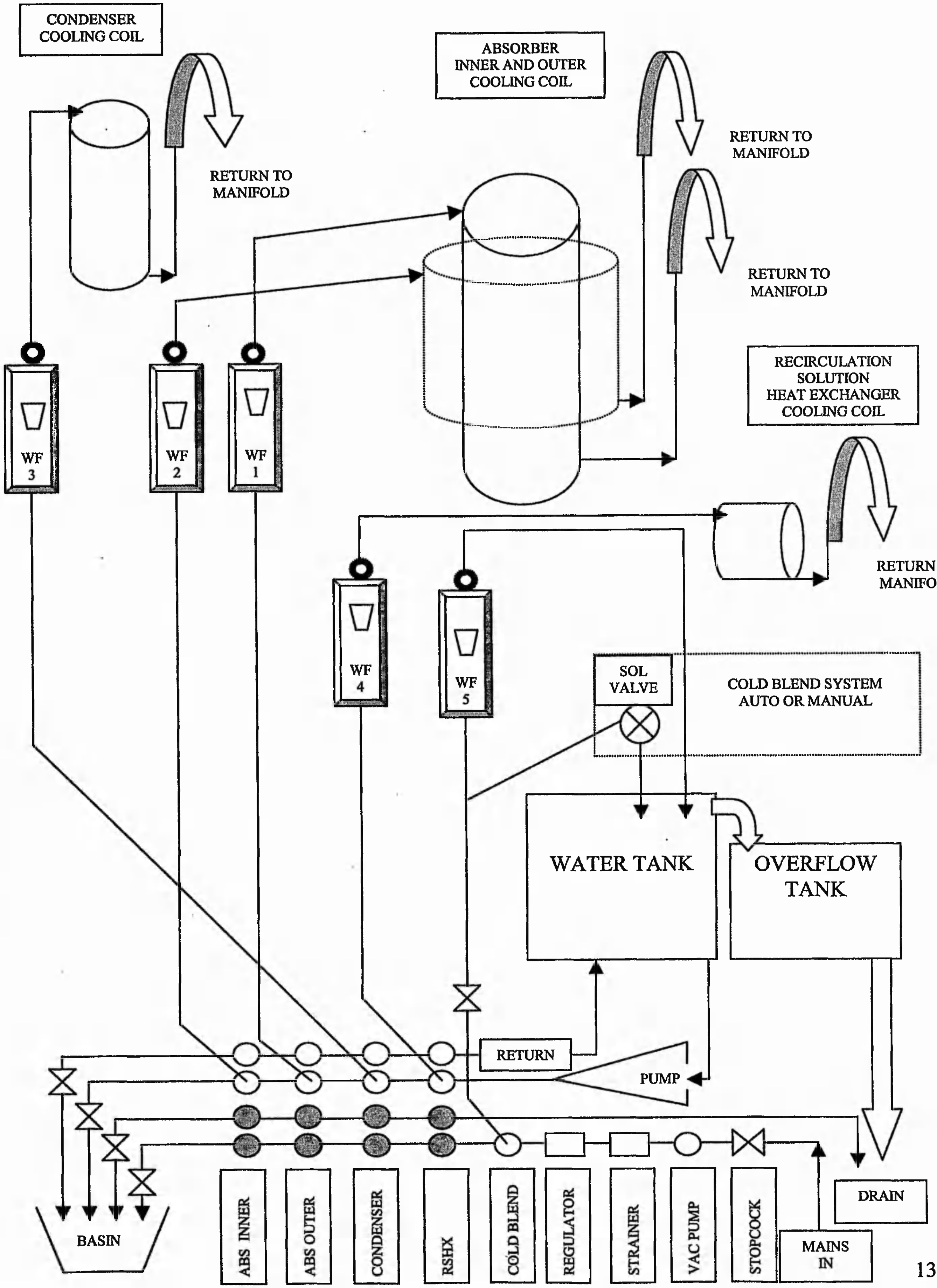

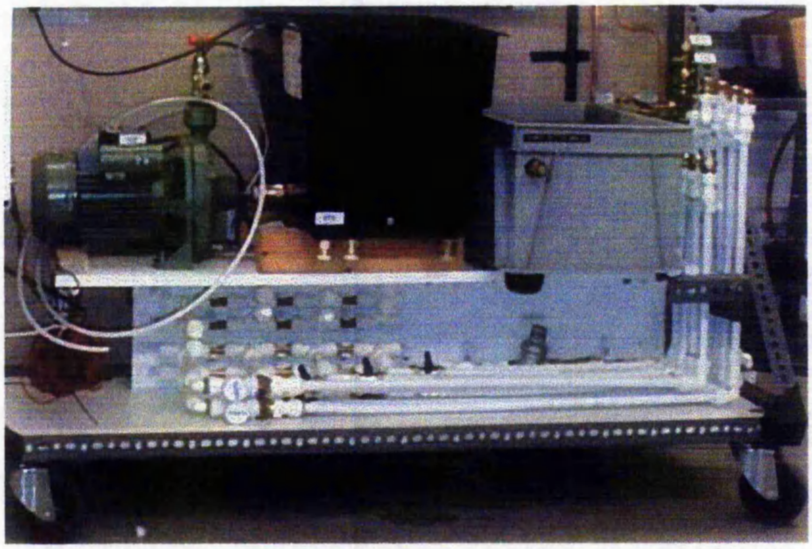

Figure 7.10 Cooling and heating water circuit

7.3 Instrumentation

In this section, the instrumentation for measuring and controlling the various parameters are reported. The instrumentation used in this work can be divided into two groups: 1. Manual, 2. Automatic (Using data logger). The use of different measuring devices were found necessary as some of the transducers such as Coriolis mass flow meter and optical fibre sensor to measure the mass concentration were considered to be too expensive. Physical measuring of fifty experimental points manually in a short space of time was found impossible and further, such measuring of all the channels will introduce additional human errors in readings of gauges. Current work addresses this problem using transducers in conjunction with a data-logging program. This proved useful in monitoring the process, thus tackling problems as they arise and even preventing them before anything more serious resulted.

7.3.1 Flow meter and transducer

Five water flow meters and three solution flow meters were installed on the control panel of the experimental rig (Figure 7.19). Two flow meters were used to measure the cooling water mass flow rate of outer (WF1) and inner (WF2) absorber coils. The other three were employed to measure water mass flow rate of the condenser (WF3) and recirculation heat exchanger (WF4) coils and cold blend respectively. The unit for these four meters are in gram/s. Two volume flow meters in cm^3/min were placed in between the generator and absorber for measuring the volume flow rate of the weak and strong solution respectively. The remaining one was used for measuring the volume flow rate of recirculation solution. All the five mass flow meters for cooling water and a volume flow meter for recirculation solution were connected to RS flow transducers. The calibration charts and conversion factors are shown in Fig. 7.11 – Fig. 7.16.

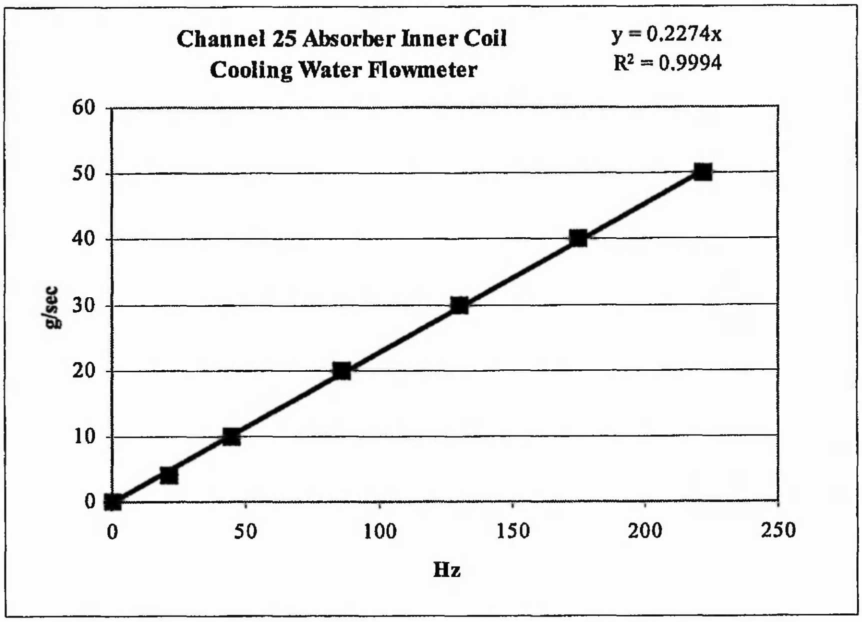

Fig 7.11Calibration chart of flow transducer for inner absorber coil

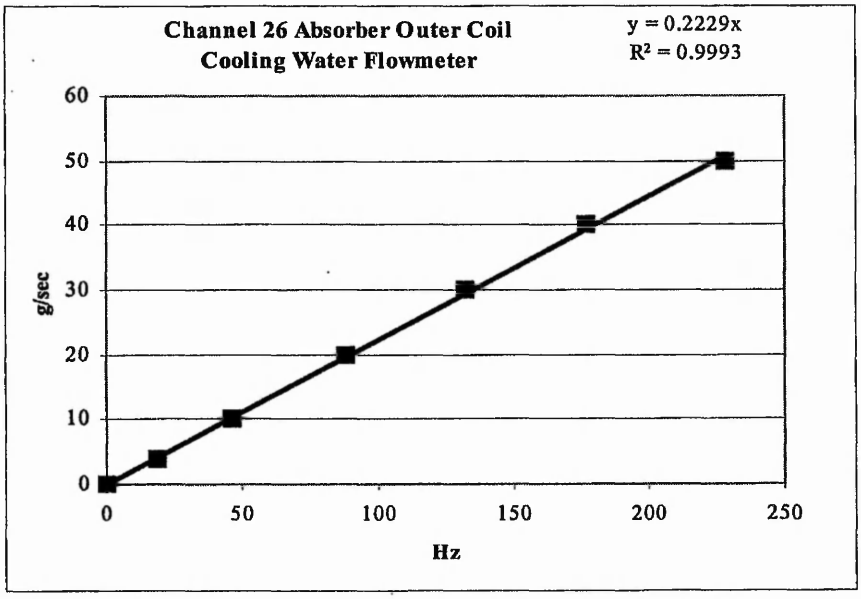

Fig 7.12Calibration chart of flow transducer for outer absorber coil

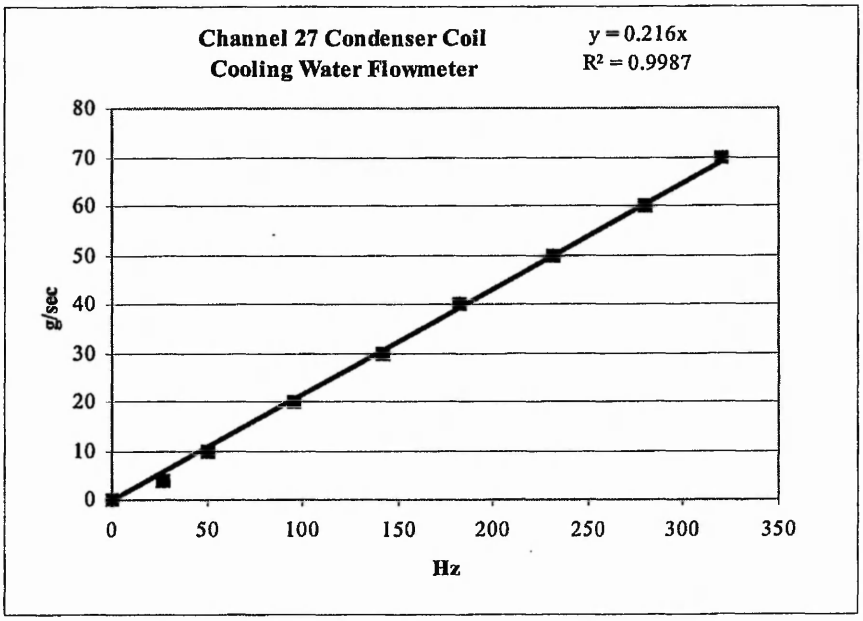

Fig. 7.13Calibration chart of flow transducer for condenser coil

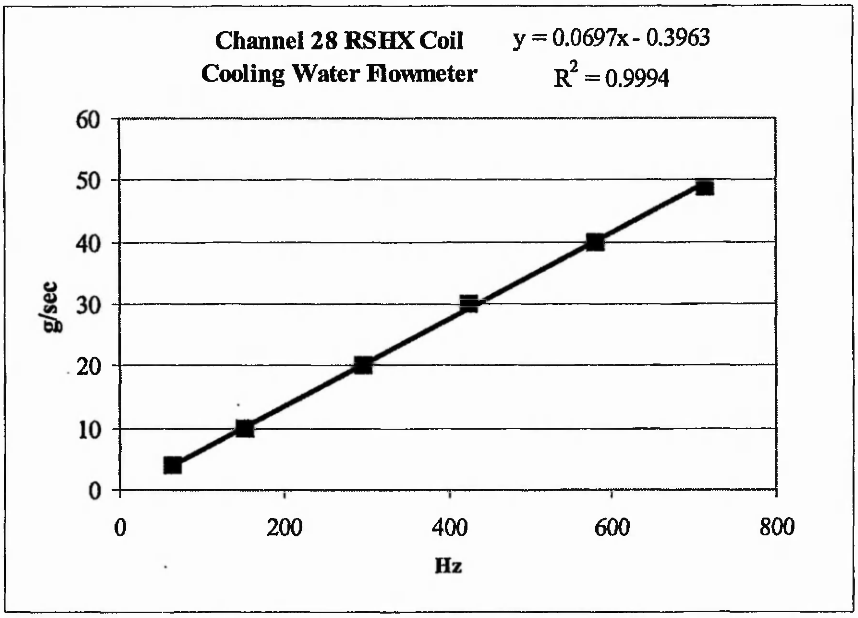

Fig. 7.14Calibration chart of flow transducer for RSHX cooling water coil

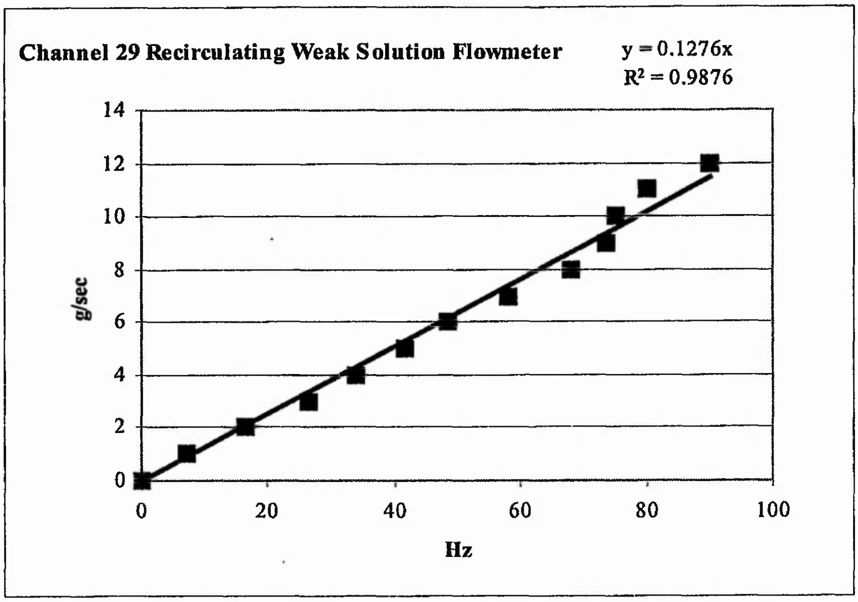

Fig. 7.15Calibration hart of flow transducer for recirculation solution

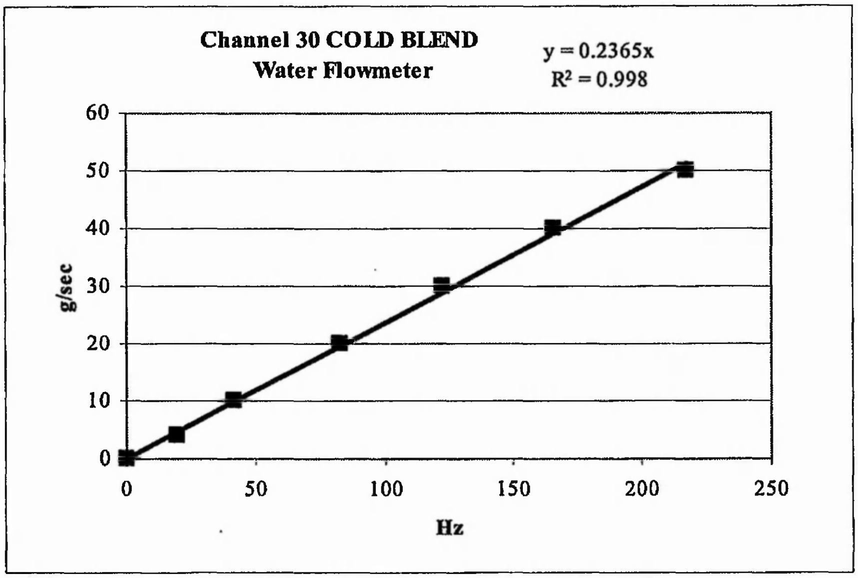

Fig. 7.16Calibration chart of flow transducer for cold blend

7.3.2 Pressure gauge and transducer

Two pressure gauges in the range of –100 kN/m^2 to 300 kN/m^2 gauge were used. Each of them was attached to pressure transducers to record the condensing pressure and evaporating pressure respectively. The initial calibration charts for the pressure transducers are shown in Fig 7.17 and Fig 7.18.

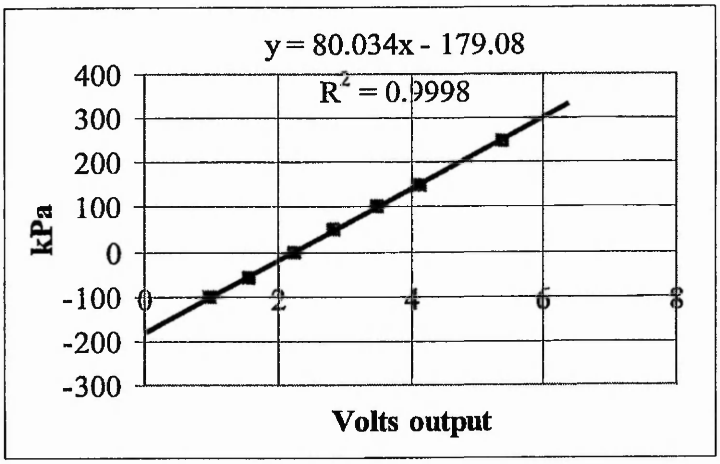

Figure 7.17 Calibration chart for pressure transducer (High pressure side)

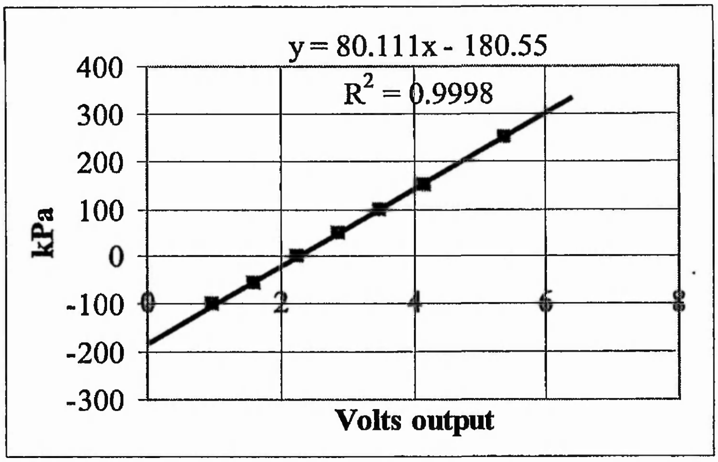

Figure 7.17 Calibration chart for pressure transducer (Low pressure side)

7.3.3 Thermocouples

There were two sets of thermocouples used in the experiment. The first set consisted of 15 thermocouples, connected to a 15 channels selector. The second set had 30 thermocouples that were connected to the data logger (See section 8.1). The thermocouples were calibrated against an ice datum at 0°C. A master thermocouple probe was used to offset the cold junction compensation of the data logger. Apart from the thermocouple probes used for measuring the water vapour in generator, absorber and evaporator, all other thermocouples were made in-house and fitted to the experimental rig. Some heat transfer compounds were applied to enhance the conduction between the thermocouple and the surface measured. The first thermocouple set was used to log the main experimental points described in Table 7.2.

Table 7.2 Description table of 15 channels selector for temperature measurement

No.	Channel Name	Description
1	T01absEwk	Absorber exit (Weak)
2	T02shxIwk	Solution heat exchanger inlet (Weak)
3	T03genIwk	Generator inlet (Weak)
4	T04genEst	Generator exit (Strong)
5	T05shxEst	Solution heat exchanger exit (Strong)
6	T06m1Est	Metering valve exit
7	T07genErv	Generator exit (Ref. vapour)
8	T08conErl	Condenser exit (Ref. liquid)
9	T09evaIrl	Evaporator inlet (Ref. liquid)
10	T10evaErv	Evaporator exit (Ref. vapour)
11	T11rhxEwk	Recirculation heat exchanger exit (Weak)
12	T12hydwk	Hydrometer weak
13	T13hydst	Hydrometer strong
14	T14aboicIcw	Absorber inner coil (Cooling water)
15	T15aboicEcw	Absorber inner coil (Cooling water)

7.3.4 Hydrometer

The mass concentrations of the aqueous lithium-bromide were monitored by using two hydrometers. Other measuring devices such as fibre optic refractometer, PZT transmitter and receiver, ultrasonic concentration analyser, capacitance sensor, electromagnetic probe, conductivity meter, IR spectrometer and Coriolis density sensor were considered for measuring the mass concentration. Heinonen and Taoscott (1999) investigated in detail of the pros and cons of these sensors. These sensors are either too expensive or the data range for aqueous LiBr were not available. Among these sensors, PZT strap-on speed-of-sound sensor has the highest potential based on cost consideration and performance. This sensor, however, is still under development and will not be available for a few years (Heinonen and Taoscott, 1999).

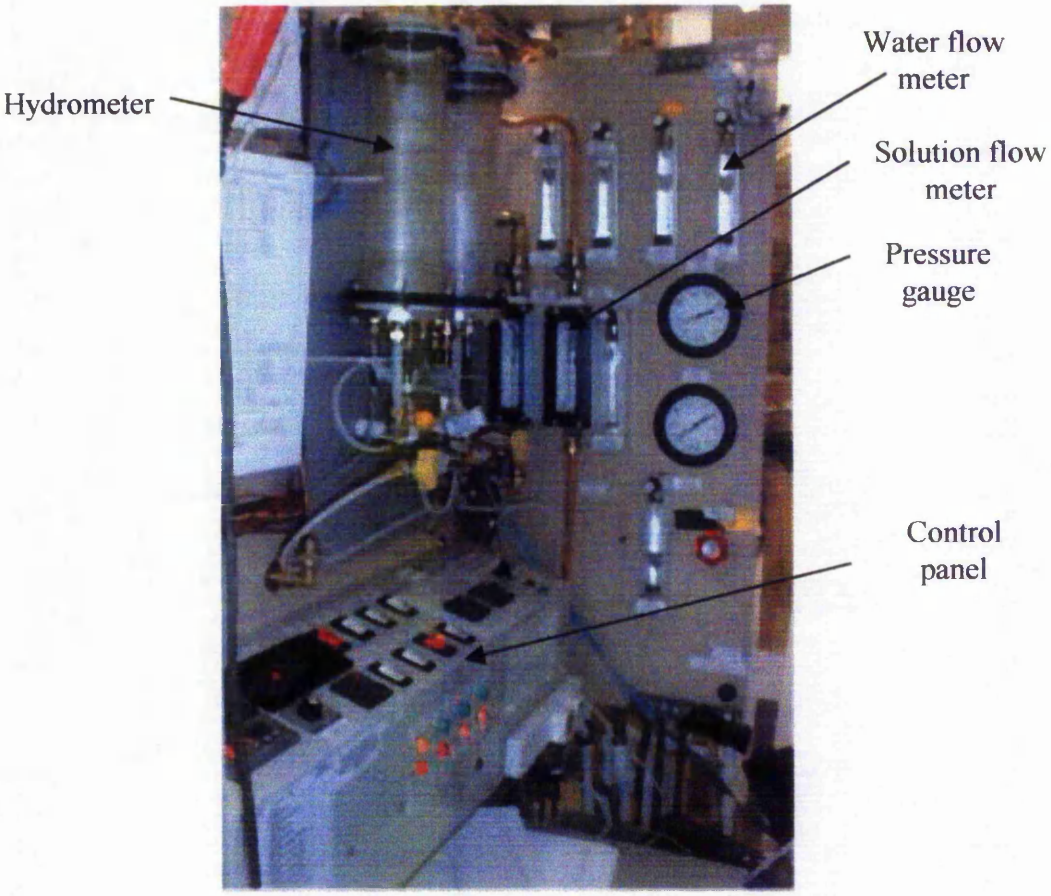

Figure 7.19 Rear view of experimental rig (hydrometer, flow meter, pressure gauges, and control/monitoring panel)

In the meantime, use of hydrometer has been found to be reliable in terms of accuracy and more importantly it is cheap. It is, however, very fragile. Three hydrometers were broken during installation in this work. A large vessel is also needed to prevent any friction between the hydrometer and the vessel's surface. Figure 7.20 shows the hydrometers used for measuring the weak and strong solution mixture.

Figure 7.20 Hydrometers for measuring strong and weak solution mixtures

The mass concentrations were computed simply by measuring the specific gravity using the hydrometer and temperature of the solution. Leverton-Clarke Ltd provided the density data for different concentrations at the temperatures used in this work.

7.4 Control system

Three temperature controllers were used for controlling the surface temperature of evaporator heater and generator lower and upper heaters. Type K thermocouple probes were brazed onto the heater surface. About 20°C difference between the heater wall temperature and the required liquid temperature were set. For instance, 110°C was set for the heaters in generator if 90°C solution temperature is required. In order to control the heat load by cutting the voltage at different rates (a build in function in the data logger namely 'burst-fire'), burst-fired rate has to be sent through the data logging software. The lower generator heater was burst-fired by the first logger.

The upper limits of generator temperature (T_4) are normally set in between 70°C to 90°C and the condition was set to 'Continuous' (See section 8.3.4). For instance, if the upper limit is set at 70°C, when the generator temperature exceeds 70°C, the data logging software will turn off the output channel until the temperature dropped below 70°C again. The burst-fired channel on second logger was used to control the cooling water temperature. It burst-fired the 2kW water heater to the preset load.

The temperature of the inlet inner absorber coil (T36) was set as the base point for operation limits. The lower limit was set in between 20°C to 30°C and the condition was set to 'Continuous' (See section 8.3.4). For example, the burst-fired channel will be activated if the cooling water temperature drops below the lower limit (°C) until it rises again above the preset lower limit temperature.

There were eight MCB switches dedicated to the solution pump, water pump, 2kW generator upper and lower heater, 2kW evaporator heater, two 0.5kW water heaters and a 2kW water heater. All of them can be switched on and off manually or through the data logger. They were also connected to neon lamp for displaying the current condition. The switching by logger is useful especially during the shut down process.

The crystallisation, which normally occurs during shut down can be prevented by diluting the solution with water from condenser and circulating in-between generator and absorber until the generator temperature reduces to the safety level. The fast dilution pipe was connected in-between condenser and absorber. Two valves were used to separate the pipe. One of them was operated manually while the other, which is a solenoid valve, was controlled by the data logging software.

7.5 Safety devices

The whole system was tested at 1.5 bars. A pressure relief valve was set to relieve at this pressure. Apart from the high temperature cut-out by the temperature controllers mentioned earlier, the float switches were also employed to protect the generator and evaporator heaters. The float switches were placed on top of the heater to make sure the heater surfaces were always covered by liquid. For safety reasons, the rig was enclosed in glass windows during operation.

7.6 Construction problem encountered

Major problems arose during connections on stub pipes. The compression fittings were found to be inappropriate due to its sharp taper end and causing breakage of glass tubes. The connections were improved after modifications to the compression fittings by creating a gradual taper. The connections were further modified into finger tight couplings with threads. The upper QVF of absorber also broke during pressure test. The pulling force when tightening the top end plate on the QVF caused the total force to exceed the original limit that the glass was designed to withstand.

Chapter 8 Data Logging

8.1 Experimental points

Figure 8.1 shows the sketch of the experimental rig with connection points to the data logger. The descriptions of the points are shown in Table 8.1 while the details of the wiring are shown in Tables ***Ca1*** and ***Ca2*** in Appendix ***C1***.

8.2 Data logger configurations/specifications

The Hilton data logger (D101/42) is a multi-channel analogue and digital unit with both input and output capability. Commands and data are transferred via a RS232 serial link using ASCII character strings sent and received by the data logging software (See section 8.3). The serial communication protocol is

Baud rate	: 9600
Parity	: None
Data bits	: 8
Stop bits	: 1

8.2.1 Analogue inputs

Temperatures (Differential input channels)

Up to 15 thermocouple inputs may be addressed in a data logger and these connect to terminals labelled D1+ D1- to D15+ D15-. Either type T or type K thermocouples may be used. There are only 35 channels on a single logger thus, the numbers of first fifteen channels for thermocouple on the second data logger will be 36 to 50. This also means that channel 36 is the first channel on the second logger.

Single ended DC voltage channels

Up to 8 low voltage DC analogue inputs may be addressed and these connect to the terminals labelled V1+ 0V … V8+ 0V.

In this project, V1 and V2 are used to connect the two pressure transducers to measure the high side (condensing) and low side (evaporating) pressure respectively. V3 is connected to a Wattmeter to measure the evaporating load.

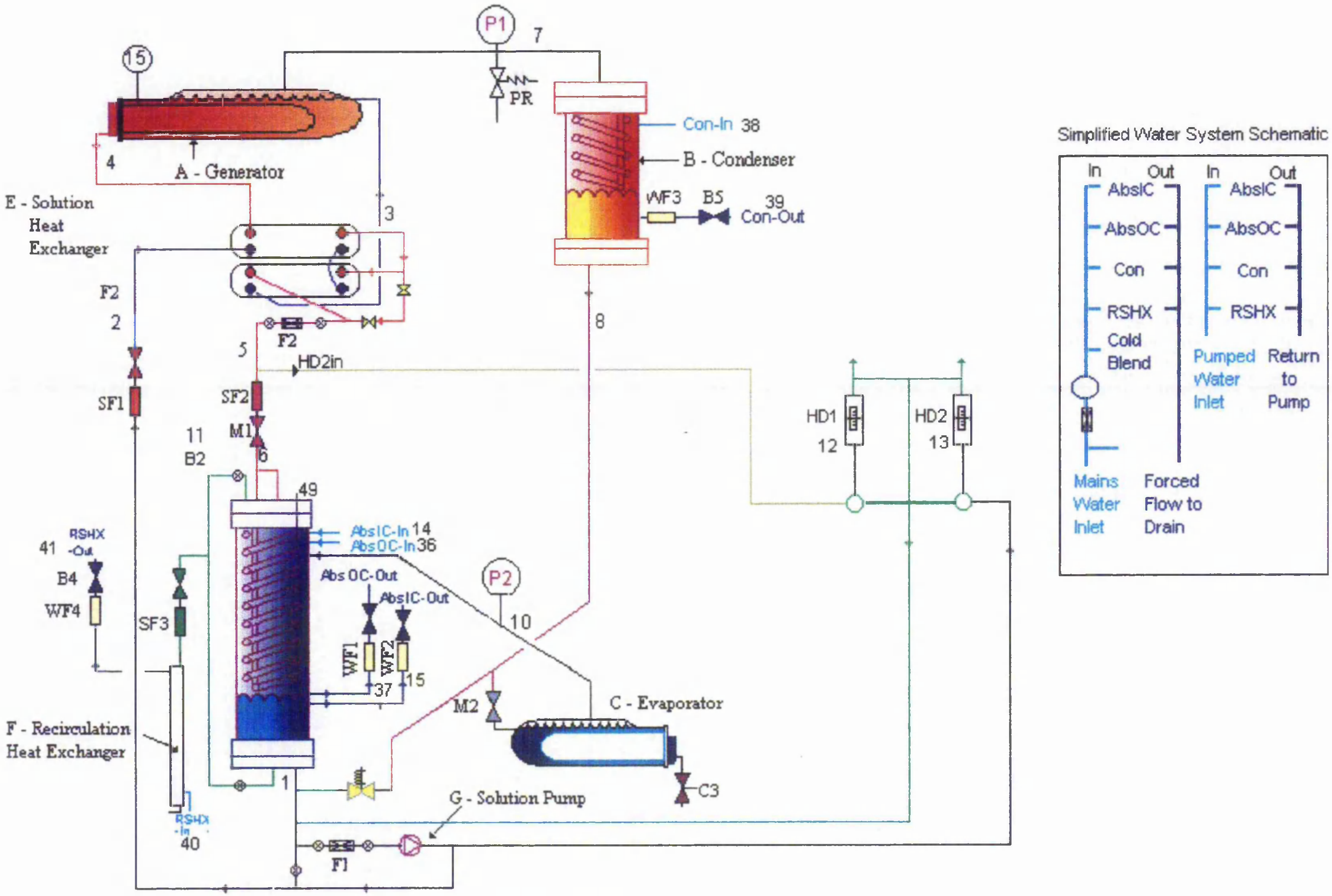

Figure 8.1 Schematic diagram of experimental rig

Table 8.1 Description of experimental points for data logging

I.D	Description	Fluid type	M	Accuracy
1	Absorber exit	Weak solution	T	±0.08 °C
2	Inlet to SHX from absorber	Weak solution	T	±0.09 °C
3	Exit from SHX to generator	Weak solution	T	±0.1 °C
4	Generator exit to SHX	Strong solution	T	±0.4 °C
5	Exit from SHX to absorber	Strong solution	T	±0.06 °C
6	Inlet to absorber	Strong solution	T	±0.1 °C
7	Vapour exit from generator	Vapour	T	±0.25 °C
8	Condenser exit	Liquid	T	±0.06 °C
9	Evaporator inlet	Liquid	T	±0.15 °C
10	Evaporator outlet	Vapour	T	±0.1 °C
11	RSHX exit	Weak solution	T	±0.1 °C
12	Hydrometer 1 T	Weak solution	T	±0.02 °C
13	Hydrometer 2 T	Strong solution	T	±0.02 °C
14	Absorber- Inner coil inlet	Water	T	±0.1 °C
15	Absorber- Inner coil outlet	Water	T	±0.04 °C
36	Absorber – Outer coil inlet	Water	T	±0.05 °C
37	Absorber – Outer coil outlet	Water	T	±0.1 °C
38	Condenser – Coil inlet	Water	T	±0.06 °C
39	Condenser – Coil outlet	Water	T	±0.05 °C
40	RSHX – Inlet	Water	T	±0.05 °C
41	RSHX – Outlet	Water	T	±0.05 °C
42	Absorber – Inner coil (Turn 1)	Weak solution	T	±0.1 °C
43	Absorber – Inner coil (Turn 4)	Weak solution	T	±0.04 °C
44	Absorber – Inner coil (Turn 7)	Weak solution	T	±0.04 °C
45	Absorber – Inner coil (Turn 10)	Weak solution	T	±0.06 °C
46	Absorber – Inner coil (Turn 13)	Weak solution	T	±0.06 °C
47	Absorber – Inner coil (Turn 16)	Weak solution	T	±0.05 °C
48	Absorber – Inner coil (Turn 19)	Weak solution	T	±0.05 °C
49	Absorber – Inside Chamber	Vapour	T	±0.05 °C
WF1	Absorber – Outer coil	Water	M	±0.7 g/s
WF2	Absorber – Inner coil	Water	M	±0.7 g/s
WF3	Condenser – Coil	Water	M	±0.32 g/s
WF4	RSHX	Water	M	Not used
SF3	RSHX	Weak solution	M	±0.26 g/s
Cold Blend	Water tank	Water	M	±0.42 g/s
P1	Generator exit	Vapour	P	±0.2 kPa
P2	Evaporator exit	Vapour	P	±0.2 kPa
A	Generator heater upper/lower	Strong solution	I	±0.02A
C	Evaporator heater	Water	W	±4W

T – temperature, P – Pressure, M – Mass flow rate, I – Current, W –Watts
M – Measurement

<u>AC current channels</u>

These channels are designed for use with Hilton AC current transformers and are connected as follows:

Channel 33 Terminals 66 C1ACF and 68 C10VF (Fast time constant)

Channel 34 Terminals 70 C2ACF and 72 C20VF (Fast time constant)

Channel 35 Terminals 74 C3ACF and 76 C30VF (Fast time constant)

Channel 33 and 34 on High Gain have a maximum input of 4mA.

Channel 33 and 34 on Low Gain have a maximum input of 16mA.

Channel 35 on High Gain has a maximum input of 0.4mA.

Channel 35 on Low Gain has a maximum input of 1.6mA.

The channel's numbers on second logger are 68, 69 and 70.

Channel 34 and 69 are used to measure the current of the 2kW generator upper and lower heaters.

8.2.2 Digital input

The D101/42 has 8 digital input channels that will accept either frequency inputs (pulses) or logic inputs. The call used by the computer determines how the channel is read, either as logic or frequency. The connectors are labelled F/I1...F/I8 from channel 25 to channel 32.

Five channels are used to measure the flow rate of cooling water while one is used to measure the flow rate of recirculation solution mixtures. Details are shown in Table 8.2. All these are frequency inputs. The logic input can also be used to monitoring the on/off of all the switches.

Table 8.2 Description of channel used for frequency inputs

Channel	Description
25	Cooling water - Inner Absorber Coil
26	Cooling water - Outer Absorber Coil
27	Cooling water – Condenser
28	Cooling water – Recirculation Heat Exchanger
29	H_2O-LiBr Solution - Recirculation Heat Exchanger
30	Cold Blend – Water Tank

8.3 Data logging software

The data logging software developed is one of the major contributions in this work. It is a major improvement to the DOS based data logging software used by P.A. Hilton. While some of the key features remain unchanged, the backbone of the program was actually reengineered to approach a higher speed communication and user-friendly interfacing with many new features included. The suit of programs was developed from scratch to a complete complex software package by the author using Visual Basic. The flow chart of the program is represented by Figure 8.2

8.3.1 System configuration

When the data logging software is first loaded from ABCON, the system configuration menu (Figure 8.3) appears. The software needs to store the information on configurations and data into five different files. The 'Channel Configuration File' is used to store information of channel names, channel functions, active channels, sample interval, upper and lower limits for the channels and high or low gain. (See section 8.3.2).

The 'Conversion Factor File' contains all the factors for each channel that convert the signals from data logger into engineering units required by the operator. The conversion factors can be exponential or polynomial up to fourth-order. The 'Output File' contains records of 8 output channels per data logger for the selected conditions. The output file with extension '.abo.gau' contains settings of computer analogue gauges and files with extensions '.abo.inp'; and '.abo.cht' stores configurations of input channels and channels that are displayed on line-charts respectively. The 'Log all data file' logs all the data at a set interval into a single file. The 'Library file' stores information of transducers' specifications. Other options include 'print and save interval', 'number of data loggers' connected in daisy chain and the 'logger port' (communication port). When the 'Online' check-box is not ticked, some configurations can be made offline and the logged data can be viewed at different intervals. (See section 8.3.6). When the configuration has been set, the main menu (Fig. 8.4) will emerge by clicking on the menu button.

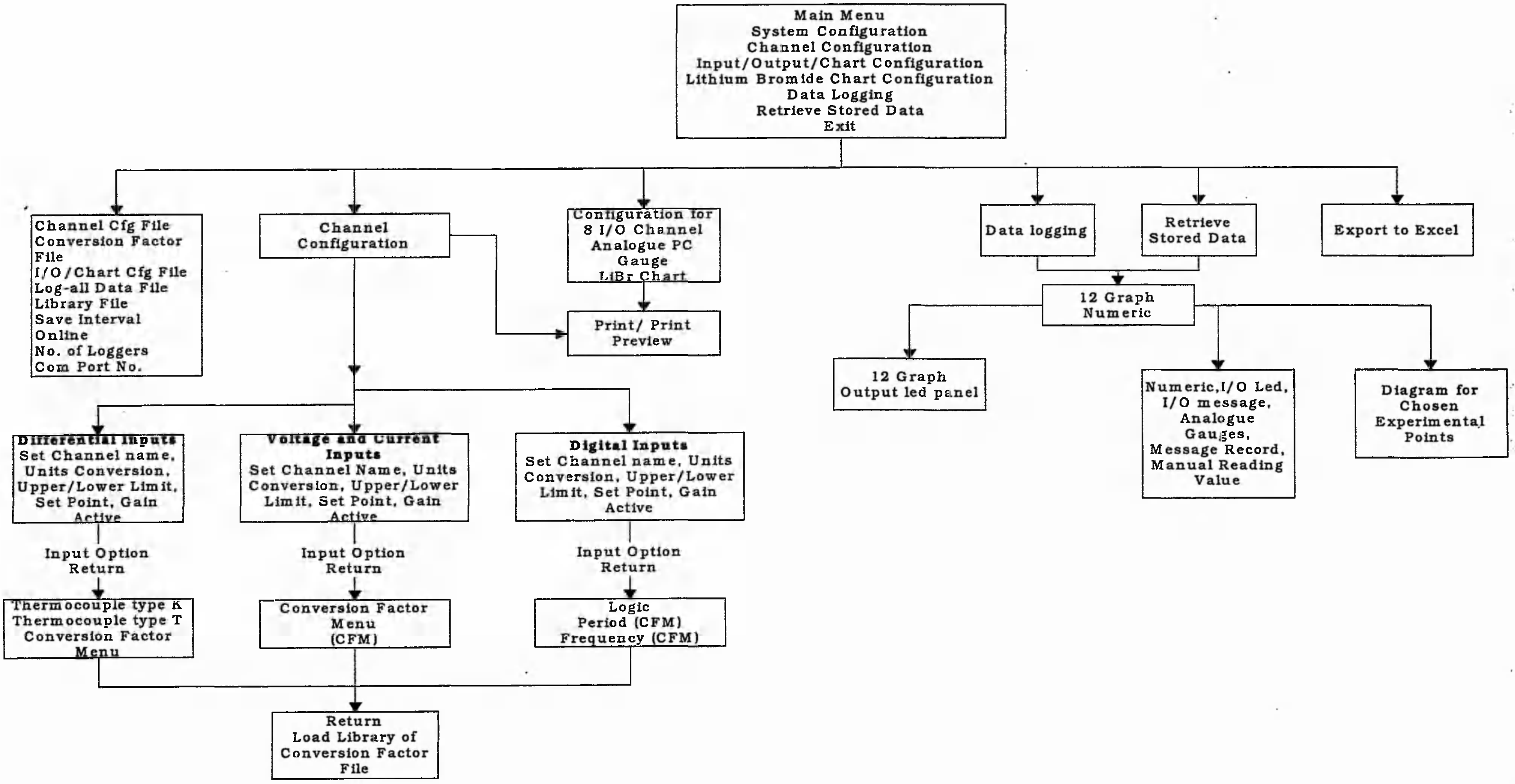

Figure 8.2 Flow chart for data logging software

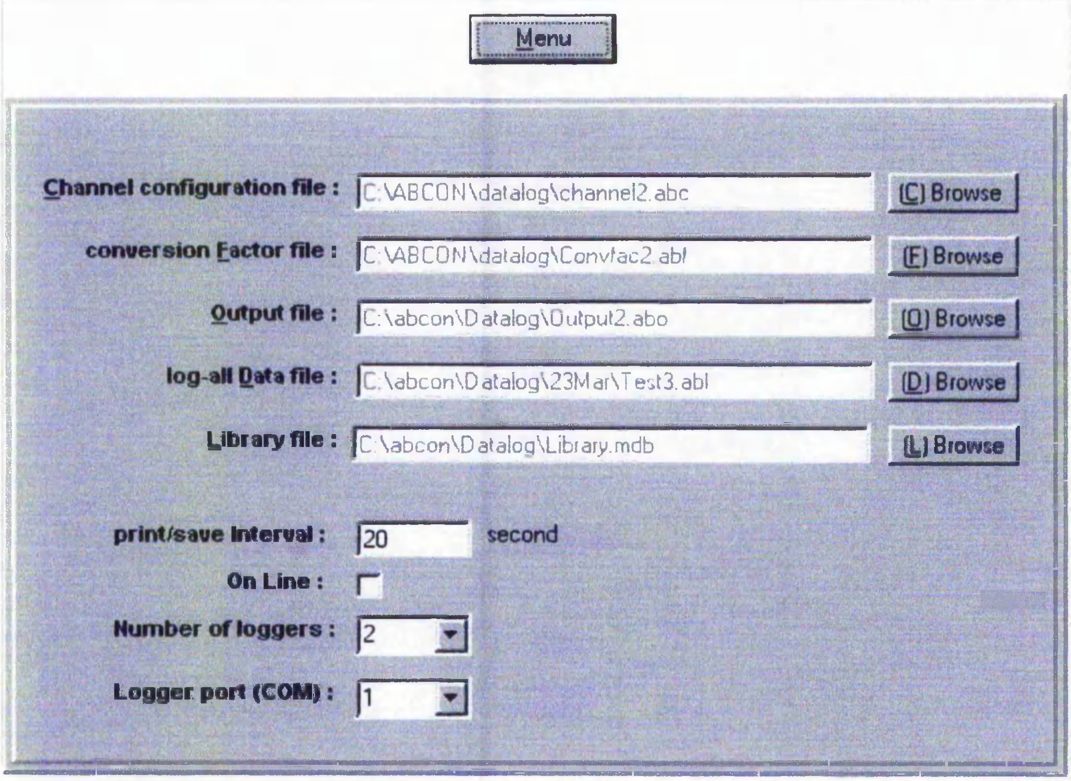

Channel configuration file : C:\ABCON\datalog\channel2.abc

conversion Factor file : C:\ABCON\datalog\Convfac2.abl

Output file : C:\abcon\Datalog\Output2.abo

log-all Data file : C:\abcon\Datalog\23Mar\Test3.abl

Library file : C:\abcon\Datalog\Library.mdb

print/save Interval : 20 second

On Line : ☐

Number of loggers : 2

Logger port (COM) : 1

Figure 8.3 System Configurations

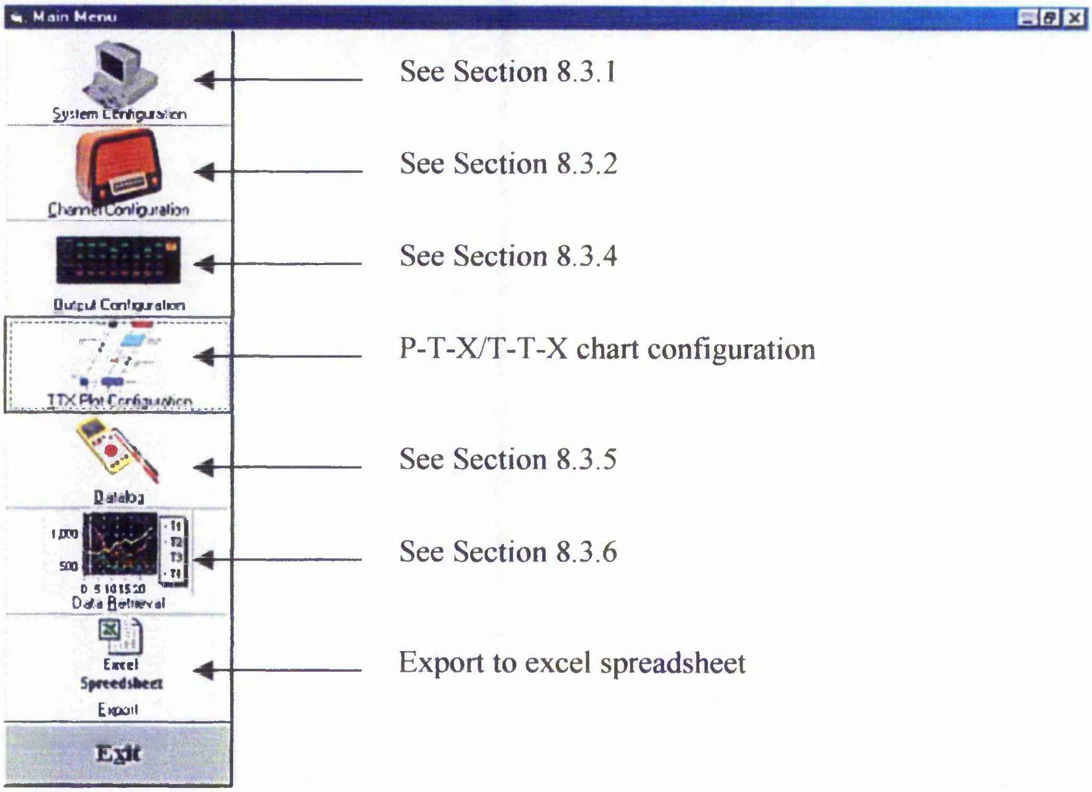

See Section 8.3.1

See Section 8.3.2

See Section 8.3.4

P-T-X/T-T-X chart configuration

See Section 8.3.5

See Section 8.3.6

Export to excel spreadsheet

Figure 8.4 Main menu of data logging software

8.3.2 Channel & conversion factor configuration

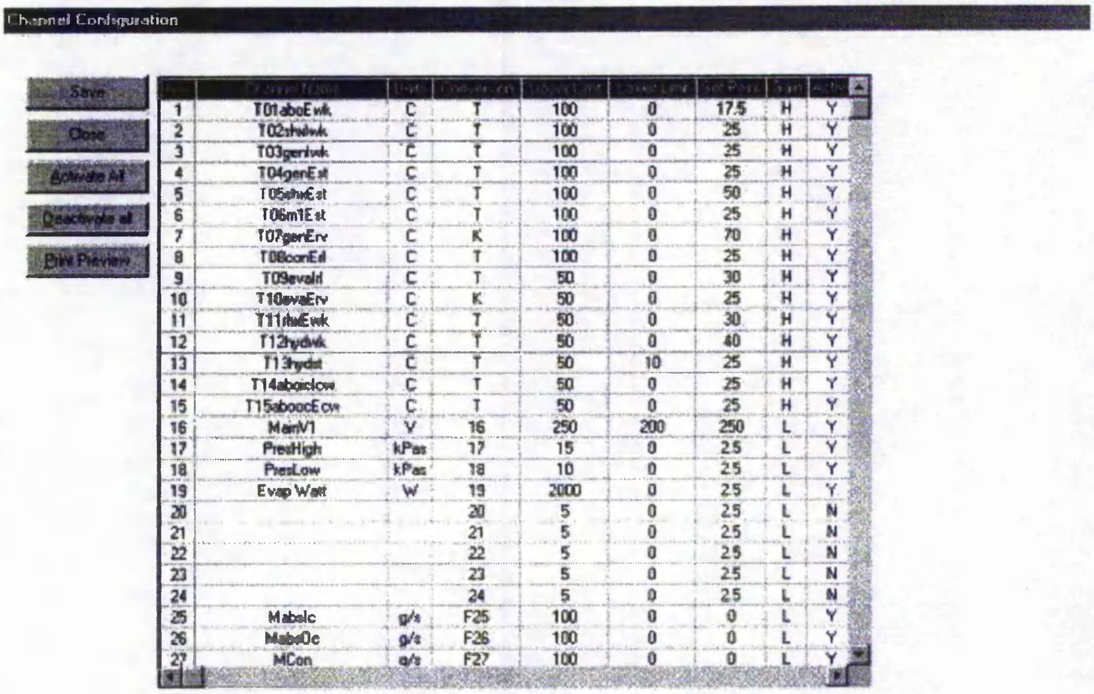

	Channel Name	Units	Conversion	Upper Limit	Lower Limit	Set Point	Gain	Activ
1	T01aboEwk	C	T	100	0	17.5	H	Y
2	T02shwlwk	C	T	100	0	25	H	Y
3	T03genlwk	C	T	100	0	25	H	Y
4	T04genEst	C	T	100	0	25	H	Y
5	T05shwEst	C	T	100	0	50	H	Y
6	T06m1Est	C	T	100	0	25	H	Y
7	T07genErv	C	K	100	0	70	H	Y
8	T08conEil	C	T	100	0	25	H	Y
9	T09evalrl	C	T	50	0	30	H	Y
10	T10evaErv	C	K	50	0	25	H	Y
11	T11rhwEwk	C	T	50	0	30	H	Y
12	T12hydwk	C	T	50	0	40	H	Y
13	T13hydst	C	T	50	10	25	H	Y
14	T14aboiclow	C	T	50	0	25	H	Y
15	T15abocclEcw	C	T	50	0	25	H	Y
16	MainV1	V	16	250	200	250	L	Y
17	PresHigh	kPas	17	15	0	2.5	L	Y
18	PresLow	kPas	18	10	0	2.5	L	Y
19	Evap Watt	W	19	2000	0	2.5	L	Y
20			20	5	0	2.5	L	N
21			21	5	0	2.5	L	N
22			22	5	0	2.5	L	N
23			23	5	0	2.5	L	N
24			24	5	0	2.5	L	N
25	Mabsic	g/s	F25	100	0	0	L	Y
26	MabsOc	g/s	F26	100	0	0	L	Y
27	MCon	g/s	F27	100	0	0	L	Y

Figure 8.4 Channel Configuration

Nine columns of settings are needed for each channel. The nine columns in the channel configuration file consist of channel number, channel name, units, conversion factor reference, lower limit and upper limit for the channel, gain and active channel. By clicking on the print preview button, the configuration table can be printed before print previewing.

On the 'conversion' column, if one of the rows between number 1 to 15 is clicked then a small option form will show (Figure 8.5). Clicking the first option will activate the internal conversion factor that converts signal from a type K thermocouple to the selected unit and type T for the second option. When third option is selected, the conversion table will be loaded (Figure 8.7).

In addition the digital channels (25 to 32) can be set (Fig. 8.6) to read logic (On or Off), pulse (Hz, or cycles/second) or period (seconds between pulses). The conversion table can be used to convert the received signal to the required unit.

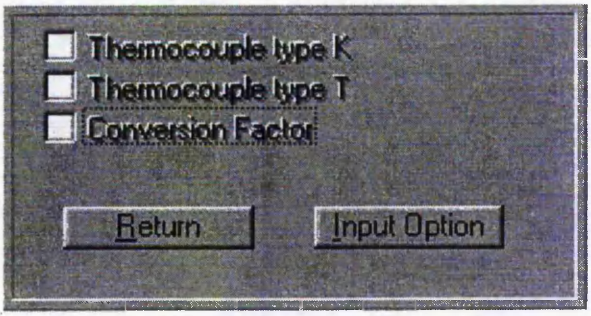

Figure 8.5 Options of differential channels

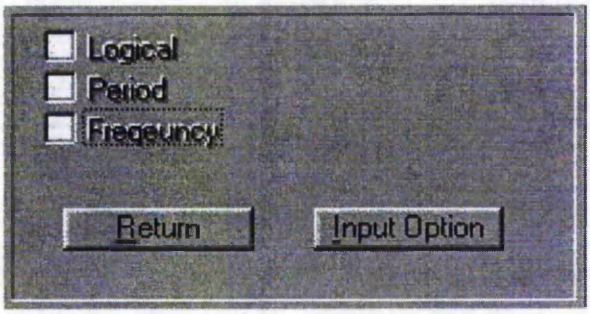

Figure 8.6 Options for digital channels

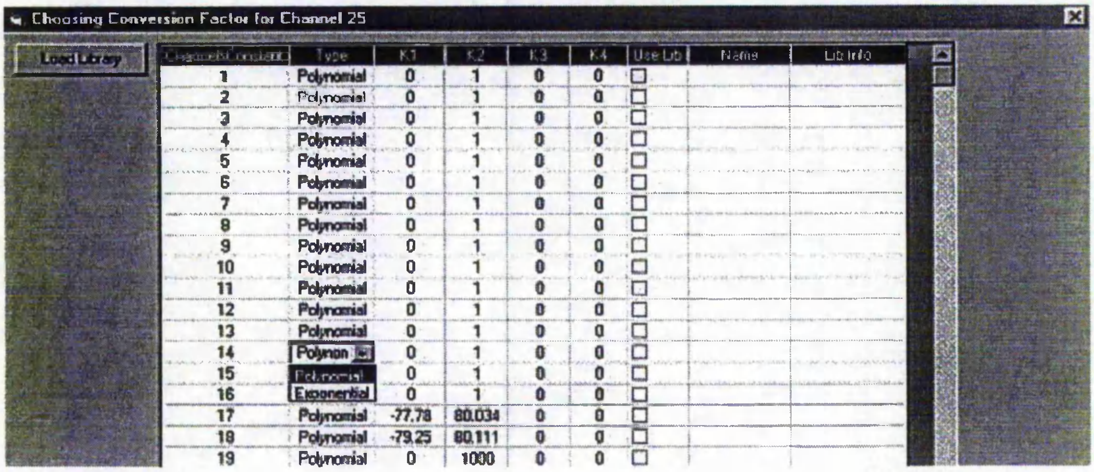

Channels\Constant	Type	K1	K2	K3	K4	Use Lib	Name	Lib Info
1	Polynomial	0	1	0	0	☐		
2	Polynomial	0	1	0	0	☐		
3	Polynomial	0	1	0	0	☐		
4	Polynomial	0	1	0	0	☐		
5	Polynomial	0	1	0	0	☐		
6	Polynomial	0	1	0	0	☐		
7	Polynomial	0	1	0	0	☐		
8	Polynomial	0	1	0	0	☐		
9	Polynomial	0	1	0	0	☐		
10	Polynomial	0	1	0	0	☐		
11	Polynomial	0	1	0	0	☐		
12	Polynomial	0	1	0	0	☐		
13	Polynomial	0	1	0	0	☐		
14	Polynon	0	1	0	0	☐		
15	Polynomial	0	1	0	0	☐		
16	Exponential	0	1	0	0	☐		
17	Polynomial	-77.78	80.034	0	0	☐		
18	Polynomial	-79.25	80.111	0	0	☐		
19	Polynomial	0	1000	0	0	☐		

Fig. 8.7 Conversion table

Figure 8.7 shows the conversion table. There are two types of conversions; 1- Pynomial, 2- Exponential. The polynomial form is as follows:

$$\mathbf{Y = K1 + K2.X + K3.X^2 + K4.\ X^3}$$

and the exponential form is

Y = K1 + K2.Exp(K3.X)

The number of available conversion factors in the menu is equal to the number of channels on the data logger. The conversion factor number selected for each channel can be any one of the 35 available on the logger. It is possible to have all the channels using the same conversion factor.

The conversion factor can be set either manually or obtained from the Library. A calibration software has been developed to store conversion factors and other information of transducers that may be used repeatedly.

8.3.3 Calibration and library of transducer

When the 'Use library' box in the conversion table is checked, the library (Fig. 8.8) will be loaded. The library can be used to store information of transducers in different categories by selecting the 'Create Table' under the 'Table' on the menu bar or clicking the toolbar button 'New Table' as shown in Fig. 8.8. Choosing the 'Open Table' under the 'Table' on the menu bar enable changing the active table (Fig 8.9).

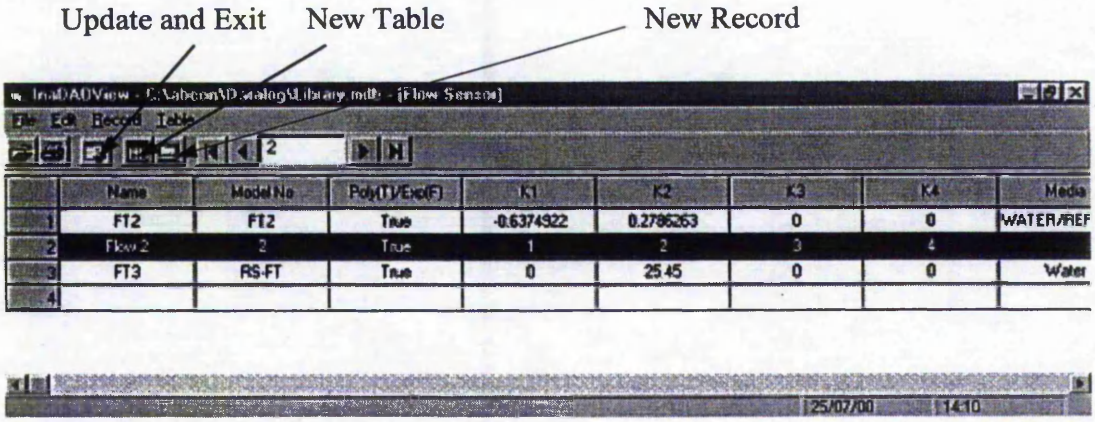

	Name	Model No	Poly(T)/Exp(F)	K1	K2	K3	K4	Media
1	FT2	FT2	True	-0.6374922	0.2786263	0	0	WATER/REF
2	Flow 2	2	True	1	2	3	4	
3	FT3	RS-FT	True	0	25.45	0	0	Water
4								

Figure 8.8 Main Menu of Library

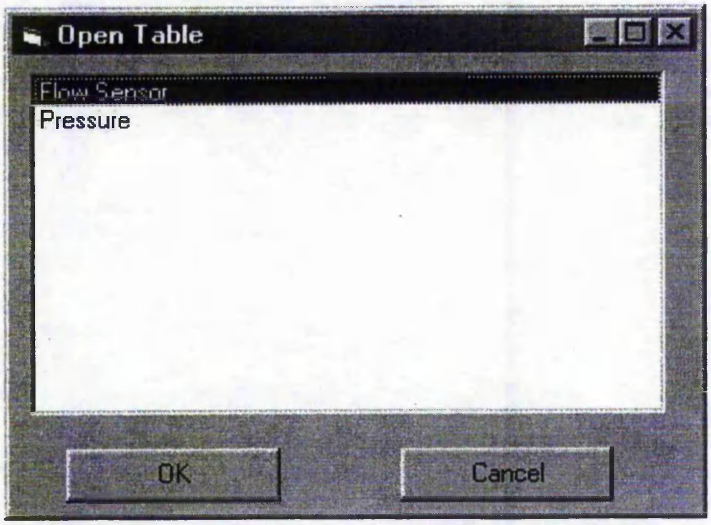

Flow Sensor
Pressure

Fig 8.9 'Open Table' – to change the active table

Adding and deleting a record can be done through the 'Edit Menu'. By double clicking on any of the rows, the record can be modified or edited (Fig 8.10).

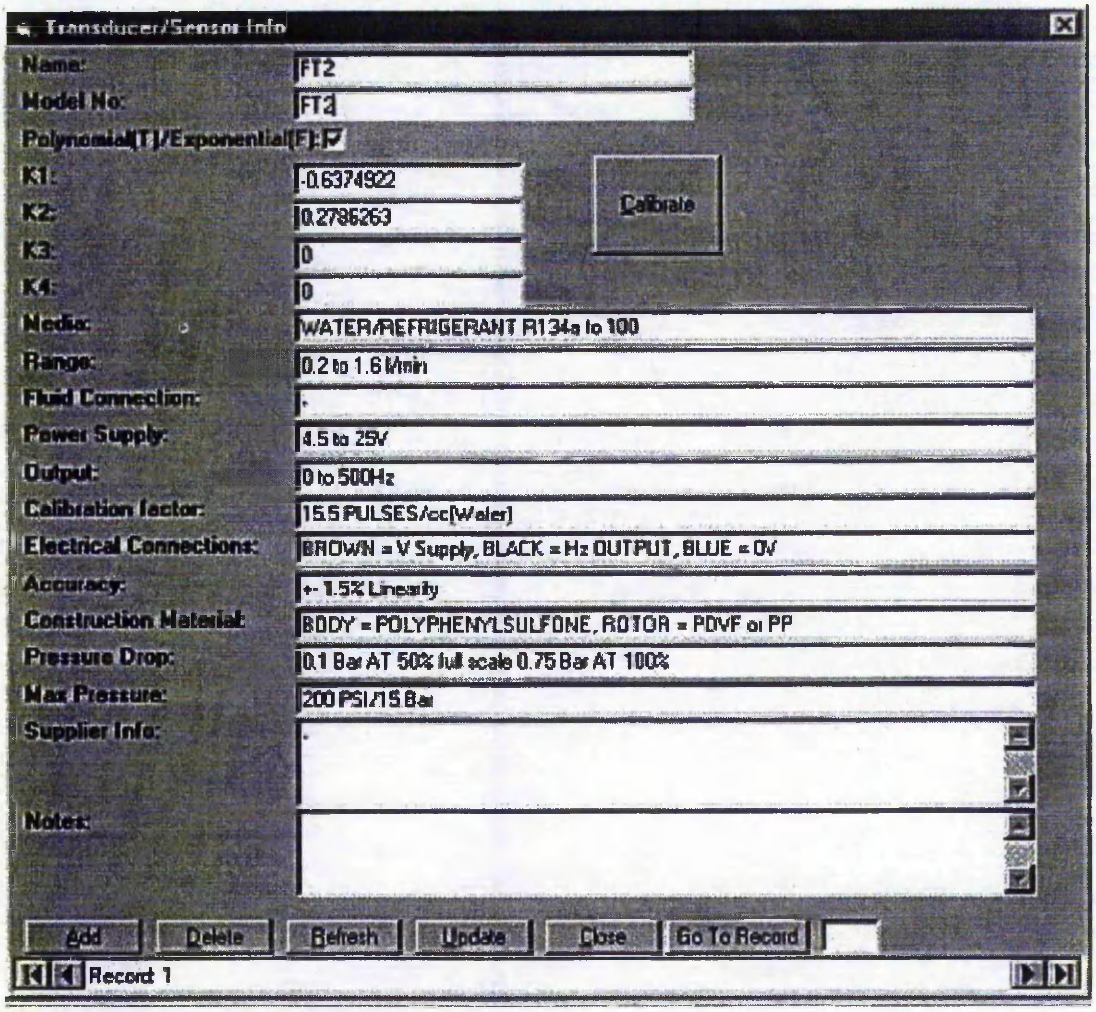

Name: FT2
Model No: FT2
Polynomial(T)/Exponential(F): ☑
K1: -0.6374922
K2: 0.2786263
K3: 0
K4: 0
Media: WATER/REFRIGERANT R134a to 100
Range: 0.2 to 1.6 l/min
Fluid Connection: -
Power Supply: 4.5 to 25V
Output: 0 to 500Hz
Calibration factor: 15.5 PULSES/cc(Water)
Electrical Connections: BROWN = V Supply, BLACK = Hz OUTPUT, BLUE = 0V
Accuracy: +- 1.5% Linearity
Construction Material: BODY = POLYPHENYLSULFONE, ROTOR = PDVF or PP
Pressure Drop: 0.1 Bar AT 50% full scale 0.75 Bar AT 100%
Max Pressure: 200 PSI/15 Bar
Supplier Info: -
Notes:

Fig 8.10 Information of transducer

The factory conversion factor can be used or re-calibrated by clicking on the 'Calibrate' button.

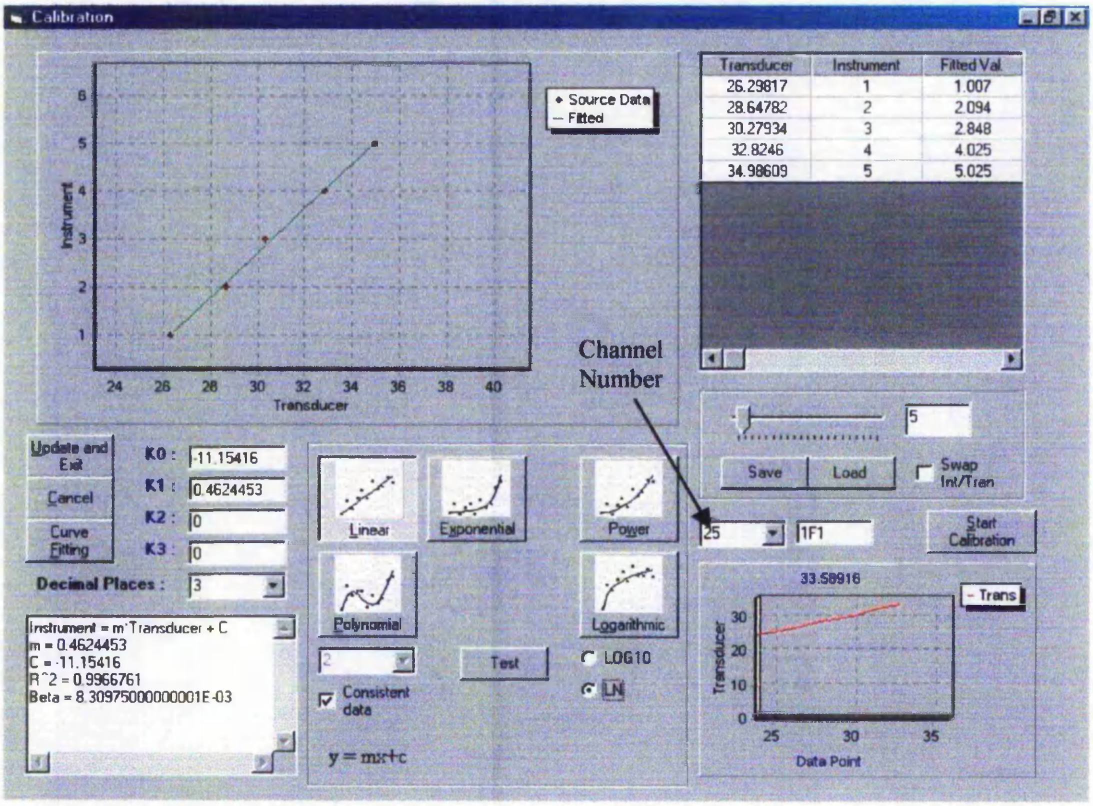

Transducer	Instrument	Fitted Val
26.29817	1	1.007
28.64782	2	2.094
30.27934	3	2.848
32.8246	4	4.025
34.98609	5	5.025

K0 : -11.15416
K1 : 0.4624453
K2 : 0
K3 : 0
Decimal Places : 3

Instrument = m*Transducer + C
m = 0.4624453
C = -11.15416
R^2 = 0.9966761
Beta = 8.30975000000001E-03

2
☑ Consistent data
○ LOG10
● LN
5
☐ Swap Int/Tran
25
1F1

Figure 8.11 Device calibration

Figure 8.11 shows an example of the calibration against a flow meter. The table on the upper right corner allows the user to enter value read from the instrument, which in this case is a flow meter. After selecting the channel number in which the transducer has been connected to and clicking on the 'Start Calibration' button, the signal will be shown on the online line chart at the lower right corner. The value is shown in the table on the 'Transducer' column in the first row where the user has entered the value read from the instruments. After a steady reading is reached, calibration is stopped temporarily. The flow rate is increased until the flow meter reads 2 litres/minute. Then the calibration is started again until a sufficient number of readings in the experimental range is reached.

The calibration factor is calculated and fitted. The results are shown in a text box on the lower left corner while the curves of the fitted value and the original data are shown on the line chart at the upper left corner. The curve fitting algorithms are the same as those discussed in Chapter 5. The calibration is done by clicking the 'Update and Exit' button. This software is particularly useful when a transducer needs calibration frequently. It also helps to organise the complex information when a large number of transducers or sensors are used.

8.3.4 Input/Output Configuration

Output configuration

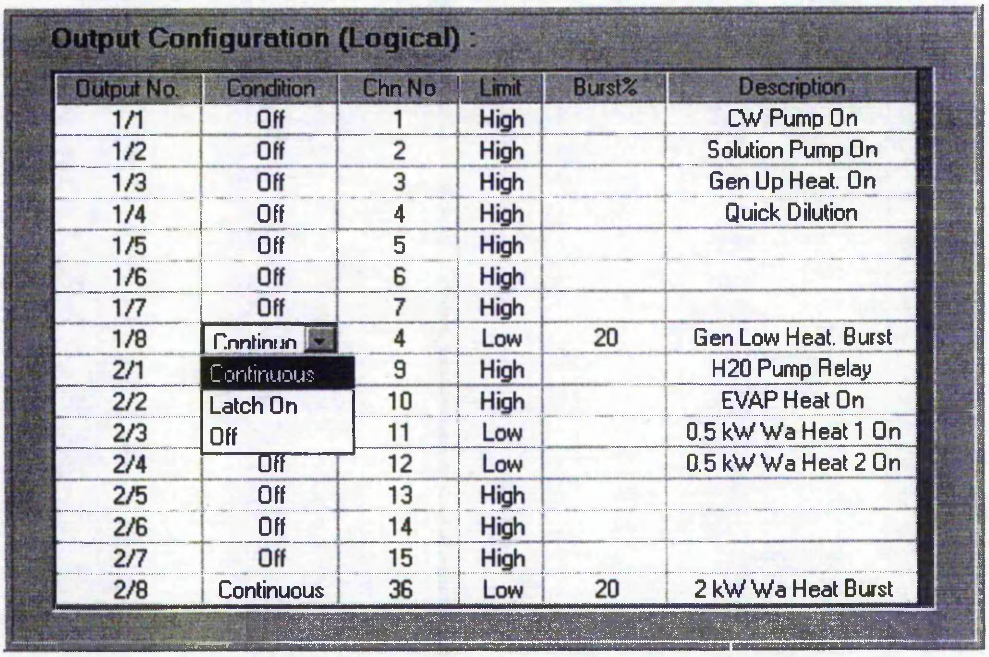

Output Configuration (Logical) :

Output No.	Condition	Chn No	Limit	Burst%	Description
1/1	Off	1	High		CW Pump On
1/2	Off	2	High		Solution Pump On
1/3	Off	3	High		Gen Up Heat. On
1/4	Off	4	High		Quick Dilution
1/5	Off	5	High		
1/6	Off	6	High		
1/7	Off	7	High		
1/8	Continuo	4	Low	20	Gen Low Heat. Burst
2/1		9	High		H20 Pump Relay
2/2		10	High		EVAP Heat On
2/3		11	Low		0.5 kW Wa Heat 1 On
2/4	Off	12	Low		0.5 kW Wa Heat 2 On
2/5	Off	13	High		
2/6	Off	14	High		
2/7	Off	15	High		
2/8	Continuous	36	Low	20	2 kW Wa Heat Burst

Fig 8.12 Output Configuration Table

The column 'Output No.' refers to the 16 available output ports. There are eight output channels in each logger. The first number refers to the logger number while the second refers to the channel number. The eighth channel of each logger is a 'Burst fire' channel where the percentage of the burst-fire rate can be set in between 0 to 100%. The 'Condition' column refers to the response of the output channel to a limit condition. The 'Chn No.' is the input channel number whose condition will be monitored relative to the limit selected in the 'Limit' column. The limit column allows the user to select the High, Low and Both (High and Low) limits that were set in the channel configuration menu (Fig 8.4) for the input channel number being associated with an output channel. For instance, the output 1/3 will be on when the input channel 3 exceeds the upper limit of 100. If the condition is set to 'Latch on', the output 1/3 will continue to be on even if the input later drops below the 100 figure. The 'Continuous' condition allows the output to switch off if the input channel falls below the set limit.

Input configuration

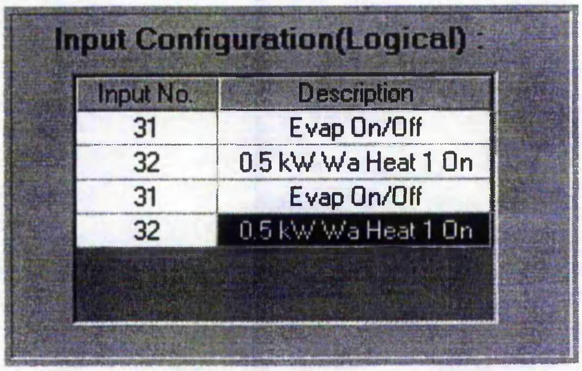

Input Configuration(Logical) :

Input No.	Description
31	Evap On/Off
32	0.5 kW Wa Heat 1 On
31	Evap On/Off
32	0.5 kW Wa Heat 1 On

Figure 8.13 Input Configuration Table

The input configuration can only be used when the digital channels are set to logical input. When the input is on, the description will be highlighted to notify the user (See Fig. 8.15).

8.3.5 Data logging and retrieval

The data-logging button on the main menu is only accessible when the online check in the system configuration box is ticked. Once the button is clicked the program will initialise the setting stored at input/output configuration. For instance, the output panel will show the conditions and limit set in the output configuration set earlier.

There are about 50 numeric displays on a single page. There is a button named 'Next Page' for viewing numeric display channels that are over 50. A Pressure-Temperature Concentration (PTX) chart and Refrigerant Temperature-Solution Temperature-Concentration (TTX) chart are also programmed. The chart may be used to monitor the process online when the operating parameters are changed. The points chosen to display at the PTX chart may be configured at the PTX/TTX configuration panel.

There are two online line charts used in this program. It gives a clear view of the process changing with time. It is also used to establish whether the process has achieved steady state. The configurations are as follows:

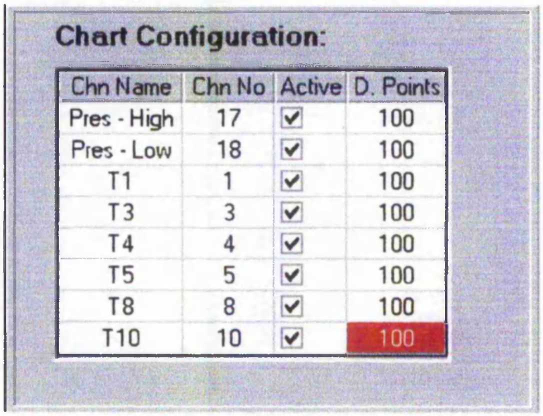

Chart Configuration:

Chn Name	Chn No	Active	D. Points
Pres - High	17	☑	100
Pres - Low	18	☑	100
T1	1	☑	100
T3	3	☑	100
T4	4	☑	100
T5	5	☑	100
T8	8	☑	100
T10	10	☑	100

Figure 8.14 Line Chart Configuration

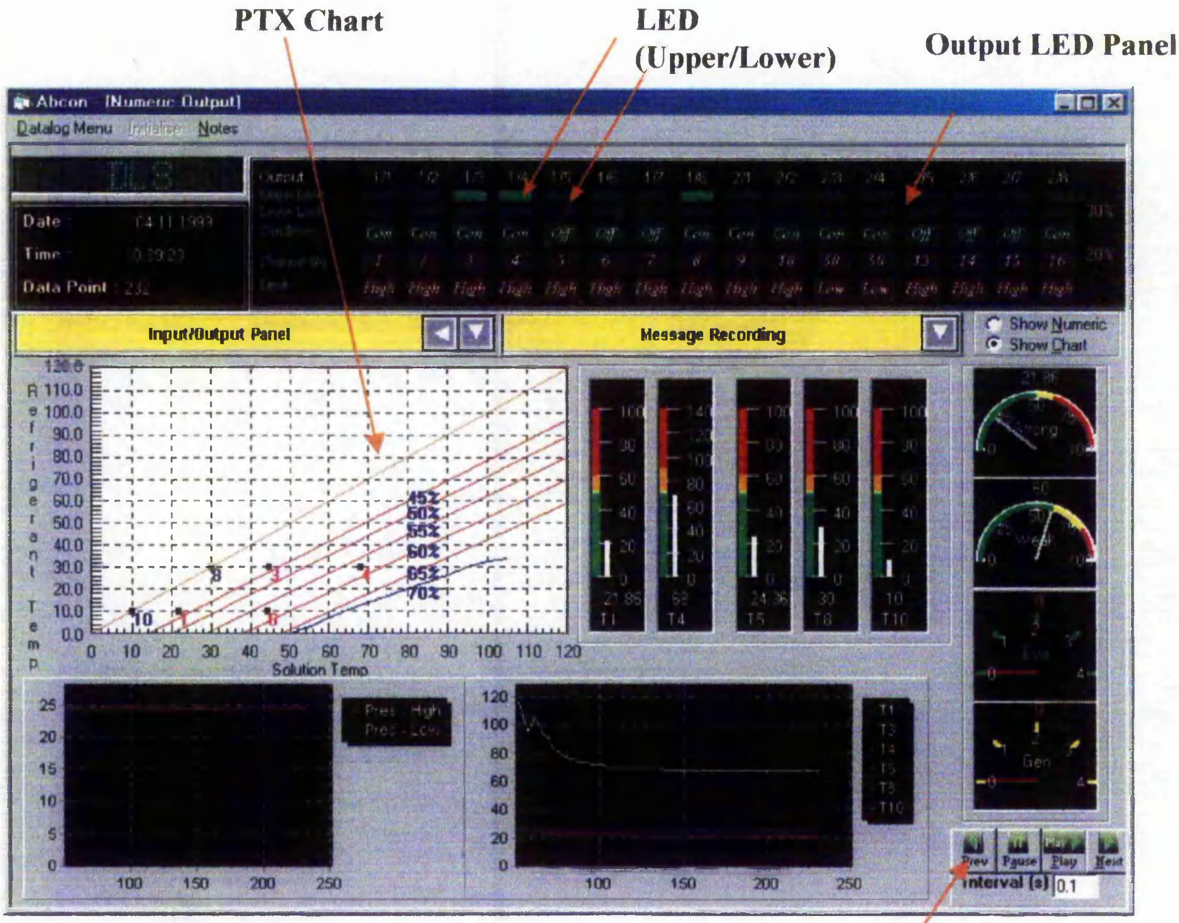

Figure 8.15 Data logging

One of the special features in this software is the computer analogue gauge. The computer analogue gauge used in this project are ActiveX components developed using Visual Basic. There are some computer analogue gauges available on the market such as those developed by Global Majic Software, Inc. However, they are too expensive and do not have functions needed in the current work. Thus it was decided to make an ActiveX which can be used repeatedly simply by changing the settings.

One of the problems with the water-lithium bromide machine is crystallisation (See Appendix E). It is therefore essential to monitor and control the process. The warning and dangerous levels can be set on these computer gauges. Once the reading has achieved the warning or dangerous level, the colour of the gauges will turn into amber and red respectively. This will help to identify problems quickly before anything worse happens. This is a big improvement over numeric display as it is difficult to notice the problem from all the numeric display simultaneously. All the settings could be entered as shown in Figure 8.16.

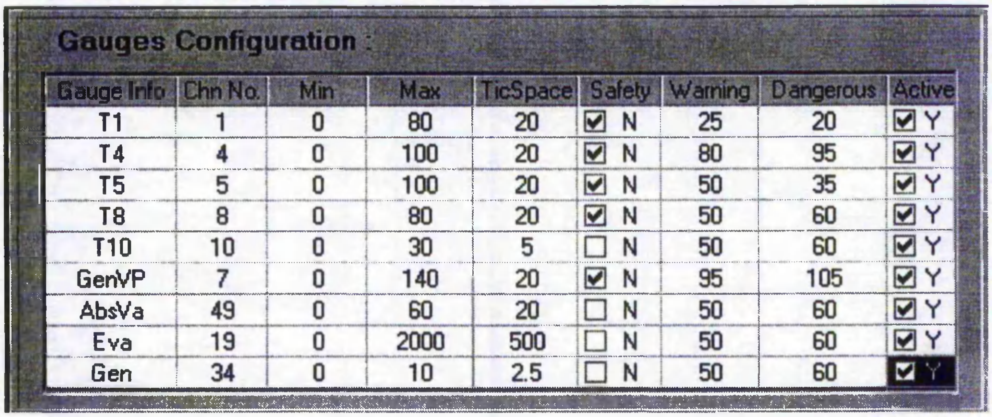

Gauges Configuration :

Gauge Info	Chn No.	Min	Max	TicSpace	Safety	Warning	Dangerous	Active
T1	1	0	80	20	☑ N	25	20	☑ Y
T4	4	0	100	20	☑ N	80	95	☑ Y
T5	5	0	100	20	☑ N	50	35	☑ Y
T8	8	0	80	20	☑ N	50	60	☑ Y
T10	10	0	30	5	☐ N	50	60	☑ Y
GenVP	7	0	140	20	☑ N	95	105	☑ Y
AbsVa	49	0	60	20	☐ N	50	60	☑ Y
Eva	19	0	2000	500	☐ N	50	60	☑ Y
Gen	34	0	10	2.5	☐ N	50	60	☑ Y

Figure 8.16

The second important feature is the output and input message panel (Fig. 8.17). Sometimes it is useful to know exactly what is on or off when the lights are turning on in the output led panel. The output led panel is useful for knowing the limits that particular values have achieved. For instance, when temperature exceeds 100 °C measured by the thermocouple in channel 3, the upper limit LED will turn into green light. The I/O message panel on the other hand will give more detailed information by highlighting the description that was configured earlier in the input/output configuration form.

The other feature is the message-recording panel. This will allow the user to record some activities in the middle of the experiment, for instance, increasing the flow and storing readings from meters that are not connected to any transducer. A small note pad will emerge at the beginning and at the ending of the experiment for recording the aims, objectives, notes, date and time.

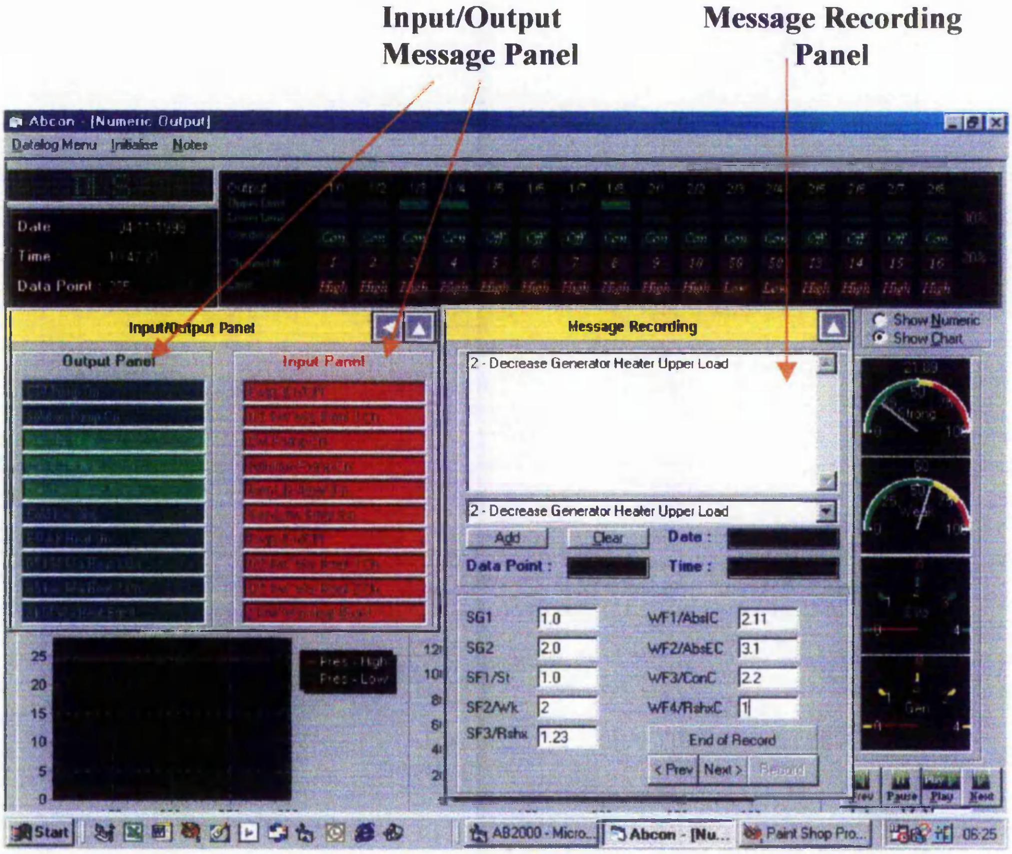

2 - Decrease Generator Heater Upper Load

2 - Decrease Generator Heater Upper Load

SG1 1.0
SG2 2.0
SF1/St 1.0
SF2/Wk 2
SF3/Rshx 1.23
WF1/AbsIC 2.11
WF2/AbsEC 3.1
WF3/ConC 2.2
WF4/RshxC 1

Figure 8.17 **Input/Output Message Panel and Message Recording Panel**

The more important experimental points have been chosen to be included in a simplified diagram (Fig. 8.18). Some of the signals such as mass flow rate and temperature have been combined into some meaningful unit such as heat load. The diagram shows the heat load of the generator and evaporator by multiplying the measured current and voltage of each heater. For the absorber and condenser, the mass flow rate of cooling water and the temperature of inlet and outlet of the coil are used to calculate the heat load. The concentration of the weak solution is estimated using the suction pressure and absorber outlet temperature (T_1) while the condensing pressure and generator outlet temperature (T_4) are used for predating the concentration of the strong solution.

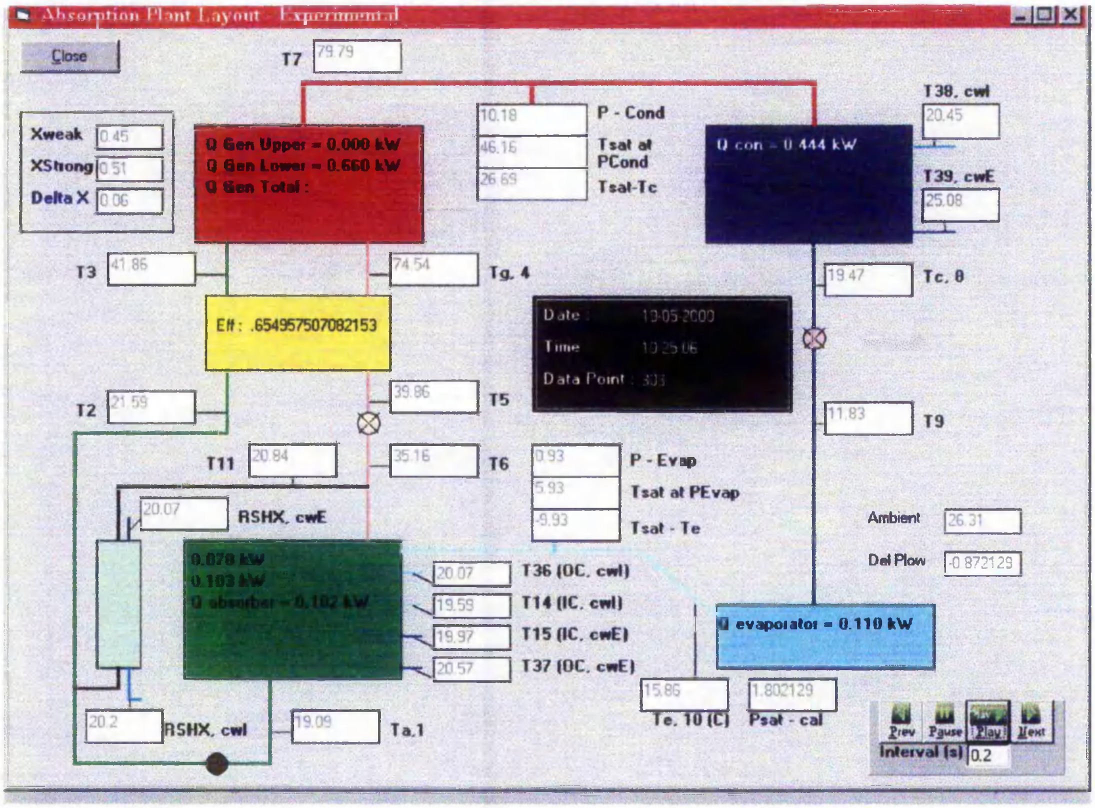

T7 79.79

Xweak 0.45

XStrong 0.51

Delta X 0.06

Q Gen Upper = 0.000 kW

Q Gen Lower = 0.660 kW

Q Gen Total :

P - Cond 10.18

Tsat at PCond 46.16

Tsat-Tc 26.69

Q con = 0.444 kW

T38, cwI 20.45

T39, cwE 25.08

T3 41.86

Tg, 4 74.54

Tc, 8 19.47

Eff : .654957507082153

Date : 13-05-2000

Time 10:25:06

Data Point : 303

T2 21.59

T5 39.86

T9 11.83

T11 20.84

T6 35.16

P - Evap 0.93

Tsat at PEvap 5.93

Tsat - Te -9.93

RSHX, cwE 20.07

Ambient 26.31

Del Plow -0.872129

0.078 kW

0.103 kW

Q absorber = 0.102 kW

T36 (OC, cwI) 20.07

T14 (IC, cwI) 19.59

T15 (IC, cwE) 19.97

T37 (OC, cwE) 20.57

Q evaporator = 0.110 kW

Te, 10 (C) 15.86

Psat - cal 1.802129

RSHX, cwI 20.2

Ta,1 19.09

Interval (s) 0.2

Fig 8.18 Simplified diagram to show important experimental points

All the logged data can be retrieved later and played at different intervals. The logged data can also be viewed in steps using the next and previous buttons on the playback panel.

Chapter 9 Experimental Results and Discussion

9.1 Experimental Procedure

Before the experimentation started, all the measuring instrumentations such as transducers and thermocouples were calibrated (Chapter 7 and Chapter 8). Initially the experiment was carried out manually by using distilled water to detect any leakage. All the instruments, controls and heaters were checked until the conditions were steady. After evacuating the system, the pressures were recorded. The experimental rig was left to idle for a week. After one week, the pressure readings were compared with the pre-recorded pressures. If there was no or negligible pressure increase detected, the experimental work was then commenced. Otherwise, the leakage had to be fixed.

9.1.1 System evacuating and charging

A home-made high-pressure water ejector vacuum pump was used to evacuate any wet air inside the test rig to prevent any contamination in the conventional vacuum pump. The conventional vacuum pump was used to pull the lowest pressure that was achievable by the pump. Three needle valves separating the high side and low side of the rig were fully closed.

The condenser and evaporator were charged with distilled water initially. The amount of distilled water charged was enough to cover the evaporator heater. The distilled water level in both evaporator and condenser were marked and recorded. The refrigerant throttling valve, was opened slightly so that the refrigerant liquid pipe could be filled with distilled water and removing any unwanted air.

The generator and absorber were filled with approximately 15kg of lithium bromide brine (55% inhibited MAC, Product code: 5139) via charging point 5 (Figure 8.1). The weight was determined by measuring the weight of the mixtures drum before and after the charging. The mixtures were charged into generator until half of the generator chamber was filled to make sure the two generator heaters were completely immersed. In the meantime, the valve M1 (Figure 8.1) fixed above strong solution flow meter was slightly opened. The mixtures were allowed to flow into the absorber until sufficient height (10cm) was reached.

9.1.2 Start up procedure

After the system was charged with distilled water and water-lithium bromide mixtures, the vacuum pump, generator and evaporator were turned on shortly in order to remove any non-condensable gas.

Soon after the vacuum pump had been switched off and the charging point were closed, the water pump was turned on. The condenser water flow meter and water heater were controlled manually to reach the required temperature and flow rate. The generator heater was switched on to separate the water from the water-lithium bromide mixtures. After a short period, the pipe connecting the generator and condenser were full of saturated water vapour. The water vapour was beginning to condense. The speed of vaporisation could be increased by controlling the heater fired-rate. By recording increased volume of water in condenser and comparing with the previous marked level, the concentration mixtures in generator can be estimated. (Section 9.2.1)

The condensing rate can be adjusted by controlling the temperature and flow rate of cooling water to the condenser. The temperature of cooling water is controlled by either regulating the cold blend from the main supply or turning the water heaters.

After the mass concentration required had been reached, the solution pump was turned on. The two metering valves above water flow meter SF1 and SF2 respectively were adjusted until the volume flow rates balanced. The evaporator heater was also turned on. The absorber was supplied with cooling water to maintain the pressure and evaporation rate. The upper and lower re-circulation sprays were also turned on.

The refrigerant liquid throttling valve, M2, was carefully controlled so that the liquid level in condenser was maintained. In the mean time, the evaporator load was also controlled so that the amount of water evaporated equals the mass of refrigerant liquid flowing from the condenser to maintain steady state..

9.1.3 Shut down procedure

Shut down procedure is very critical in this experimental work as the highest possibility of crystallisation occurs during shut down of an ACS. This is because of the remaining heat in generator after shutting down will continue to boil the water from the mixtures. If the concentration becomes too high, it will form crystals when it cools down to room temperature. In order to prevent the crystallisation happens, the generator has to be turned off first while the solution pump and water pump are allowed to run so that the solution will continue to absorb water vapour from evaporator and dilute the solution in generator. The refrigerant liquid throttling valve M2 is also closed to prevent any water flow from condenser to evaporator. At the same time, cooling water to the condenser is stopped. The pumps remain on until the evaporator level return to its original level.

Alternatively the fast dilution valve can be turned on to allow the water from the condenser to flow into the absorber until the water drops to the initial marked level in the condenser.

At the end of the experiment, the evaporator heater, solution pump and cooling water pump are turned off. The absorber and generator temperatures will drop to the ambient conditions. Before the test rig is shut down, the mass concentration of strong solution has to be checked so that the concentration is not too high to form crystals when it returns to ambient conditions.

9.2 Measurements

9.2.1 Mass concentration

9.2.1.1 Water level method

As mentioned earlier, the concentration of mixtures in the generator can be estimated by recording the increased volume of water in condenser and comparing this with the previous marked level. The calculations are shown below:

The volume of the half filled generator was calculated as

$$\mathbf{V_{hf}} = \frac{1}{2}\pi \times d_{gen} \times \mathbf{l_{gen}} \qquad \textbf{(9.1)}$$

$$= 0.00283 \text{ m}^3$$

where

d_{gen} = 0.15 (diameter of generator chamber), m

l_{gen} = 0.60 (length of generator chamber), m

The volume of the mixture (V_{mix}) was obtained after the deduction of the two heater volumes from Equation 9.1, as shown below:

$$\text{i.e. } \mathbf{V_{mix}} = \mathbf{V_{hf}} - 2 \times \mathbf{l_{rh}} \times \pi \frac{d_{rh}^2}{4} \qquad \textbf{(9.2)}$$

where

l_{rh} = 2.134 (length of rod heater), m

d_{rh} = 0.008 (diameter of rod heater), m

The mass of the mixtures in the generator was calculated by multiplication of the volume (V_{mix}) and the density of the mixture at room temperature as follows:

$$\text{i.e. Mass of mixture} = V_{mix} \text{ x } \rho_{mix, 20\,^\circ C}$$

$$= 4.152 \text{ kg}$$

where $\rho_{mix, 20\,^\circ C} = 1589 \text{ kg/m}^3$

The initial mass of lithium-bromide and water in the mixture was calculated as follows:

Mass of lithium-bromide in the generator,

$\mathbf{m_{LiBr} = 4.152 \times 55/100\ (kg)}$

$= 2.2836$

Mass of water in the generator,

$\mathbf{m_{H_2O,\,GEN} = 4.152 - m_{LiBr}\,(kg)}$

$= 1.8684$

If 1 cm^3 was collected, the mass of water in condenser was computed as

$\mathbf{m_{H_2O,\,CON} = 1 \times 10^{-6}\ [m^3] \times \rho_{H_2O,\,T_C}\ \ [kg/m^3]}$

where $\rho_{H2O,\,Tc}$ is the density of water at condensing temperature

The mass concentration of water-lithium bromide mixture in generator was calculated in the following manner:

$$\frac{\mathbf{m_{LiBr}}}{\mathbf{m_{LiBr} + (m_{H_2O,GEN} - m_{H_2O,CON})}} \times 100\% \qquad (9.3)$$

9.2.1.2 Hydrometer method

The hydrometers were evacuated every time before the measurement took place. First, the water ejector vacuum pump was turned on. Then the pipes were connected to the Schraeder valves above each hydrometer. Each hydrometer was isolated with the system with two ball valves.

The strong solution flows to the hydrometer automatically due to gravity when the B1 and B2 valves (Figure 9.1) are in the vertical and horizontal position respectively. The T1 valve is in 270 degree during the fill-in of strong solution mixtures to the hydrometer. Once level of mixtures is sufficient for the hydrometer to float, the Ball valves B1 and B2 are set to vertical and horizontal positions respectively. The temperature and the specific gravity of the solution are measured. The mass concentration can then be calculated by solving a non-linear equation (Equation 3.62) in chapter 3 using False-position method. After the measurement, B2 is changed into a vertical position while the T1 is set to 270 degrees. The flow will return to absorber to the solution pump inlet. The mass concentration of weak solution in absorber can be measured by pumping the solution to the weak side hydrometer. The steps are basically similar to measurement of strong solution except for the position of T2 valve. Table 9.1 shows the procedures of measuring the density of the solution in detail.

Table 9.1 Action table for measuring the density of H_2O-LiBr mixtures

	Hydrometer (Strong)			Hydrometer (Weak)		
Action\Valves	B1	B2	T1 (degree)	B3	B4	T2 (degree)
Fill the Hydro.	V	H	270^0	V	H	0^0
Measure	H	V	0^0	H	V	270^0
Discharge	V	V	0^0	V	V	270^0
After Discharge	H	V	270^0	H	V	0^0

V – Vertical, H – Horizontal.

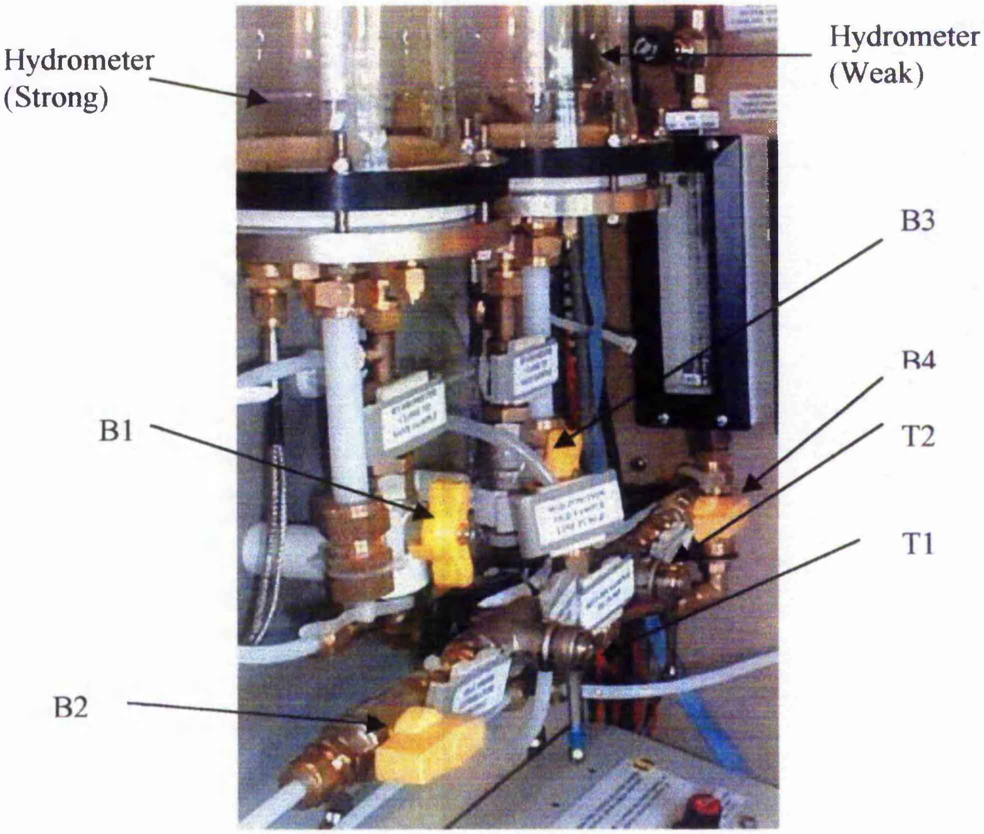

Figure 9.1 Picture of hydrometers

9.2.2 Mass flow rate

The condensing mass flow rate of refrigerant vapour could be measured by recording the time taken for 1cm^3 of refrigerant liquid collected in the condenser. The mass flow rates of weak and strong solutions were monitored by a two Platen volume flow meter. No flow transducer was found suitable to measure this slow flow rate except the Coriolis flow meter. However, previous work by Zaltash et al (1991) showed significant error in this type of meter and moreover the price of Coriolis flow meter is quite high. Thus, it was decided to record the mass flow rate of the solutions manually.

The flow meters used for measuring the volume flow rate of solutions were originally calibrated by the manufacturer against water at 20°C and the unit used is cm^3/min. In order to preserve the original data and accuracy, the values reported in the Appendix E are not changed. However, it has to be converted into proper unit in order to carry out the performance analysis. Unit conversion is also required for the recorded data of the flow rate of re-circulation spray. Other flow transducers and meters for measuring cooling water do not need the conversion factor as there were calibrated against cooling water from the supply. The volume flow rate (cm^3/min) measured from the solution flow meters can be changed to mass flow rate (kg/s) as follows:

$$\textbf{Mass flow rate (kg/s)} = \frac{V_{H2O} \times 10^{-6} \times \rho_{H2O}}{60} \qquad \textbf{(9.4)}$$

where

ρ_{H2O} = density of water (kg/m^3)

V = Volume flow rate measured (cm^3/min)

The mass flow rate of water can then be converted to mass flow rate of water-lithium bromide by multiplication the Equation 9.4 with specific gravity (S.G.) of water-lithium bromide.

The flow transducer records the flow rate in unit Hertz. The transducer was calibrated using water against a water flow meter in unit gram/sec (Figure 7.15). Thus, the conversion can be done by multiply the mass flow rate recorded directly with S.G. of water-lithium bromide and dividing the result by 1000 if unit of kilogram per second is required.

9.2.3 Heat transfer in absorber

The heat loads of the generator and evaporator were calculated by multiplication of the recorded current (obtained from current transformer) and the voltage recorded by data logger. The condenser load can be calculated as follows:

$$\dot{Q}_{con} = \dot{m}_{cw} c_{pw} (T_{cwi} - T_{cwo}) \tag{9.4}$$

where

T_{cwi} = Inlet cooling water temperature to condenser (°C)
T_{cwo} = Outlet cooling water temperature from condenser (°C)
$\dot{m}_{cw}$ = mass flow rate of cooling water (kg/s)
c_{pw} = specific heat (kJ.kg^{-1} °C^{-1})

The absorber load can also be calculated based on Equation 9.4 as follows:

$$\dot{Q}_{abs,\,ic} = \dot{m}_{cw,ic}\, C_{pw,\,inc}\, (T_{cwi,\,ic} - T_{cwi,\,ic}) \tag{9.5}$$

$$\dot{Q}_{abs,\,oc} = \dot{m}_{cw,oc}\, C_{pw,\,oc}\, (T_{cwi,\,oc} - T_{cwi,\,oc}) \tag{9.6}$$

where subscripts ic and oc represent the inner and outer coil respectively

The heat balance yields

$$\dot{Q}_{abs} = U_{total} A \Delta T_m = \dot{m}_{cw} C_p (T_{cwi} - T_{cwo}) \tag{9.7}$$

The heat transfer coefficient can the be determined as follows:

$$U_{total} = \frac{\dot{Q}_{abs}}{A \Delta T_m} \tag{9.8}$$

where A is the absorber heat transfer area and ΔT_m is the log mean temperature difference which is represented as follows:

$$\Delta T_m = \frac{(T_{si} - T_{cwo}) - (T_{so} - T_{cwi})}{\ln\left[\dfrac{(T_{si} - T_{cwo})}{(T_{so} - T_{cwi})}\right]} \tag{9.9}$$

where T_{si} and T_{so} represent the inlet and outlet of solution temperatures respectively. The inlet and outlet temperatures of solution and cooling water are obtained from experiments. From Equation 6.58, the overall heat transfer coefficient is defined in the following way:

$$\frac{1}{U}=\frac{1}{h_c}+\frac{r_i\ln(r_o/r_i)}{k_{pyrex}}+\frac{A_i}{h_sA_{eff}}$$

Where the h_c is the heat transfer coefficient for the cooling water side (inner tube). The heat transfer coefficient can be computed as follows:

$$h_s=\frac{A_i}{A_{eff}}\left[\frac{1}{U}-\frac{1}{h_c}-\frac{r_i\ln(r_o/r_i)}{k_{pyrex}}\right]^{-1} \tag{9.10}$$

9.2.4 Mass transfer in absorber

From the solute mass balance,

$$\dot{m}_{si}x_{si}=\dot{m}_{so}x_{so} \tag{9.11}$$

$$\dot{m}_{so}=\dot{m}_{si}\frac{x_{si}}{x_{so}} \tag{9.12}$$

The conservation of mass yields

$$\dot{m}_{abs}=\dot{m}_{so}-\dot{m}_{si} \tag{9.13}$$

where

$\dot{m}_{abs}$ is the absorbed refrigerant rate. $\dot{m}_{si}$ and $\dot{m}_{so}$ are inlet and outlet mass flow rate of solution respectively. x_{si} and x_{so} are the inlet and outlet solution concentration respectively which can be obtained from experiments.

By substituting Equation 9.12 into Equation 9.13, $\dot{m}_{abs}$ can also be expressed as follows:

$$\dot{m}_{abs}=\dot{m}_{si}\left(\frac{x_{si}}{x_{so}}-1\right) \tag{9.14}$$

The mass absorbed rate is also generally defined as follows:

$$\dot{m}_{abs} = h_m \rho A\left(x_{in} - x_{eq}(T_c, P_v)\right) \tag{9.15}$$

where

h_m = mass transfer coefficient (W/m^2 °C)

ρ = the solution density (kg/m^3)

x_{eq} = the solution equilibrium concentration at the cooling water temperature and the absorber vapour pressure

A = the total effective area (m^2)

The mass transfer coefficient can be determined by manipulating Equations 9.14 and 9.15 as follows:

$$h_m = \frac{\dot{m}_{si}}{\rho A x_{so}} \Delta x \tag{9.16}$$

where

$$\Delta x = \frac{x_{si} - x_{so}}{x_{si} - x_{eq}\left(T_c, P_v\right)} \tag{9.17}$$

If the re-circulation sprays are turned on the solute mass balance becomes,

$$\dot{m}_{si} x_{si} + \dot{m}_{us} x_{so} + \dot{m}_{ls} x_{so} = \dot{m}_{so} x_{so} \tag{9.18}$$

Dividing both sides of Equation 9.18 by x_{so} yields

$$\dot{m}_{so} = \dot{m}_{si} \frac{x_{si}}{x_{so}} + \dot{m}_{us} + \dot{m}_{ls} \tag{9.19}$$

where $\dot{m}_{us}$ and $\dot{m}_{ls}$ are the mass flow rate of upper and lower re-circulations spray

The mass balance is as follows:

$$\dot{m}_{abs} + \dot{m}_{si} + \dot{m}_{us} + \dot{m}_{ls} = \dot{m}_{so} \tag{9.20}$$

By Equating Equation 9.19 and 9.20 yields a similar result to Equation 9.14 as follows:

$$\dot{m}_{abs} = \dot{m}_{si}\left(\frac{x_{si}}{x_{so}} - 1\right)$$

Thus the Equation 9.15 can be used to find out the mass transfer coefficient for both configurations.

9.3 Experimental observation

9.3.1 Initial stage

The following effects were observed during the period before the system reached the steady state conditions:

1. Increase of pressure in generator/condenser. (Figure 9.1)
2. Slight decrease in pressure in evaporator/absorber. (Figure 9.1)
3. Temperatures increased in generator, absorber and condenser. (Figure 9.2)
4. Evaporating temperature dropped slowly. (Figure 9.2)

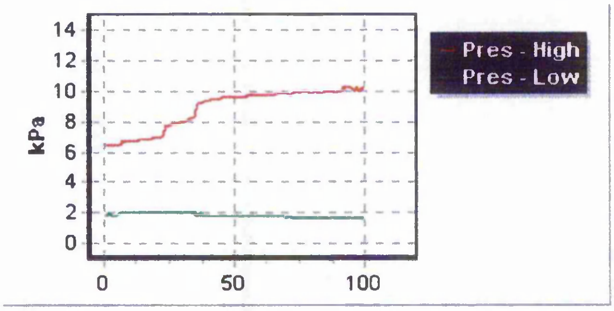

Figure 9.1 Pressure changes versus samples taken at preset interval

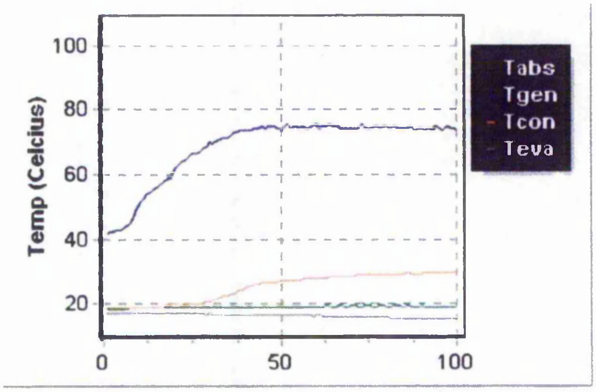

Figure 9.2 Pressure changes versus samples taken at preset interval

From the line charts (Figure 9.1 and Figure 9.1), it is clear that after the number of samples reached 50 (1 sample = interval of 20 seconds), the system has gradually approached steady state. Once the steady state is reached, the recording of experimental data can begin.

9.3.2 Changes of pressure with variation of temperatures

The evaporating temperature depends on the saturation pressure in evaporator (Figure 9.3a and Figure 9.3b) which is controlled by varying the evaporator load or the cooling water flow rate and temperature in absorber. The lower the cooling water temperature supplied, the higher the evaporator load that can be achieved. The high pressure side is determined by the temperature and mass flow rate of the cooling water supplied to the condenser. If the conditions in condenser are maintained, the increase of generator load will cause the rise in generator temperature, mass concentration and vapour pressure. Figure 9.3a and Figure 9.3b show the relation of high side pressure and generator temperature at various samples. If the conditions in absorber are also maintained, then the mass absorption rate will increase due to the higher difference in the weak and strong mass concentration.

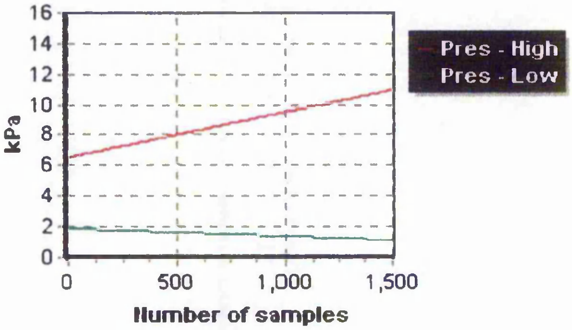

Figure 9.3a Constant changes of high and low side pressure in 1500 samples

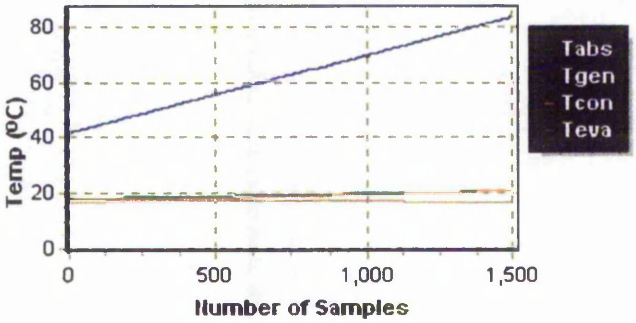

Figure 9.3b Variation of absorber, condenser, generator and evaporator temperatures in 1500 samples

9.3.3 Inlet solution temperature effects

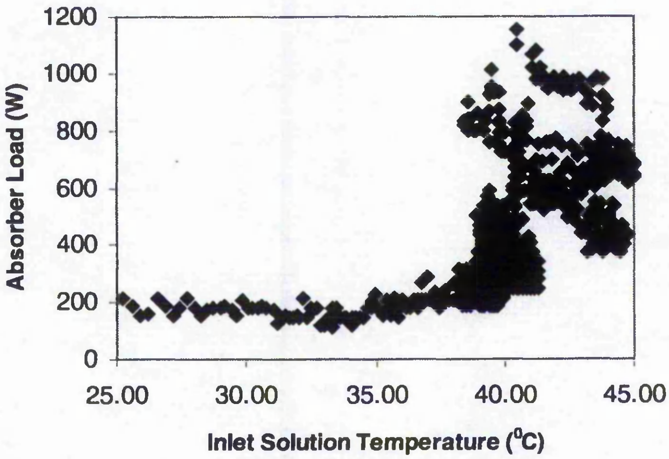

Figure 9.4 Changes absorber load with variation of inlet solution temperatures

9.3.3.1 Absorber load v.s. inlet solution temperature

Figure 9.4 shows the changes of absorber load with different inlet solution temperatures. The inlet solution temperature is determined by the generator load and the efficiency of the solution heat exchanger. The data in Figure 9.4 were obtained from 1500 experimental records. The inlet cooling water temperatures to the absorber inner and outer coils were controlled at 20 °C. From the Figure 9.4, it is clear that inlet solution temperature between 25 °C to 35 °C the absorber can conveniently remove the heat at around 200 Watts. The heat load rises exponentially up to 1200 Watts at temperature 35°C and above. However, the performance drops (Chapter 4) with increasing absorber temperature as shown in Figure 9.5. The data above 35 °C begin to scatter because a higher mass flow rate of cooling water is required to remove the heat and maintain the absorption rate. The high temperature and concentration of the solution mixtures flow from generator were more viscous causing a reduction of the velocity of solution droplets and falling film on the coil tubes. At high inlet solution temperature, the steady state condition is difficult to be maintained as the vapour pressure in the evaporator and absorber continue to fluctuate causing changes in evaporator temperature.

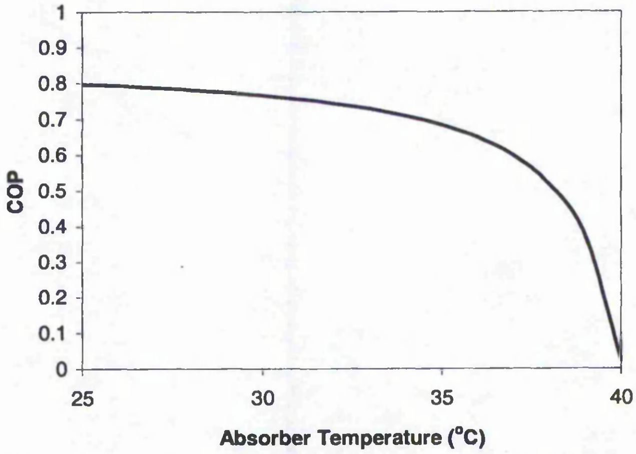

Figure 9.5 Changes of COP with absorber temperature

The experimental data shown in Figure 9.4 suggest that in order to maintain the performance for a constant evaporator load, large amount of heat has to be removed if the inlet solution temperature to the absorber is increased. Although the high temperature in absorber can help to decrease the size of the absorber, it can prevent the absorption process and thus reducing the overall performance.

9.3.3.2 Overall heat transfer coefficient v.s. inlet solution temperature

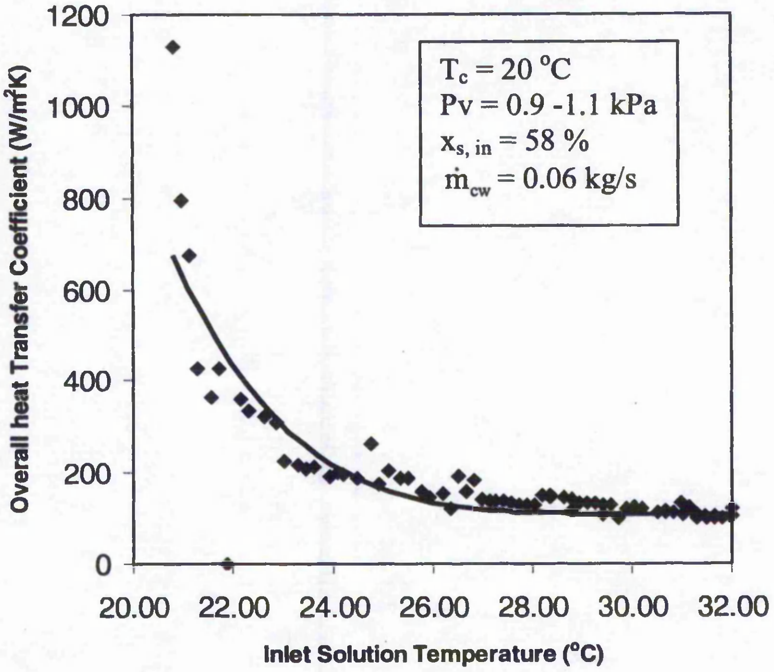

Figure 9.6 Effects of inlet solution temperature on the overall heat transfer coefficient

The experimental results in Figure 9.6 were compiled using Equation 9.8 as follows

$$U = \frac{\dot{Q}_{abs}}{A \Delta T_m}$$

where

$\dot{Q}_{abs}$ = Absorber load (W), A = effective area and ΔT_m = log mean temperature difference. From experiment data (Figure 9.6), it can be seen that the overall heat transfer coefficient reduces when the inlet solution temperatures increase. This trend also confirms the theoretical model which shows the decrease in performance shown in Figure 9.5.

9.3.3.3 Solution side heat transfer coefficient v.s. inlet solution temperature

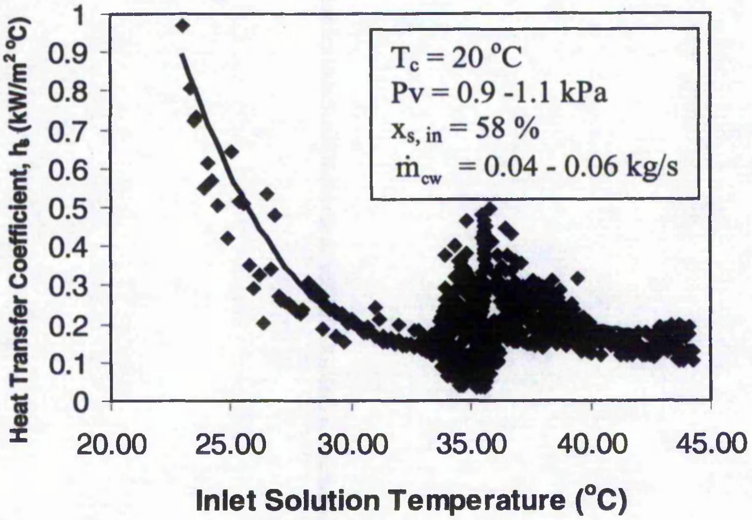

Figure 9.7 Effects of inlet solution temperature on the solution side heat transfer coefficient

The heat transfer coefficients in Figure 9.7 were obtained by using the Equations 9.7-9.10 where inlet and outlet of solution temperatures and cooling water temperature were recorded from the experiments. As shown in Figure 9.7, the general trend of heat transfer coefficient at solution side of the absorber drops with increasing inlets solution temperature. The similar trend in Figure 9.7 and Figure 9.6 show the direct impact of inlet solution temperature to the overall performance. The data at temperature between 35 °C and 40 °C is more scattered because this range was used to study different effects on the absorber performance such as variation of vapour pressure, coolant flow rate and temperature. The data suggest that the inlet temperature should be kept as low as possible where the heat transfer coefficient is high. The performance chart in Figure 9.5 is partly explained by the observation in this section.

9.3.3.4 Changes of wall temperature at various turns v.s. inlet solution temperature

Six thermocouples were placed at the inner coil of the absorber at interval of three turns. Figure 9.8 shows the wall temperature from top to bottom of the inner coil absorber. The wall temperatures increase with inlet solution temperature as it flows from solution heat exchanger to the absorber. It can be observed that the difference of temperature is reducing from T1 to T6. For instance, at the inlet solution temperature 31 °C, the temperature solution temperature rise about 0.4 °C from T1 to T2, but on rise 0.1 °C towards the end of the coil. This observation proves that the theoretical modelling in Chapter 6 (Figure 6.13) is correct in predicting the trend of heat transfer. In Figure 6.13, it shows the heat transfer at first few turns are high but drop drastically when it approaches the end of the coil. This means that the design should be large in

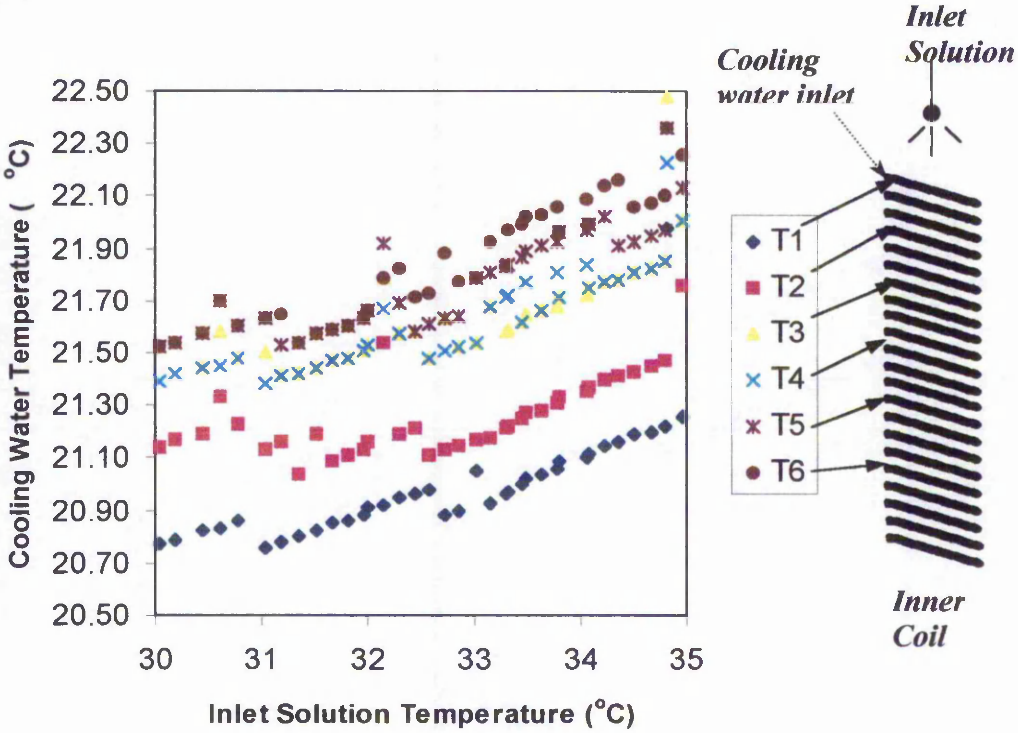

Figure 9.8 Variation of the inner coil wall temperatures from top to bottom for various inlet solution temperatures.

diameter but shorter in height. The figure also shows that the difference between the first and last recorded temperatures increase when the inlet solution temperature increases indicating that more heat has to be removed.

9.3.3.5 Changes of concentration v.s. inlet solution temperature

Figure 9.9 shows that the effect of inlet solution temperature to the concentration changes (Δx) is significant. From the trend of the experiment data, it is clear that absorption will be minimal at higher inlet solution temperatures.

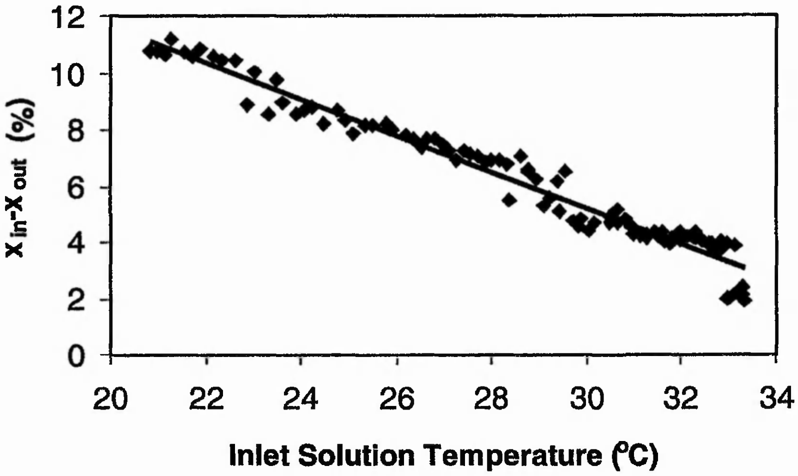

Figure 9.9 Difference of inlet and outlet concentration with variation of inlet solution temperatures.

9.3.3.6 Mass absorbed and mass transfer coefficient v.s inlet solution temperature

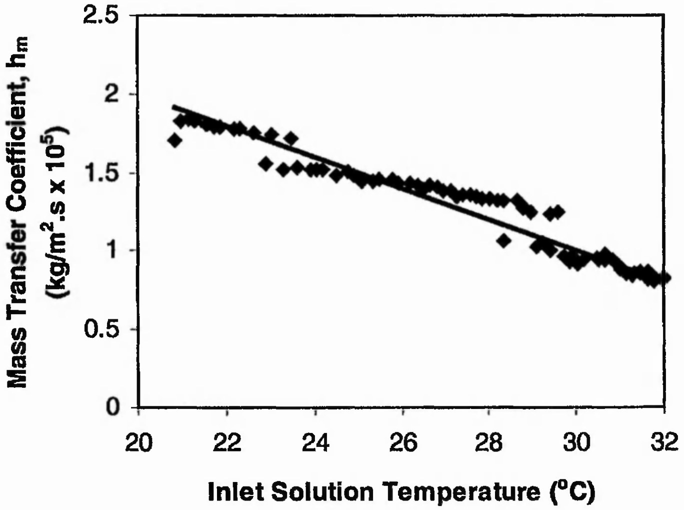

Figure 9.10 The inlet solution temperature effect on the mass transfer coefficient

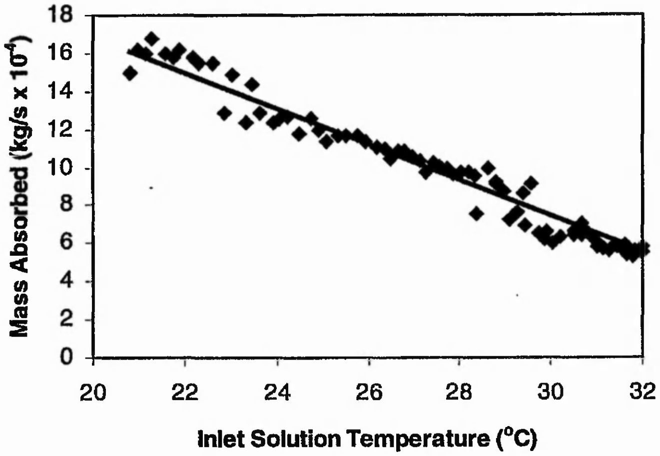

Figure 9.11 The inlet solution temperature effect on the rate mass absorbed

Figure 9.10 shows the effect of the inlet solution temperature on the mass transfer coefficient. The mass transfer coefficient decreases slightly with the increase of inlet solution temperature. Figure 9.11 shows that the mass absorption rate drops when the inlet solution temperature is increased. In order to maintain the mass absorption rate, either larger or more effective absorber has to be employed or the inlet solution temperature will need to be reduced by using the solution heat exchanger. The latter is preferable as the heat exchange will also decrease the heat input required and hence improve the performance.

9.3.4 Changes of performance with evaporating temperature

Figure 9.12 shows the changes of evaporator load with varying evaporator temperatures while the generator load was controlled to be constant. The coefficient of performance (COP) increases with higher evaporator temperatures. This is because when the evaporator temperature increases, the vapour pressure also increases. The pressure in the absorber is also increased. Larger the difference between the pressure of refrigerant vapour and the partial pressure of water in the water-lithium bromide mixture will increase absorption rate. Thus, the performance of the overall system will be improved.

The average COP and evaporator temperature achieved in the experiment are 0.5 and 13°C respectively. The trend of the COP is similar to the theoretical predictions previously discussed in Section 4.1.4.

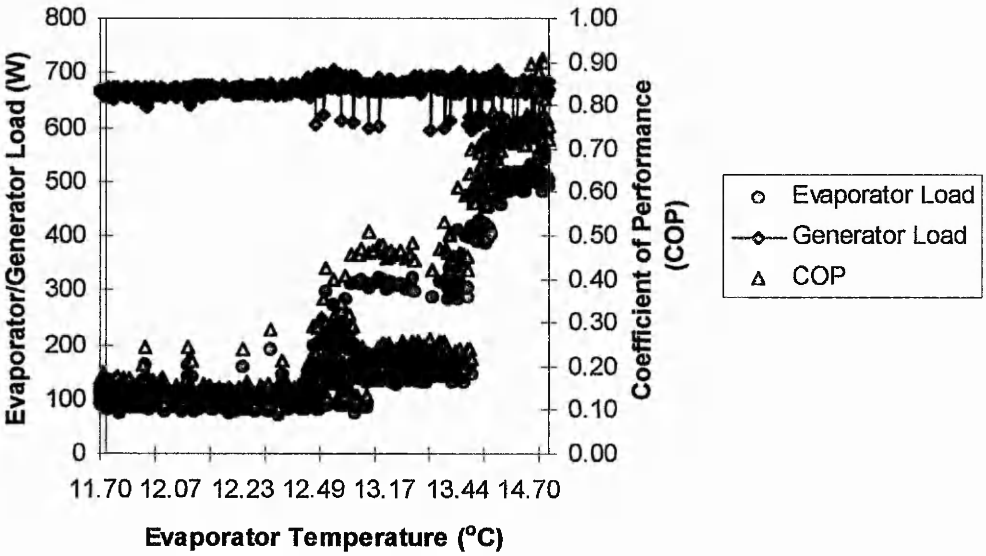

Figure 9.12 Effects on performance with variation of evaporator temperature

9.3.5 Solution Reynolds number effects

Figures 9.13 and 9.14 show the results obtained from one of the experiments over a whole day. The mass flow rates of the solution were changed gradually. The uncertainties at Reynolds at 270, 300, 320 and 345 are explained by the changes of other parameters such as inlet solution temperature, cooling water temperature and etc while the mass flow rates of solution mixtures were maintained.

The aim of this experiment is to study the general trend of effects of increasing Reynolds number on the heat and mass transfer. The trends from the whole day experimental results show that the increasing Reynolds number causes a higher mass absorbed rate and increase of heat transfer coefficient. However the effect is not significant compared to inlet solution temperature. Moreover, the solution flow is also restricted by the power of the pump and also the evaporator load required. The uncertainties at Reynolds numbers 275, 300,320 and 340 are explained by the increased of mass flow rate at various times, when other factors such as inlet solution temperature, concentration and evaporator temperature were also studied.

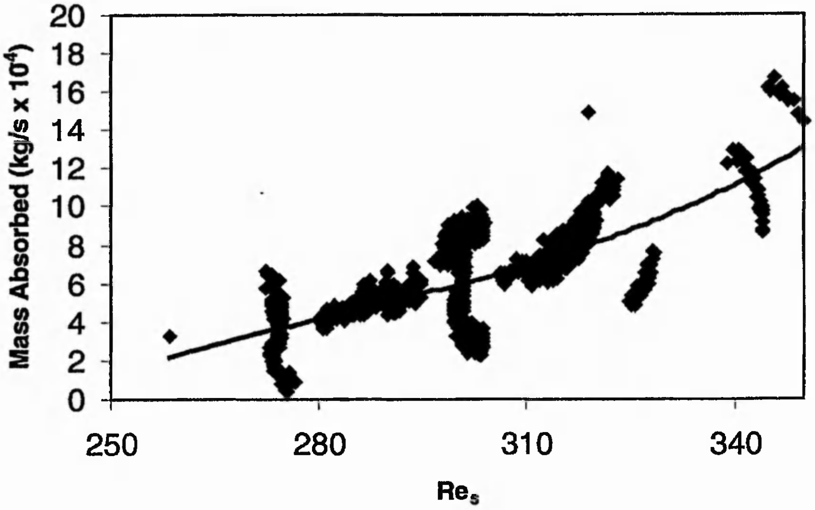

Figure 9.13 The effects of solution Reynolds number on mass absorbed rate

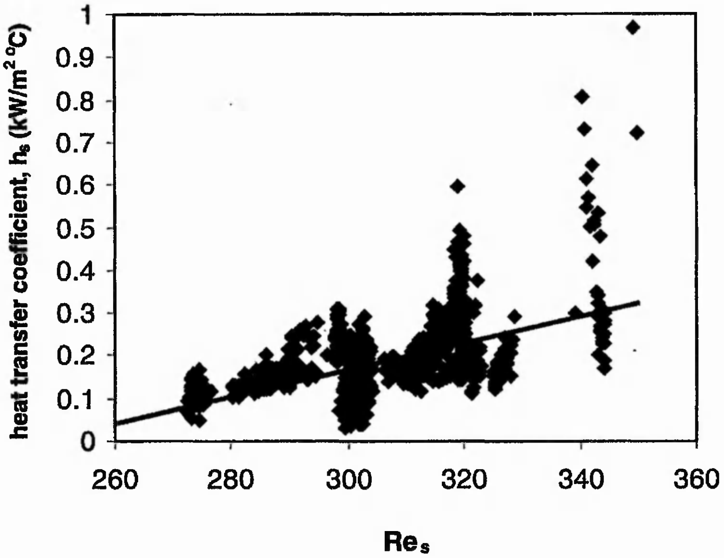

Figure 9.14 The effects of solution Reynolds number on heat transfer coefficient

9.4 Summary

In this chapter, the experimental results have been presented. The critical parameters such as the inlet solution temperature and evaporator temperature and pressure have been studied. The importance of the inlet solution temperature which was derived theoretically (Chapter 4) has been validated with the experiments in this work. Though other parameters such as cooling water temperature was shown to be important theoretically, the effects of these are not reported, as the temperature is restricted by the supply water.

All the results shown in Section 9.3.3 show that the increase of solution temperature is not favourable. The heat from the strong solution flow from the generator can be useful in using it to reheat the colder weak solution mixtures exit the absorber before it enters the generator. The high temperature of the solution mixture also affects the absorption process. The large temperature differences between the inlet solution and the cooling water may cause the water in the mixture to flash into vapour. The absorption system rig studied in previous literature (Deng and Ma, 1999; Kim et al, 1995) normally comprise of an absorber, evaporator and pump which require the regeneration of the water absorbed in the mixtures at the end of each experiments. The experiments in this work have enabled a better view of the effects of parameters on absorber performance in different ways. Some of the results may be different from previous literatures in which the open loop system was employed. For instance, the mass flow rate and the temperature of the solution are determined by several factors such as the evaporator and generator load. The changes in any one of these factors may affect the stability of the overall system. The pressures in both the high and low side may also be changed. This effect cannot be studied by using the open loop system where the pressure is constantly control by external cooling device. The experiments in this work have addressed this problem despite the fact that collected data is more scattered due to the changes of stability.

Chapter 10 Comments, Conclusions and Recommendations

10.1 General

Global warming caused by ozone depletion and greenhouse gases such as carbon dioxide is now making a serious impact on the northern hemisphere, threatening to melt ice caps and raise sea levels round the world. The recent floods and storms in the UK could also be part of a pattern of more extreme weather occurring as a result of climate change. Other indications are hot summers; six of the 10 warmest years ever recorded occurred in the 1990s; the other four all happened in the late 1980s and the declining ice sheet. The Arctic ice cover is shrinking by an area the size of the Netherlands every year (Guardian News, Sunday October 22, 2000). The recent predictions by scientists show that the worst-case scenario raises the global average land temperatures by 6 °C above the 1990 level in the next 100 years (BBC News, Sunday, 12 November, 2000).

Absorption systems have played a predominant role in reducing CO_2 emission by utilising free heat source such as waste heat and solar energy. As increasing number of people begin to use the air-conditioning systems due to the temperature rise, absorption system which uses the natural refrigerant will help to reduce CFCs and HFCs released by conventional air-conditioning systems. However, there is still plenty of room for improvement. The improvements can be achieved by increasing component efficiency, using the energy effectively and using alternative working fluids. These approaches were considered in this work and can be broadly represented by Figure 10.1. The main objective of this work were to identify the opportunities from the available technology by a comprehensive literature review and incorporate the techniques into a powerful computer program to facilitate the analysis in a design process. The contributions of this work are briefly summarised in the following sections:

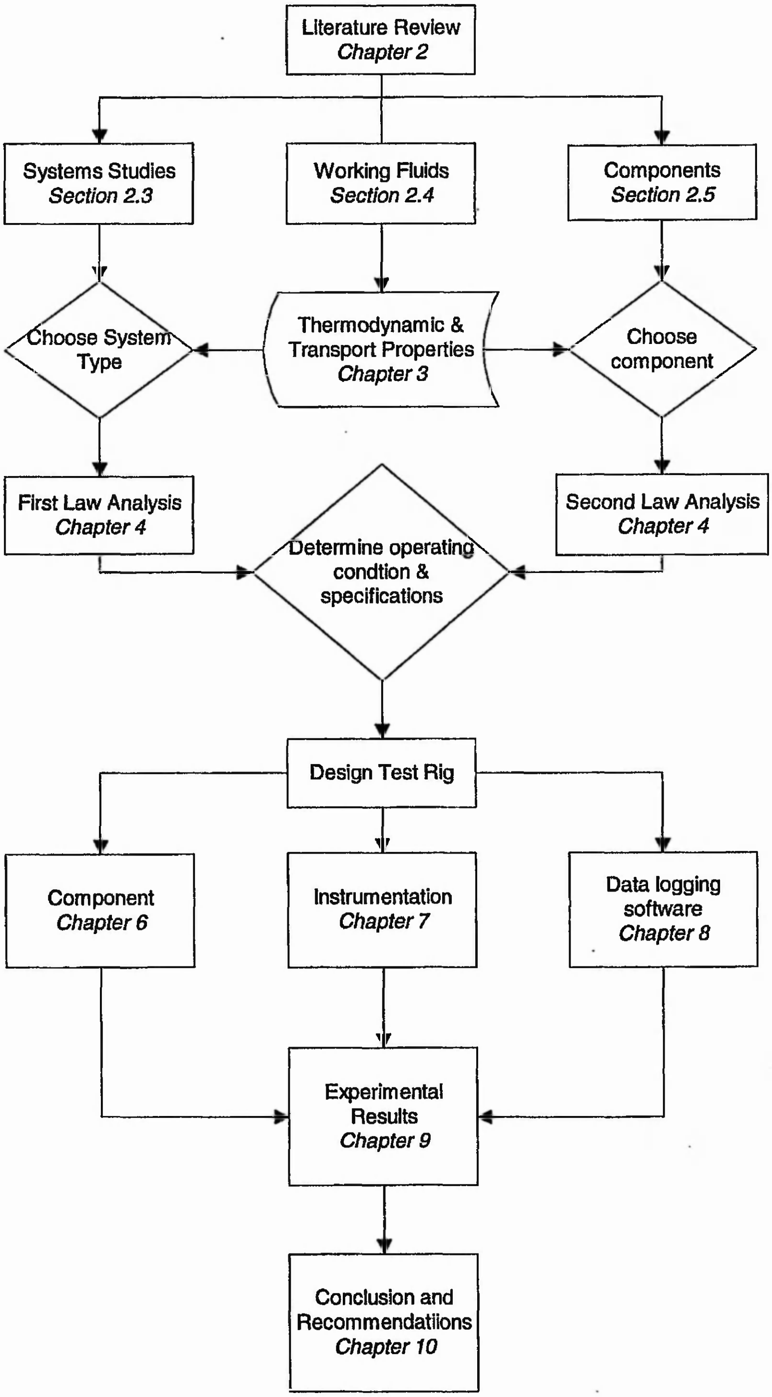

Figure 10.1 Flow chart of the structure in this work

10.2 Conclusions

The main contributions to this work can be broadly divided into four areas namely: system studies and modelling (First Law), component design and analysis (Second Law analysis and absorber modelling), the development of a user-friendly computer programs (ABCON) and building a versatile experimental rig.

10.2.1 System studies and modelling

From the review, it was concluded that the single effect type is more suitable for utilising low-grade energy at temperatures below 90 °C and has less components. However, the overall performance of the single stage system is lower than other advanced systems such as GAX cycle. Thus, the focus was set on the selection of alternative working fluids. The First law (Section 4.1) was used to study the effect of parameters such as generator temperature, absorber temperature, condenser temperature and evaporator temperature on the system performance and circulation ratio. From the studies, it was found that there is an optimal generator temperature for every combination of parameters. The main achievement in this area is the establishment of optimal points for various conditions which were fitted into two simple equations (Tan, 1999). The optimal generator temperature required can be calculated easily by inserting the absorber temperature, evaporator temperature and condenser temperature without the need to know the thermodynamic properties of the mixtures.

First law of thermodynamics model developed was also used as the preliminary tool to filter the various alternative working fluids. Water-lithium bromide and ammonia-water systems were used as benchmark for comparisons. From the modelling, it was found that the operation of the absorption system depends on the temperature of cooling water for removing heat from the absorber and condenser. Having said this, the system will only run above a cut-off temperature (minimum generator temperature) and this is restricted to the supply available and the characteristics of the working fluid mixtures. Therefore, it is important to choose a working fluid that is capable of operating at a temperature as low as possible. The overheating of the mixtures may pose problems of crystallisation when the mixtures cool down. Thus, any mixture which can work at a low cut-off temperature need also be required to work at a high concentration to avoid crystallisation. With the knowledge of three thermodynamic properties, various working fluid mixtures were compared. Water-lithium chloride is one example shown in this work which has this potential.

10.2.2 Component design & Second Law analysis

If an alternative working fluid is not available, improvements to the system will rely on the ability to utilize the heat from existing supply and precise control of the absorption process. This can only be achieved by moving the focus to a level down from the overall system studies to the design of the components. It was found that the questions regarding the effects of the control parameters are still not well understood. This work has addressed the problem by developing a model using Second Law of thermodynamics. The exergetic analysis in Section 4.2 has highlighted the importance of the absorber in the absorption system. Optimum generator temperatures for finding maximum exergetic coefficient of performance (ECOP) have been presented in a novel carpet plot form. In this work, two new equations were derived for maximum ECOP and COP at optimum generator temperature which may be conveniently stored in a control system to achieve optimised conditions during operation.

The Second Law was used to remedy the First Law model to study effect of control parameters on the individual component. The Second Law model developed was used to study in detail the extent of exergy lost from each individual component and the results show that the largest exergy lost occurred in the absorber and the generator. Since comprehensive research on the generator had been previously done by Wang (1996), this work only focuses on the absorber.

The vital role of the absorber has been further emphasised by the development of a semi-empirical model in Section 6.6. The model suggested in this work is the first one, not identified in previous literature to include the droplet formation for the coil configuration. The model built is based on an analytical method to the droplet falling upon the coil tube and forming a triangular shape. The model results have shown that the traditional approach which favoured the use of a counter flow heat exchanger may not be necessarily true in this case. Figures 6.9a and 6.9b show that parallel flow is slightly better than the counter-current absorber for less than 40 turns.

The results in Figure 6.10a and 6.10b suggest that a larger coil diameter possessing less number of turns is better than a coil with high number of turns but small in diameter. The computer modelling results (Figures 6.11a and 6.11b) show that the mass absorbed and heat transferred increase with the number of droplet sites. This again proves that a larger diameter coil is more favourable. Detailed design of the condenser, evaporator and generator are reported (Chapter 6).

10.2.3 The computer program

All of the design work and analysis mentioned earlier will take a considerable amount of time if carried out manually. The learning curve is steep due to the massive amount of literature available but mostly provide no hints at all to the detailed design. The unpopularity of absorption systems may be partly due to its complexity and the lack of information compared to vapour compression cycles. This work is aimed to providing a bridge of understanding of the system and simplifying the design process by incorporating all the necessary tools into an integrated user-friendly package named ABCON (Figure 5.2).

The published literature on thermodynamic and transport properties are massive, however, most of them are either in tabular form or incomplete for the full range of interest. This work has addressed this problem by incorporating the crucial working fluid properties of eight mixtures into computer functions which can be recalled anytime in a convenient way. The properties can be printed into tables and carpet plots for the range of interest.

In this work, not only the available properties in tabular form were correlated into equations, several analytical methods are also reported to correlate the enthalpy and entropy from other commonly available properties such as specific heat (Chapter 3). Comprehensive reference tables of thermodynamic and transport properties for binary (Table 2.4), ternary (Table 2.5) and tertiary (Table 2.6) were also reported in this work.

The thermodynamic analysis has been made easier to designers through using comprehensive software developed in this work. By setting the working fluid, a main parameter and its range, the program (Figure 5.6) will enable the user to obtain the performance curves and a parametric study. The results can be further interpreted by using the overlay plot to investigate the various effects on one another in a single chart. Furthermore, the results can be fitted into any one of the six types of curve fitting routines from exponential to polynomial fits (Figure 5.8). In this program, a database of about four hundred publications and a hundred theses have been compiled as a database that can be easily retrieved for further reference.

Another important outcome from this work is the development of a powerful data logging system for absorption systems (Chapter 8). The ability of not only logging data from a variety of transducers but also controlling the output load such as evaporator, generator and pumps will help to understand the absorption system more thoroughly. A pressure-temperature-concentration chart and custom made computer gauges will help to monitor the process so that crystallisation limits are not reached. This facility is not normally available from any other commercial software packages. The data-logging software developed is also a great improvement from the one presently used by P.A. Hilton Ltd., which works under DOS and inefficient in terms of speed, functionality and user-friendliness.

10.2.4 Experimental rig and results

The instrumentations used in this work have been discussed in detail in Chapter 7. An absorption rig was built using borosilicate glass so that the process can be easily observed. It was designed to be flexible and used as a benchmark for comparison in studying and developing new cycles and absorbent/refrigerant combinations for future work. This rig could be used for further work in studying the effects of cooling water flow in series or parallel, single solution heat exchanger or two heat exchangers in series, inner or outer absorber coil and two different sprays. The rig is capable of working for different capacities.

The experiments show the effect of the inlet solution temperature on the heat and mass transfer coefficients, concentration changes, mass absorption rate and absorber load. The effects of evaporator temperature, which reflects the low side pressure on the system performance, were also demonstrated. The evaporator temperature and pressure clearly depends on the evaporator load.

As mentioned earlier, two of the main parameters namely the generator temperature and cooling water temperature are subjected to change at anytime and solely depend on the supply despite their dependence on the mass concentration at inlet and outlet of the absorber. If air-cooled absorber and condenser are used, the ambient conditions such as humidity and temperature will affect the cooling load. The remaining controllable parameters are the inlet solution temperature and the flow rates of the solution and cooling water. Thus only the effects of the inlet solution temperature and Reynolds number were investigated.

The results have been validated against the theoretical model and shown to be in good agreement to the trends predicted under different conditions. It is clearly seen that both the heat (Figure 9.7) and mass transfer (Figure 9.9) coefficients decrease with increase of the inlet solution temperature.

The results from both the theoretical model (Figure 9.5) and the experiments (Figure 9.7) suggest that the inlet solution temperature has to be kept lower than 35 ^{o}C if water is used as a cooling medium.

Two feasible approaches to reduce the inlet solution temperature are 1. The use of strong solution heat exchanger so that heat from the generator can be used to reheat the colder weak solution mixture from the absorber before it enters the generator 2. The use of re-circulation spray. The re-circulation sprays will not only help to keep the surface well covered with solution, it also reduces the heat to the inlet solution through the mixing process. The strong solution may not absorb enough initially and the re-circulation allows the opportunity for the solution to absorb more vapour and thus reduce the workload of generator and the inlet solution temperature to the absorber.

From the experiments, it is found that the crucial factor to achieving a good system performance lies under the control of the system pressure especially the pressure difference between the evaporator and absorber. The distance between the evaporator and absorber has to be kept as close as possible to increase the absorption rate.

10.3 Further recommendations

The following are suggested for improvement:

1. Copper coil which has a higher thermal conductivity should be used in the future so that enhanced heat transfer can be achieved.
2. The tube used in this work can be replaced with other advanced tubes that were tested in vertical and horizontal tubes absorber. Among the advanced tubes, several configuration are generally considered better in terms of heat and mass transfer namely:
   - KoroChil (Wolverine)
   - Fluted tube
   - Axial Groove fins
   - Thermoexcel-A (Hitachi)
3. The effects of additives such as 2-ethyl-1-hexanol (2EH) on the performance of the coil absorber should be studied. The additives will increase both the heat and mass transfer rates.
4. The design of the evaporator and absorber should be combined into a single unit so that the cost can be reduced. The pressure drop in the pipeline can be avoided thus increasing the absorption rate.
5. Spray nozzles should be used in evaporator and generator.
6. The absorber coil should be made large in diameter with smaller number of turns which help to increase the heat and mass transfer rates.
7. Alternative working fluid such as H_2O-LiCl and H_2O-LiBr+LiCl+$ZnCl_2$, which can work at lower generator temperature and higher performance, should be tested.

Although the hydrometer used is this work are accurate but it can only be used to measure the concentration periodically. The measurement also affects the system stability due to the large amount of mixtures needed to fill the hydrometer chamber. In the future, electric conductance cell type should be used for speed provided the cell is calibrated periodically.

The absorber model suggested in this work can be further improved by studying the randomness of the droplets fall. The model in the future should also consider the movement of the droplet around the coil. The effect of non-condensable gases on the performance can be included into the model.

Although the current work has highlighted key factors for improvement of the absorption system, more research is required for stepping towards the development of a robust small-scale chiller with high performance. With the help of the tools developed in this work, the above recommendations may be carried out easier in the future towards a thorough understanding of the system characteristics and contributing towards a better environment.

References

Abovsky, V., 1996, Thermodynamic of ammonia-water mixture. *Fluid Phase Equilibria*, **116**, 170-176.

Adegoke, C.O., 1987, Evaluation of a refrigerant/absorbent combination for vapour absorption refrigeration systems utilizing solar heat. *PhD Thesis, The King's College*, London.

Adegoke, C.O. and Gosney, W.B., 1991, Vapour pressure data for (2LiBr+$ZnBr_2$)-H_20 solutions. *Int. J. Refrig.*, **14**(Jan), 39-45.

Akiyama, T., Arai, S., Sato, H. and Watanabe, K., 1996, Thermodynamic equations for lithium bromide-water solution covering a wide range of concentrations. *I.I.F.-I.I.R. - Commissions B1, B2, E1 and E2 – Aarhus*, Denmark, **3**, 329-337

Alizadah, S., Bahar, F. and Geoola, F., 1979, Design and optimisation of an absorption refrigeration system operated by solar energy. *Solar Energy*, **22**, 149-154.

Alvares, S.G. and Trepp, Ch., 1987, Simulation of a solar driven aqua-ammonia absorption refrigeration system. *Int. J. Refrig.*, **10**, 40-48.

Andberg, J.W., 1986, Absorption of vapors into liquid films flowing over cooled horizontal tubes. *PhD thesis, The Univ. of Texas at Austin.*

Antonopoulos, K.A., 1992, Absorption panel cooling using a TFE-NMP mixture. *Heat Recovery Systems & CHP*, **12**(3), 203 – 210.

Aphornratana, S. and Eames, I.W., 1995, Thermodynamic analysis of absorption refrigeration cycles using the second law of thermodynamics method. *Int. J. Refrig*, **18**(4), 244-252.

Ataer, O. E. and Gogus, Y., 1991, Comparative study of irreversibilities in an aqua-ammonia absorption refrigeration system. *Int. J. Refrig.*, **14**(2), 86-92.

Ameel, T.A., Kim, K.J., Wood, B.D., 1997, Non-absorbable gas effects on heat and mass transfer in wavy laminar falling film absorption. *Solar Energy*, **60**(6), 301-311.

Bayramoglu, M. and Bulgan, A.T., 1995, Sensitivity analysis of an aqua-ammonia-absorption refrigeration systems (AARS). *Energy*, **20**(6), 567-571.

Best, R., Eisa, M.A.R. and Holland, F.A., 1987, Thermodynamic design data for absorption heat transformers - I. operating on ammonia-water-Part I .cooling. *Heat Recovery Systems & CHP*, **7**(2), 167-175.

Best, R., Islas, J. and Martinez, M., 1993, Exergy efficiency of an ammonia-water absorption system for ice production. *Applied Energy*, **45**, 241-256.

Beutler, A.S., Feuerecker, G.R. and Alefeld, G., 1996, A hydroxide mixture as working fluid for absorption heat pumps. *ASHRAE Transactions*, **102**(1), pp.12

Bogart, M., 1981, Ammonia absorption refrigeration in industrial processes. *Gulf Publishing Company.*

Boryta, D.A., 1970, Solubility of lithium bromide in water between -50 and 100 C (45 to 70% lithium bromide). *J. Chem. Eng. Data*, **15**(1), 142-144.

Bourseau, P. and Bugarel, R., 1986, Absorption diffusion machines : comparison of the performances of NH_3-H_2O and NH_3-NaSCN. *Int. J. Refrig.*, **9**, Jul, 206-214.

Bourseau, P., 1983, Contribution a l'etude des machines frigorifiques solaires de faible maintenance. These de Docteur-Ingenieur Institut du Genie Chimique de Toulouse, Jun.

BS4434, 1995, Safety aspects in the design, construction and installation of refrigeration appliances and systems. *BRISTISH STANDARDS INSTITUTION.*

Bulgan, AT, 1995, Optimisation of the thermodynamic model of aqua-ammonia absorption refrigeration systems. *Energy Conversion and Management*, **36**(2), Feb, 135-143.

Bulgan, A.T., 1997, Use of low temperature energy sources in aqua-ammonia absorption refrigeration systems. *Energy Convers. Mgmt*, **38**(4), 1431-1438.

Butterworth, 1977, Introduction of heat transfer. Engineering design guides, *Oxford university press.*

Carmody S.A. and Shelton, S.V., 1993, Direct second law analysis of advanced absorption cycles utilizing an ideal solution model. *AES, International Absorption Heat Pump Conference*, **31**.

Chapman, J.F., Rees, G.W. and Tucker, R.J., 1996, Advanced technologies for gas-fired air conditioning. *British Gas R & T*, Paper No. T318.

Choudhury, S.K., Hisajima, D., Ohuchi, T., Nishiguchi, A., Fukushima, T. and Sakaguchi, S., 1993, Absorption of vapours into liquid films flowing over cooled horizontal tubes. *ASHRAE Transactions*, **99**(2), 81-89.

Cui, X. Y., 1998, The theory and experiment research on water-lithium bromide falling film absorption process. *PhD. Thesis, University of Shanghai for Science and Technology.*

Clerx, M., and G.J. Trezek. 1987, Performance of an aqua-ammonia absorption solar refrigerator. *Solar Energy*, **39**, 379-388.

Davidson, I., 1999, The "CFC" issue: an overview. *Private contact.*

Dence, A.E., Nowak, C.C. and Perez-Blanco, H., 1996, A transient computer simulation of an ammonia-water heat pump in cooling mode. *Proc. of the Intersociety Energy Convers. Eng. Conf.*, **416**, 1041-1046.

DiGuilio, R.M., 1990, Properties of lithium bromide-water solutions at high temperatures and concentrations-I. Thermal conductivity. *ASHRAE Transaction*, **96**(1), 702-708.

Dincer, I., Dost, S., 1996, Energy analysis of an ammonia-water absorption refrigeration system, *Energy Sources*, **18**(6), 727-733.

Eames, I.W. and Wu, S., 1999, Theory and practice of H_2O-LiBr vapour absorption cycle refrigerators. *I Mech E Seminar S615, Recent development in refrigeration and heat pump technologies.*

Eisa, M.A.R. and Holland, F.A., 1987, A study of the optimum interaction between the working fluid and the absorbent in absorption heat pump systems. *Heat Recovery System & CHP*, **7**(2), 107-117.

El-Sayed, Y.M. and Tribus, M., 1985, Thermodynamic properties of water-ammonia mixtures theoretical implementation for use in power cycles analysis. *ASME Adv. Energy Systems Div.*, **1**, Jul, 89-95.

Engler, M., Grossman, G. and Hellmann, H.-M., 1997, Comparative simulation and investigation of ammonia-water : absorption cycles for heat pump applications. *Int. J. Refrig.*, **20**(7), 504-516.

Feuerecker, G., Scharfe, J., Greiter, I., Frank, C. and Alefeld, G., 1993, Measurement of thermophysical properties of aqueous Libr-solutions at high temperatures and concentrations. *Int. Absorp. Heat Pump Conf., ASME, AES* **31**, 493-499.

Gillespie, P.C., Wilding, W.V. and Wilson, G.M., 1987, Vapour-liquid equilibrium measurements on the ammonia-water system from 313 K to 589 K. *AICHE Symposium Series*, **83**(256), 97-127.

Gomez, A.L. and Mansoori, G.A., 1983, Thermodynamic equation of state approach for the choice of working fluids of absorption cooling cycles. *Solar Energy*, **31**(6), 557-566.

Grigor'eva, N.I. and Nakoryakov, V.E., 1977, Exact solution of combined heat and mass transfer problem during film absorption. *J.Eng. Physics*, **33**, 1349-1353.

Grossman, G., 1983, Simultaneous heat and mass transfer in film absorption under laminar flow. *Int. J. of Heat Mass Transfer*, **26**(3), 357-371.

Grossman, G., 1990, Film absorption heat and mass transfer in the presence of non-condensables. *Int. J., of Heat Mass Transfer*, **6**, 247-252.

Grossman, G., 1995, Modular simulation of absorption systems. *User's guide and reference, OAK Ridge National Laboratory, Contract No. DE-AC05-96OR22464.*

Grossman, G. and Gommed, K., 1997, Heat and mass transfer in film absorption in the presence of non-condensable gases. *Int. J. of Heat & Mass Transfer*, **40**(15), 3595-3606.

Grover, G.S., Eisa, M.A.R. and Holland, F.A., 1988, Thermodynamic design data for absorption heat pump systems operating on water-lithium chloride - Part I. Cooling. *Heat Recovery Systems & CHP*, **8**(1), 33-41.

Guillevic, J.L., Richon, D., and Renon, H., 1985, Vapour-liquid equilibrium data for the binary system water-ammonia at 403.1, 453.1, and 503.1 K up to 7.0 MPa. *J. Chem. Eng. Data*, **30**(3), 332-335.

Haar, L. and Gallaghar, J., 1978, Thermodynamic properties of ammonia. *J. Phys. Chem. Ref. Data*, **7**(3), 635-792.

Hasaba, S., Kawai, K., Kawasaki, K. and Uemura, T., 1960, Specific heat of aqueous solution of LiBr. *Reito*, Japan, **35**, 815-819.

Heinonen, E.W. and Tapscott, R.E., 1999, Secondary properties of aqueous lithium bromide solutions. *ASHRAE Transactions*, **105**(1).

Hellmann , H.M. and Grossman, G., 1996, Improved property data correlations of absorption fluids for computer simulation of heat pump cycles. *ASHRAE Trans.* **102**(1), 980-997.

Herold, K.E. and Moran, M.J., 1987, Thermodynamic properties of lithium bromide/water solutions. *ASHRAE Transactions*, **93**(1), 35-43.

Herold, K.E. and Radermacher, R., 1996, Absorption chillers and heat pumps. *CRC Press.*

Herold, K.E. and Radermacher, R., Howe, L. and Erickson, D.C., 1991, Development of an absorption heat pump water heater using an aqueous ternary hydroxide working fluid. *Int. J. Refrig.*, **14**(May), 156-167.

Holman, J.P., 1997, Heat transfer. *McGraw Hill Inc.*

Huang, B.J. and Chang, T.Y., 1978, Design analysis of ammonia-water absorption refrigeration systems. *Proc. of the Intersociety Energy Convers. Eng. Conf.*, 798-804.

Ibrahim, G.A., , 1991, An investigation into liquid film absorbers for refrigeration systems. *PhD thesis, King's College London.*

Ibrahim, O.M., 1993, Thermodynamic properties of ammonia-water mixtures. *ASHRAE Transactions*, **99**(1), 1495-1502.

Ibrahim, O.M., Barnett, S.M., Balamuru, V.G., 1997, Improving the performance of ammonia-water absorption cycles using salt additives and membranes. *ASHRAE Transactions*, **103**(1), 439-443.

Iyoki, S., Ohmori, S. and Uemura, T., 1990, Heat capacities of the water-lithium bromide-lithium iodide system. *J. Chem. Eng. Data*, **35**, 317-320.

Iyoki, S., Iwasaki, S., Kuriyama, Y. and Uemura, T., 1993a, Densities, viscosities, and surface tensions for the two ternary systems H_2O+LiBr+LiI and H_20+LiCl+$LiNO_3$. *J. Chem. Eng. Data*, **38**, 302-305.

Iyoki, S., Iwasaki, S., Kuriyama, Y. and Uemura, T., 1993b, Integral enthalpies of mixing for water-lithium bromide-lithium iodide and water-lithium chloride-lithium nitrate at 298.15K. *J. Chem. Eng. Data*, **38**, 299-301.

Iyoki, S., Iwasaki, S., Kuriyama, Y. and Uemura, T., 1990, Solubilities for the two ternary systems water+lithium bromide+lithium iodide and water+lithium chloride+lithium nitrate at various temperatures. *J. Chem. Eng. Data*, **35**, 396-398.

Iyoki, S. and Uemura, T., 1989a, Physical and thermal properties of the water-lithium bromide-zinc chloride-calcium bromide system. *Int. J. Refrig.*, **12**(Sep), 272-277.

Iyoki, S. and Uemura, T., 1989b, Vapour pressure of the water-lithium bromide system and the water-lithium bromide-lithium chloride system at high temperatures. *Int. J. Refrig.*, **12**(Sep), 278-282.

Iyoki, S. and Uemura, T., 1990, Physical and thermal properties of the water-lithium bromide-zinc bromide-lithium chloride system. *ASHRAE Transactions*, 2, 328.

Jain, P.C. and Gable, K.C., 1971, Equilibrium property data equations for ammonia-water mixtures. *ASHRAE Trans.*, **77**(1), 149-151.

Jambunathan K., Tan Y.W. and Ashforth-Frost S., 2000, Optimised design tools for small scale ammonia-water absorption coolings systems, *Int. Conf. & Exhib. on Gearing, Transmissions and Mech. Systems,* 791-803.

Jennings, B.H. and Shannon F.P., 1938, The thermodynamics of absorption refrigeration. *Refrig. Eng.*, **35**, p.333.

Jennings, B.H., 1981, The thermodynamic properties of ammonia-water mixtures: A reassessment in tabular format. *ASHRAE Transactions*, **87**(2), 419-433.

Jeong, S., Kang, B.H., Lee, C.S. and Karng, S.W., 1993, Computer simulation on dynamic behaviour of a hot water driven absorption chiller. *AES, International Absorption Heat Pump Conference*, **31**, 333-338.

Kandlikar, S.G., 1982, A new absorber heat recovery cycle to improve COP of aqua-ammonia absorption refrigeration system. *ASHRAE Transaction*s, **88**(1), 141-158.

Karakas, A., Egrican, N. and Uygur, S., 1990, Second-law analysis of solar absorption cooling cycles using lithium-bromide/water and ammonia/water as working fluids. *Applied Energy*, **37**, 169-187.

Katzel, J., 1992, The rediscovery of absorption chillers. *Plant Engineering*, Apr., 40-45.

Kaushik, S.C. and Bhardwaj, S.C., 1982, Theoretical analysis of ammonia-water absorption cycles for refrigeration and space conditioning systems. *Energy Research*, **6**, 205-225.

Keizer, C., 1982, Absorption refrigeration machines. *PhD. Thesis, Delft University of Technology*, April, 208p.

Kern, D., Seaton, R., A theoretical analysis of thermal surfaces fouling, *Brit, Chem. Engin.*, 4(5), 258-262, 1959

Kirby, M.J. and Perez-Blanco, H., 1994, A design model for horizontal tube water/lithium bromide absorbers. *AES, Heat Pump and Refrigeration Systems Design, Analysis and Applications*, **32**, 1-10.

Knudsen, H.J., 1980, Static simulation of absorption refrigeration system, *IIR - Commisstion B1, B2, E1 and E2: Mons (Belgium).*

Koo, K.K., Lee, H.R. and Jeong, S., 1998, Solubilities, vapour pressures, densities, and viscosities of the (water+lithium bromide+lithium iodide+lithium chloride) system. *J. Chem. Eng. Data*, **43**, 722-725.

Kouremenos, D.A., Kakatsios, X.K. and Floratos, O.E., 1996, Development of a computer program describing the real gas isentropic expansion of an ammonia-water vapour mixture. *Advances in Eng. Soft*, **26**, 65-72.

Kumar, R. and Kaushik, S.C., 1991, Thermodynamic evaluation of a modified aqua-ammonia absorption refrigeration. *Energy Convers. Mgmt*, **32**(2), 191-195.

Lee, R.J., DiGuilio, R.M., Jeter, S.M. and Jeter, S.M., 1990, Properties of lithium bromide-water solutions at high temperatures and concentrations – II: density and viscosity. *ASHRAE Transaction*, **96**(1), 709-714.

Macriss, R.A., Eakin, B.E., Ellington, R.T. and Huebler, J., 1964, Physical and thermodynamic properties of ammonia-water mixtures. *Institute of Gas Technology, Chicago*, Research Bulletin No. **34**.

Macriss, R.A., Gutraj, J.M. and Zawacki, T.S., 1995, Absorption fluids data survey : Final report on worldwide data. *Working fluids and transport phenomena in advanced absorption heat pumps, Annex 14*, HPP-AN14-1, **2**, 19-1 – 19-15.

Manago, A., 1995, Research and development on working fluids. *Working fluids and transport phenomena in advanced absorption heat pumps*, *Annex 14* HPP-AN14-1,. **2**, 4-1 – 4-56.

Mao, J., 1996, Falling film absorption on horizontal and coiled tubes. *PhD Thesis, The Ohio State University.*

McLinden, M. and Radermacher, R., 1985, An experimental comparison of ammonia-water and ammonia-water lithium bromide mixtures in an absorption heat pump. *ASHRAE Transactions*, **91**(2b), 1837-1845.

McNeely, L.A., 1979, Thermodynamic properties of aqueous solutions of lithium bromide, *ASHRAE Transactions* **85**(1), 413-434.

Merkel, F. and Bosnjakovic, F., 1929, Diagrams and tables for the calculation of absorption refrigeration. *Berlin: Julius Springer.*

Miller, W.A., 1998, The experimental analysis of aqueous lithium bromide vertical falling film absorption. *PhD thesis, The Univ. of Tennessee, Knoxville.*

Miller, W.A., Perez-Blanco, H. and Patnaik, V., 1992, Advanced surfaces for vertical tube absorbers. *Gas Research Institute GRI-93/0061.*

Mumah, S.N., Adefila, S.S. and Arinze, E.A., 1994, First law thermodynamic evaluation and simulation of ammonia-water absorption heat pump systems. *Energy Convers. Mgmt,* **35**(8), 737-750.

Ng, K.C., Tu, K. and Chua, H.T., 1998, Thermodynamic analysis of absorption chillers: Internal dissipation and process average temperature. *Applied Thermal Eng.*, **18**(8), 671-682.

Ogawa, K., 1980, Thermodynamic properties of aqueous solution of lithium bromide. *Reito*, Japan, **55**, 347-351.

Patnaik, V. and Perez-Blanco, H., 1996, Roll waves in falling films: an approximate treatment of velocity field. *Int. J. Heat and Fluid Flow*, **17**(1), 63-70.

Patnaik, V., Perez-Blanco, H. and Ryan, W.A., 1993, A simple analytical model for the design of vertical tube absorbers. *ASHRAE Transactions*, **99**(2), 69-80.

Palmer, S.C., 1995, Dual-pressure absorption cycles – the second law and working fluids. *PhD Thesis, Georgia Institute of Technology*, Dec, 204p.

Park, Y.M. and Sonntag, R.E., 1990, Thermodynamics properties of ammonia-water mixtures : A generalized equation-of-state approach. *ASHRAE Transactions*, **9**(1), 150-159.

Patek, J. and Klomfar, J., 1995, Simple functions for fast calculations of selected thermodynamic properties of the ammonia-water system. *Int. J. Refrig.*, **18**(4), 228-234

Patil, K.R., Chaudhari, S.K. and Katti, S.S., 1991a, Thermodynamic design data for absorption heat pump systems operating on water-lithium iodide - part 1. Cooling. *Heat Recovery Systems & CHP*, **11**(5), 341-350.

Patil, K.R., Chaudhari, S.K. and Katti, S.S., 1991b, Thermodynamics properties of aqueous solutions of lithium iodide : Simplified method for predicting the enthalpies from the vapor-pressure data. *Applied Energy*, **39**(3), 189-199.

Patterson M.R. and Perez-Blanco, H., 1988, Numerical fits of the properties of lithium-bromide water solutions. *ASHRAE Trans.* **94**(2), 2059-2076.

Phillips, B.A., 1976, Absorption cycles for air-cooled solar air conditioning. *ASHRAE Transactions*, **81**(1), 966-974.

Polak, J. and Lu, B.C.Y., 1975, Vapour-liquid equilibria in system ammonia-water at 14.69 and 65 Psia. *J. Chem. Eng. Data*, **20**(2), 182-183.

Qasrawi, A.M.S., 1980, Absorption heat pump generators. *Proceedings of the NATO advanced study institute on heat pump fundamentals, Espinho, Spain*, 400-424.

Rane, M.V., Lalvani, S.B. and Helmer, W.A., 1998, New method to correlate and predict vapor-liquid equilibrium data for salt solutions to be used for heat pump simulations. *ASHRAE Transactions*, **94**(2), 2078-2094.

Reid, S.S.H., and Heidemann, R.A., 1987, Vapour-liquid equilibria in the ammonia-water system. *J. Chem. Eng. Data*, **32**(2), 183-191.

Reistad, B., 1969, Thermodynamic properties of ammonia-water mixtures. *Electrolux Technical Report* 11108, 24 September.

Rogdakis, E.D. and Antonopoulos, K.A., 1991, Effect of the interface heat exchanger in composite NH_3/H_20 - H_20/LiBr absorption-refrigeration systems. *Heat Recovery Systems & CHP*, **11**(6), 495-504.

Rogdakis, E.D.. and Antonopoulos, K.A., 1992, Performance of a solar driven H_2O/LiBr absorption panel cooling system. *AES, Thermodynamics and the design, analysis, and improvement of energy systems*, **27**, 135-140.

Rogers, G.F.C. and Mayhew, Y.R., 1964, Heat transfer and pressure loss in helically coiled tubes with turbulent flow. *Int. J. of Heat Mass Transfer*, **7**, 1207-1216.

Rohsenow, W.M. and Griffith, P., 1955, Correlation of maximum heat flux data for boiling of saturated liquids. *AIChE-ASME Heat transfer symp.*, Louisville, Ky.

Ru, Y., 1987, Heat and mass transfer in laminar wavy film absorption with the presence of non-absorbable gases. *PhD. Thesis, Arizona State University.*

Ruiter, J.P., 1990, Simplified thermodynamic description of mixtures and solutions. *Int. J. Refrig.*, **13**(Jul), 223-236.

Sabir, H.M. and Eames, I.W., 1998, Theoretical comparison between Lithium Bromide/Water vapour resorption and absorption cycles. *Applied Thermal Eng.*, **18**(8), 683-692.

Sabir, H.M. and Eames, I.W., 1999, Performance of film absorbers under the effect of a contaminant non-absorbable gas. *Applied Energy*, **63**, 255-267.

Sabir, H. and Suen, K.O., 1996, Investigation of effects of wave motion on the performance of a falling film absorber. *Int. J. Heat & Mass Transfer*, **39**(12), 2463-2472.

Saito, T., 1995, Working fluids and transport phenomena in advanced absorption heat pumps. *IEA Heat Pump Centre, Annex 14*, HPP-AN14-1,. **1.**

Saravanan, R. and Maiya, M.P., 1998, Thermodynamic comparison of water based working fluid combinations for a vapour absorption refrigeration system. *Applied Thermal Eng.*, **18**(7), 553-568.

Sassen, C.L., Kwartel, R.A.C.V., Kooi, H.J.V.D. and Arons, J.D.S., 1990, Vapour-Liquid equilibria the system ammonia + water up to the critical region. *J. Chem. Eng. Data*, **35**(2), 140-144.

Satha, A., 1995, Research on absorption refrigerators and heat pumps. *Int. Energy J.*, **17**(1), Jun, 1-19.

Scatchard, G., 1947, Thermodynamic properties of saturated liquid and vapour of ammonia-water mixtures. *Refrig. Eng.*, **53**, 413-417.

Schulz, S.C.G., 1972, Equation of state for the system ammonia-water for use with computers. *Proc. Int. Congress of Refrigeration, Washington*, **2**, 431-436.

Seewald, J.S. and Perez-Blanco, H., 1992, A model for calculating the performance of a lithium-bromide/water absorber, *B.Eng. (Hon) Thesis, The Pennsylvania State Univ.*.

Shiran, Y., Shitzer, A. and Degani, D., 1982, Computerized design and economic evaluation of an aqua-ammonia solar operated absorption system. *Solar Energy*, **29**(1), 43-54.

Smith, I.E., 1986, Design and development of absorption heat pump. *Commission of the European Communities*, EUR 10808.

Smith, R.A., 1986, Vaporisers (selection, design & operation). *Longman Scientific & Technical.*

Stoecker, W.F. and Reed, L.D.,1971, Effect of operating temperatures on the coefficient of performance of aqua-ammonia refrigerating systems. *ASHRAE Transactions*, **77**(1), 163-170.

Sun, D.W., 1997a, Thermodynamic design data and optimum design maps for absorption refrigeration systems. *Applied Thermal Eng.*, **17**(3), 211-221.

Sun, D.W., 1997b, Computer simulation and optimization of ammonia-water absorption refrigeration systems. *Energy Sources*, **19**(7), 677-690

Sun, D.W., 1998, Comparison of the performances of NH_3-H_2O, NH_3-$LiNO_3$ and NH_3-NaSCN absorption refrigeration systems. *Energy Convers. Mgmt*, **39**(5/6), 357-368.

Tan, Y.W., 1999, Development of a novel absorption principle water cooling system for the domestic sector. *MPhil/PhD Transfer Report*, p.39.

Tan, Y.W. and Jambunathan, K., 2000, Development of a small-scale H_20 – LiBr absorption cooling system, *Heat Transfer Science & Technology., Uni. Of Tsinghua, Beijing*, 803-808.

Thomas, E.D., 1985, Chemical engineering thermodynamics. *McGraw-Hill Book Company.*

Thomas, M.S., David B.M., and Bruce, E.P., 1991,Vapour-liquid equilibrium data for the NH3-H20 system and its description with a modified cubic equation of state. *J. Chem. Eng. Data*, **36**(2), 202-208.

Tillner-Roth, R. and Friend, D.G., 1998, A Helmholtz free energy formulation of the thermodynamic properties of the mixture {Water +Ammonia}. *J. Phys. Chem. Ref. Data,* **27**(1), 63-96.

Tozer, R., 1997, ABO Newsletter, *IEA Annex 24*, **1-4.**

Tyagi, K.P. and Rao, K.S., 1984, Choice of absorbent-refrigerant mixtures. *Energy Research*, **8**, 361-368.

Tyagi, K.P., 1988a, Technical Note - Cut-Off Temperatures of Aqua-Ammonia Absorption Refrigeration System. *Heat Recovery Systems & CHP*, **8**(4), 371-373.

Tyagi, K.P., 1988b, Technical Note - Design Parameters of an Aqua-Ammonia Vapour Absorption Refrigeration System, *Heat Recovery Systems & CHP*, **8**(4), 375-377.

Vliet, G.C. and Chen, W., 1993, Location of non-absorbable gases in a simplified absorber geometry. *AES, International Absorption Heat Pump Conference ASME*, **31**, 171-177.

Wagner, W. and Pruss, A., 1993, International equations for the saturation properties of ordinary water substance. Revised according to the international temperature scale of 1990. *J. Physics. Chem. Ref. Data,*22(3), 783-787.

Wang, C.Q., 1996, Research of heat and mass transfer of lithium bromide falling film generator. *PhD Thesis, Shanghai Jiaotong University*, China.

Wang, J., Hu, X., and Liu, C., 1992, Coefficient of performance of an ideal absorption cycle. *ASHRAE Transactions*, **98**(2), 185-187.

Ward, J.A., Moss, S.Y., Finney, G.W. and Harvey, J, 1987, A study of absorption cycle heat pump based heating units and their potential in the UK domestic central heating market : Low temperature heat utilisation. *United Kingdom Atomic Energy Authority, Harwell.*

Wekken, B.J.C. and Wassenaar, R,H., 1988, Simultaneous heat and mass transfer accompanying absorption in laminar flow over a cooled wall. *Int. J. Refrig.*, **11**, 123-136.

Wimby, J.M. and Berntsson T.S., 1994a, Viscosity and density of aqueous solutions of LiBr, LiCl, ZnBr2, CaCl2 and LiNO3. 1. Single salt solutions. *J. Chem. Eng. Data*, **39**(1), 68-72.

Wimby, J.M. and Berntsson T.S., 1994b, Viscosity and density of aqueous solutions of Libr, LiCl, $ZnBr_2$, $CaCl_2$, and LiNO3. 2. Two-salt solutions. *J. Chem. Eng. Data*, **39**, 73-78.

Wood, B.D., Berman, N.S., Kim, K. and Chau, D.S.C., 1992, Heat transfer additives for absorption cooling system fluids. *Gas Research Institute*, GRI-92/0051.

Woschni, G., 1959, Untersuchung des Warmeubergangs und des Druckverlusts in gekrummten Rohren. Dr.-Ing. Diss. *TH Dresden, DDR*.

Wu, C., 1993, Cooling capacity optimisation of a waste heat absorption refrigeration cycle. *Heat Recovery Systems & CHP*, **13**(2), 161-166.

Xu S., 1998, Cycle analysis of absorption refrigeration system based on the second law of thermodynamics. *J. of Dalian Univ. of Tech., In Mandarin* **38**(1), 70-75.

Yang, R. and Jou, T., 1998, Non-absorbable gas effect on the wavy film absorption process. *Int. J. Heat Mass Transfer*, **41**, 3657-3668.

Yigit, A., 1999, A numerical study of heat and mass transfer in falling film absorber. *Int. Comm. Heat Mass Transfer*, **26**(2), 269-278.

Yih, S.M. and K.Y. Chen, 1982, Gas absorption into wavy and turbulent falling liquid films in a wetted-wall column. *Chemical Engineering Communications*, **17**, 123-136.

Yih, S.M. and Seagrave, R.C., 1980, Mass transfer in laminar liquid falling films with accompanying heat transfer and interfacial shear. *Int. J. Heat Mass Transfer*, **23**, 749-758.

Zaltash, A., Alley, M., Klatt, L.N., and Linkous, R.L., 1991, Densities and refractive indexes of aqueous (Li, K, Na) NO_3 Mixtures. *J. Chem. Eng. Data*, **36**, 209-213.

Ziegler, B. and Trepp, Ch., 1984, Equation of state for ammonia-water mixtures. *Int. J. Refrig.*, 7(2), Mar, 101-106.

Zinner, K., 1934, Effects of composition and temperature on the heat content of mixtures of ammonia and water. *Z.Gesamt. Kalte-Ind.*, **41**, p.21.

Appendix A - Report /Summary of constants for equation

The following report was generated for Equation 3.59

For concentration range $0 \leq x\% \leq 30$

Source	DF	Sum of Squares	Mean Square
Regression	16	77.82418	4.86401
Residual	131	1.240645E-04	9.470571E-07
Uncorrected Total	147	77.82430	
(Corrected Total)	146	16.59275	

R squared = 1 - Residual SS / Corrected SS = 0.99999

For concentration range $30 < x\% < 55$

Source	DF	Sum of Squares	Mean Square
Regression	16	31.25271	1.95329
Residual	89	2.057995E-05	2.312354E-07
Uncorrected Total	105	31.25273	
(Corrected Total)	104	6.26322	

R squared = 1 - Residual SS / Corrected SS = 1.00000

For concentration range $55 \leq x\% \leq 70$

Source	DF	Sum of Squares	Mean Square
Regression	16	10.55803	.65988
Residual	45	1.119437E-05	2.487638E-07
Uncorrected Total	61	10.55804	
(Corrected Total)	60	1.53771	

R squared = 1 - Residual SS / Corrected SS = .99999

Appendix B –Least Square Fit

Given n data points (x_1,y_1), (x_2,y_2)…. (x_n,y_n), the best fit function can be written in the form

$$\mathbf{F}(x) = \mathbf{C}_1\mathbf{f}_1(x) + \mathbf{C}_1\mathbf{f}_1(x) + \ldots. + \mathbf{C}_k\mathbf{f}_k(x) \qquad (\mathbf{B_A1})$$

Where $f_j(x)$, $j = 1,2\ldots k$ are chosen functions of x and the C_j, $j = 1,2\ldots k$ are constants which are initially unknown. The sum of the squares of the difference between f(x) and the actual values of y is given by

$$\begin{aligned} E &= \sum_{i=1}^{n} \left[f(x_i) - y_i\right]^2 \\ &= \sum_{i=1}^{n} \left[C_1 f_1(x_i) + C_2 f_2(x_i) + \ldots + C_k f_k(x_i) - y_i\right]^2 \end{aligned} \qquad (\mathbf{B_A2})$$

This error term is minimised by taking the partial first derivative of E with respect to each of the constants, C_j, $j = 1,2,\ldots.k$ and putting the result to zero, thus

$$\frac{\partial E}{\partial C_1} = 2\sum_{i=1}^{n} \left\{\left[C_1 f_1(x_i) + C_2 f_2(x_i) + \ldots + C_k f_k(x_k) - y_i\right] f_1(x_i)\right\} = 0$$

$$\frac{\partial E}{\partial C_2} = 2\sum_{i=1}^{n} \left\{\left[C_1 f_1(x_i) + C_2 f_2(x_i) + \ldots + C_k f_k(x_k) - y_i\right] f_2(x_i)\right\} = 0$$

$$\vdots \qquad\qquad\qquad \vdots$$

$$\frac{\partial E}{\partial C_k} = 2\sum_{i=1}^{n} \left\{\left[C_1 f_1(x_i) + C_2 f_2(x_i) + \ldots + C_k f_k(x_k) - y_i\right] f_k(x_i)\right\} = 0 \qquad (\mathbf{B_A3})$$

This symmetric system of k equation is linear, can be written in matrix form as

$$\begin{bmatrix} \sum_{i=1}^{n} f_1(x_i)f_1(x_i) \sum_{i=1}^{n} f_1(x_i)f_2(x_i) \ldots \sum_{i=1}^{n} f_1(x_i)f_k(x_i) \\ \sum_{i=1}^{n} f_2(x_i)f_1(x_i) \sum_{i=1}^{n} f_2(x_i)f_2(x_i) \ldots \sum_{i=1}^{n} f_2(x_i)f_k(x_i) \\ \vdots \\ \sum_{i=1}^{n} f_k(x_i)f_1(x_i) \sum_{i=1}^{n} f_k(x_i)f_2(x_i) \ldots \sum_{i=1}^{n} f_k(x_i)f_k(x_i) \end{bmatrix} \left\{\begin{bmatrix} C_1 \\ C_2 \\ \vdots \\ C_k \end{bmatrix}\right\} = \left\{\begin{matrix} \sum_{i=1}^{n} f_1(x_i)y_i \\ \sum_{i=1}^{n} f_2(x_i)y_i \\ \vdots \\ \sum_{i=1}^{n} f_k(x_i)y_i \end{matrix}\right\}$$

which can be solved for C_1, C_2, ….., C_k using Guess elimination.

APPENDIX C – Allocation of Channels

Table Ca1 - ALLOCATION OF CHANNELS FOR USE ON: ABSORPTION CHILLER, LOGGER 1.

		LOWER		UPPER			
CHANNEL NAME	**No**	**No**	**TERMINAL NAME**		**No**	**No**	**CHANNEL NAME**
T1 white +	1	02	D1+	D5+	01	5	T5 white +
BLUE NEG **T**		04	D1-	D5-	03		BLUE NEG **T**
T2 white +	2	06	D2+	D6+	05	6	T6 white +
BLUE NEG **T**		08	D2+	D6-	07		BLUE NEG **T**
T3 white +	3	10	D3+	D7+	09	7	T7 BROWN +
BLUE NEG **T**		12	D3-	D7-	11		BLUE NEG **K**
T4 white +	4	14	D4+	D8+	13	8	T8 white +
BLUE NEG **T**		16	D4-	D8-	15		BLUE NEG **T**
T9 white +	9	18	D9+	D13+	17	13	T13 BROWN +
BLUE NEG **T**		20	D9-	D13-	19		BLUE NEG **K**
T10 BROWN +	10	22	D10+	D14+	21	14	T14 white +
BLUE NEG **K**		24	D10-	D14-	23		BLUE NEG **T**
T11 white +	11	26	D11+	D15+	25	15	T15 white +
BLUE NEG **T**		28	D11-	D15-	27		BLUE NEG **T**
T12 BROWN+	12	30	D12+	CAL+	29		
BLUE NEG **K**		32	D12-	CAL-	31		
	20	34	V4+	L +5V	33	15	Chan 25/26/27/30 RS Flow RED
Chan 25/26/27/30RSflow SCREEN		36	ØV	L+	35		
	21	38	V5+	L-	37		
		40	ØV	L -5V	39		
	22	42	V6+	ØV	41		HIGH Px BROWN
		44	ØV	V1+	43	17	HIGH Px GREEN
	23	46	V7+	ØV	45		LOW Px BROWN
		48	ØV	V2+	47	18	LOW Px GREEN
	24	50	V8+	ØV	49		EVAP WATTS BLACK
Chan 28/29 FT2 flow BROWN		52	+12V	V3+	51	19	EVAP WATTS RED
RSHX & Recirc FT2 flow BLUE		54	ØV	+12V	53		HIGH & LOW Px Tx WHITE
RSHX FT2 flow BLACK	28	56	F/I 4	F/I 1	55	25	Inner coil RS flow BLUE
Recirculation FT2 flow BLACK	29	58	F/I 5	F/I 2	57	26	Outer coil RS flow BLUE
Cold blend RS flow BLUE	30	60	F/I 6	F/I 3	59	27	Condenser coil RS flow BLUE
	31	62	F/I 7	O +V	61	OUT +V	Link to 80 Relays supply RED
	EXT ØV	64	ØV	O1	63	OUT 1	2 kW Generator 1 upper 25A SSR BLACK (310)
	33	66	C1 ACF	O2	65	OUT 2	Solution pump 12V relay BLACK (386)
		68	C1 ØVF	O3	67	OUT 3	2 kW evaporator 25A SSR BLACK (314)
Generator 2 lower RED S2	34	70	C2 ACS	O4	69	OUT 4	Quick dilution Solenoid 5A SSR BLACK (327)
Generator 2 lower RED S1		72	C2 ØVS	O5	71	OUT 5	
	35	74	C3 ACS	O6	73	OUT 6	
		76	C3 ØVS	O7	75	OUT 7	
(388)	OUT ØV	78	O ØV	O8/B	77	OUT 8 BURST	2 kW Generator 2 lower 25A SSR BLACK (313)
(312 EV) OUT 1/2 Relay & 1/3 EvapSSR+12vlamp supply RED,+LINK 61		80	+12V	O ØV	79	OUT ØV	
SUPPLY VOLTS AC	16	SUPPLY V120/240V 50/60 Hz					(311) (315) (326)
	32	82	F/I8	+15V	81	OUT 1/1, 1/4 & 1/8 SSRs RED	
		84	ØV	-15V	83		
		LOWER		UPPER			

Table Ca2 - ALLOCATION OF CHANNELS FOR USE ON: ABSORPTION CHILLER, LOGGER 2.

		LOWER		UPPER			
CHANNEL NAME	**No**	No	**TERMINAL NAME**		**No**	**No**	**CHANNEL NAME**
T36 white +	36	02	D1+	D5+	01	40	T40 white +
BLUE NEG **T**		04	D1-	D5-	03		BLUE NEG **T**
T37 white +	37	06	D2+	D6+	05	41	T41 white +
BLUE NEG **T**		08	D2+	D6-	07		BLUE NEG **T**
T38 white +	38	10	D3+	D7+	09	42	T42 BROWN +
BLUE NEG **T**		12	D3-	D7-	11		BLUE NEG **K**
T39 white +	39	14	D4+	D8+	13	43	T43 BROWN +
BLUE NEG **T**		16	D4-	D8-	15		BLUE NEG **K**
T44 BROWN +	44	18	D9+	D13+	17	48	T48 BROWN +
BLUE NEG **K**		20	D9-	D13-	19		BLUE NEG **K**
T45 BROWN +	45	22	D10+	D14+	21	49	T49 BROWN +
BLUE NEG **K**		24	D10-	D14-	23		BLUE NEG **K**
T46 BROWN +	46	26	D11+	D15+	25	50	T50 BROWN +
BLUE NEG **K**		28	D11-	D15-	27		BLUE NEG **K**
T47 BROWN +	47	30	D12+	CAL+	29		
BLUE NEG **K**		32	D12-	CAL-	31		
	55	34	V4+	L +5V	33	50	
		36	0V	L+	35		
	56	38	V5+	L-	37		
		40	0V	L -5V	39		
	57	42	V6+	0V	41		
		44	0V	V1+	43	52	
	58	46	V7+	0V	45		
		48	0V	V2+	47	53	
	59	50	V8+	0V	49		
		52	+12V	V3+	51	54	
		54	0V	+12V	53		
	63	56	F/I 4	F/I 1	55	60	
	64	58	F/I 5	F/I 2	57	61	
	65	60	F/I 6	F/I 3	59	62	
	66	62	F/I 7	O +V	61	OUT +V	Link to 80 Relays supply RED
EXT 0V		64	0V	O1	63	OUT 1	H2O pump Relay BLACK (389)
	68	66	C1 ACF	O2	65	OUT 2	0.5 kW water 5A SSR BLACK (319)
		68	C1 0VF	O3	67	OUT 3	0.5 kW water 5A SSR BLACK (323)
Generator 1 upper RED S2	69	70	C2 ACS	O4	69	OUT 4	Cold blend solenoid 5A SSR BLACK (331)
Generator 1 upper RED S1		72	C2 0VS	O5	71	OUT 5	
	70	74	C3 ACS	O6	73	OUT 6	
		76	C3 0VS	O7	75	OUT 7	
OUT 0V		78	O 0V	O8/B	77	OUT 8 BURST	2 kW water 25A SSR BLACK (309)
OUT 2/1Relay 12V supply RED (391) +LINK 61		80	+12V	O 0V	79	OUT 0V	
SUPPLY VOLTS AC	51	SUPPLY V120/240V 50/60 Hz					(308) (318) (322) (330)
	67	82	F/I8	+15V	81	OUT 2/2, 2/3, 2/4 & 2/8 SSRs RED	
		84	0V	-15V	83		
		LOWER		UPPER			

APPENDIX D1 - ABSORPTION DIN RAIL

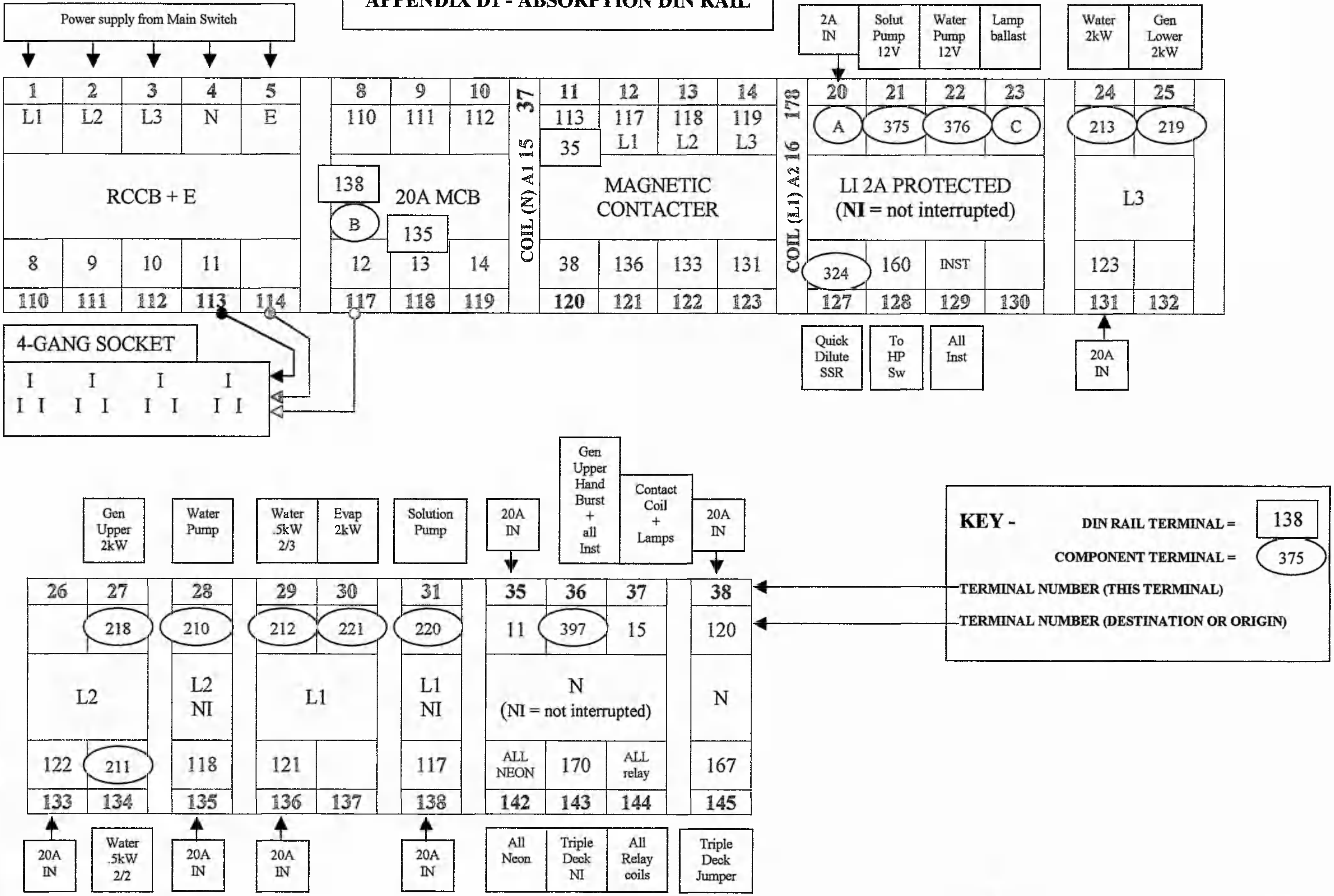

APPENDIX D2 - ABSORPTION TRIPLE-DECKERS

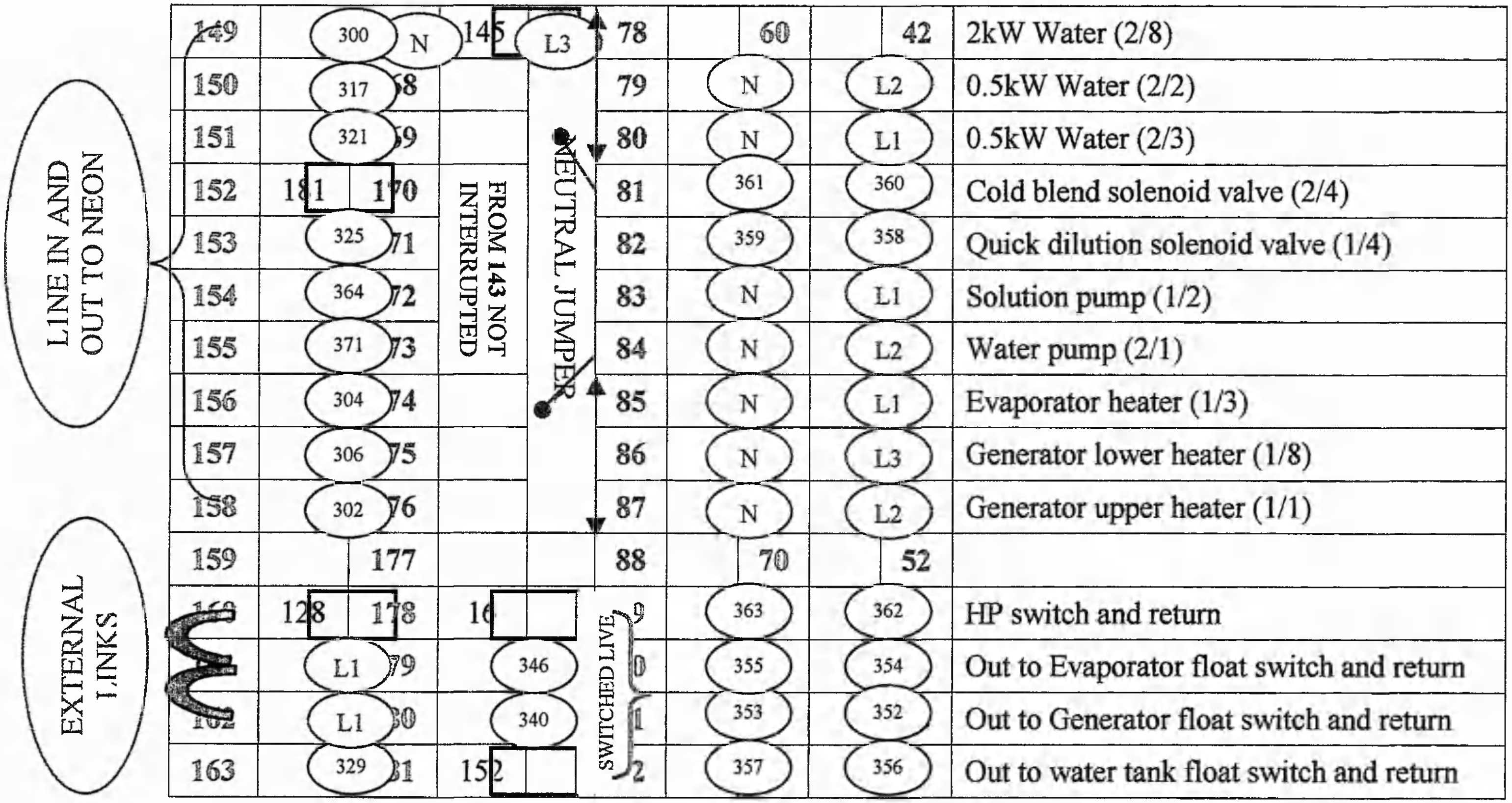

APPENDIX E – Crystallisation

Crystallisation is one of the major problems in absorption systems. The reason why crystallisation occurs is that the lithium bromide (salt) in the aqueous solution precipitates when the mass fraction of salts exceeds the solubility limit. The solubility limit is a strong function of mass fraction and temperature and a weak function of pressure. Furthermore, crystal nucleation is a process that is sensitive to the presence of nucleation sites. If no suitable nucleation sites are present, supersaturation can occur where the salt content of the liquid is greater than the solubility limit. Once crystals begin to form, the crystals themselves provide favourable nucleation sites and the crystals grow on themselves. The detail of the phase diagram explaining this phenomenon was presented by Herold (1996).

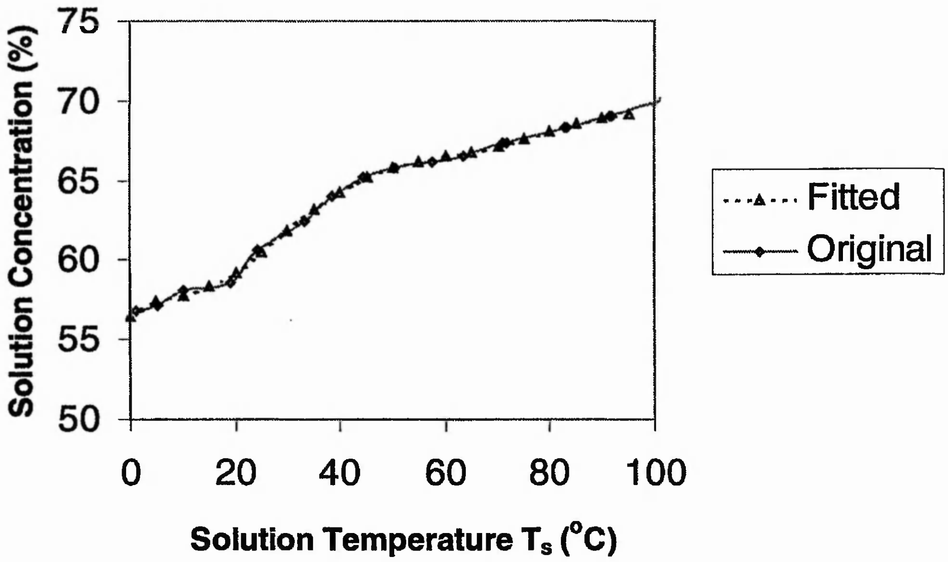

Figure E1, Solubility chart

Figure E1 shows the solubility line (Boryta,1970) of the water-lithium bromide mixtures. The line shows the saturation concentration at a particular concentration where crystallisation begins. It is a function of solution temperature and concentration. The solubility line was fitted by the author into an equation which can be readily used in computer control to avoid crystallisation. The equation is as follows:

$$\mathbf{So\,(T_s) = a + b \cdot T + c \cdot T^2 + d \cdot T^3 + e \cdot T^4 + f \cdot T^5 + g \cdot T^6 + h \cdot T^7}$$

where

a = 56.442591528, b = 0.328517912, c = -3.833257E-2, d = 2.530692E-3

e = -7.1546E-5, f = 9.9759E-7, g = -6.81493E-9, h = 1.82669E-11

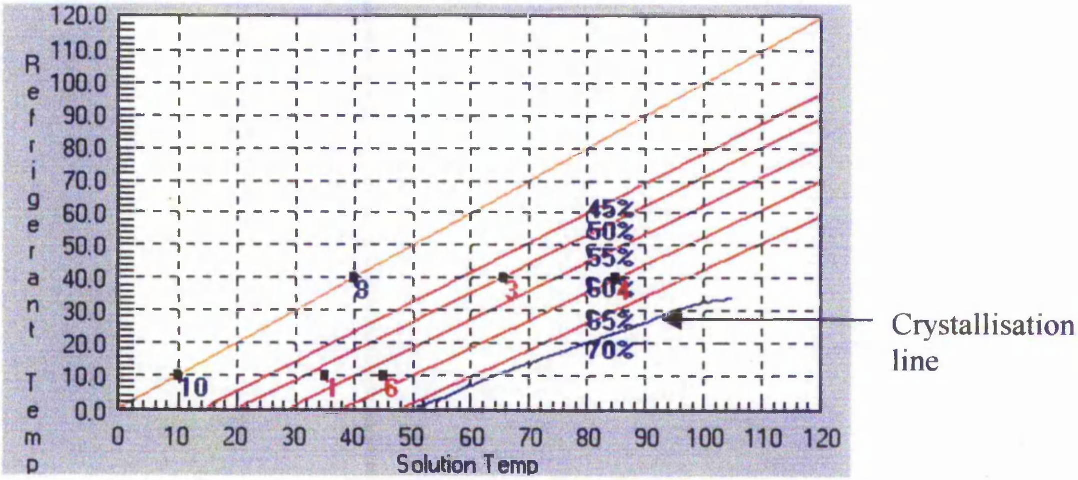

Figure E2, Refrigerant temperature against solution temperature for different concentrations

Figure E2 shows the condition based on experimental points. Point 4 represents the outlet solution from generator. For instance, at refrigerant temperature 30 °C, if the solution temperature reaches 92 °C, the solution concentration will be at 68.9%. When the solution temperature falls back to ambient, crystallization will occur.

The method to minimise the possibility of crossing the phase boundary is to ensure a sufficiently low sink temperature for cooling the absorber accompanied by the low absorber solution concentration. The strong solution mixture has to be kept below 63%.

When crystallisation occurs, the recovery method is to dilute it with distilled water from condenser or evaporator. The portion where crystals form has to be heated and continuously diluted by the circulating low-concentration mixture or water until the crystals disappear.